

INSTITUTE OF MOUNTAIN RISK ENGINEERING
UNIVERSITY OF NATURAL RESOURCES AND APPLIED LIFE SCIENCES
VIENNA

NUMERICAL MODELLING OF
BEDLOAD TRANSPORT IN
TORRENTS AND MOUNTAIN STREAMS

PhD THESIS

presented by

Michael Chiari

For the degree of

Doctor rerum naturalium technicarum

Vienna, October 2008

Supervisor and first assessor:

Univ.Prof. Dipl.Ing.ETH-Zür. Dr.sc.techn. Dieter Rickenmann

Second assessor:

Ao.Univ.Prof. Dipl.-Ing. Dr.nat.techn. Helmut Habersack

Abstract

Floods with substantial bedload transport have a high potential for damage. In particular inhabited fans are often heavily affected by deposits of sediment. Aim of the study is to improve an existing sediment transport model and to evaluate numerical simulations of bedload transport at steep slopes with field observations.

A sediment routing model for steep torrent channel networks called SETRAC has been developed at the University of Natural Resources and Applied Life Sciences, Vienna. SETRAC is the acronym for Sediment TRansport in Alpine Catchments. The main purpose of the model is the simulation of bedload transport at steep channel slopes. The SETRAC model has been further developed in collaboration with the programmer of the original version. Flow resistance and bedload transport equations appropriate for torrents and mountain streams are implemented. To take form roughness losses into account several approaches are available to modify the calculated transport capacity to better match observations on bedload transport. Armouring effects can also be considered. In addition it is possible to calculate fractional bedload transport by taking grain sorting effects in combination with mobile bed conditions into account. Flow hydrographs are routed through the channel network by using the kinematic wave approach.

The improved sediment routing model for steep torrent channel networks is presented. The model has been tested with two flume studies to examine the models ability to simulate morphologic changes as well as sorting effects. In addition, SETRAC has been applied to well documented case studies on flood events in torrential catchments with substantial sediment transport in the Austrian, Swiss and French Alps. The simulation results show the importance of form roughness losses when computing bedload transport in torrents and mountain streams. Neglecting form drag in rough steep channels often results in an overestimation of the calculated bedload transport.

Zusammenfassung

Geschiebeführende Hochwässer haben ein hohes Schadenspotential. Insbesondere bewohnte Schwemmkegel sind oft von den Auswirkungen der Geschiebeablagerung betroffen. Ziel der vorliegenden Arbeit ist es, ein numerisches Simulationsmodell für Geschiebetransport zu verbessern und Simulationsergebnisse anhand von Feldbeobachtungen zu evaluieren.

An der Universität für Bodenkultur in Wien wurde ein Modell zur numerischen Simulation von Geschiebetransport in Alpinen Einzugsgebieten entwickelt. SETRAC ist das Akronym für SEDiment TRansport in Alpine Catchments. Im Rahmen der vorliegenden Arbeit wurde das Modell in Zusammenarbeit mit dem Programmierer der ursprünglichen Version erweitert und verbessert. Der Fließwiderstand und der Geschiebetrieb werden mit für Gebirgsflüsse und Wildbäche geeigneten Formeln berechnet. Die Abminderung der Transportkapazität durch Formverluste kann mit verschiedenen Ansätzen berücksichtigt werden. Deckschichtbildung und fraktionsweiser Geschiebetransport kann in Kombination mit einer mobilen Gerinnesohle simuliert werden. Abflussganglinien werden als kinematische Welle durch ein Gerinnesystem geleitet.

Im Rahmen der vorliegenden Arbeit wird die neue Version von SETRAC vorgestellt. Das Modell wurde anhand von Laboruntersuchungen getestet, wobei sowohl morphologische Veränderungen als auch Sortiereffekte durch selektiven Geschiebetransport simuliert wurden. Des Weiteren wurde SETRAC anhand von gut dokumentierten Hochwasserereignissen in Österreich, der Schweiz und Frankreich getestet. Die Simulationsergebnisse zeigen die Bedeutung von Formverlusten bei der Berechnung des Geschiebetransports in Gebirgsflüssen und Wildbächen. Werden Formverluste nicht berücksichtigt, wird Geschiebetransport in steilen Gerinnen mit großer Rauigkeit meist stark überschätzt.

Acknowledgements

I would like to express my appreciation to Dieter Rickenmann for his encouragement to work on the topic of bedload transport at steep slopes and his supervision and criticism at all stages of this work.

I would like to express my gratitude to Helmut Habersack for assessing the thesis and providing interesting discussions.

Kurt Friedl, the programmer of the SETRAC model, essentially contributed to this work by continually extending and improving the model according to our needs. For his support and understanding I express my special gratitude.

Philippe Frey and Nicolle Mathys from CEMAGREF Grenoble provided important discussions in Vienna and Grenoble and field data for model comparisons between SETRAC and the ETC model. Therefore I would like to thank them.

I would like to thank the staff of the research unit Mountain Hydrology and Torrents of the Swiss Federal Institute for Forest, Snow and Landscape Research (WSL) for providing important data for the back-calculation of extreme flood events. The Swiss Federal Office of Environment (BAFU) provided post-event LiDAR data, and the Swiss Federal Office of Topography (swisstop) pre-event LiDAR data for three mountain rivers which were analyzed in the context of a BAFU project on the flood events 2005.

Thanks are extended to all colleagues from the Institute of Mountain Risk Engineering for their kindness and their help. Special thanks are addressed to Christian Scheidl for supporting my work through discussions, conversations and being a friend.

I would like to thank the Austrian Science Fund (FWF) for the financial support through the Translational Research Program L147 on *Sediment routing model for steep torrent channels* which enabled this work to be undertaken.

The Austrian Exchange Service (ÖAD) supported the scientific exchange between CEMAGREF (Grenoble) and our Institute through the program WTZ - Scientific and Technological Cooperation.

My parents supported and encouraged me during my whole life. For that reason I would like to express my gratefulness.

Finally I would like to thank my beloved wife Billy for her love and understanding.

Contents

I	Introduction	16
1	Bedload transport at steep slopes	17
2	Modelling bedload transport	18
3	Objectives of the study	20
II	Flow and Sediment Transport in Mountain Streams	21
4	Flow resistance approaches	22
4.1	Total flow resistance	22
4.2	Flow resistance due to grain roughness, form roughness and the resistance of the transported sediment	24
4.2.1	Approach of Palt and Rickenmann	24
4.2.2	Other approaches to estimate form resistance	27
4.2.3	Resistance of the transported sediment	31
5	Sediment transport capacity and initiation of motion at steep slopes	34
5.1	Initiation of motion	34
5.1.1	Critical shear stress	35
5.1.2	Critical flow discharge	36
5.2	Sediment transport	37
5.2.1	Effect of armour layer on bedload transport	39
5.2.2	Fractional bedload transport	40
5.2.3	Two phase transport	43
III	SETRAC - A Sediment Transport Simulation Model for Torrents and Mountain Streams	44
6	The SETRAC Model	45
6.1	Purpose	45
6.2	General approach	45
6.3	Hydrodynamic model	47
6.3.1	Kinematic wave approach	48
6.3.2	Numerical model	49
6.3.3	Flow resistance approaches	50

6.4	Sediment transport model	51
6.4.1	Morphologic changes	51
6.4.2	Erosion, deposition and sediment layers	54
6.4.3	Flow resistance due to form roughness	56
6.4.4	Sediment transport capacity and initiation of motion	56
6.4.5	Armour layer effect on transport threshold	57
6.4.6	Fractional bedload transport	57
6.5	Possible combinations of the formula sets	58
6.6	Limitations of the SETRAC model	58
6.7	Note on availability of the SETRAC model	59
6.8	Note on history of SETRAC	59
IV	Model Verification	60
7	Laboratory experiments to optimize a bedload deposition basin	61
8	Development of armour layer	64
V	Sensitivity Analysis	66
9	Effect of mobile bed approach	67
10	Effect of spatial and temporal discretisation	70
10.1	Effect of spatial discretisation	70
10.2	Effect of temporal discretisation	71
11	Effect of fractional bedload transport	72
11.1	The hiding function	72
11.2	Active layer thickness	74
11.3	Comparison with sediment transport formula for sediment mixtures	75
12	Effect of grain size distribution	78
VI	Event Documentation of Case Study Streams	82
13	Event documentation	83
13.1	Hydrology	83
13.2	Morphologic changes	84
13.2.1	Sediment budget based on field investigations	84
13.2.2	Airborn LiDAR Data	87
VII	Application of SETRAC to Case Study Streams	94
14	Simulation design	95

15 Extreme events August 2005	97
15.1 Sessladbach	98
15.1.1 Simulations of the Sessladbach extreme event	101
15.2 Schnannerbach	106
15.2.1 Simulations of the Schnannerbach extreme event	109
15.3 Suggadinbach	114
15.3.1 Simulations of the Suggadinbach extreme event	117
15.4 Chirel	122
15.4.1 Simulations of the Chirel extreme event	125
15.5 Chiene	129
15.5.1 Simulations of the Chiene extreme event	131
15.6 Schwarze Lutschine	136
15.6.1 Simulations of the Schwarze Lutschine extreme event	139
16 Case study in France	144
16.1 Draix	144
16.1.1 Model comparison	145
VIII Discussion	148
17 Discussion of simulation results	149
17.1 Agreement of predicted and observed loads and likely influence of form resistance	149
17.2 Effect of armour layer criteria in combination with one grain model . . .	150
17.3 Importance of form roughness losses	151
17.4 Comparison between transport capacity and observed transport on a channel reach basis	155
17.5 Back calculated form roughness losses on a channel reach basis	158
17.6 One grain-size model versus fractional bedload transport	161
18 Application of other simulation models	162

IX Conclusions	164
Nomenclature	167
Bibliography	170
Curriculum vitae	181
X Appendix	185
A SETRAC	186
A.1 Possible formula combination	186
A.2 SETRAC file formats	190
A.2.1 Cross-section file format	190
A.2.2 Point file format	192
A.2.3 Section file format	193
A.2.4 Grain size distribution file format	195
A.2.5 Signal file format	202
A.2.6 Output file format	204
B Precipitation-discharge simulation	210

List of Figures

4.1	Comparison of two approaches to estimate the proportion of form and grain roughness in steep streams	26
4.2	Comparison between different approaches to calculate losses due to form roughness	29
4.3	Contribution of grain roughness to total roughness calculated with Equation 4.14, 4.15 and 4.35.	30
4.4	Calculated resistance coefficients versus the relative submergence R/d with consideration of slope.	32
4.5	Contribution of flow resistance of the transported sediment for fix and mobile bed conditions to total flow resistance versus $S * h/d$. Data taken from Hu and Abrahams (2005).	33
5.1	Effect of varying γ on the relative mobility of grain size fractions . . .	42
6.1	Structured cross-section with visualization of the specific bedload transport rate in the strips	46
6.2	$\frac{\partial Q}{\partial x}$ as difference quotient at the timeline j . The arrows indicate the flow of information.	50
6.3	Example of a cross-section with morphologic changes due to erosion and deposition	52
6.4	Concept of enhancement or lowering of the cross-section	53
6.5	At confluences the erosion or deposition volumes are weighted by the bedload transport of the parent sections	54
6.6	Sediment routing of size fractions	55
7.1	The experimental setup for the bedload deposition basin	61
7.2	Water and sediment discharge for the HQ150 experimental run	62
7.3	Measured deposition heights after the experimental run	63
7.4	Comparison of modelled and measured deposition heights for the laboratory experiment HQ150	63
8.1	Grain size distribution for the experimental run 8 and comparison with SETRAC simulation	65
9.1	Time evolution of a longitudinal profile	67
9.2	Comparison of accumulated bedload transport after 40 minutes simulation time	68
9.3	Comparison of accumulated bedload transport after 80 minutes simulation time	69

9.4	Comparison of accumulated bedload transport after 240 minutes simulation time	69
10.1	Comparison of different spatial discretisations for the Laval case study	70
11.1	Grain size distribution obtained by variation of γ	73
11.2	Bedload transport for varying γ	73
11.3	Grain size distribution obtained by different discharges	74
12.1	Grain size distributions used for the simulations	78
12.2	Bedload transport at $0.1 \text{ m}^3/\text{s}$	79
12.3	Bedload transport at $1.0 \text{ m}^3/\text{s}$	80
12.4	Bedload transport at $10.0 \text{ m}^3/\text{s}$	80
13.1	Calculation procedure for the back calculation of the peak discharge after Rickenmann (1990)	85
13.2	Example of the erosion and deposition volumes for one of the case study torrents (including fibne material for erosion, and pore space) . .	85
13.3	Example of the accumulated bedload transport for one of the case study torrents (excluding fine material and pore space)	86
13.4	Reflection depending on the target (source: www.riegl.com)	87
13.5	River reach with confluence of the Chirel mountain stream. Hill shades were generated with DSM and DTM.	88
13.6	River reach of the Chirel mountain stream before and after the August 2005 flood event	90
13.7	Calculated erosion and deposition heights with discretisation of the active channel reaches	91
13.8	River reach of the Lütshine mountain stream before and after the August 2005 flood event	93
15.1	72-hours precipitation from 21. - 24. August 2005 (source: MeteoSchweiz (2006))	97
15.2	Overview Sesslabach project area	99
15.3	Grain size distribution for the Sesslabach project	100
15.4	Accumulated bedload transport for the Sesslabach case study	100
15.5	Longitudinal profile of the Sesslabach with slope and possible erosion depth for each section	101
15.6	Hydrograph and related critical discharge values for a cross-section at fan apex of the Sesslabach ($S = 0.20$ and $W = 5.5 \text{ m}$).	102
15.7	Comparison of the reconstructed bedload transport and SETRAC simulations for the cases Sesslabach S1, S2 and S7	103
15.8	Comparison of the reconstructed bedload transport and SETRAC simulations for the cases Sesslabach S3 and S8	103
15.9	Comparison of the reconstructed bedload transport and SETRAC simulations for the cases Sesslabach S4 and S9	104
15.10	Comparison of the reconstructed bedload transport and SETRAC simulations for the cases Sesslabach S5 and S10	104

15.11	Comparison of the reconstructed bedload transport and SETRAC simulations for the cases Sesslabach S6 and S11	105
15.12	Overview Schnannerbach project area	107
15.13	Grain size distribution for the Schnannerbach project	107
15.14	Accumulated bedload transport for the Schnannerbach case study . . .	108
15.15	Longitudinal profile of the Schnannerbach with slope and possible erosion depth for each section	109
15.16	Hydrograph and related critical discharge values for a cross-section at fan apex of the Schnannerbach ($S = 0.20$ and $W = 5.5 m$).	110
15.17	Comparison of the reconstructed bedload transport and SETRAC simulations for the cases Schnannerbach S1, S2 and S7	111
15.18	Comparison of the reconstructed bedload transport and SETRAC simulations for the cases Schnannerbach S3 and S8	111
15.19	Comparison of the reconstructed bedload transport and SETRAC simulations for the cases Schnannerbach S4 and S9	112
15.20	Comparison of the reconstructed bedload transport and SETRAC simulations for the cases Schnannerbach S5 and S10	112
15.21	Comparison of the reconstructed bedload transport and SETRAC simulations for the cases Schnannerbach S6 and S11	113
15.22	Overview Suggadin project area	115
15.23	Grain size distribution for the Suggadinbach project	115
15.24	Accumulated bedload transport for the Suggadinbach case study . . .	116
15.25	Longitudinal profile of the Suggadin mountain stream with slope and possible erosion depth for each section	117
15.26	Hydrograph and related critical discharge values for a cross-section at km 0.5 of the Suggadinbach ($S = 0.06$ and $W = 12 m$).	118
15.27	Comparison of the reconstructed bedload transport and SETRAC simulations for the cases Suggadinbach S1, S2 and S7	119
15.28	Comparison of the reconstructed bedload transport and SETRAC simulations for the cases Suggadinbach S3 and S8	119
15.29	Comparison of the reconstructed bedload transport and SETRAC simulations for the cases Suggadinbach S4 and S9	120
15.30	Comparison of the reconstructed bedload transport and SETRAC simulations for the cases Suggadinbach S5 and S10	120
15.31	Comparison of the reconstructed bedload transport and SETRAC simulations for the cases Suggadinbach S6 and S11	121
15.32	Overview Chirelbach project area	123
15.33	Grain size distribution for the Chirel project	123
15.34	Accumulated bedload transport for the Chirelbach case study	124
15.35	Longitudinal profile of the Chirel mountain stream with slope and possible erosion depth for each section	125
15.36	Hydrograph and related critical discharge values for a cross-section at km 1.2 of the Chirel mountain stream ($S = 0.026$ and $W = 15 m$). . .	126
15.37	Comparison of the reconstructed bedload transport and SETRAC simulations for the cases Chirelbach S1, S2 and S7	127

15.38	Comparison of the reconstructed bedload transport and SETRAC simulations for the cases Chirelbach S3 and S8	127
15.39	Comparison of the reconstructed bedload transport and SETRAC simulations for the cases Chirelbach S4 and S9	128
15.40	Comparison of the reconstructed bedload transport and SETRAC simulations for the cases Chirelbach S5 and S10	128
15.41	Overview Chiene project area	129
15.42	Grain size distribution for the Chiene project	130
15.43	Accumulated bedload transport for the Chiene case study	130
15.44	Longitudinal profile of the Chiene mountain stream with slope and possible erosion depth for each section	131
15.45	Hydrograph and related critical discharge values for a cross-section at <i>km</i> 0.75 of the Chiene mountain stream ($S = 0.022$ and $W = 18 m$).	132
15.46	Comparison of the reconstructed bedload transport and SETRAC simulations for the cases Chiene S1, S2 and S7	133
15.47	Comparison of the reconstructed bedload transport and SETRAC simulations for the cases Chiene S3 and S8	133
15.48	Comparison of the reconstructed bedload transport and SETRAC simulations for the cases Chiene S4 and S9	134
15.49	Comparison of the reconstructed bedload transport and SETRAC simulations for the cases Chiene S5 and S10	134
15.50	Comparison of the reconstructed bedload transport and SETRAC simulations for the cases Chiene S6 and S11	135
15.51	Overview Lüttschine project area	137
15.52	Grain size distribution for the Lüttschine project	137
15.53	Accumulated bedload transport for the Lüttschine case study	138
15.54	Longitudinal profile of the Lüttschine mountain stream with slope and possible erosion depth for each section	139
15.55	Hydrograph and related critical discharge values for a cross-section at <i>km</i> 4.0 of the Schwarze Lüttschine mountain stream ($S = 0.022$ and $W = 20 m$).	140
15.56	Comparison of the reconstructed bedload transport and SETRAC simulations for the cases Lüttschine S1, S2 and S7	141
15.57	Comparison of the reconstructed bedload transport and SETRAC simulations for the cases Lüttschine S3 and S8	141
15.58	Comparison of the reconstructed bedload transport and SETRAC simulations for the cases Lüttschine S4 and S9	142
15.59	Comparison of the reconstructed bedload transport and SETRAC simulations for the cases Lüttschine S5 and S10	142
15.60	Comparison of the reconstructed bedload transport and SETRAC simulations for the cases Luetschine S6 and S11	143
16.1	Overview Laval project area	144
16.2	Rainfall and runoff measurements for the Laval case study	145
16.3	Longitudinal profile of the Laval torrent with slope and possible erosion depth for each section	146

16.4	Channel bed with fine sediment in the Laval catchment	147
16.5	Comparison of simulation results obtained with the SETRAC and ETC models for the Laval case study	147
17.1	Relation between discharge and effective water volume after Badoux and Rickenmann (2008)	152
17.2	Hydrograph and sedi-graphs for the channel outlet of the Schnannerbach	152
17.3	Hydrograph and sedi-graphs for the channel outlet of the Sesslabach	153
17.4	The calibrated exponent a for the Sesslabach	154
17.5	The calibrated exponent a for the Schnannerbach	154
17.6	The calibrated exponent a for the Chiene mountain stream	154
17.7	The calibrated exponent a for the Lütshine mountain stream	154
17.8	Ratio of transport capacity and reconstructed bedload transport for all field data	156
17.9	Ratio of transport capacity and reconstructed bedload transport for all torrents and mountain streams	156
17.10	Ratio of transport capacity and reconstructed bedload transport for all field data where the ratio is >1	157
17.11	Ratio of transport capacity and reconstructed bedload transport for all field data where the ratio is >1 and the slope is steeper than 0.02	157
17.12	Contribution of form roughness to total roughness as a function of slope if $a = 2$ is used in Equation 17.5.	159
17.13	Contribution of form roughness to total roughness as a function of slope if $a = 1.35$ is used in Equation 17.5.	159
17.14	Contribution of form roughness to total roughness as a function of slope for channel reaches in alluvium if $a = 2$ is used in Equation 17.5.	160
A.1	Possible formula combinations for SETRAC simulations for sediment mixtures, using the $q_b - q$ form	187
A.2	Possible formula combinations for SETRAC simulations for sediment mixtures, using the $\Phi_b - \theta$ form	188
A.3	Possible formula combinations for SETRAC simulations for sediment mixtures for sediment transport calculations by size fractions	189
A.4	Example of DXF file export in SETRAC.	209

List of Tables

4.1	Values of Coefficients c and e from Pagliara and Chiavaccini (2006) . . .	28
4.2	Parameters for the comparison of different approaches to estimate form roughness losses	28
8.1	Selected experimental run	64
8.2	Grain size distribution of the sediment mixture used in the experiment and obtained by Günter and SETRAC simulations	65
10.1	Discretisation length and simulated river/flume length for the case studies.	71
11.1	Initial grain size distribution of the bed sediment	72
11.2	Duration for the development of a constant grain size distribution for different discharges and varying active layer depth	75
11.3	Comparison of bedload discharge obtained by the one-grain model and the fractional bedload transport with $\gamma = 0.80$. All values in m^3/s	77
12.1	Characteristic grain sizes for the one grain model. All values in cm . . .	78
12.2	Comparison of bedload discharge obtained by the one-grain model and the fractional bedload transport at $0.1 m^3/s$. All values in m^3/s	81
12.3	Comparison of bedload discharge obtained by the one-grain model and the fractional bedload transport at $1.0 m^3/s$. All values in m^3/s	81
12.4	Comparison of bedload discharge obtained by the one-grain model and the fractional bedload transport at $10.0 m^3/s$. All values in m^3/s	81
13.1	Point density for the active channels before and after the August 2005 flood event in Switzerland.	92
14.1	Formulas used for the simulations	96
16.1	Formulas used for the model comparison	146
A.1	Tags for the cross-section file	190
A.2	Tags for the point file	192
A.3	Tags for the section file	193
A.4	Tags for the grain size distribution file	196
A.5	Structure of the signal file	202
A.6	Variables for txt the output file	205
A.7	Variables for the dxf output file	207
B.1	Parameters for the precipitation-discharge simulations of the Sesslabach	210

B.2	Parameters for the precipitation-discharge simulations of the Schnannerbach	210
B.3	Parameters for the precipitation-discharge simulations of the Suggadinbach	211
B.4	Parameters for the precipitation-discharge simulations of the Chirelbach	211
B.5	Parameters for the precipitation-discharge simulations of the Chiene mountain stream	211
B.6	Parameters for the precipitation-discharge simulations of the Lütschiene mountain stream	211
B.7	Parameters for the precipitation-discharge simulations of the Laval case study	212

Part I

Introduction

1 Bedload transport at steep slopes

In contrast to studies on lowland gravel bed rivers, relatively few were made on sediment transport in steep headwater channels, with stream gradients steeper than about 0.05. Bathurst et al. (1987) defined a mountain stream as a river in an upland area or an area with steep topography. Channel slopes are steep (ranging from 0.01 to 0.1 or steeper) and bed sediment contains a high proportion of gravel, cobbles and boulders. For the most upstream reaches in mountainous catchments the term torrent can be used, which is typically associated with catchment areas smaller than about 25 km^2 and mean channel gradients larger than 0.05 to 0.10 (Rickenmann et al., 2008). Sediment transport dynamics in these channels may be quite different from low-gradient channels. Sediment storage in torrents and mountain streams is often limited, whereas the transport capacity during flood events is very high resulting in fast changes in the cross-section geometry during flood events. There is often a strong interaction between hill slope processes and the channel network. Sediment pulses and sediment supply disturbances influence the transport of bedload (Cui and Parker, 2005). Sediment transport may be supply limited (Bathurst, 2007) rather than controlled by the sediment transport capacity under given discharge and channel conditions. Steep headwater streams are characterized by a wide range of sediment sizes and temporally- and spatially-variable sediment sources. Bed morphology and channel structures may be influenced by the presence of large boulders, woody debris and bedrock constrictions. This can result in large variations in channel geometry, stream flow velocity and roughness (Hassan et al., 2005). Flow resistance in steep mountain streams with irregular bed topography includes both grain friction and important form drag. Flows are typically characterized by low relative flow depths. Recent investigations and discussions of such flow conditions were made by Aberle and Smart (2003), Bathurst (2002), Lee and Ferguson (2002), and Smart et al. (2002). Especially form roughness losses can reduce the actual bedload transport at steep slopes. The application of theoretical sediment transport equations derived from laboratory experiments may be problematic (Gomi and Sidle, 2003). Quantitative measurements of sediment and bedload transport in steep streams are very limited ((Rickenmann, 2001). Measured transport rates in natural streams may differ substantially from values predicted with such formulas (e.g. Bathurst et al., 1987; Gomez and Church, 1989). Yager et al. (2007) demonstrated that accurately predicting bedload transport in steep, rough streams requires accounting for the effects of local sediment availability and drag due to rarely mobile, loose particles. Also, measured transport rates in gravel-bed rivers and boulder-bed streams may vary by several orders of magnitude at similar (mean) flow conditions (e.g. Bathurst et al., 1987; Gomez, 1987; Reid and Laronne, 1995; Hegg and Rickenmann, 1999; Rickenmann, 2001).

2 Modelling bedload transport

Several models have been developed for modelling bedload transport. Most of these models are mainly applicable to rivers, but have not been tested for steep channels found in torrents and mountain streams. Few models are applicable for stream gradients steeper than about 0.05.

In principle there are two opportunities to sediment routing in steep streams. The first approach consists in using a hydraulic simulation model including sediment transport and accounting for variations in bed geometry due to erosion or deposition. These models typically include the full Saint Venant equations for one- or two-dimensional flow. A sediment transport equation is used in combination with the so-called Exner equation to account for sediment transport and storage effects in the riverbed. Examples are the one dimensional 3ST1D model (Papanicolaou et al., 2004), the 1.5 dimensional FLORIS-2000 model (Reichel et al., 2000) or the semi two-dimensional stream tube SDAR model (Bahadori et al., 2006). Most two-dimensional bedload transport models have been mainly developed for large riverine or estuarine environments. An example of a two-dimensional model applicable for steep slopes is the Flumen model (Beffa, 2005). A second group of hydro-sedimentologic models considers sediment transfer processes at the catchment scale, including channel sediment transfer with different degrees of details. These models can typically be linked to a rainfall-runoff model and a module to account for sediment transfer from hill slopes into the channel network. Examples are the ETC rainfall-runoff-erosion model (Mathys et al., 2003), the SHESED model (Wicks and Bathurst, 1996), the DHSVM model (Doten et al., 2006) or the Promab-GIS model (Rinderer et al., ip).

Modelling bedload transport in steep headwater channels is rather challenging, as flow data - generally needed for the calibration of a hydraulic model - are mostly absent in small catchments. The input hydrographs, necessary for the simulation model, need to be generated with a rainfall runoff model and calibrated with measured or reconstructed hydrographs. Flood marks at cross-sections without morphological change have to be used for the recalculation of the peak discharge if no stream flow measurements are available. An important hydraulic model parameter, the roughness coefficient, is typically estimated by approximate techniques (Kidson et al., 2006), because no measurements for high discharges are available. The space occupied by the transported sediment is non negligible for flood events with substantial bedload transport at steep slopes (Rickenmann, 1990). For the calibration of the sediment transport model additional data about morphologic changes can be obtained by field investigations or by remote sensing techniques (e.g. differential elevation models obtained by LiDAR). In the case of a flood event a movable-boundary, unsteady-state calibration (Thomas and Chang, 2008) is required for computational modelling. If a real model calibration is not possible due to the lack of adequate calibration data, Thomas and Chang (2008) suggest computational analysis. Computational analysis is the application of a computational

model to a problem in which a reliable model calibration is not possible. For the case of a flood reconstruction with bedload transport at steep slopes measured water levels are used for the back-calculation of the peak discharge and therefore they cannot be used for the calibration of the hydraulic part of the model. Hence the simulated water levels are obtained by estimates of the channel roughness and therefore not very reliable. For that reason Schoklitsch-type bedload transport equations are recommended for the calculation of bedload transport at steep slopes (Bathurst et al., 1987). Hence modelling bedload transport at steep slopes and recalculations of sediment laden floods can be regarded as computational analysis.

3 Objectives of the study

A one dimensional sediment transport model for steep headwater catchments has been developed at the University of Natural Resources and Applied Life Sciences (Friedl, 2004). Aim of the study is to evaluate and improve the existing SETRAC model. Therefore the SETRAC model is applied to back-calculations of well documented flood events with substantial bedload transport. In order to evaluate the performance, simulation results are compared with observed sediment transport during flood events with high flow intensities. Large discrepancies between observed and calculated bedload volumes have been reported for low to medium flow intensities (see e.g. Rickenmann, 2001; Bathurst, 2007). Back-calculations of well documented torrential flood events show the needs for enhancements of the existing SETRAC model. Form roughness losses caused by the roughness of the channel bed can be considered by different approaches. The role of form resistance losses with respect to reduced sediment transport rates are evaluated. The suitability of other models for sediment transport simulations in steep channels is discussed.

Part II

Flow and Sediment Transport in Mountain Streams

4 Flow resistance approaches

4.1 Total flow resistance

Flow resistance is composed of three distinct, but related elements (Morvan et al., 2008):

- Skin drag (e.g. roughness due to surface texture, grain roughness)
- Form drag (e.g. roughness due to surface geometry, bed forms, dunes, separation)
- Shape drag (e.g. roughness due to overall channel shape, meanders bends)

Flow resistance in steep headwater streams cannot be described sufficiently by a characteristic percentile of the grain size distribution (Aberle and Smart, 2003). Bed forms and bed structures, grains, discharge and the channel slope as well as the presence of large woody debris influence the flow resistance of torrents and mountain streams (Wilcox and Wohl, 2006).

For steep streams with gradients larger than about 0.1 there are only few velocity measurements, and in most cases no information is available on flow depth. For the calculation of turbulent flow over a rough channel bed different approaches to calculate the flow resistance have been derived. This can be empirically derived formulas to calculate the mean flow velocity or can be based on the logarithmic flow resistance law.

The well known Manning-Strickler equation (Strickler, 1923) is an empirical relation for the calculation of the mean flow velocity which is often used for engineering applications:

$$v = k_{St} R^{0.67} S^{0.5} \quad (4.1)$$

where v is the mean flow velocity, k_{St} is Strickler's roughness coefficient, R is the hydraulic radius and S is the channel gradient.

The Strickler roughness coefficient k_{St} is a cumulative value of total roughness and therefore not independent of the flow depth. Due to the lack of flow depth data in steep streams, Rickenmann (1994, 1996) developed a set of empirical equations where the mean flow velocity, the Strickler coefficient and the surface width of the flow, respectively, can be expressed as a function of discharge, channel gradient, and a characteristic grain size of the surface bed material. All the equations are dimensionally homogeneous; they are based on more than 300 measurements in torrents and gravel-bed rivers. The equations to estimate the Strickler roughness coefficient k_{St} are (Rickenmann, 1996):

$$k_{St} = \frac{0.97g^{0.41}Q^{0.19}}{S^{0.19}d_{90}^{0.64}} \quad \text{for } S \geq 0.008 \quad (4.2)$$

$$k_{St} = \frac{4.36g^{0.49}Q^{0.02}}{S^{0.03}d_{90}^{0.23}} \quad \text{for } S \leq 0.008 \quad (4.3)$$

where g is the acceleration due to gravity, Q is the discharge and d_{90} is the grain size of the surface bed material for which 90% of the bed material is finer. The equations are based on stream flow velocity observations covering a wide range of flow conditions, including mountain streams with channel gradients of up to 0.2 and relative flow depth as small as about 0.4. The original regression equations were derived using dimensionless parameters.

Alternatively Rickenmann (1991, 1994) developed a power law equation to express the mean flow velocity as a function of discharge instead of flow depth:

$$v = \frac{1.3g^{0.2}q^{0.6}S^{0.2}}{d_{90}^{0.4}} \quad (4.4)$$

where q is the flow rate per unit width. Equation (4.4) was originally proposed by Takahashi (1987) based on laboratory experiments on debris flows, and successfully applied by Rickenmann (1991) to experimental sediment transporting flows.

Equation (4.4) was applied to field data by Rickenmann (1996), resulting in a similar scatter between predicted and observed velocities, as when applying equation (4.2) in combination with equation (4.1). With $q = vh$ equation (4.4) can be transformed to (Rickenmann et al., 2006):

$$v = \frac{1.93g^{0.5}h^{1.5}S^{0.5}}{d_{90}} \quad (4.5)$$

where h is the flow depth.

Approaches based on the logarithmic law are developed after Colebrook and White (1937), who found a flow law for turbulent flow in pipes. The mean velocity can be expressed as a function of slope and the friction factor f

$$v = \sqrt{\frac{8}{f}} \sqrt{gRS} \quad (4.6)$$

where f is the Darcy-Weisbach friction factor. For wide channels the hydraulic Radius R can be approximated by the flow depth h .

$$v = \sqrt{\frac{8}{f}} \sqrt{ghS} \quad (4.7)$$

Aberle and Smart (2003) derived an empirical relationship for the calculation of $(8/f)^{0.5}$ for low relative submergence ($h/d_{84} < 3$) based on laboratory experiments with slopes ranging from 0.02 to 0.1:

$$\sqrt{\frac{8}{f}} = 3.54 \ln \left(\frac{h}{d_{84}} \right) + 4.41 \quad (4.8)$$

Another flow resistance equation for steep channels was introduced by Smart and Jäggi (1983). The formula is based on laboratory data. The increasing flow resistance at

low relative flow depth is taken into account by the term in the first brackets, modifying the traditional logarithmic velocity equation:

$$v = 2.5v^* \left(1 - e^{\frac{-0.05h_m}{S^{0.5}d_{90}}} \right)^{0.5} \ln \left[\frac{12.3h_m}{1.5d_{90}} \right] \quad (4.9)$$

Where h_m is the mixture flow depth. The shear velocity is defined as $v^* = (ghS)^{0.5}$. The mixture flow depth h_m accounts for the space occupied by moving particles. This formula is valid for channels with gradients up to 0.20. The increase compared to the fluid flow depth, $h_f = q/v$ was found to be important for channel gradients steeper than about 0.1 in the laboratory experiments. To account for increased flow depth at high sediment concentrations, the following empirical relation for h_f/h_m (Rickenmann, 1990) was introduced, based on flume experiments of Smart and Jäggi (1983) and Rickenmann (1990):

$$\frac{h_f}{h_m} = 1 - 1.64S^{0.42} \left(\frac{q_b}{q} \right)^{0.63} \quad (4.10)$$

where q_b is the bedload transport rate per unit channel width. The equation was derived from experiments with channel gradients up to 0.2.

4.2 Flow resistance due to grain roughness, form roughness and the resistance of the transported sediment

For steep mountain streams with irregular bed topography and low relative flow depth form drag becomes very important. Sediment transport formulas derived from steep experimental flumes are generally based on rather uniform bed material where the moveable bed had a more or less planar surface without bed form structures (Smart and Jäggi, 1983; Rickenmann, 1990). Therefore essentially skin drag was present in these experiments.

Apart from limited sediment supply this can be regarded as a reason why these formulas often overestimate bedload transport when they are applied to channels where bed forms can not be neglected.

4.2.1 Approach of Palt and Rickenmann

A procedure is presented to separate the slope of the energy line into a part associated with skin friction only. The procedure assumes that grain friction losses depend on the power of a characteristic grain size, and these losses are compared to the total (measured) friction losses. This part of the energy line is available for bedload transport when calculated with a formula derived from laboratory experiments without consideration of form drag (no bed forms were present in the flume experiments) and shape drag (flume is straight). Generally form drag and shape drag are regarded together. In the following the term form roughness includes shape drag.

Rickenmann (1996) proposed equations to calculate the Manning's coefficient of total roughness n_{tot} for torrents steeper than 0.6%

$$\frac{1}{n_{tot}} = \frac{0.56g^{0.44}Q^{0.11}}{S^{0.33}d_{90}^{0.45}} \quad (4.11)$$

and for torrents steeper than 0.8% the following equation was proposed:

$$\frac{1}{n_{tot}} = \frac{0.97g^{0.41}Q^{0.19}}{S^{0.19}d_{90}^{0.64}} \quad (4.12)$$

Equation 4.11 is derived from velocity and discharge measurements in combination with a regime relation for the channel width to adopt the Manning Strickler equation by replacing the hydraulic radius by the flow depth, whereas Equation 4.12 is derived by direct regression.

Wong and Parker (2006) reanalyzed the Meyer-Peter and Mueller (1948) data and suggested that the roughness coefficient associated with skin friction only n_r can be expressed as:

$$\frac{1}{n_r} = \frac{23.2}{\sqrt[6]{d_{90}}} \quad (4.13)$$

The contribution of skin roughness to total roughness can be expressed by dividing Equation (4.11) by Equation (4.13)

$$\frac{n_r}{n_{tot}} = \frac{0.0756Q^{0.11}}{g^{0.06}d_{90}^{0.28}S^{0.33}} \quad (4.14)$$

or by dividing Equation (4.12) by Equation (4.13).

$$\frac{n_r}{n_{tot}} = \frac{0.133Q^{0.19}}{g^{0.096}d_{90}^{0.47}S^{0.19}} \quad (4.15)$$

Rickenmann (2005) proposed a procedure to estimate flow resistance losses due to form drag as a function of slope and relative submergence. Taking into account (4.11), equation (11) and (9a) from Rickenmann (1996) in combination with (4.13) the equation becomes:

$$\frac{n_r}{n_{tot}} = 0.092S^{-0.35} \left(\frac{h}{d_{90}} \right)^{0.33} \quad (4.16)$$

or derived from 4.12), equation (11) and (9a) from Rickenmann (1996) in combination with (4.13) the equation becomes:

$$\frac{n_r}{n_{tot}} = 0.185S^{-0.22} \left(\frac{h}{d_{90}} \right)^{0.55} \quad (4.17)$$

Palt (2001) derived a similar approach from natural data for the slope range $0.002 < S < 0.12$ (Equation 4.18).

$$\frac{n_r}{n_{tot}} = 0.13S^{-0.28} \left(\frac{h}{d_{90}} \right)^{0.21} \quad (4.18)$$

If there is no information about the cross-section and the water level available alternatively the following expression can be used for the estimation of n_r/n_{tot} (Palt, 2001):

$$\frac{n_r}{n_{tot}} = 0.1S^{-0.36} \quad (4.19)$$

For comparison with Equation 4.19 a potential equation has been fitted for Equation 4.14:

$$\frac{n_r}{n_{tot}} = 0.09S^{-0.52} \quad (4.20)$$

and for Equation 4.17:

$$\frac{n_r}{n_{tot}} = 0.12S^{-0.34} \quad (4.21)$$

A comparison of Equation 4.15 and Equation 4.17 is made in Figure 4.1 where they are applied to the data set of flow velocity measurements used by Rickenmann (1994, 1996). A large variation of the n_r/n_{tot} values is observed for channel gradients up to about 0.1. For steeper channels form roughness appears to be more important than grain roughness, based on the limited data available.

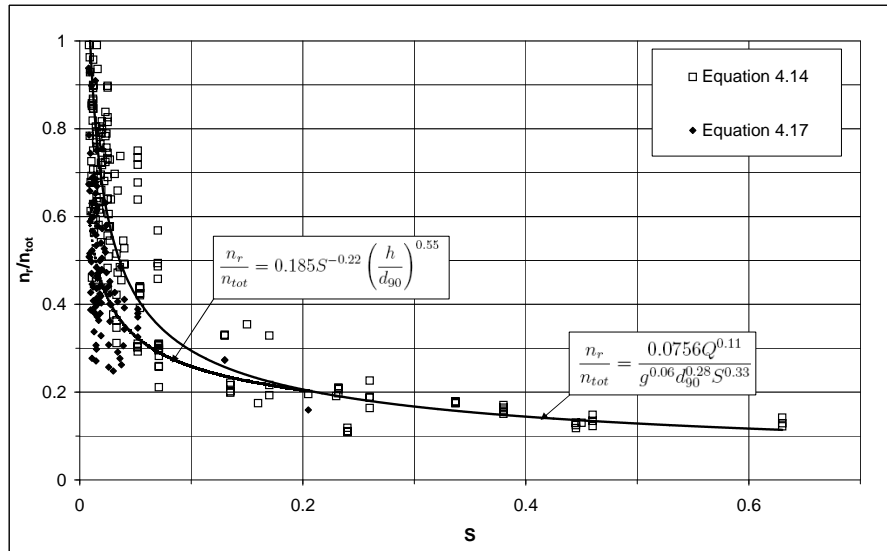


Figure 4.1: Comparison of two approaches to estimate the proportion of form and grain roughness in steep streams

To account for skin roughness only in the bedload transport capacity calculations, the slope of the energy line S can be partitioned into a fraction S_{red} associated with grain friction only. According to the Manning-Strickler equation the total slope can be expressed by Equation 4.22 and the slope associated with skin friction only can be determined by Equation 4.23:

$$S = \frac{v^2 n_{tot}^2}{R^{4/3}} \quad (4.22)$$

$$S_{red} = \frac{v^2 n_r^2}{R^{4/3}} \quad (4.23)$$

$$S_{red} = S \left(\frac{n_r}{n_{tot}} \right)^2 \quad (4.24)$$

where S_{red} is the component of the energy line related with skin friction.

Meyer-Peter and Mueller (1948) argued that the exponent in the Equation 4.24 may be different from 2, and from their experiments they empirically determined a value of 1.5. To adopt the reduction of the energy slope to observations on bedload transport the exponent in Equation 4.24 is replaced by the variable a (similar to Palt (2001)), which is allowed to vary between the values 1 and 2. Therefor the exponent a serves as calibration parameter.

$$S_{red} = S \left(\frac{n_r}{n_{tot}} \right)^a \quad (4.25)$$

The procedure assumes that grain friction losses depend on the power of a characteristic grain size, and these losses are compared to the total (measured) friction losses. Using a similar procedure, (Palt, 2001) accounted for form losses and found much better agreement with his bedload measurements in Himalayan rivers and the bedload transport formula of Meyer-Peter and Mueller (1948).

The relative proportion of form resistance is equal to $(1 - n_r/n_{tot})$.

4.2.2 Other approaches to estimate form resistance

Pagliara and Chiavaccini (2006) made flume experiments to estimate flow resistance of rock chutes with protruding boulders. The slope of the experiments was in the range from 0.04 to 0.4 and the relative submergence (h/d_{84}) varied from 0.5 to 10.5. Without protruding boulders they propose an equation to estimate flow resistance for uniform material:

$$\sqrt{\frac{8}{f}} = \log_{10} \left(S^{-2.5} \frac{h}{d_{84}} \right) + 2.8 \quad (4.26)$$

where d_{84} is the characteristic grain size for which 84 % by weight is finer. Taking into account form roughness losses due to protruding boulders in rock chutes Pagliara and Chiavaccini (2006) proposed the following equation:

$$\sqrt{\frac{8}{f_{tot}}} = 3.1 (1 + \Gamma)^c S_0^{-0.17} \left(\frac{h}{d_{84}} \right)^{0.1} \quad (4.27)$$

where Γ is the boulder concentration and the exponent c depends on the disposition (random or in rows) and on the surface of the boulders (rounded or crushed). Possible values for c are given in table 4.1.

The contribution of grain roughness to total roughness can be expressed by dividing equation 4.27 with 4.26.

$$\frac{\sqrt{\frac{8}{f_{tot}}}}{\sqrt{\frac{8}{f}}} = \frac{3.1 (1 + \Gamma)^c S_0^{-0.17} \left(\frac{h}{d_{84}} \right)^{0.1}}{\log_{10} \left(S_0^{-2.5} \frac{h}{d_{84}} \right) + 2.8} \quad (4.28)$$

It is possible to express the Manning coefficient and the total Manning coefficient in the same manner.

Equation 4.29 was proposed by Rice et al. (1998)

$$n_r = 0.029(d_{50}S)^{0.147} \quad (4.29)$$

Adding the form roughness effect of the boulders to Equation 4.29 the following relationship was obtained by Pagliara and Chiavaccini (2006).

$$n_{tot} = 0.064(1 + \Gamma)^e(d_{50}S_0)^{0.11} \quad (4.30)$$

Possible values for the parameter e are given in Table 4.1.

The contribution of form roughness to total roughness can be expressed by dividing Equation 4.29 by 4.30.

$$\frac{n}{n_{tot}} = \frac{29(\Gamma + 1)^{-e}(d_{50}S_0)^{0.037}}{64} \quad (4.31)$$

Table 4.1: Values of Coefficients c and e from Pagliara and Chiavaccini (2006)

Coefficient	Random	Rows	Random	Rows
	disposition rounded surface	disposition rounded surface	disposition crushed surface	disposition crushed surface
c (Eq. 4.27 and 4.28)	-1.60	-1.80	-2.40	-3.00
e (Eq. 4.30 and 4.31)	1.00	1.20	1.80	2.30

Figure 4.2 shows a comparison for the contribution of form roughness to total roughness for the Equations 4.14, 4.15, 4.16, 4.17 and 4.28. A boulder concentration of 0.25 for crushed boulders in rows was assumed (to simulate a typical step-pool sequence). All parameters for the comparison are listed in Table 4.2. For Equation 4.28 the different flow depth h for considering grain friction and total friction was taken into account (i.e. the same specific discharge q has been assumed). For the Equations 4.14 and 4.15 a channel width (W) of 5 meters was assumed for comparison. With Equation 4.28 a minimum value is achieved at $S = 0.05$ and the influence of form roughness decreases again with increasing slope. Therefore Equation 4.28 is not in accordance with the other approaches.

Table 4.2: Parameters for the comparison of different approaches to estimate form roughness losses

Parameter	range
S	0.0025 - 0.7
q	0.5 - 2.5
W	5
d_{90}	0.348
h/d_{84}	0.7-6.5

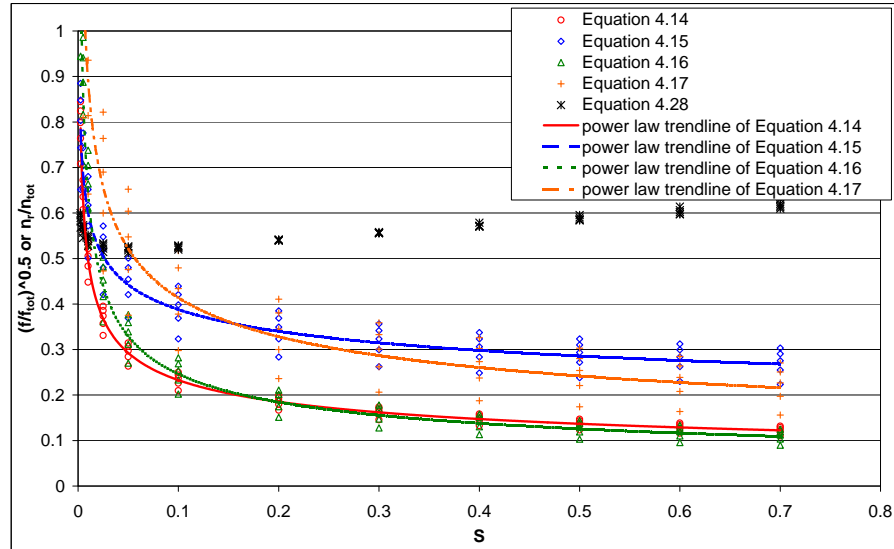


Figure 4.2: Comparison between different approaches to calculate losses due to form roughness

Other authors report on the contribution of step-pool sequences on the total roughness (e.g. Wohl and Thompson, 2000; Lee and Ferguson, 2002). Investigations from Zimmermann and Church (2001) suggest that in step-pool channels only the slope within the pools is available for bedload transport. Currently the ability to predict hydraulic geometry and quantify roughness characteristics based on the morphology of step-pool systems is lacking (Church and Zimmerman, 2007).

Lee and Ferguson (2002) derived a power law relation to estimate flow resistance in step-pool systems based on field and laboratory measurements. The slope of the investigated rivers varied from 0.03 to 0.18 and the slope of the flume experiments was 0.07:

$$\sqrt{\frac{8}{f_{tot}}} = 4.186 \left(\frac{R}{d_{84}} \right)^{1.8} \quad (4.32)$$

Canovaro and Solari (2007b) applied Equation 4.32 to natural data ($0.03 < S < 0.18$) and laboratory experiments ($0.01 < S < 0.08$) with step-pool configurations and found an agreement between the calculated and measured total roughness. For comparison with the other approaches presented above the related grain resistance is calculated by the relation:

$$\sqrt{\frac{8}{f}} = \frac{1}{n} R^{1/6} \quad (4.33)$$

with Equation 4.13 grain roughness can be calculated with Equation 4.33 resulting in:

$$\sqrt{\frac{8}{f}} = \frac{23.2}{d_{90}^{1/6}} R^{1/6} \quad (4.34)$$

The contribution of grain roughness to total roughness can be expressed by dividing Equation (4.32) by Equation (4.34):

$$\frac{\sqrt{\frac{8}{f_{tot}}}}{\sqrt{\frac{8}{f}}} = \frac{4.186 \left(\frac{R}{d_{s4}}\right)^{1.8}}{\frac{23.2}{d_{90}^{1/6}} R^{1/6}} \quad (4.35)$$

For comparison with the other approaches presented in this study Equation 4.35 has been tested for the same dataset used for Figure 4.2. All parameters for the comparison are listed in Table 4.2. The contribution of grain roughness to total roughness for different slopes and flow depth is presented in Figure 4.3 and compared with Equation 4.14 and 4.15. For the calculation of the hydraulic radius a rectangular channel width of 5 m has been considered (as for Figure 4.2). The general trend and the range of values is comparable with the approach of Equation 4.14 based on data compiled by Rickenmann (1996), particularly for slopes steeper than 0.1. Equation 4.14 and 4.15 are based on the same dataset and show the level of uncertainty.

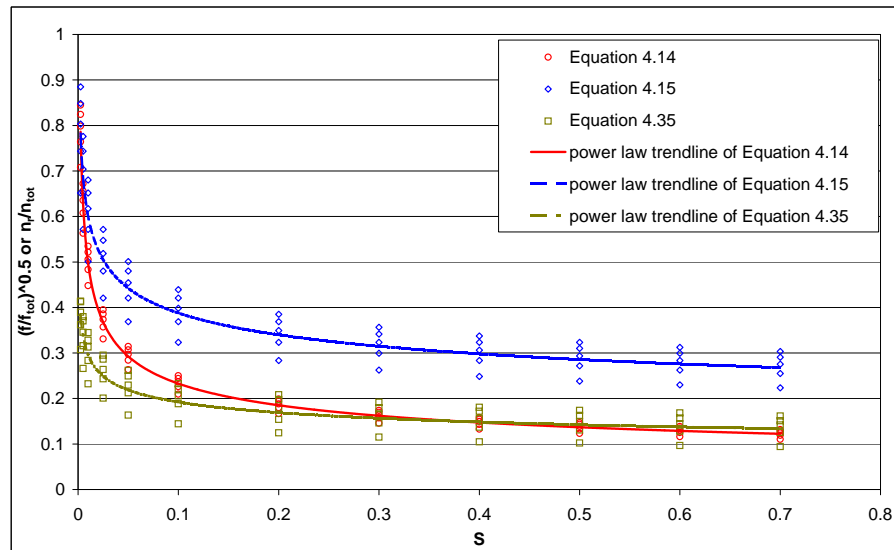


Figure 4.3: Contribution of grain roughness to total roughness calculated with Equation 4.14, 4.15 and 4.35.

Canovaro and Solari (2006) investigated flow resistance associated with schematic step-pool pattern and found that flow resistance is maximum for in the case of macro-roughness with regularly spaced stripes of pebbles with spacing between the stripes about 10 times the stripe height. In this condition flow resistance consists almost entirely in form resistance. Canovaro et al. (2007) expanded their experiments for different arrangements of roughness elements (transversal stripe pattern, longitudinal stripe pattern and random pattern) and concluded, that for a spatial density of these immobile elements in the range between 0.20 and 0.40 flow resistance is maximum. Then flow resistance is mainly associated with form drag, whereas skin friction plays a minor role. Therefore classical flow resistance formulas developed for low-land rivers cannot explain flow resistance in the presence of macro roughness such as found in steep mountain streams (Canovaro et al., 2007)

Research done by Hu and Abrahams (2006) indicate that the contribution of form roughness to total roughness is greater on rough fixed beds than on rough mobile beds. The deformation of the bed streamlines the flow and therefore form drag decreases. They made flume experiments with sediment-laden water flowing over a cylinder covered bed. The slope of the experiments was 0.114. According to the findings from Hu and Abrahams (2006) the contribution of form roughness to total roughness ranges from 0.030 to 0.332 and averages 0.179.

4.2.3 Resistance of the transported sediment

Recking et al. (2008a) observed a change in flow resistance caused by the transported sediment. They made flume experiments with slopes ranging from 0.01 to 0.09 and included other flume studies with slopes ranging from 0.001 to 0.3 in their analysis. Equations for the estimation of total roughness for clear water flows and flows with bedload transport were derived. For flows without bedload the total roughness can be calculated by:

$$\sqrt{\frac{8}{f}} = 3.6 + 3.2 \ln \left(\frac{R}{d} \right) \quad (4.36)$$

where d is the uniform grain diameter. For flows with bedload Equation 4.36 becomes:

$$\sqrt{\frac{8}{f}} = 0.67 + 3.2 \ln \left(\frac{R}{d} \right) \quad (4.37)$$

Recking et al. (2008a) showed that before incipient motion conditions the total resistance is the friction coefficient, which decreases with increasing flow depth. With bedload transport flow resistance is maximum and corresponds to a roughness parameter, which is approximately 2.5 (for $R/d = 10$) times higher than for clear water flows. Between these two states, the bedload layer thickness increases with the bedload transport rate, and the resistance coefficient can be approximated by a constant value for a given slope. Recking et al. (2008a) interpret this behavior as an increasing additional bedload resistance, that compensates for the decreasing friction factor for increasing values of R/d obtained for the clear water flow. In Figure 4.4 the resistance coefficient f is plotted versus the relative submergence R/d to show the increase in roughness due to the transported sediment.

Smart (2006) reanalyzed the flume data of Smart and Jäggi (1983) concerning the resistance of the transported sediment. The drag of the transported sediment was studied in terms of force balances. Smart (2006) concludes that the energy spent on transporting sediment for high sediment loads at steep slopes can be more than 90% of the available energy. Song et al. (1998) also observed an increase of the friction factor in flows with bedload transport. They attribute the consumption of additional energy in the flow to the collision of the sediment particles. Gao and Abrahams (2004) expanded the database from Song et al. (1998) and derived an equation for the estimation of the bedload transport resistance f_{bt} in terms of Darcy-Weisbach friction factor:

for flows with sediment transport where $C_{bc} \geq C_b > 0$:

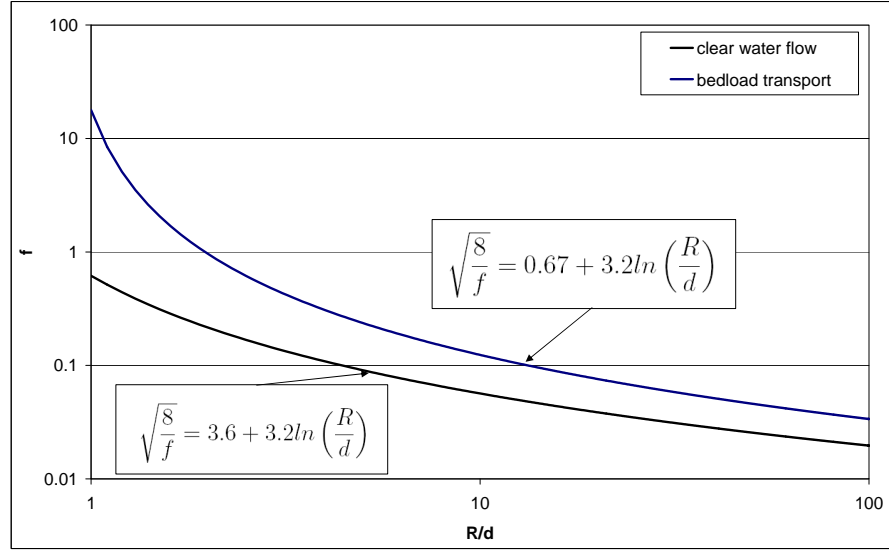


Figure 4.4: Calculated resistance coefficients versus the relative submergence R/d with consideration of slope.

$$f_{bt} = 0.048 C_{bc}^{0.25x} d_*^{0.5} \left(\frac{h}{d} \right)^{-0.75y} \quad (4.38)$$

and for flows without bedload transport ($C_b = 0$) the equation becomes:

$$f_{bt} = 0 \quad (4.39)$$

where C_b is the volumetric bedload concentration, C_{bc} is the volumetric bedload concentration at capacity, $x = (C_b/C_{bc})^\alpha$, $y = (C_b/C_{bc})^\beta$, α and β are empirical coefficients determined by non-linear regression and d_* is the dimensionless grain diameter defined by:

$$d_* = \left(\frac{g(s-1)}{\nu^2} \right)^{1/3} d_{50} \quad (4.40)$$

where ν is the kinematic viscosity of the water. Gao and Abrahams (2004) determined values for $\alpha = -0.41$ and $\beta = 0.77$. For Equation 4.38 data from two flumes with fixed and mobile beds and previously published data were used with relative submergences between 1 and 20. The magnitude of the bedload transport resistance f_{bt} was investigated for fully rough turbulent flows with no suspended load. Bedload particles were moved entirely by saltation.

Hu and Abrahams (2004) expanded the study from Gao and Abrahams (2004) and identified two additional factors for grain resistance: Froude number F and slope S . The advantage of the derived equation is the prediction of f_{bt} without the need to know the bedload transport rate:

$$f_{bt} = 267.3 d_*^{-1} \left(\frac{h}{d} \right)^{0.5} F^{-3} S^2 \quad (4.41)$$

Analyzing flume data from 38 experiments Hu and Abrahams (2004) found that the resistance of the transported sediment f_{bt} is about 22 % of the total flow resistance for sediment transport over a fix bed and about 32 % for mobile bed conditions (Hu and Abrahams, 2006). Mobile beds offer greater resistance to the flow than fixed beds (Hu and Abrahams, 2005) because grain collisions with mobile beds are less elastic than those with fixed beds. The contribution of resistance caused by the transported sediment $(f_{bt}/f)^{0.5}$ for fix bed and mobile bed conditions versus $S * h/d$ is shown in Figure 4.5. Logarithmic regressions have been fitted to show the trend. Data are taken from flume studies by Hu and Abrahams (2005) with channel slopes between 0.055 and 0.166.

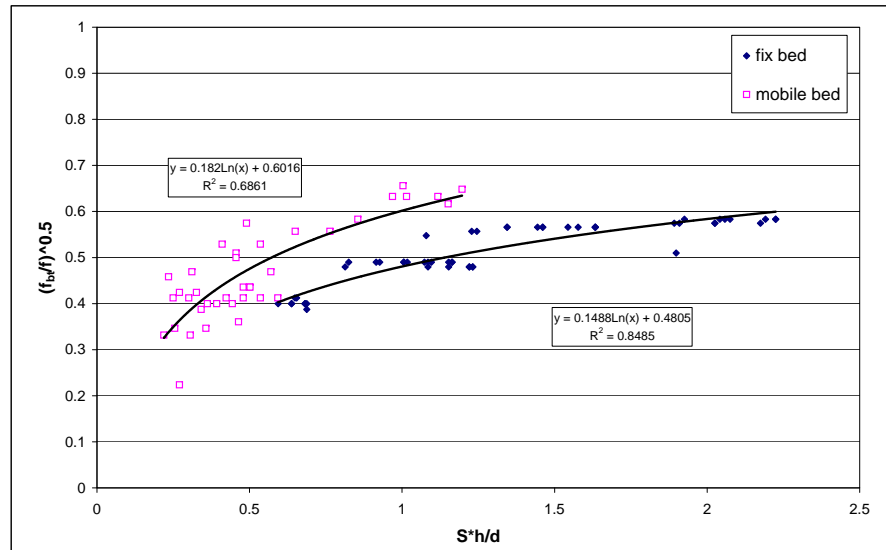


Figure 4.5: Contribution of flow resistance of the transported sediment for fix and mobile bed conditions to total flow resistance versus $S * h/d$. Data taken from Hu and Abrahams (2005).

5 Sediment transport capacity and initiation of motion at steep slopes

5.1 Initiation of motion

The forces acting on particles in a high gradient river bed are the drag force F_D , the lift force F_L and the submerged weight W (Yang et al., 2006).

$$F_D = C_D \frac{\pi d^2}{4} \frac{\rho_s U^2}{2} \quad (5.1)$$

$$F_L = C_L \frac{\pi d^2}{4} \frac{\rho_s U^2}{2} \quad (5.2)$$

$$W = (\rho_s - \rho_f) \frac{\pi d^3}{6} \quad (5.3)$$

where C_D and C_L are the coefficients of drag and lift forces, ρ_s and ρ_f are the density of sediment and fluid and π is the circular frequency. The drag coefficient C_D depends mainly on the flow regime near the particle (Yang et al., 2006).

$$C_D = F_1 \left(\frac{h}{d}, S \right) \quad (5.4)$$

and the lift coefficient can be obtained as:

$$C_L = F_2 \left(\frac{h}{d}, S \right) \quad (5.5)$$

Armanini and Gregoretti (2005) stress the importance of exposure effects on the initial motion of bed sediment at steep slopes. The influence of exposure increases with increasing slope, due to the increase in velocity corresponding to the exposed surface of the particle. Therefore a model is proposed considering the flow depth instead of the dimensionless critical shear stress.

Kirchner et al. (1990) claim that distinct initial motion or selective entrainment thresholds may not exist. The critical shear stress is dependent on grain projection, exposure and friction angle. These values can vary from point to point within a channel bed. Therefore the critical shear stress of a single grain size is not a single value. Instead a probability distribution which becomes broader with decreasing grain size and increasing bed roughness could be used.

Shvidchenko and Pender (2000) found that critical flow conditions for uniform sediment motion are dependent not only on the grain size but also on the ratio of flow depth to grain diameter (relative submergence). The lower the relative depth for steeper slopes is, the higher is the value of critical shear stress for a given grain size. This effect can be explained by the greater resistance of the grains caused by reduced relative submergence. Vollmer and Kleinhans (2007) considered turbulence-generated pressure fluctuations in the bed down to the bottom of the particles in an analytical model for incipient motion.

Mao et al. (2008) investigated the sediment entrainment in two high gradient streams. They observed an apparent increase in critical shear stress due to additional roughness effects of step-pool morphology. They also report that differences in the methodology to determine the incipient motion are a certain source of bias in comparing critical conditions for bedload entrainment in mountain rivers. Lamb et al. (2008) found that the critical dimensionless shear stress for incipient motion of sediment increases with the channel slope. They conclude that the local velocity about the grains decreases with increasing slope. The change in relative roughness with increasing slope, since flow depth is inversely related to channel slope for a given bed-shear stress and particle size may explain the observed behavior. Very high values for the incipient motion at the Rio Cordon in Italy (Lenzi et al., 2006) indicate a high proportion of non bedload effective shear stress in step-pool systems.

5.1.1 Critical shear stress

Shields (1936) introduced the critical dimensionless shear stress θ_c :

$$\theta_c = \frac{\tau_c}{(\rho_s - \rho_f)gd} \quad (5.6)$$

where θ_c is the critical dimensionless shear stress at beginning of motion for the grain size d and τ_c is the critical shear stress. Critical shear stress relationships developed for uniformly sized sediment, such as the Shields (1936) criteria cannot be applied for channels with steep slopes without correction. The threshold shear stress for initial motion of gravel at steep slopes is more difficult to determine accurately than for finer materials in alluvial streams (Wieberg and Smith, 1987). Meyer-Peter and Mueller (1948) determined the critical initiation of motion criteria θ_c visually and found values ranging from 0.03 to 0.05. Whereas an extrapolation of the shear stress where the transport rate becomes zero yields a value of $\theta_c = 0.047$. Buffington and Montgomery (1997) found published values in literature ranging from 0.02 to 0.065. For rough, turbulent flow characteristic of gravel-bed rivers there is no definitive θ_c (Buffington and Montgomery, 1997), but rather there is a range of values that differs between investigative methodologies. Palt (2001) found values of θ_c ranging from 0.03 to 0.15 for Himalayan mountain rivers.

Smart and Jäggi (1983) considered the influence of gravity on incipient of motion at steep slopes and derived following to Stevens et al. (1976) an equation for the initiation of bedload transport:

$$\theta_{crS} = \theta_c \cos \arctan S \left(1 - \frac{S}{\tan \varphi} \right) \quad (5.7)$$

where θ_{crS} is a corrected critical Shields parameter for high slopes and φ is the angle of repose.

Lamb et al. (2008) analysed a large set of experimental and field data from incipient motion studies and found a trend of increasing critical Shields stress with channel slope:

$$\theta_c = 0.15S^{0.25} \quad (5.8)$$

5.1.2 Critical flow discharge

For flows with steep slopes and low relative submergence the flow depth is difficult to measure (Bathurst et al., 1987). Therefore the Shields equation can be converted to a discharge-based equation by means of a flow resistance relationship. Schoklitsch (1950) developed a formula to calculate the critical discharge q_c at beginning of bedload transport based on field and laboratory data:

$$q_c = 0.26(s - 1)^{1.67} d_{40}^{1.5} S^{-1.17} \quad (5.9)$$

where s is the ratio between sediment to fluid density ($s = \rho_s / \rho_f$) and d_{40} is the characteristic grain size for which 40 % by weight is finer. For steep slopes ($0.0025 < S < 0.20$) Bathurst (1985) introduced an equation for the beginning of bedload transport.

$$q_c = 0.15g^{0.5} d_{50}^{1.5} S^{-1.12} \quad (5.10)$$

where d_{50} is the characteristic grain size for which 50 % by weight is finer. Rickenmann (1990) modified Equation 5.10 to include a density factor given in Equation 5.9.

$$q_c = 0.065(s - 1)^{1.67} g^{0.5} d_{50}^{1.5} S^{-1.12} \quad (5.11)$$

Whittacker and Jäggi (1986) investigated the stability of block ramps at slopes between 0.05 and 0.25. For the destruction of ramps with rather uniform blocks they derived:

$$q_c = 0.257(s - 1)^{0.5} g^{0.5} d_{65}^{1.5} S^{-1.167} \quad (5.12)$$

where d_{65} is the characteristic grain size for which 65 % by weight is finer.

Bezzola et al. (2005) investigated the stability of block ramps and found good agreement with Equation 5.12. Rickenmann (1990) modified Equation 5.12 to include the same density factor given in Equation 5.11.

$$q_c = 0.143(s - 1)^{1.67} g^{0.5} d_{65}^{1.5} S^{-1.167} \quad (5.13)$$

5.2 Sediment transport

Only a very limited number of bedload transport formulas have been developed for steep gravel bed streams. At ETH in Zurich, experiments on bedload transport in gravel-bed channels were performed both for gradients of 0.0004 to 0.023 (Meyer-Peter and Mueller, 1948) and for gradients of 0.03 to 0.20 (Smart and Jäggi, 1983; Rickenmann, 1990).

Smart and Jäggi (1983) expanded the database obtained by Meyer-Peter and Mueller (1948) for the steep slope range up to 0.20. They performed flume experiments to estimate the maximum transport capacity of mountain streams:

$$q_b = \frac{4}{s-1} \left(\frac{d_{90}}{d_{30}} \right)^{0.2} q S^{1.6} \left(1 - \frac{\theta_{crI}}{\theta} \right)$$

for $0.002 \leq S \leq 0.20$ *and* $d_{90}/d_{30} \leq 10$ (5.14)

where d_{30} is the characteristic grain size for which 30 % by weight is finer. Equation 5.14 can be transformed in dimensionless form:

$$\Phi_b = 4 \left(\frac{d_{90}}{d_{30}} \right)^{0.2} S^{0.6} e \theta^{0.5} (\theta - \theta_{cr})$$
(5.15)

where $\Phi_b = q_b / [(s-1)gd_m^3]^{0.5}$ is the dimensionless bedload transport rate and e is a resistance factor defined by the ratio $e = v_m/v^*$ with v_m the mean flow velocity.

Replacing the weak influence of the correction term for sediment mixtures $(d_{90}/d_{30})^{0.2}$ by 1.05, setting $s = 2.68$ for sand and gravel ($s=2.68$) and assuming turbulent flow, Equation 5.14 can be simplified to (Smart and Jäggi, 1983):

$$q_b = 2.5qS^{0.6} \left(S - \frac{d_m}{12.1h_m} \right)$$
(5.16)

Rickenmann (1991) performed flume experiments with unlimited sediment supply conditions for slopes ranging from 0.07 to 0.20 and investigated the influence of the fluid density on the bedload transport capacity. Fluid densities from 1000 to 1400 kg/m^3 were used for the experiments. A total of 252 experiments including flume data obtained by Meyer-Peter and Mueller (1948) and Smart and Jäggi (1983) were used for the development of the following dimensionless bedload transport equation (Rickenmann, 1991):

$$\Phi_b = \frac{3.1}{(s-1)^{-0.5}} \left(\frac{d_{90}}{d_{30}} \right)^{0.2} \theta^{0.5} (\theta - \theta_c) Fr^{1.1}$$
(5.17)

where d_m is the mean grain size and Fr is the Froude number equal to $v/(gh)^{0.5}$. For the steep slope range, i.e. $0.03 \leq S \leq 0.20$, a more accurate representation of the steep flume data on bedload transport obtained at ETH Zurich is given by the following equation Rickenmann (1990):

$$q_b = 12.6 \left(\frac{d_{90}}{d_{30}} \right)^{0.2} (q - q_c) S^{2.0} (s - 1)^{-1.6} \quad (5.18)$$

Rickenmann (2001) slightly modified equation (5.17) to facilitate comparison with other formulas and with sediment transport observations specifically from streams with steep gradients.

$$q_b = 3.1 \left(\frac{d_{90}}{d_{30}} \right)^{0.2} (q - q_c) S^{1.5} (s - 1)^{-1.5} \quad (5.19)$$

These formulas can be combined with approaches for the critical discharge q_c .

Palt (2001) derived a bedload transport equation with flume data obtained by Meyer-Peter and Mueller (1948) and Smart and Jäggi (1983) and his own measurements from Himalayan mountain rivers:

$$\phi_b = 1203.5 \left(\left[\frac{n_r}{n_{tot}} \right]^2 \theta \right)^{4.48} \quad (5.20)$$

The combination of field and flume data is interpreted by Palt (2001) as follows: At low flow rates bedload transport in natural rivers follows the measured bedload transport, after the braking up of morphological structures, the flume data can serve as reference conditions. This combination can be justified by the fact that measurements of bedload transport at high flow rates are difficult to obtain.

D'Agostino and Lenzi (1999) tested several bedload transport equations for steep slopes at the Rio Cordo and found the best agreement between computed and measured values of accumulated bedload volumes with the Bagnold (1956), Smart and Jäggi (1983) and Rickenmann (1991) bedload transport equation in combination with measured incipient motion conditions.

Barry et al. (2004) tested eight variations of four popular bedload transport equations with natural data for mountain gravel-bed rivers in Idaho and conclude, that formulas containing a threshold for bed load transport commonly predict a substantial number of incorrect zero-transport rates and typically perform worse than nonthreshold formulas. Although they found differences in formula performance, no consistent relationship between performance and complexity of the formula could be found for their application. Therefore they also fitted a simple power law function of discharge to describe their available bedload transport data of the form:

$$q_b = \alpha Q^\omega \quad (5.21)$$

The variables α and ω are site specific and have to be empirically fitted to the observed data.

For many streams no within-event sediment measurements are available Rickenmann (2001). Therefore the use of time integrated bedload transport equations is required for event analysis:

$$Q_b = ES^\beta (Q_m - Q_c) \quad (5.22)$$

where E is an empirical coefficient, Q_b is the average bedload transport rate, Q_m is the average flow rate, Q_c is the critical discharge at initiation of motion and the exponent β can vary between 1.5 and 2.0 (as in many bedload transport equations for steep slopes).

Equation 5.22 can be time integrated for flood events:

$$G_E = ES^\beta V_{re} \quad (5.23)$$

where G_E is the total load volume per flood event and V_{re} is the integral of the discharge above the critical discharge (bedload effective runoff).

5.2.1 Effect of armour layer on bedload transport

Mountain streams can develop an armour layer when the finer sediment fractions are more likely to be transported than the coarser fractions. The critical conditions for the destruction of the armour layer in terms of the dimensionless shear stress $\theta_{c,D}$ are defined by Jäggi (1992) and Hunziker and Jäggi (2002) as:

$$\theta_{c,D} = \theta_c \left[\frac{d_{m,D}}{d_{m,S}} \right]^{2/3} \approx \theta_c \left[\frac{d_{90}}{d_m} \right]^{2/3} \quad (5.24)$$

where $\theta_{c,D}$ is the dimensionless critical shear stress for an armour layer, $d_{m,D}$ is the mean diameter of the armour layer and $d_{m,S}$ the mean diameter of the subsurface layer. The $d_{m,D}$ can be approximated by the d_{90} (Jäggi, 1992). Using the Manning-Strickler equation, the specific discharge can be related to dimensionless shear stress as $q \sim h^{5/3} \sim \theta^{5/3}$. The critical specific discharge $q_{c,D}$ to break up an armor layer can then be expressed accordingly by (Badoux and Rickenmann, 2008):

$$q_{c,D} = q_c \left[\left(\frac{d_{90}}{d_m} \right)^{2/3} \right]^{5/3} = q_c \left[\frac{d_{90}}{d_m} \right]^{10/9} \quad (5.25)$$

Bathurst (2007) studied the effect of a coarse surface layer on bedload transport. He suggested that the limited supply of bedload available for transport may be explained by the degree of armoring. Data from natural rivers for phase II (see Chapter 5.2.3) transport were investigated. A Schoklitsch type bedload transport equation was modified to take the degree of armoring into account. Phase II bedload transport (see Chapter 5.2.3) is given as:

$$g_s = r\rho(q - q_{c2}) \quad (5.26)$$

$$r = 29.2S^{1.5} \frac{d_{50}^{-3.3}}{d_{50s}} \quad (5.27)$$

$$q_{c2} = 0.0513g^{0.5} d_{50}^{1.5} S^{-1.20} \quad (5.28)$$

or

$$q_{c2} = 0.0133g^{0.5} d_{84}^{1.5} S^{-1.23} \quad (5.29)$$

where g_s is the bedload mass discharge per unit width (kg/sm), r is (mathematically) the rate of change of bedload discharge with water mass discharge and q_{c2} is the critical discharge ($m^3m^{-1}s^{-1}$) for the phase II transport (see Chapter 5.2.3). The d_{50s} is the subsurface median particle size (m). These equations have been empirically derived from slopes from 0.00048-0.048, d_{50} from 12 to 146 mm and the ratio d_{50}/d_{50s} varied from 1.52 to 11. The derived equations refer to bulk bedload discharge and are not valid for fractional transport.

5.2.2 Fractional bedload transport

For refined sediment transport investigations bedload transport can be calculated by size fractions instead of computing bedload transport for the whole sediment mixture. Therefore changes in the grain size distribution due to selective transport can be considered. Coarser grains are intrinsically less mobile than finer grains.

For the calculation of vertical sediment fluxes, Hirano (1971) introduced the concept of a mixing or surface layer. The mixing processes are described by mass balances of individual grain size classes. The concept has been further developed by Armanini (1995) to precise the physical meanings of the theoretical formulations. Avoiding the limitations of the active layer concept Parker et al. (2000) proposed a probabilistic Exner sediment continuity equation for mixtures. The deeper a particle is buried in the bed sediment the lower is the probability of being entrained. An implementation of the probabilistic formulation would require the specifications of functional relations of the probability distribution for sediment entrainment and deposition. But these functional relations have not yet been developed. For future applications the concept could be very interesting for modelling the vertical structure of the stratigraphy produced by aggrading streams (Parker et al., 2000).

Gessler (1965) investigated mixtures with slopes of 0.195 and 0.4 % and $0.6 < d_{max} < 1.2 cm$, where d_{max} is the maximum particle size. He performed long experiments (duration approximately 2 weeks) with constant discharge and relative low bed shear stress $\bar{\tau}$. As expected, a static armour layer with coarser substrate than the initial substrate developed. The armour layer was mainly composed of the coarsest grains of the initial material, but also fine grains were found, because they were hidden from the flow by coarser grains.

Günter (1971) observed the development of an armoured channel bed due to selective transport in a laboratory flume with long experimental durations and low transport rates. Hunziker and Jäggi (2002) reevaluated the Meyer-Peter/Mueller data to account for fractional bedload transport including a hiding function.

Fractional bedload transport after Rickenmann

For sediment mixtures Rickenmann (1991) developed the following dimensionless bedload transport equation:

$$\Phi_b = 3.1 \left(\frac{d_{90}}{d_{30}} \right)^{0.2} \theta^{0.5} (\theta - \theta_c) Fr^{1.1} (s - 1)^{0.5} \quad (5.30)$$

To use this kind of equation for fractional bedload transport some modifications are necessary. If the relation $(d_{90}/d_{30})^{0.2}$ is set to 1.05 and a θ_{ci} is used for each size fraction the equation becomes:

$$\Phi_{bi} = \frac{3.255}{(s-1)^{0.5}} \theta^{0.5} (\theta_i - \theta_{ci}) Fr^{1.1} \quad (5.31)$$

where Φ_{bi} is the dimensionless transport rate per size fraction, θ_i is the dimensionless shear stress per size fraction and θ_{ci} is the dimensionless critical shear stress for a size fraction.

$$\theta_i = \frac{hS}{(s-1)d_{gi}} \quad (5.32)$$

where θ_{ci} is a corrected value that takes into account a power law hiding function after Parker (2008) and d_{gi} is the geometric mean diameter of the size fraction. Parker et al. (1982a,b) presented the concept of power relations for hiding functions. The following surface based relation for reference conditions is related to the d_{50} :

$$\frac{\theta_{ci}}{\theta_{c50}} = \left(\frac{d_i}{d_{50}} \right)^{-\gamma} \quad (5.33)$$

where θ_{ci} is the dimensionless critical shear stress for the size fraction of the surface sediment and θ_{c50} is the dimensionless critical shear stress of the surface median grain size. The exponent γ can be selected between 0 and 2 by the user to adopt the model to the observed behavior of the stream. A value of $\gamma = 0$ corresponds to size-independence and a value of $\gamma = 1$ corresponds to equal-threshold conditions. The equal mobility hypothesis does not imply that all grains are of intrinsically equal mobility regardless of size. Coarser grains are still less mobile than finer grains, even having balanced out hiding effects against weight effects. The equal mobility is achieved by coarsening of the surface layer (Parker and Toro-Escobar, 2002). A value of $\gamma > 1$ can be used for the case of mobility reversal (Solari and Parker, 2000; Brummer and Montgomery, 2003). Solari and Parker (2000) describe the phenomenon of mobility reversal in sediment mixtures, when the bed slope is higher than approximately 0.02. Coarser grains become more mobile than finer grains in a mixture. The authors suggest, that the mobility reversal is due to the direct effect of gravity acting on sediment grains. Further investigations are required to investigate sorting effects at steep slopes.

The effect of varying exponents γ in Equation 5.33 is visualized in Figure 5.1.

Then the critical θ_{ci} for each size fraction can be expressed as:

$$\theta_{ci} = \left(\frac{d_i}{d_{50}} \right)^{-\gamma} \theta_{c50} \quad (5.34)$$

where possible values for θ_{c50} are in the range from 0.03 to 0.06.

The bedload transport rate for each (q_{bi}) size fraction becomes:

$$q_{bi} = F_i \Phi_{bi} \left[g(s-1)d_{gi}^3 \right]^{0.5} \quad (5.35)$$

and

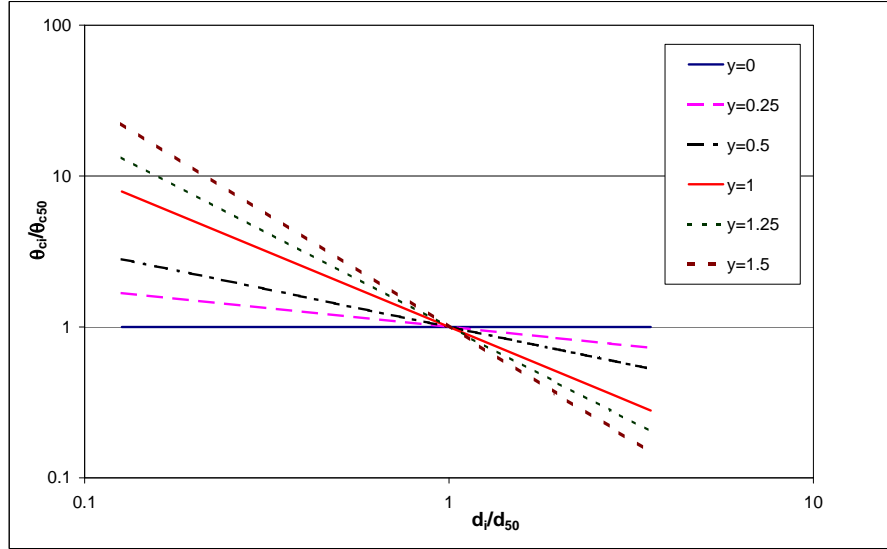


Figure 5.1: Effect of varying γ on the relative mobility of grain size fractions

$$q_b = \sum q_{bi} \quad (5.36)$$

where F_i is the proportion of each size fraction within the grain size distribution and d_{gi} is the geometric mean of the size fraction.

Other approaches for steep slopes

Lenzi et al. (2006) investigated the critical conditions for bedload motion in the Rio Cordon, a steep boulder bed stream in the Italian Alps and report that the mobility of each particle size in steep mountain channels is a function of both relative submergence (R/d_{84}) and relative size (d_i/d_{90}).

$$\theta_{ci} = 0.054 \left(\frac{d_i}{d_{90}} \right)^{-0.737} \quad (5.37)$$

where d_i is the characteristic grain diameter for a size fraction.

In terms of critical discharge, Equation 5.37 (Lenzi et al., 2006) can be transformed to:

$$q_{ci} = 0.745 \left(\frac{d_i}{d_{90}} \right)^{-0.857} g^{0.5} d_i^{1.5} \quad (5.38)$$

To explain the findings from Bathurst et al. (1987) that the critical discharge for entraining of poorly sorted sediment increases much more slowly with grain size than predicted by the the Schoklitsch (1950, 1962) equation, Ferguson (1994) developed a critical discharge criteria including hiding and exposure effects for sediment sediment size fractions for poorly sorted gravel beds:

$$q_{ci} = 0.134 d_{50}^{1.5} \left(\frac{d_i}{d_{50}} \right)^{0.19} S^{-1.37} \quad (5.39)$$

5.2.3 Two phase transport

Bedload transport can be separated in two phases: Transport rates are relatively low until a certain level is reached (Phase I). Once a certain flow is exceeded, transport rates increase substantially (Phase II). Phase one transport represents transport of finer fractions, whereas Phase II includes the mobility of coarser fractions and an increase of the total transport (Ryan et al., 2002). The distinction between these two phases is not always so clear.

Ryan et al. (2005) investigated 19 gravel-bedded channels ranging from stable step-pool systems to channels with more mobile beds and braided behavior. Most of the channels exhibited two phases of bedload transport. The slope range of the investigated channels is ranging from 0.019 to 0.055. According to their findings, a change in phase occurs over a narrow range of discharge, typically between 60 and 100 per cent of bank full discharge.

Recking et al. (2008b) distinguish between three flow domains:

1. domain 1 ($\theta < \theta_c$) - no bedload transport
2. domain 2 ($\theta_c < \theta < 2.5\theta_c$) - bedload transport with no constant bedload layer and no constant bedload layer thickness
3. domain 3 ($\theta > 2.5\theta_c$) - bedload transport with continuous bedload layer and constant bedload layer thickness of several times the grain diameter

Domain 2 is comparable to phase I bedload transport and domain 3 corresponds to phase II transport. A bedload transport equation based on the tractive force concept of the general form has been fitted for the different domains (Recking et al., 2008b) based on flume experiments with slopes ranging from 0.1 to 0.20. A total of 1567 data sets from literature and own experiments were considered for the bedload transport equation. The general form is:

$$\Phi = A\theta^\alpha(\theta - \theta_c)^\beta \quad (5.40)$$

where A is a efficiency ratio and α and β are exponents. The corresponding critical Shields value for the transition from domain 1 to domain 2 transport was found to be slope-dependent:

$$\theta_c = 0.13S^{0.24} \quad (5.41)$$

For domain 2 transport the best fit of Equation 5.40 was obtained by:

$$\Phi = 15.6(\theta - \theta_c)^2 \quad (5.42)$$

with a slightly modified value of θ_c :

$$\theta_c = 0.15S^{0.275} \quad (5.43)$$

For domain 3 bedload transport the slope effect was negligible and Equation 5.40 is transformed to:

$$\Phi = 14\theta^{2.45} \quad (5.44)$$

Part III

SETRAC - A Sediment Transport Simulation Model for Torrents and Mountain Streams

6 The SETRAC Model

6.1 Purpose

The SETRAC model has been developed for the simulation of bedload transport at steep slopes. Flow resistance and bedload transport equations appropriate for torrents and mountain streams are implemented. Several approaches to take form roughness losses into account are also available to calibrate the calculated bedload transport with field observations. Armouring can also be considered with regard to the threshold of bedload movement in the the one grain model. Within the SETRAC simulation environment it is also possible to calculate fractional bedload transport taking grain sorting effects into account.

6.2 General approach

SETRAC is a stand-alone simulation software tool with a graphical user interface (GUI). In SETRAC the Channel network is represented by nodes, cross-section and sections. Nodes contain the information about the location of the related cross-sections. Cross-sections are described by pairs of points containing information about the distance from the left bank and the altitude. Each slice of the cross-section can be of the type main channel, bank or riparian. Erosion and deposition, as well as bedload transport can only occur in slices of the type main channel. Each cross-section contains information about the grain size distribution. The order of cross-sections in the channel network is described by the section file. This file contains information about possible erosion depths in the sections. The flow lengths between the cross-sections can also be specified if they differ from the direct (three-dimensional) distance between the cross-sections. Sediment information is stored in an extra file, containing characteristic grain sizes for the sediment mixture as well as for the sediment fractions in classes. The number of sediment classes is specified by the user. The grain size class definition has to be constant for one project, and each cross-section is related to a grain size distribution for the active layer, and one for the bedload layer.

Input hydrographs can be related to cross-sections as time series. Sediment input as time series is also possible. The channel-network is visualized within the user interface. Longitudinal sections as well as all cross-sections can be shown within the graphical user interface. For calculations, the cross-section is divided into strips to get a representative discretization of the profile. The number of strips depends on the number of points that are used to specify a cross-section, implying that the number of strips increases with the complexity of the cross-section (Figure 6.1).

The cross-section editor also serves as dimensioning tool, because a visualization of velocity and bedload transport can be carried out for different discharges. These

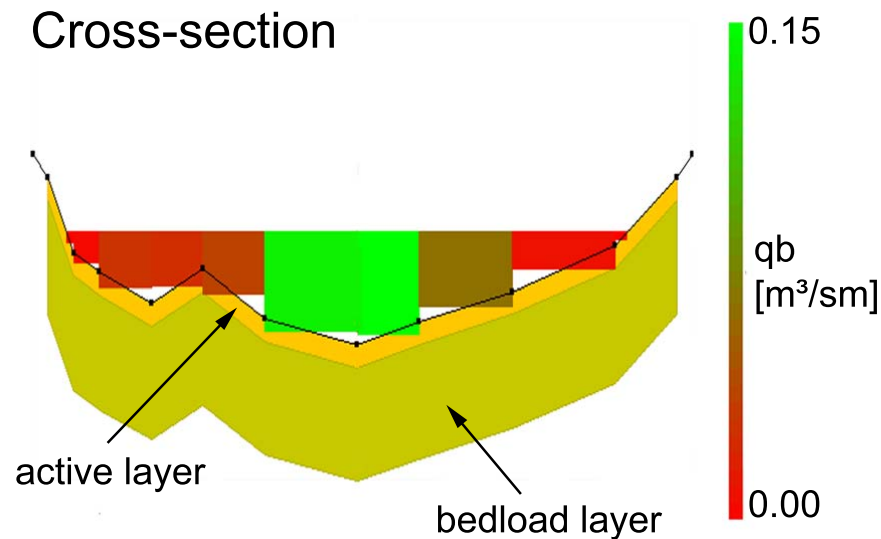


Figure 6.1: Structured cross-section with visualization of the specific bedload transport rate in the strips

visualizations are also important for fault finding of the input data. A sidebar informs the user about the correct usage of the model and shows warnings in case of improper model applications.

During the simulation all input hydro graphs and sedi graphs are shown in a simulation window. The same data are also shown for the outlet and selected cross-sections.

All simulation results can be stored as longitudinal profiles as well as time series for all cross-sections in user defined time intervals as text files for further analysis. The last time step with information about the highest values can also be exported as DXF file for plotting the results for engineering applications.

Within the simulation environment the user can represent the channel with different degrees of detail. For a first fast estimation of the bedload transport, the model can be run as one-grain model without morphologic changes due to erosion and deposition. The changes of the bedload stock in the sections are treated as numerical bedload volumes. Due to the fact that the morphology of the cross-section is constant over the simulation time, the model calculates the stage-discharge relation for each cross-section and the results are stored in a table. During the unsteady simulation the model interpolates the stage discharge relation in the stored table, resulting in a faster computation compared to the iterative solution of the water surface elevation.

If morphologic changes are considered as non-negligible, the erosion module can be activated. The table solution of the water surface is deactivated and an iterative solution is activated, to account for bedlevel changes in the cross-section and the change of the channel slope due to erosion and deposition is considered. For more detailed investigations the fractional bedload module can be activated. It is possible to combine this module with or without the erosion module.

6.3 Hydrodynamic model

The motion of water can be described by the Navier-Stokes equations. When the horizontal length scale is much greater than the vertical length scale the Navier-Stokes equations can be depth integrated resulting in the shallow water equations. Under these conditions conservation of mass implies that the vertical velocity of the fluid is very small and from the momentum equation it can be shown that the vertical pressure gradients are nearly hydrostatic. These equations are also known as Saint-Venant equations. They describe the flow below a pressure surface in a fluid and are a set of hyperbolic partial differential equations.

For the application of the Saint-Venant equations for one dimensional flow situations the following assumptions have to be fulfilled (Maniak, 2005; Habersack et al., 2007).

- The flow can be described as streamtube, i. e. the flow is constant for the regarded cross-section (assumption of mean water depth and mean velocity)
- The pressure can be treated as hydrostatic and waves are translatory waves. The vertical acceleration is negligible i.e.the bending of the streamtubes is small.
- The velocity and the impulse in vertical direction can be neglected.
- The velocity transverse to the main flow direction are small compared to the velocity in main flow direction and can be neglected.
- The height of the waves is much smaller than the length (shallow water assumption).
- The boarder of the channel is only affected by gravity and friction and the influence of side friction and turbulence can be described by friction laws
- The average channel slope is small: $\cos \alpha \approx 1$

With the above mentioned assumptions the shallow water equations can be derived from equations of conservation of mass and conservation of momentum (Navier-Stokes-equations).

The conservation of mass can be expressed as:

$$\frac{\partial h}{\partial t} + v \frac{\partial h}{\partial x} + h \frac{\partial v}{\partial x} = 0 \quad (6.1)$$

where t is the time and x is the coordinate in x direction.

the conservation of momentum can be expressed as:

$$\frac{1}{g} \frac{\partial v}{\partial t} + \frac{v}{g} \frac{\partial v}{\partial x} + \frac{\partial h}{\partial x} - S_0 + S_f = 0 \quad (6.2)$$

where $\frac{1}{g} \frac{\partial v}{\partial t}$ is the local acceleration, $\frac{v}{g} \frac{\partial v}{\partial x}$ is the convective acceleration and $\frac{\partial h}{\partial x}$ is the pressure term. S_0 and S_f are the channel and the friction slope.

In Equation (6.1) and (6.2) the velocity v is the dependent variable of the Saint-Venant equations. With the discharge Q as dependent variable, the equations can be transformed to:

- conservation of mass

$$\frac{\partial A}{\partial t} + \frac{\partial Q}{\partial x} = 0 \quad (6.3)$$

- conservation of momentum

$$\frac{\partial Q}{\partial t} + \frac{\partial}{\partial x} \left(\frac{Q^2}{A} \right) + g A \left(\frac{\partial h}{\partial x} - S_0 + S_f \right) = 0 \quad (6.4)$$

where A is the wetted area of the cross-section.

6.3.1 Kinematic wave approach

For the solution of the hydrodynamics the kinematic wave approach is used in SETRAC. According to Maniak (2005) the kinematic wave can be used for overland flow, mountain streams with steep slopes or for rivers with slow temporal change of the discharge without backwater effects. The kinematic wave approach neglects the acceleration terms and the pressure term of the full Saint Venant equations. In order to neglect the pressure term the channel slope has to be sufficiently steep ($>0.2\%$) (USACE, 1994) and the change of the water depth has to be small.

Hager and Hager (1985) investigated application limits for the kinematic wave approximation. The application limits for any plane or channel reach are summarized in Singh (1996)

$$\eta_1 = \frac{1}{n_{tot}} \sqrt{S} < 3 \quad (6.5)$$

and

$$\eta_2 = \frac{p(1/n_{tot})^3 \sqrt{S}}{g^2} < 0.07 \quad (6.6)$$

where p is the lateral inflow per unit width. Equation (6.5) eliminates dynamic effects such as roll waves and Equation (6.6) excludes diffusive effects (Singh, 1996).

According the kinematic wave approximation the water level is then only dependent on the discharge Q and independent of the time t . With this simplification no backwater effects can be calculated. With the following equations the kinematic wave can be described (Chow et al., 1988):

- conservation of mass

$$\frac{\partial A}{\partial t} + \frac{\partial Q}{\partial x} = 0 \quad (6.7)$$

- conservation of momentum

$$S_0 = S_f \quad (6.8)$$

According to the momentum equation (6.8) the wetted cross-section area is only a function of the discharge $A = f(Q)$. The first term of the continuity equation can be expressed as: $\frac{\partial A}{\partial t} = \frac{\partial A(Q)}{\partial Q} \frac{\partial Q}{\partial t}$. In combination with equation (6.7) the kinematic wave can be written as:

$$\frac{\partial Q}{\partial x} + \frac{\partial A(Q)}{\partial Q} \left(\frac{\partial Q}{\partial t} \right) = 0 \quad (6.9)$$

The velocity of propagation of the kinematic wave is $c_k = \frac{\partial Q}{\partial A}$.

6.3.2 Numerical model

Equation 6.9 represents the combination of the Saint Venant continuity and Saint Venant momentum equation. Concerning the momentum equation only the kinematic terms are accounted. Therefore the momentum equation can be written as $I_0 = I_f$ respectively $A = f(Q)$. In case of lateral inflow p Equation 6.9 can be rewritten as

$$\frac{\partial Q}{\partial x} + \frac{\partial A(Q)}{\partial Q} \left(\frac{\partial Q}{\partial t} \right) = p \quad (6.10)$$

where the indices i and j are for the length step and time step respectively. Equation 6.10 cannot be solved analytically except for simplified assumptions. Because it is a partial differential equation, it must be solved by numerical methods. In SETRAC equation 6.10 is converted into a finite difference equation replacing the differential quotients by difference quotients according to equation 6.11 and 6.12.

$$\frac{\partial Q_i^{j+1}}{\partial x} \approx \frac{Q_i^j - Q_{i-1}^j}{\Delta x} \quad (6.11)$$

$$\frac{\partial Q_i^{j+1}}{\partial t} \approx \frac{Q_i^{j+1} - Q_i^j}{\Delta t} \quad (6.12)$$

The resulting difference equation 6.14 is solved by an explicit algorithm. This kind of conversion also stands for an non-automatic stability of the algorithm. Therefore the user must define the ideal spatial discretization and the Courant-Friedrichs-Lewy condition (CFL condition) (Courant et al., 1967).

For the explicit solution schemes of the advection equation the CFL condition has to be fulfilled in order to be convergent. Otherwise the simulation can produce incorrect results. For the case of a wave the timestep must be less than the time required to travel to the next grid point. For pure advection schemes the CFL condition can be written as:

$$\frac{v\Delta t}{\Delta x} < CFL \quad (6.13)$$

where Δt is the time step and Δx is the discretisation length and CFL is a critical value. The CFL condition ($CFL < 1$) has to be fulfilled for the whole simulation system. In order to optimize computation time, the time step in SETRAC is not constant. Depending on the flow conditions the minimum time step required to fulfill the CFL

condition is calculated within each time step for the simulated channel. This routine allows for large time steps for lower discharges and lower damping of the wave. The maximum CFL number can be chosen by the user within the GUI. Values close to 1 (for example 0.99) are recommended. If a special application requires smaller time steps, smaller values for the CFL number can be chosen. The quotient $\frac{\partial Q}{\partial x}$ of equation 6.10 is calculated at the timeline j (Figure 6.2).

$$Q_i^{j+1} = Q_i^j - \frac{v\Delta t}{\Delta x} (Q_i^j - Q_{i-1}^j) \quad (6.14)$$

Equation 6.14 defines an explicit finite-difference solution for an advection equation as a backward or upwind difference scheme, which is used in SETRAC.

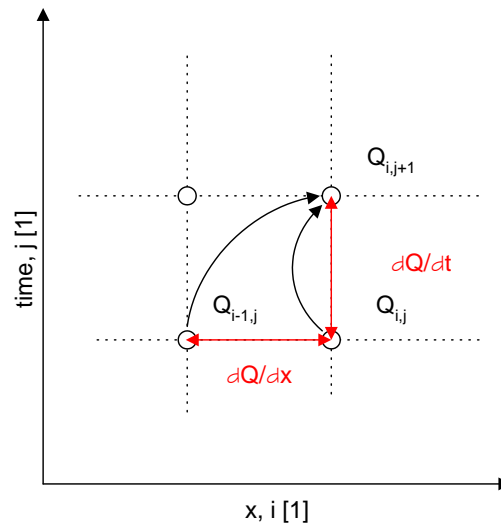


Figure 6.2: $\frac{\partial Q}{\partial x}$ as difference quotient at the timeline j . The arrows indicate the flow of information.

The upwind-scheme is used at all nodes of the model, except at (i) beginning nodes, (ii) the outlet, (iii) confluences of reaches and (iv) signal charged nodes.

The advantage of the upwind scheme is its simplicity and relatively stability.

6.3.3 Flow resistance approaches

Within the SETRAC simulation environment several flow resistance approaches can be selected. All equations are described in Chapter 4.

Strickler (1923):

$$v = k_{St} R^{0.67} S^{0.5} \quad (6.15)$$

The roughness coefficient is not independent of the flow depth, and therefore a calibration is only valid for a specific discharge. Due to the lack of calibration data for steep torrents in SETRAC the total roughness k_{St} coefficient is calculated for every cross-section at each time step after Rickenmann (1996):

$$k_{St} = \frac{0.97g^{0.41}Q^{0.19}}{S^{0.19}d_{90}^{0.64}} \quad \text{for } S \geq 0.008 \quad (6.16)$$

$$k_{St} = \frac{4.36g^{0.49}Q^{0.02}}{S^{0.03}d_{90}^{0.23}} \quad \text{for } S \leq 0.008 \quad (6.17)$$

Alternatively the mean flow velocity can also be calculated as a function of flow depth with Rickenmann et al. (2006):

$$v = \frac{1.93g^{0.5}h^{1.5}S^{0.5}}{d_{90}} \quad (6.18)$$

Now with Smart and Jäggi (1983):

$$v = 2.5v^* \left(1 - e^{\frac{-0.05h_m}{S^{0.5}d_{90}}} \right)^{0.5} \ln \left[\frac{12.3h_m}{1.5d_{90}} \right] \quad (6.19)$$

The empirical relation h_f/h_m of Rickenmann (1990) is used in SETRAC to obtain the mixture flow depth h_m :

$$\frac{h_f}{h_m} = 1 - 1.64S^{0.42} \left(\frac{q_b}{q} \right)^{0.63} \quad (6.20)$$

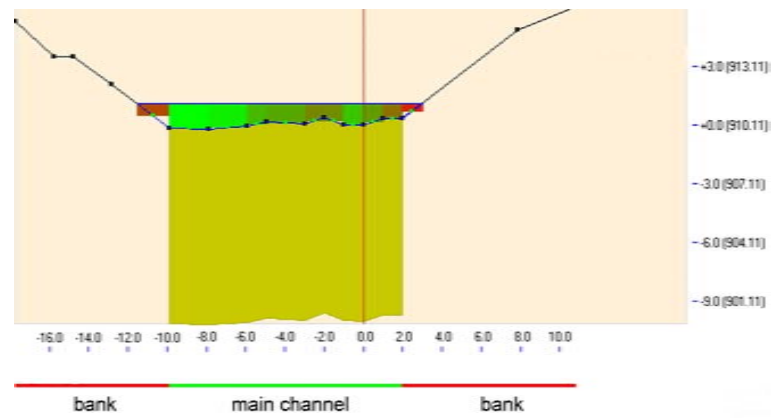
The equation was derived from experiments with channel gradients up to 0.2. The minimum value of h_f/h_m is limited by 0.2 to avoid unrealistic extrapolations. This value corresponds approximately to the maximum packing density of natural sediment.

For the calculation of the water level an iterative solution is required to obtain the discharge and flow velocity in every strip of the cross-section. Then the bedload transport is calculated for every strip and summed for the whole cross section.

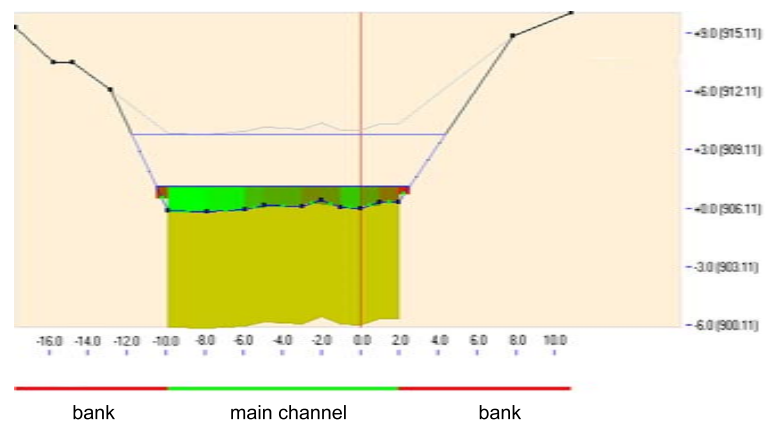
6.4 Sediment transport model

6.4.1 Morphologic changes

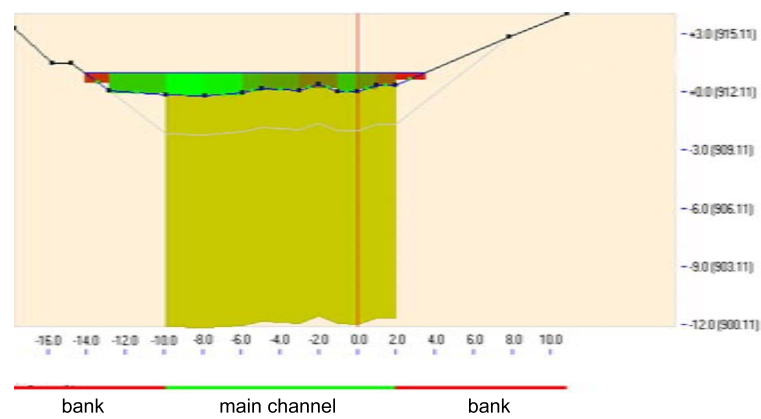
If the erosion module is activated, morphologic changes due to erosion and deposition are modelled. The total erosion or deposition is integrated over the cross-section. All slices of the type main channel of the structured cross-section cross-section are affected by the morphologic change. Morphologic changes are integrated over the cross-section slices defined as main channel. An example of erosion and deposition is illustrated in Figure 6.3. A mean erosion or deposition depth is subtracted or added to the type "main channel" of the original cross-section geometry, which is thus largely preserved.



(a) original cross-section



(b) cross-section with erosion



(c) cross-section with deposition

Figure 6.3: Example of a cross-section with morphologic changes due to erosion and deposition

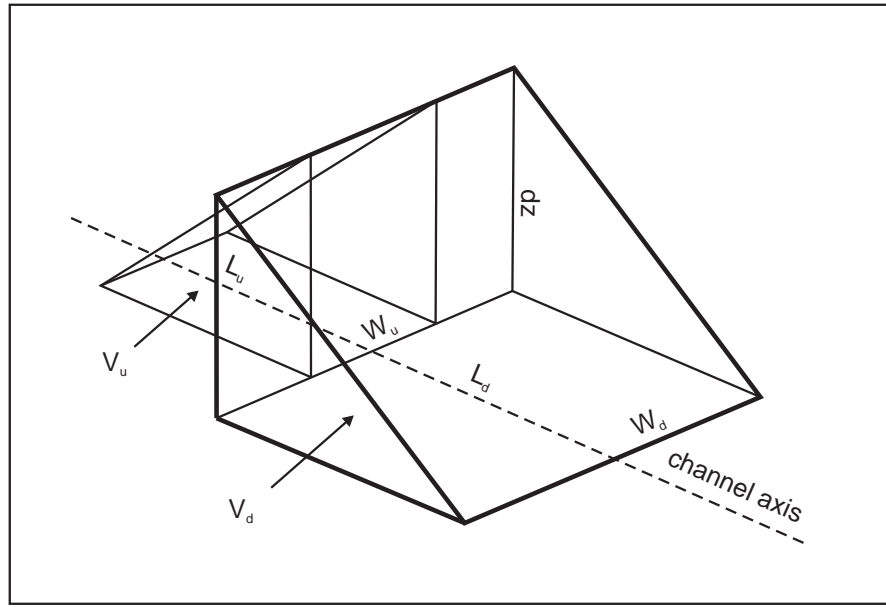


Figure 6.4: Concept of enhancement or lowering of the cross-section

The calculated erosion or deposition volume is split wedge-shaped upstream and downstream depending on the length of the subsection and the width of the main channel in these sections. The enhancement or lowering of the cross-section δz is calculated by:

$$\delta z = \frac{2V_{tot}}{W_d L_d + W_{u,1} L_{u,1} \dots W_{u,n} L_{u,n}} \quad (6.21)$$

where V_{tot} is the total bedload volume W_d is the width of the main channel downstream and L_d is the length of the (sub-) section downstream. W_u and L_u are the downstream values. Figure 6.4 shows the presented concept of bed level variations.

For the first node Equation (6.21) can be written as:

$$\delta z = \frac{V_{tot}}{W_d L_d} \quad (6.22)$$

And for the last node Equation (6.21) can be written as:

$$\delta z = \frac{V_{tot}}{W_u L_u} \quad (6.23)$$

At confluences the channel geometry of all contributing channels is considered. The influence of the bedload transport of the parent sections is weighted to calculate the erosion or deposition volumes in these sections (Figure 6.5).

$$k_{i,z} = \frac{Q_{B,i-1,z}}{\sum Q_{B,i-1,z}} \quad (6.24)$$

Where $k_{i,z}$ is the weighting factor and $Q_{B,i}$ is the volumetric sediment input from the tributaries.

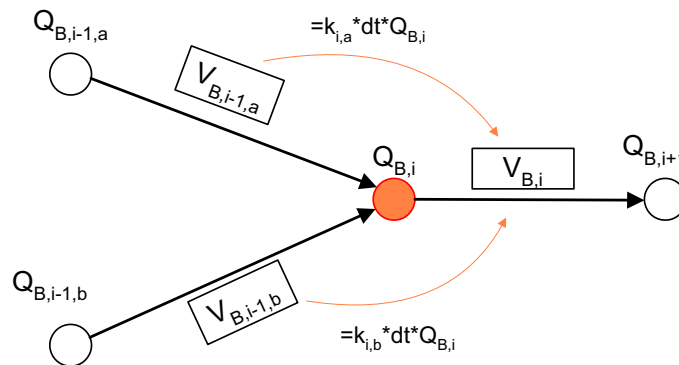


Figure 6.5: At confluences the erosion or deposition volumes are weighted by the bedload transport of the parent sections

6.4.2 Erosion, deposition and sediment layers

If the calculated transport capacity exceeds the sediment input from the upstream section, erosion occurs in the section as long as sediment stock is available in the bedload layer. The erosion is limited by the depth of the bedload layer. The maximum erosion depth can be set individually for each section or globally as uniform erosion depth for the whole channel system. Morphologic changes can only occur in cross-section parts (strips) of the type main channel.

If the sediment input from the parent section is higher than the transport capacity in the section deposition occurs. During deposition it is possible that the cross-section becomes blocked by the deposited sediment and the discharge can not flow through this profile any more. Then the model fails. This can especially occur at changes of the channel slope. When this problem occurs it is possible to limit the maximum deposition height for sediment globally or by a special routine. As soon as the maximum deposition height for the actual discharge is reached the model keeps (or even lowers) the cross-section geometry to allow the discharge to flow through the cross-section. If there is further deposition in this reach the cross-section height remains constant and the deposition is recorded numerically. In the case, that erosion processes follow, first the numerical sediment storage is emptied, and then the cross-section can be eroded again. The user is warned within the graphical user interface about the cross-sections that are affected by this routine. This is a solution to complete a computation with high amounts of sediment deposition in combination with bed level changes and shows a limit of the 1d approach concerning morphologic changes in the cross-section geometry. A larger description of the cross-section can avoid this problem, by allowing higher depositions in the reach.

6.4.3 Flow resistance due to form roughness

Losses due to form roughness can be considered optionally in SETRAC. All presented formulas are described in detail in Chapter 4.2.

$$\frac{n_r}{n_{tot}} = \frac{0.0756Q^{0.11}}{g^{0.06}d_{90}^{0.28}S^{0.33}} \quad (6.25)$$

$$\frac{n_r}{n_{tot}} = \frac{0.133Q^{0.19}}{g^{0.096}d_{90}^{0.47}S^{0.19}} \quad (6.26)$$

$$\frac{n_r}{n_{tot}} = 0.092S^{-0.35} \left(\frac{h}{d_{90}} \right)^{0.33} \quad (6.27)$$

$$\frac{n_r}{n_{tot}} = 0.185S^{-0.22} \left(\frac{h}{d_{90}} \right)^{0.55} \quad (6.28)$$

$$S_{red} = S \left(\frac{n_r}{n_{tot}} \right)^2 \quad (6.29)$$

To adopt the reduction of the slope to observations on bedload transport, the exponent in equation (6.29) is replaced by the variable a and can be varied between the values 1 and 2 (Rickenmann et al., 2006). Therefore a can be used as a calibration parameter.

$$S_{red} = S \left(\frac{n_r}{n_{tot}} \right)^a \quad (6.30)$$

6.4.4 Sediment transport capacity and initiation of motion

Different incipient motion criteria are available for bedload transport simulations within SETRAC. All formulas are described in detail in Chapter 5.

Smart and Jäggi (1983)

$$q_b = \frac{4}{s-1} \left(\frac{d_{90}}{d_{30}} \right)^{0.2} q S^{1.6} \left(1 - \frac{\theta_{crI}}{\theta} \right) \quad (6.31)$$

For the steep slope range a modified critical Shields parameter θ_{crS} for the begin of motion was introduced:

$$\theta_{crS} = \theta_{cr} \cos \arctan S \left(1 - \frac{S}{\varphi} \right) \quad (6.32)$$

Due to the early programming newer findings concerning the slope effect on incipient motion conditions (Lamb et al., 2008) as shown in Equation 5.8 have not been considered.

Rickenmann (1991):

$$\Phi_b = \frac{3.1}{(s-1)^{0.5}} \left(\frac{d_{90}}{d_{30}} \right)^{0.2} \theta^{0.5} (\theta - \theta_{cr}) F_r^{1.1} \quad (6.33)$$

Rickenmann (1990):

$$q_b = 12.6 \left(\frac{d_{90}}{d_{30}} \right)^{0.2} (q - q_c) S^{2.0} (s - 1)^{-1.6} \quad (6.34)$$

Rickenmann (2001):

$$q_b = 3.1 \left(\frac{d_{90}}{d_{30}} \right)^{0.2} (q - q_c) S^{1.5} (s - 1)^{-1.5} \quad (6.35)$$

These formulas can be combined with the critical discharge q_c .

$$q_c = q_{c,min} = 0.065 (s - 1)^{1.67} g^{0.5} d_{50}^{1.5} S^{-1.12} \quad (6.36)$$

$$q_c = q_{c,blockramp} = 0.143 (s - 1)^{1.67} g^{0.5} d_{90}^{1.5} S^{-1.167} \quad (6.37)$$

In the original form of Equation 6.37, d_{65} is used as characteristic grain size and was replaced by d_{90} to describe the incipient motion condition for coarse channel beds.

6.4.5 Armour layer effect on transport threshold

If armouring seams to be non negligible this effect can be considered in combination with the one grain model. The approaches used in SETRAC are explained in detail in Chapter 5.2.1.

For the $\phi - \theta$ formulation (Jäggi, 1992):

$$\theta_{c,D} = \theta_c \left[\frac{d_{90}}{d_m} \right]^{2/3} \quad (6.38)$$

In combination with the critical discharge q_c :

$$q_{c,D} = q_c \left[\frac{d_{90}}{d_m} \right]^{10/9} \quad (6.39)$$

6.4.6 Fractional bedload transport

The relation $(d_{90}/d_{30})^{0.2}$ is set to 1.05 (Smart and Jäggi, 1983) and θ_i and θ_{ci} are used for each size fraction i . The equation 6.33 becomes:

$$\Phi_{bi} = \frac{3.255}{(s - 1)^{0.5}} \theta^{0.5} (\theta_i - \theta_{ci}) Fr^{1.1} \quad (6.40)$$

For direct comparison with (6.33) the relation $(d_{90}/d_{30})^{0.2}$ of the whole grain size distribution can also be used in SETRAC resulting in higher transport capacity for wider sorted sediment mixtures.

$$\Phi_{bi} = \frac{3.1}{(s - 1)^{0.5}} \left(\frac{d_{90}}{d_{30}} \right)^{0.2} \theta^{0.5} (\theta_i - \theta_{ci}) Fr^{1.1} \quad (6.41)$$

with

$$\theta_i = \frac{hS}{(s-1)d_{gi}} \quad (6.42)$$

where θ_{ci} is a corrected value that takes into account a power law hiding function after Parker (2008)

$$\frac{\theta_{ci}}{\theta_{c50}} = \left(\frac{d_i}{d_{50}} \right)^{-\gamma} \quad (6.43)$$

The exponent γ can be selected between 0 and 2 by the user to adjust the model to the observed behavior of the stream. A value of $\gamma = 0$ corresponds to size-independence and a value of $\gamma = 1$ corresponds to equal-threshold conditions. A value of $\gamma > 1$ can be used for the case of mobility reversal (Solari and Parker, 2000; Brummer and Montgomery, 2003).

The critical value θ_{ci} for each size fraction can be expressed as:

$$\theta_{ci} = \left(\frac{d_i}{d_{50}} \right)^{-\gamma} \theta_{c50} \quad (6.44)$$

where possible values for θ_{c50} are in the range from 0.03 to 0.06 and can be selected within the GUI.

The bedload transport rate for each size fraction becomes:

$$q_{bi} = F_i \Phi_{bi} \left[g(s-1)d_{gi}^3 \right]^{0.5} \quad (6.45)$$

and the total bedload transport rate is then:

$$q_b = \sum q_{bi} \quad (6.46)$$

6.5 Possible combinations of the formula sets

The flow resistance approaches 6.15 and 6.18 can be combined with the sediment transport formulas 6.34 and 6.35 and with the critical discharge 6.36 and 6.37. Whereas the flow resistance approach 6.19 can be combined with 6.31 and 6.33.

For the computation of fractional bedload transport the flow resistance approach 6.19 is combined with the sediment transport formulas 6.40 or 6.41.

The flow resistance losses due to form drag 6.25, 6.26, 6.27 or 6.28 may or may not be taken into account with a sediment transport equation. Optionally the armour layer criteria 6.38 can be combined with the sediment transport formulas 6.31 and 6.33, whereas 6.39 can be combined with the critical discharge 6.36.

All possible formula combinations are visualized in Appendix A.1.

6.6 Limitations of the SETRAC model

SETRAC has been designed for steep headwater channels and mountain streams. Due to the kinematic wave approach no counter slope or backwater effects can be modelled.

Sediment routing and bed variation is limited to the main channel. Neither erosion nor deposition can be modelled on the floodplain. The transport formulas implemented in SETRAC take only bedload into account, suspended transport and washload are not considered. For each cross-section only one grain size distribution for the active layer and one for the bedload layer can be specified. The number of grain classes is unlimited, but has to be the same for the whole project. The number of cross-sections, strips within the cross-sections and the number of branches is unlimited, or may only be limited by the computation power of the computer used. In the actual version of SETRAC, the number of input hydro- and sedigraphs is limited by 14, but this will change in a later version of the simulation model.

6.7 Note on availability of the SETRAC model

SETRAC as well as a user guide, a technical manual and tutorials will be available soon as free download at www.alpine-naturgefahren.at.

6.8 Note on history of SETRAC

The first version of SETRAC has been developed in the framework of the project "Abschätzung von Naturgefahren" from 1998 to 2002 (Fuchs and Friedl, 1999, 2000, 2002; Friedl, 2004), which was funded by the Federal Ministry of Agriculture, Forestry, Environment and Water Management. Since July 2005 SETRAC has been substantially modified and further developed and tested (Rickenmann et al., 2006; Chiari and Rickenmann, 2007; Chiari et al., 2007, 2008) within the project "Evaluierung von Sediment-Transport Modellen in Wildbachgerinnen". This project is financed by the Austrian Science Fund. The actual version of the presented model is SETRACv20080929.

Part IV

Model Verification

7 Laboratory experiments to optimize a bedload deposition basin

Laboratory experiments were made to optimize a bedload retention basin in the context of a hazard assessment (Kaitna et al., 2007). Different flow and sediment scenarios were modelled to investigate the deposition behavior of quite uniform sand. The physical model is a Froude scaled model with a scale of 1:30. The modelled deposition area is 6 m long and between 0.8 and 1.0 m wide. The experimental setup is illustrated in Figure 7.1. Sediment in- and output is controlled by 7 load cells. The water depth is measured with 8 ultrasonic sensors.

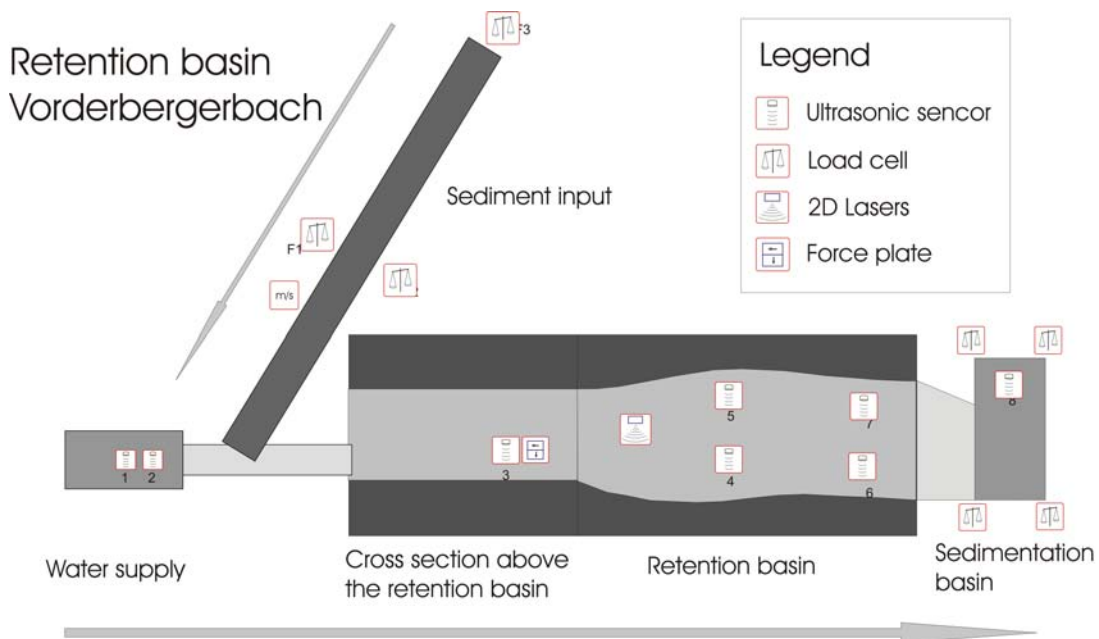


Figure 7.1: The experimental setup for the bedload deposition basin

A design event for a flood with a recurrence period of 150 years was used to study the deposition of quite uniform sand in a deposition basin. Figure 7 shows the design input hydrograph as well as the sediment input. The sediment input was calculated according the transport capacity of the upstream reach with Formula 6.34 and was fed by a conveyor belt followed by a mixing reach before the sediment water mixture was released into the channel which flows into the deposition basin. After the experimental run the deposition of bedload in the basin was measured by a 2d laser scan device mounted on a rail above the retention basin. Therefore the deposition was measured

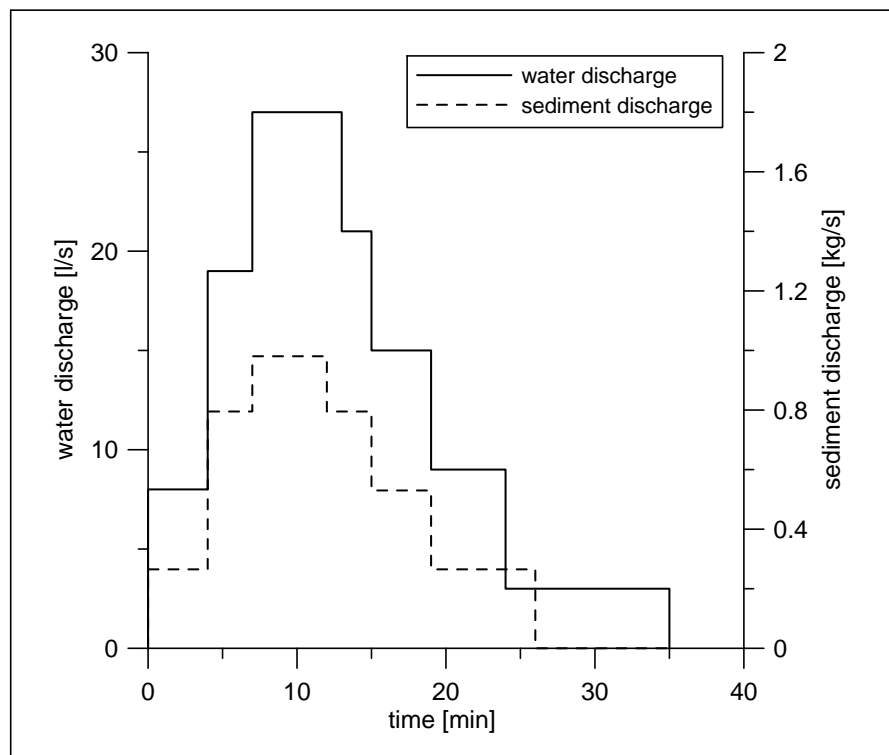


Figure 7.2: Water and sediment discharge for the HQ150 experimental run

with high accuracy. The measured deposition heights are shown in Figure 7.3.

To get a better representation of the 2-d deposition pattern, the average lateral deposition heights were determined at cross-sections with a separation distance of 25 cm in longitudinal direction. The deposition heights simulated with SETRAC are compared to the average deposition of the physical model (Figure 7). The spatial discretization for the SETRAC simulation was 0.1 m with $\Theta_{cr} = 0.035$. In SETRAC the flow velocity was calculated with Formula (6.19) and the bedload transport with Formula 6.33, where the incipient motion condition Θ_{cr} served as calibration parameter.

The deposition behavior as well as the slope of the deposited material could be modelled accurately with the exception of the scour close to the inlet of the basin which could not be reproduced with the simplified hydraulics of SETRAC. The longitudinal slope of the sediment deposits was 0.02. Due to the defined outlet boundary conditions of the experiment (critical depth) the simplified hydraulics in SETRAC were no limitation for the modelling of the experiment.

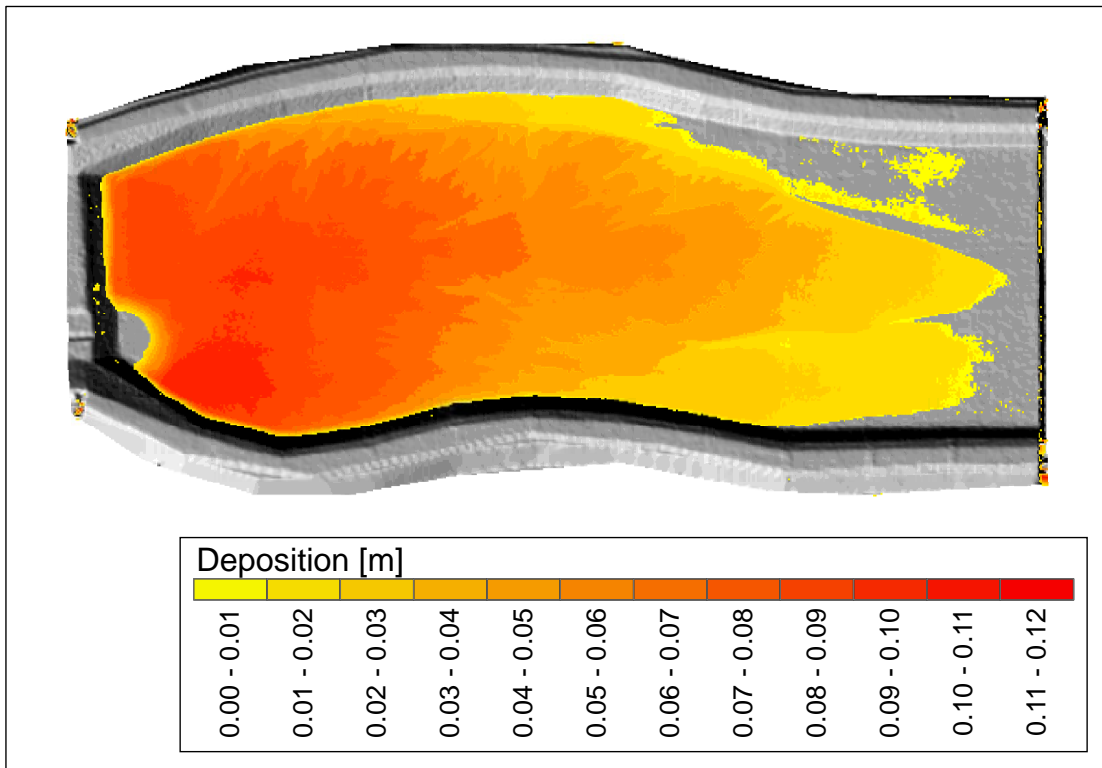


Figure 7.3: Measured deposition heights after the experimental run

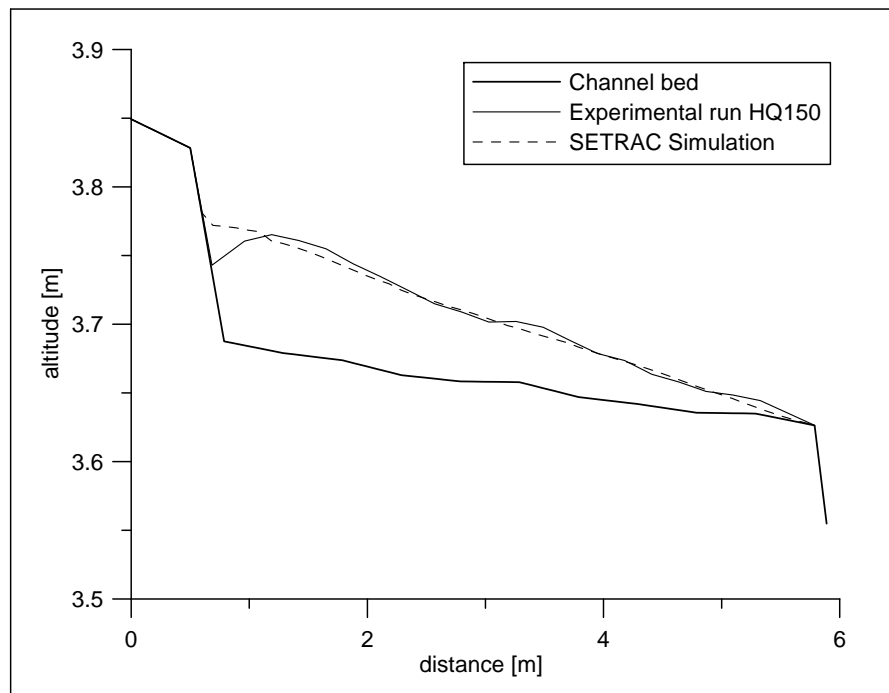


Figure 7.4: Comparison of modelled and measured deposition heights for the laboratory experiment HQ150

8 Development of armour layer

The fractional bedload transport module of SETRAC has been evaluated by using the experimental data from Günter (1971). The development of an armour layer and a rotation of the bed was observed in a 40 *m* long and 1 *m* wide concrete channel.

For comparison with SETRAC simulations the steepest experiment has been modelled. The selected experiment with the channel slope at the beginning and the discharge is shown in Table (8.1). The sediment mixture used for the experiment is presented in Table 8.2.

Because of the simplified hydraulics in SETRAC the experimental setup could not be rebuilt exactly. The boundary conditions of the inlet and outlet of the channel cannot be modelled with the kinematic wave approach used in SETRAC.

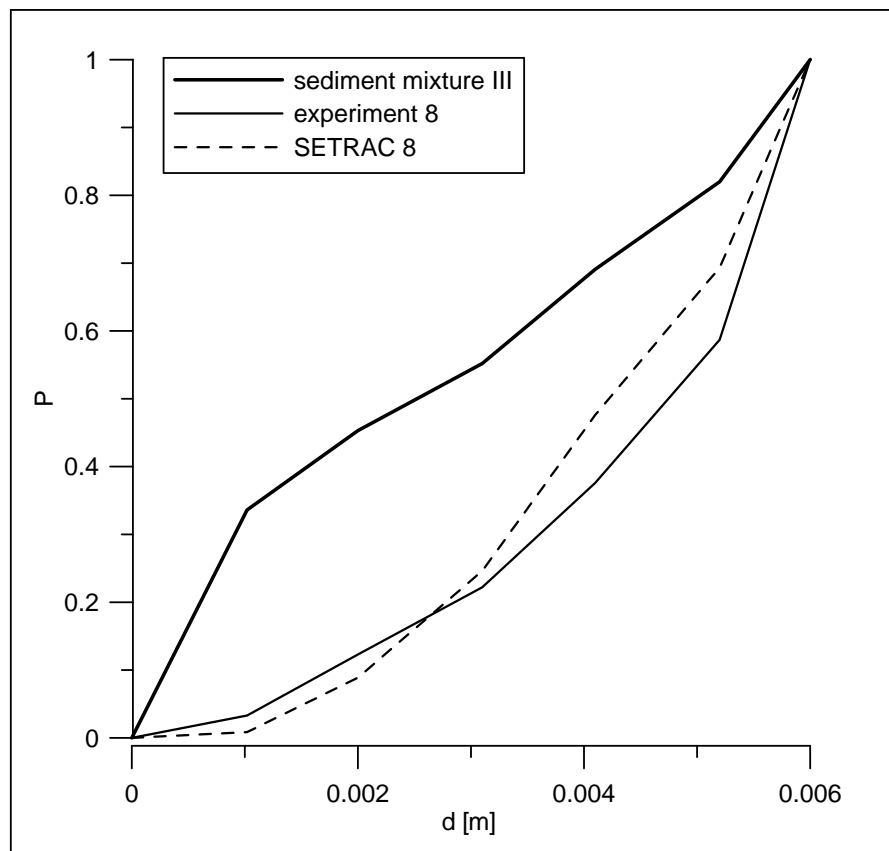
The critical Shields parameter for the whole sediment mixture was set at $\Theta_{cr50} = 0.040$. The exponent in the hiding function (5.34) and the active layer depth was used as calibration parameter. The duration of the laboratory experiments was 4 to 6 weeks. The experiments of Günter (1971) were stopped, when there was no more change in channel slope. For the SETRAC simulations a duration of 6 weeks was modelled for the selected run. The grain size distribution reported by Günter (1971) and the one obtained with the SETRAC simulation are compared in Table 8.2 and are visualized in Figure 8.1. A comparable average grain size distribution for the inner 20 *m* of the concrete channel was achieved with $\gamma = 0.97$ and an active layer depth of 2.2 *cm*.

Table 8.1: Selected experimental run

sediment mixture	experiment	discharge [l/s]	Slope at begin [%]
III	8	29.7	0.550

Table 8.2: Grain size distribution of the sediment mixture used in the experiment and obtained by Günter and SETRAC simulations

grain size	d [cm]	0	0.102	0.200	0.310	0.410	0.520	0.600
fraction	III	0	0.336	0.453	0.552	0.691	0.820	1
finer than	Günter	0	0.033	0.132	0.222	0.376	0.587	1
d	SETRAC	0	0.006	0.081	0.256	0.481	0.696	1

**Figure 8.1:** Grain size distribution for the experimental run 8 and comparison with SETRAC simulation

Part V

Sensitivity Analysis

9 Effect of mobile bed approach

The movable bed boundary condition allows for changes of the longitudinal profile. Erosion and deposition have an effect on the channel slope. Changes in channel slope can be made smoothed depending on the spatial discretisation.

Figure 9.1 shows the temporal evolution of a longitudinal profile with changing slope. The most upstream reach is 1000 *m* long and the slope is 0.1. This reach is followed by a 1000 *m* long reach with a slope of 0.05. The downstream reach is 400 *m* long and again 0.1 steep (black line in Figure 9.1).

Unlimited sediment stock was assumed (possible erosion depth 100 *m*). The channel outlet was considered as estuary. Therefore no erosion was allowed in the last cross-section. A constant discharge of 60 m^3/s without sediment input from upstream was applied. The spatial discretisation was defined as 50 *m*. The temporal evolution of the longitudinal profile shows a decreasing slope for the most upstream reach. Deposition in the second reach, followed by erosion in the most downstream reach develop a first smoothing in the channel slope. A balanced slope of 0.075 is obtained for the two downstream reaches and the lower 300 *m* of the upstream reach at the end of the simulation.

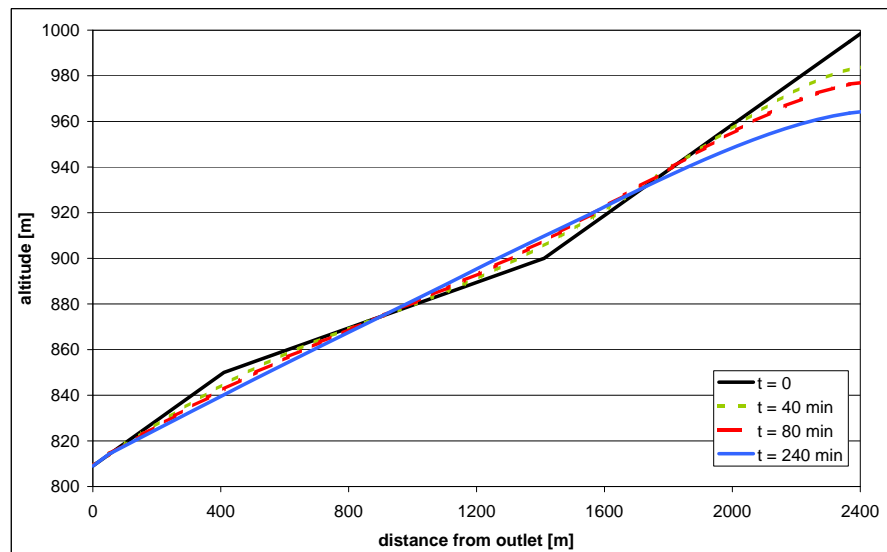


Figure 9.1: Time evolution of a longitudinal profile

The changing slope also influences the transport capacity of the reaches, resulting in lower accumulated transport in the steeper reaches but also an increased transport for the lesser steep reaches compared to calculations without morphologic changes. A comparison of the accumulated bedload transport for fixed and mobile bed boundary

conditions at certain time steps is made in Figures 9.2, 9.3 and 9.4. After 40 minutes of simulation time the two approaches do not differ very much. The main differences are at the locations where the slope changes and of course at the upper end where erosion causes a decrease of the channel slope. After 40 more minutes (Figure 9.3) the change of the bed geometry (compare Figure 9.1) influences the total amount of transported sediment for the whole channel. An increased transport in the middle reach and decreased transport in the steeper reaches can be observed. This trend increases with simulation time (Figure 9.4).

For this comparison no form roughness correction has been used. The time evolution and degree of differences in accumulated bedload transport for fixed and mobile bed conditions depend on the level of transport rates.

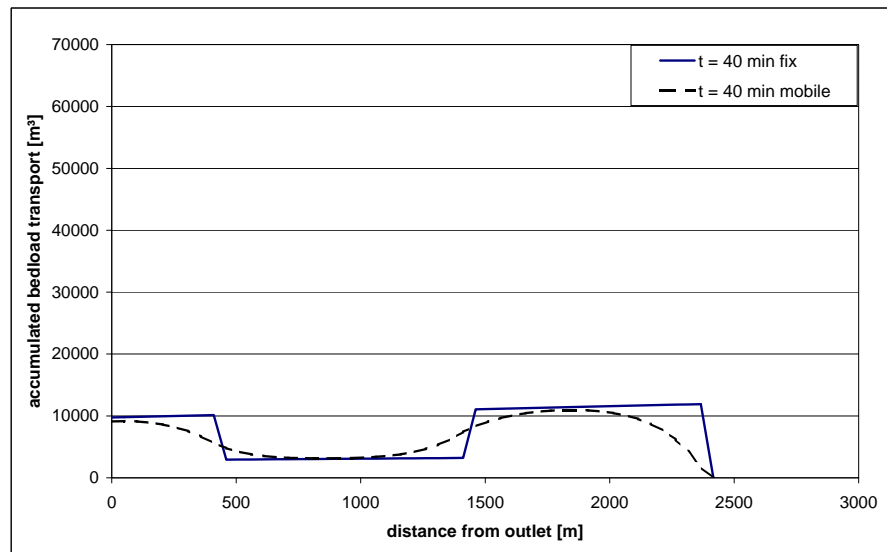


Figure 9.2: Comparison of accumulated bedload transport after 40 minutes simulation time

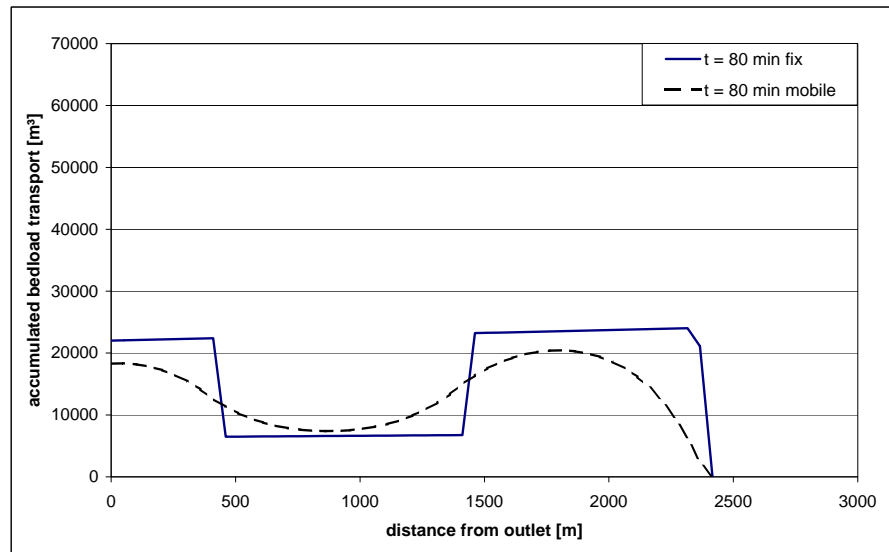


Figure 9.3: Comparison of accumulated bedload transport after 80 minutes simulation time

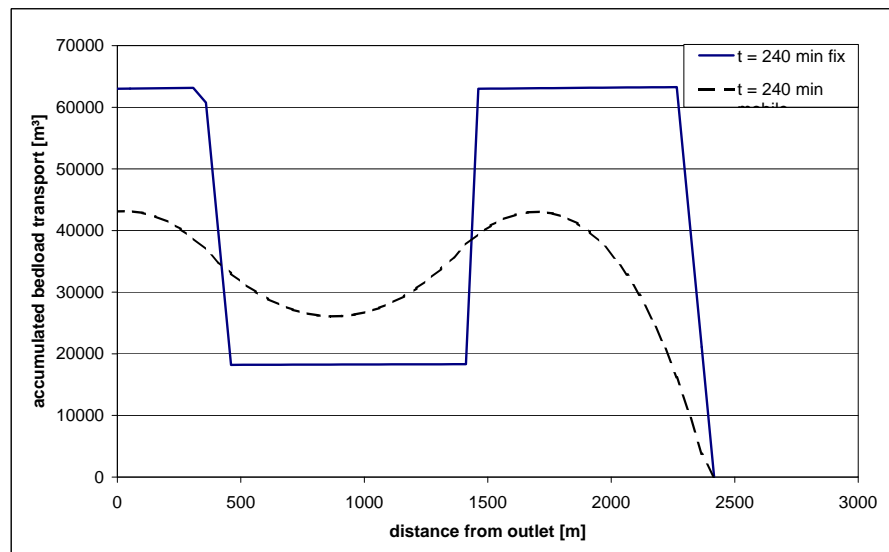


Figure 9.4: Comparison of accumulated bedload transport after 240 minutes simulation time

10 Effect of spatial and temporal discretisation

10.1 Effect of spatial discretisation

Especially when bedload is calculated under mobile bed conditions the change of the longitudinal profile has an effect on the bedload transport capacity. The spatial discretisation along the channel describes the length of a calculation unit (e.g. distance between the cross-sections). If the distance between the cross-section is longer than the discretisation length, subsections are used to obtain uniformly distributed calculation units. The length of these units is responsible for the ability to adjust to morphologic changes caused by erosion and deposition. The discretisation length can not be determined a priori. Figure 10.1 shows the Laval case (see Chapter 16.1) study modelled with different discretisation lengths. Starting with no refined spatial discretisation (cross-section distance equals the discretisation length), the spatial discretisation was refined from 100 m, 50 m, 25 m, 10 m, 5 m to 2.5 m. The rough discretisations (down to 50 m) show very different results for the accumulated bedload transport, whereas the finer discretisations result in similar amounts of transported bedload.

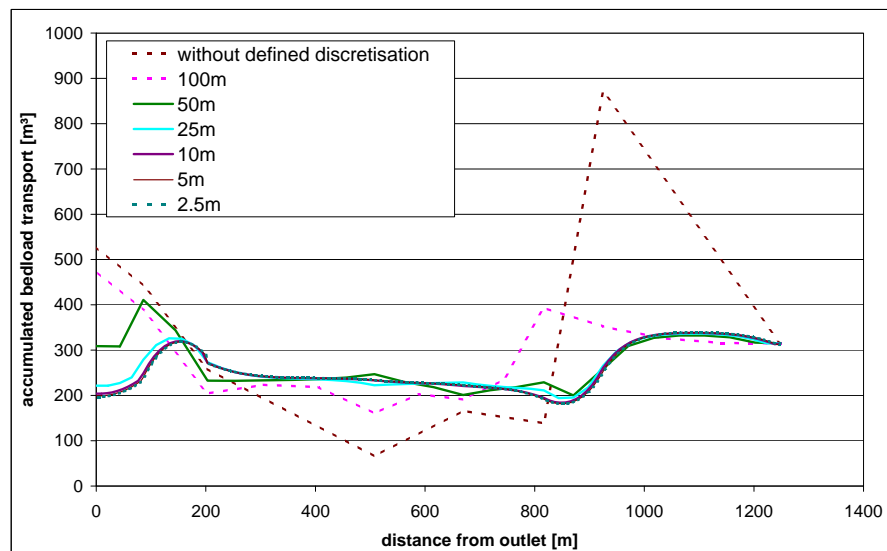


Figure 10.1: Comparison of different spatial discretisations for the Laval case study

The discretisation length has to be refined until there is no significant difference between the simulation results. Then the coarsest discretisation without loss of accuracy can be chosen to achieve an optimized combination of simulation time and accuracy. For

the example shown in Figure 10.1 a spatial discretisation of 10 m is necessary to obtain the required accuracy. Smaller channels tend to require finer spatial discretisation than bigger channels. The same observation was made by Bahadori et al. (2006) when they applied the SDAR model to rivers and laboratory studies.

For this study discretisation lengths from 0.10 to 5 m were used for the recalculation of laboratory experiments. The field studies were calculated with spatial discretisation varying from 10 to 50 m depending on the catchment area and cross-section width. An overview of the required discretisation length and river/flume length for the simulations made in this study is given in Table 10.1.

Table 10.1: Discretisation length and simulated river/flume length for the case studies.

Simulated case study	length of simulated flume/river	discretisation length
Günter (1971) flume study	40 m	5 m
Kaitna et al. (2007) flume study	8 m	0.10 m
Sessladbach field study	3 250 m	25 m
Schnannerbach filed study	3 000 m	25 m
Suggadinbach field study	8 800 m	50 m
Chirelbach field study	7 800 m	50 m
Chiene field study	8 250 m	50 m
Lütschine field study	12 800 m	50 m
Draix Laval field study	1 250 m	10 m

10.2 Effect of temporal discretisation

As the flow hydraulics in SETRAC is solved with an explicit solution scheme for the partial differential equations the minimal time step required for numerical stability is depending on the Courant-Friedrichs-Lewy (Courant et al., 1967) condition (see Chapter 6.13). To simplify a correct temporal discretisation in SETRAC the CFL number instead of the time step is chosen by the user. Therefore the temporal discretisation has to be regarded in combination with the spatial discretisation.

For normal applications the CFL number is set close to 1 (e.g. $CFL = 0.99$) to optimize numerical stability, numerical diffusion and computation time. For some special cases a small CFL number can be chosen to force smaller time steps in SETRAC. This can be the case for the fractional bedload transport module at high transport rates. When a small active layer is needed, which must not be depleted within one time step it is possible to decrease the CFL number. To avoid problems concerning the numerical stability, Armanini and Di Silvio (1988) recommend that the active layer should not be thinner than 0.05 h . With lower CFL numbers numerical diffusion increases and a damping of the wave can be observed. Instead it is possible to increase the active layer depth to avoid this problem, by damping the rate of change in the active layer (see Chapter 11.2).

11 Effect of fractional bedload transport

For the following analysis a test channel has been used. The channel is one kilometer long channel with a constant slope of 0.1. Unlimited sediment supply (maximum erosion depth 100 *m*) has been considered. Calculations are made with the fixed bed option to keep the slope constant. The cross-section of the channel is trapezoidal with a bottom width of 5 *m* and a side slope of 1:1. The initial bed sediment is homogeneous for the active layer and the bedload layer and consists of five fractions. Table 11.1 shows the initial grain size distribution.

Table 11.1: Initial grain size distribution of the bed sediment

sediment size class	[cm]	proportion
K1	0-4	0.425
K2	4-8	0.195
K3	8-12	0.160
K4	12-16	0.145
K5	16-20	0.075

11.1 The hiding function

The hiding function describes the relative mobility of the fractions of the grain size distribution. Depending on the streams transport behavior, effects of downstream fining or even downstream coarsening (Solari and Parker, 2000; Brummer and Montgomery, 2003) can be reproduced with a power law hiding function. The exponent in the hiding function determines whether finer or coarser particles are more mobile compared to the mean grain size d_m of the total sediment mixtures.

The above described channel has been modelled with a constant discharge of 1 m^3/s until a constant grain size distribution has been obtained. No sediment input from upstream and unlimited sediment availability was assumed. The active layer is specified as 0.3 *m* ($2d_{90}$). To investigate the influence of the exponent γ in the hiding function (Equation 6.44) it has been varied between 0.0 and 1.6. Figure 11.1 shows the initial grain size distribution and the grain size distribution obtained with different values of γ . A value smaller than one has the effect of downstream fining. The resulting grain size distribution is coarser than the initial grain size distribution. Setting γ equal to one, the initial grain size distribution remains constant - all sediment fractions are equally mobile and there are no hiding effects. A value of γ greater than one reproduces the effect of downstream coarsening. Finer sediment fractions are less mobile than the coarser

fractions of the grain size distribution. The resulting active layer becomes finer than the initial grain size distribution.

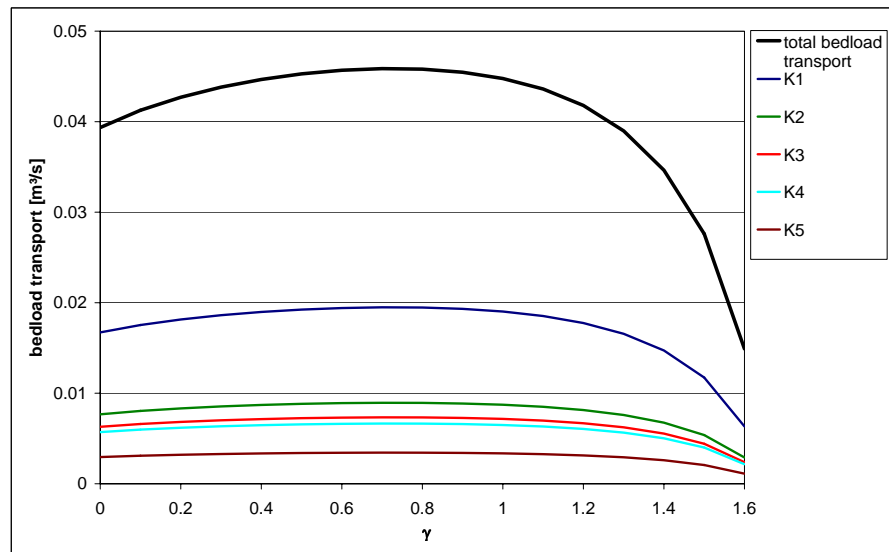


Figure 11.1: Grain size distribution obtained by variation of γ .

Figure 11.2 shows the total bedload transport after the development of a constant grain size distribution for the single sediment size classes as well as accumulated as total bedload transport. The highest total transport is obtained by a γ between 0.6 and 1.0. Lower values of γ result in slightly smaller bedload transport. Values of $\gamma > 1$ result in a strong reduction of the bedload transport. This can be explained by the selective transport behavior of the hiding function. Fractions that are less mobile accumulate in the active layer whereas more mobile fractions are eroded and transported downstream. Thus the time integrated amount of transported bedload is reduced compared to non selective transport.

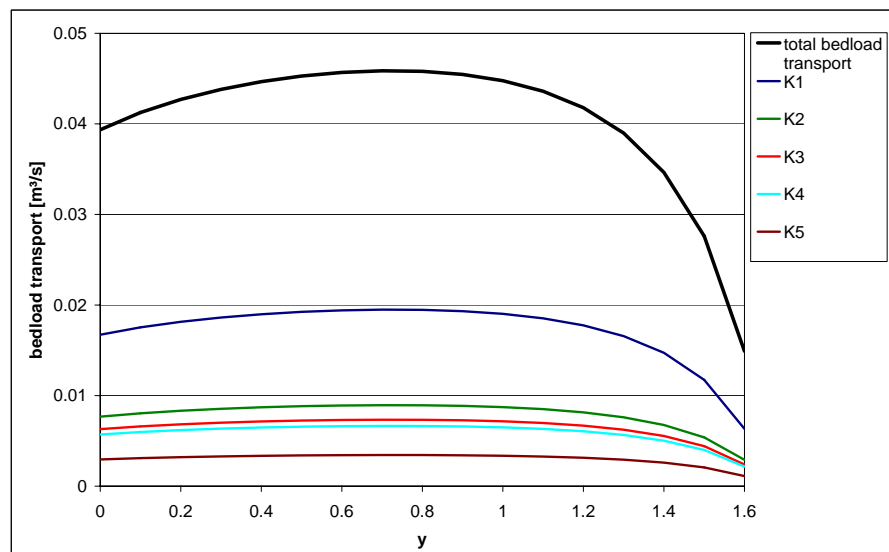


Figure 11.2: Bedload transport for varying γ .

11.2 Active layer thickness

Computing fractional bedload transport at steep slopes requires more data for calibration. The rate of change of the grain size distribution due to selective transport is dependent on the hiding function and the active layer thickness. Hassan and Church (1994) investigated vertical mixing in gravel bed rivers and found that the burial depth of particles is dependent on the magnitude and duration of the flow event. In addition the number of events and the surface structure and texture influence vertical mixing, too. Hence the determination of the active layer thickness is not a priori known and can be used as a calibration parameter to adjust the rate of change in the grain size distribution to observations. Because of numerical stability Armanini and Di Silvio (1988) observed that the active layer should not be thinner than $0.05 h$. According to our findings the active layer should not be depleted within one time step to avoid unrealistic transport rates and grain size distributions (see Chapter 10.2).

The influence of the active layer thickness has been investigated with several experimental runs. The in Chapter 11 presented test channel has been modelled with different discharges. The simulation has been stopped when a constant grain size distribution for the whole channel was achieved. For each discharge the active layer thickness has been varied from $0.01 m$ to $0.5 m$. Each discharge produces a specific grain size distribution independent of the active layer thickness for a given exponent $\gamma = 0.85$. The difference is only the time span when it is achieved. The active layer thickness influences the rate of change of the grain size distribution. The initial grain size distribution and the obtained grain size distributions are shown in Figure 11.3.

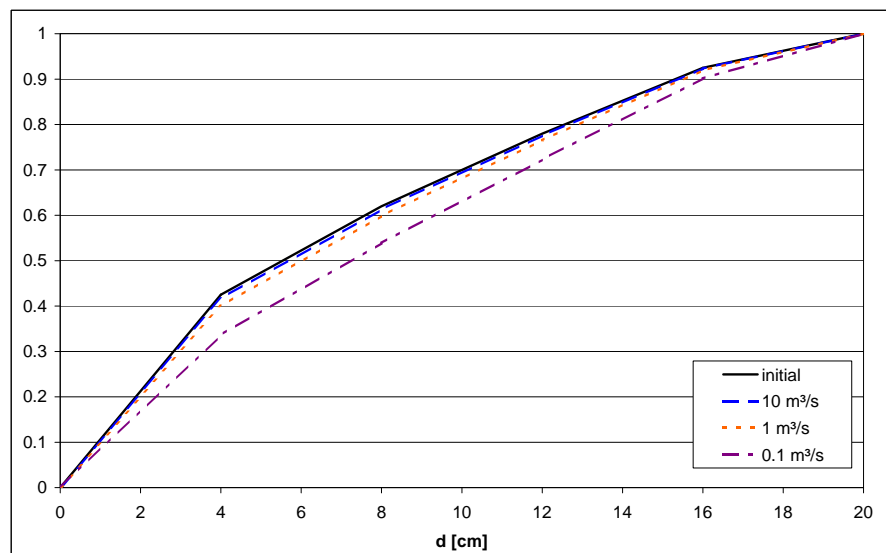


Figure 11.3: Grain size distribution obtained by different discharges

Coarsening of the bed is dependent on the hiding function used (see Chapter 11.1) and on the discharge applied to the channel. The lower the discharge the coarser is the active layer developed after a certain time. The time until a constant grain size distribution for the whole channel is developed is shown in Table 11.2. The spatial discretisation for the simulation is $50 m$. In SETRAC the fractional bedload transport module in combination with Equation 6.40 was used to model the grain size distribution. Morphologic changes

of the longitudinal profile were neglected for this comparison. Each discharge produces a certain grain size distribution. The active layer thickness influences the time required to obtain the specific grain size distribution. A thick active layer produced by a low discharge takes longer to develop than a thin active layer in combination with a high discharge. Therefore the sensitivity of the active layer thickness is dependent on the time scale. For long term developments the active layer thickness has not a major influence on the resulting grain size distribution. For events with short duration and fast changes of the discharge (e.g. flood events in torrents with steep hydrographs) the active layer thickness has an influence on the grain size distribution of the active layer.

Table 11.2: Duration for the development of a constant grain size distribution for different discharges and varying active layer depth

active layer thickness	10 m^3/s	1 m^3/s	0.1 m^3/s
0.500 m	9 900 s	104 400 s	2 221 200 s
0.300 m	6 000 s	70 200 s	1 346 400 s
0.200 m	4 200 s	46 800 s	1 015 200 s
0.100 m	2 100 s	20 700 s	444 000 s
0.050 m	1 200 s	12 000 s	222 000 s
0.025 m	600 s	6 000 s	111 000 s
0.010 m	not stable	2 400 s	44 100 s

11.3 Comparison with sediment transport formula for sediment mixtures

For high flow rates with mobility of all fractions the total transport rate is comparable with the bedload transport obtained by a one-grain model. However at low transport rates (below incipient motion conditions for the one grain model) the total amount of transported sediment is be higher. This is caused by the effect of selective transport, when finer fractions are already transported, but coarser still remain in the channel bed. Self-evident the exponent γ is responsible for the relative mobility of the size fractions.

For direct comparison of the one grain model with the fractional bedload transport module Equation 6.40 has been expanded for the correction term $(d_{90}/d_{30})^{0.2}$. Therefore Equation 6.41 was applied to the same channel presented at the beginning of Chapter 11. An active layer thickness of 0.30 m ($2d_{90}$) has been considered. Varying discharges from 0.01 to 100 m^3/s were modelled. The results are compared with bedload discharges obtained by the one grain model calculated with the bedload transport Equation 6.33. Table 11.3 shows a comparison of the two different approaches. The bedload discharge of the sediment size classe K1-K5 are also given. In Table 11.3 an exponent $\gamma = 0.80$ has been considered. Close to incipient motion of bedload transport the calculation of fractional bedload transport results in higher amounts of total bedload transport. This can be explained by the hiding function with the exponent $\gamma = 0.80$. Finer fractions are more mobile then coarser fractions, therefore the incipient motion criteria is lower compared to the sediment mixture calculated with the one grain model. Thus sediment

transport starts earlier. As soon as the incipient motion criteria for the one grain model is fulfilled, both models deliver comparable transport rates.

Table 11.3: Comparison of bedload discharge obtained by the one-grain model and the fractional bedload transport with $\gamma = 0.80$. All values in m^3/s .

discharge	one grain model	Sum fractional	K1	K2	K3	K4	K5
0.001	0.00000	0.00000	0.00000	0.00000	0.00000	0.00000	0.00000
0.005	0.00000	0.00001	0.00001	0.00000	0.00000	0.00000	0.00000
0.01	0.00000	0.00009	0.00009	0.00000	0.00000	0.00000	0.00000
0.02	0.00026	0.00025	0.00024	0.00001	0.00000	0.00000	0.00000
0.05	0.00137	0.00113	0.00069	0.00021	0.00013	0.00009	0.00003
0.1	0.00487	0.00463	0.00251	0.00082	0.00059	0.00048	0.00023
0.5	0.02769	0.02710	0.01292	0.00508	0.00395	0.00344	0.00172
1	0.06655	0.06547	0.02918	0.01267	0.01011	0.00897	0.00455
5	0.37356	0.37065	0.15753	0.07228	0.05930	0.05374	0.02780
10	0.77155	0.76732	0.32611	0.14963	0.12277	0.11126	0.05755
50	4.23888	4.22837	1.79706	0.82453	0.67654	0.61311	0.31713
100	8.56779	8.55226	3.63471	1.66769	1.36836	1.24008	0.64142

12 Effect of grain size distribution

The effect of the grain size distribution concerning the transport rate has been investigated using the channel presented in Chapter 11. The grain size distribution as well as the discharge have been varied. For comparison both, the one grain model as well as the fractional bedload transport module have been used in the simulations. The grain size distribution for the different simulation runs are shown in Figure 12.1. Table 12.1 lists the corresponding characteristic grain sizes for the one grain model.

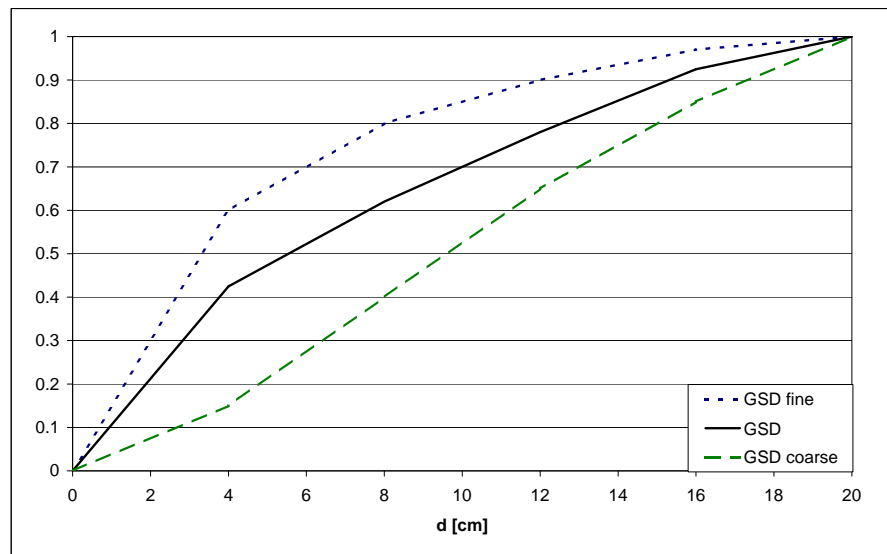


Figure 12.1: Grain size distributions used for the simulations

Table 12.1: Characteristic grain sizes for the one grain model. All values in *cm*.

	GSD fine	GSD	GSD coarse
d_{30}	2.00	2.75	6.30
d_{50}	3.30	5.50	9.60
d_{90}	12.00	15.25	17.25

Like in Chapter 11.3 the fractional bedload transport module Equation 6.40 has been expanded for the correction term $(d_{90}/d_{30})^{0.2}$. Therefore Equation 6.41 was applied. An active layer thickness of 0.30 m ($2d_{90}$) has been considered. Varying discharges from 0.1 to $10\text{ m}^3/\text{s}$ were modelled. The results are compared with bedload discharges obtained by the one grain model in combination with the bedload transport Equation 6.33. The simulations were stopped when a static armour layer was achieved. The exponent in the hiding function was set at $\gamma = 0.85$. Figures 12.2 to 12.4 compare the bedload transport for the one grain model and the fractional bedload transport. The ratio $q_{b,frac}/q_b$

is also given. The influence of the grain size distribution can be explained by the fact that the initial grain size distribution is responsible for the incipient motion criteria used in the hiding function as well as for the sediment mixture. Therefore the the grain size distribution influences the bedload discharge. The finer the grain size distribution is the higher is the bedload discharge for the sediment mixture as well as for the specific fractions. Depending on the exponent γ in the hiding function the differences between the two modelling approaches are not independent of the discharge. At $0.1 \text{ m}^3/\text{s}$ (Figure 12.2) the differences between the bedload transported by the one grain model compared to the fractional bedload transport are most noticeable. The differences increase with coarser grain size distributions. That can be explained by the hiding function. With an exponent $\gamma = 0.85$ finer fractions are more likely to be transported than coarser fractions. The coarser the grain size distribution is the smaller is the proportion of the finer fraction. Thus the total transport decreases. At $1.0 \text{ m}^3/\text{s}$ (Figure 12.3) the differences are smaller compared to the smaller discharge. With the high discharge of $10 \text{ m}^3/\text{s}$ (Figure 12.4) both models deliver nearly identical results.

Tables 12.2 to 12.4 show the bedload discharge for the one grain model as well as for the sediment size fractions at different discharges.

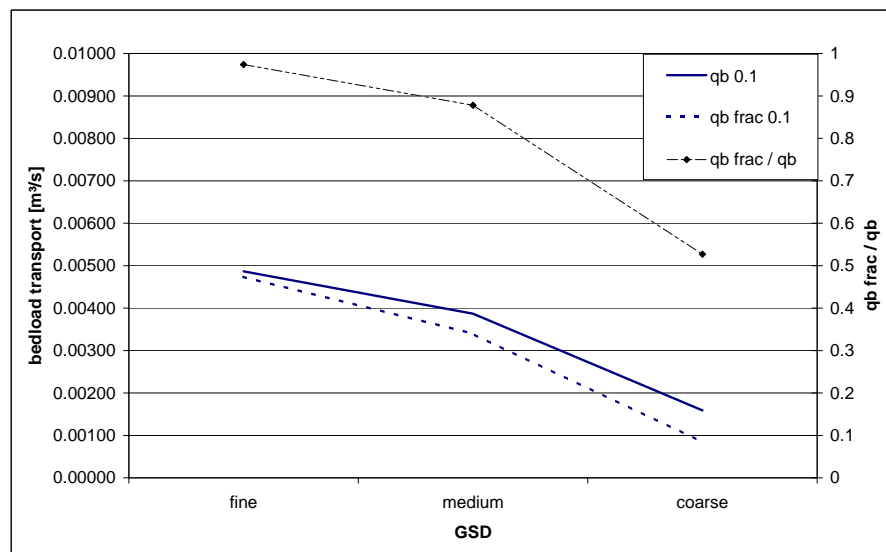


Figure 12.2: Bedload transport at $0.1 \text{ m}^3/\text{s}$

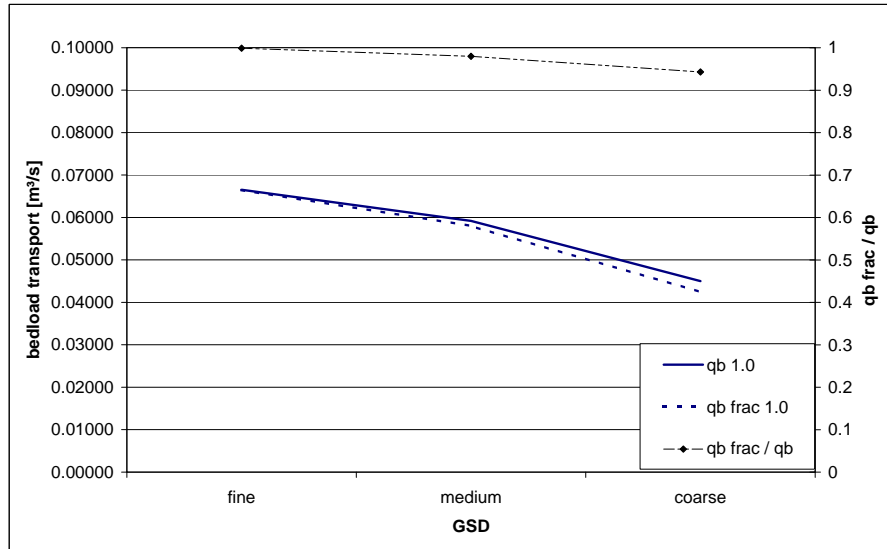


Figure 12.3: Bedload transport at $1.0 \text{ m}^3/\text{s}$

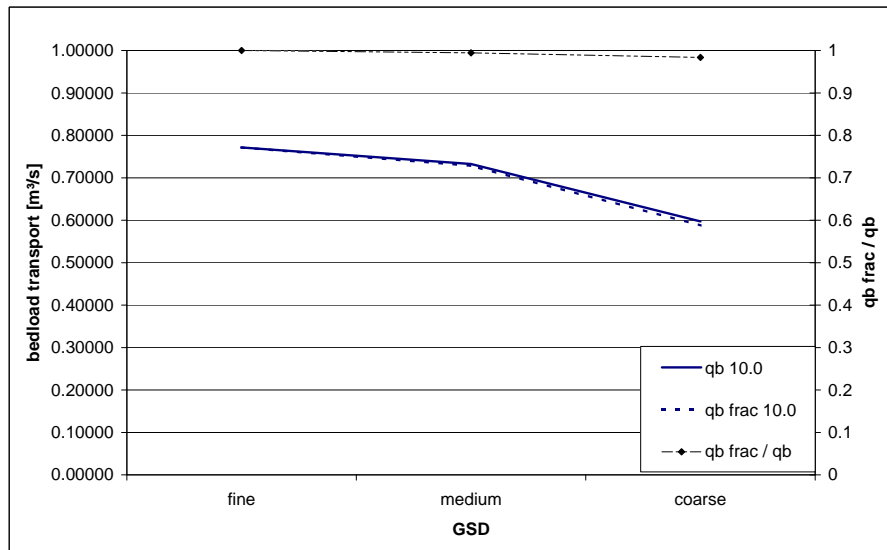


Figure 12.4: Bedload transport at $10.0 \text{ m}^3/\text{s}$

Table 12.2: Comparison of bedload discharge obtained by the one-grain model and the fractional bedload transport at $0.1 m^3/s$. All values in m^3/s .

grainsize distribution	one grain model	Sum fractional	K1	K2	K3	K4	K5
GSD fine	0.00487	0.00474	0.00284	0.00095	0.00047	0.00033	0.00014
GSD	0.00387	0.00340	0.00144	0.00066	0.00054	0.00049	0.00025
GSD coarse	0.00159	0.00084	0.00013	0.00026	0.00026	0.00013	0.00006

Table 12.3: Comparison of bedload discharge obtained by the one-grain model and the fractional bedload transport at $1.0 m^3/s$. All values in m^3/s .

grainsize distribution	one grain model	Sum fractional	K1	K2	K3	K4	K5
GSD fine	0.06655	0.06647	0.03988	0.01329	0.00665	0.00465	0.00199
GSD	0.05920	0.05800	0.02465	0.01131	0.00928	0.00841	0.00435
GSD coarse	0.04500	0.04244	0.00637	0.01061	0.01061	0.00849	0.00637

Table 12.4: Comparison of bedload discharge obtained by the one-grain model and the fractional bedload transport at $10.0 m^3/s$. All values in m^3/s .

grainsize distribution	one grain model	Sum fractional	K1	K2	K3	K4	K5
GSD fine	0.77155	0.77165	0.46299	0.15433	0.07716	0.05402	0.02315
GSD	0.73239	0.72824	0.30950	0.14201	0.11652	0.10559	0.05462
GSD coarse	0.59731	0.58756	0.08813	0.14689	0.14689	0.11751	0.08813

Part VI

Event Documentation of Case Study Streams

13 Event documentation

For the purpose of a sediment transport model validation, field data are required. Most important data are flood hydrographs and sedigraphs for extreme events if the model should serve as a tool for hazard assessment. For small mountain catchments these data are rarely available. Therefore event documentation shortly after an extreme event is essential for the reconstruction of torrential events. The back-calculation of the peak discharge at several cross-sections is necessary. The time evolution of the event may be obtained from rainfall records to reconstruct the temporal sequence of the flood hydrograph. Sedigraphs are not commonly available in mountain catchments except for experimental catchments. Therefore sediment budgets for single reaches have to be made in order to reconstruct the time integrated morphologic changes along the active channel.

13.1 Hydrology

For the back calculation of extreme events in ungauged catchments field investigations are necessary. The cross-section geometry, channel slopes and the grain size characteristics can be obtained in the field. Silent whitenesses allow the estimation of the maximum wetted perimeter of the cross-section. Vegetation is often a good indicator of the maximum flow depth, but flood marks can often be seen on bedrock too. Cross-sections without major morphologic change during the event have to be identified in the field. Extreme events in steep catchments often carry substantial amounts of bedload. The flood marks indicate the mixture flow depth. For the back calculation of the peak discharge one has to verify the assumption, that the flood marks are caused by more or less steady uniform flow and were not caused by a debris flow. Rickenmann (1990) presented a calculation procedure for the field case (Figure 13.1). With the known parameters h_m , S , $(s - 1)$, d_{90} , d_m , and d_{30} the unknown parameters q_b , q , h_f and v can be calculated. The recommended range of application is given with: $0.2\% \leq S \leq 20\%$; $\alpha = 0.05$ and $\beta = 1.5$ for $S \geq 5\%$; $d_m \geq 1\text{ mm}$. For $S < 5\%$ the space occupied by the transported sediment can be neglected ($h_f \cong h_m$).

Modelling bedload transport in ungauged catchments requires an estimate of not only the peak discharge, but also the total amount of water as well as the shape of the hydrograph. On inhabited fans eye witnesses may give additional informations about the temporal evolution of the event. They often can tell when and where the flow overtopped the channel banks and when bedload was deposited outside the channel. Additionally they may indicate time of the peak: "When was it worst?". Fire brigades can also deliver important information about the temporal evolution and locations of flow overtopping.

Analyzing flow data from discharge gauges upstream and downstream of the outlet of the investigated river can deliver additional information about the flow hydrograph.

One has to consider all the tributaries between the two discharge gauges.

It is also necessary to analyze all rainfall gauges in or close to the catchment. Spatial information about the rain can be obtained by analyzing radar precipitation data and relate them with the rainfall gauges.

All these informations help calibrating a rainfall-runoff model to generate the flow hydrographs for the catchment and its sub-catchments required for the hydraulic- and sediment transport simulation.

13.2 Morphologic changes

To obtain information on the morphologic changes after a flood event, different investigation methods can be used to identify and assess the processes of erosion and deposition along the whole channel. Remote sensing techniques are a new opportunity to determine erosion and deposition volumes for extreme flood events. Field investigations after events are important to get qualitative and quantitative information about the relevant processes in torrents and mountain streams.

13.2.1 Sediment budget based on field investigations

Shortly after extreme flood events a channel can be surveyed. Erosion and deposition volumes are measured (whenever possible) or estimated in the field for (quasi-)uniform reaches with similar bed, erosion/deposition and channel gradient. Separate measurements can be made for the main channel, the banks and sediment input from the banks or hill slopes. The erosion and deposition volumes are then accumulated for the entire channel starting from the most upstream point. The differences between accumulated erosion and deposition is the transported sediment volume. These volumes have to be corrected for the pore volumes and the amount of fine sediment transported as suspended load further downstream. For this study it is assumed, that the pore volume and the content of fine sediment makes up about 50 % of the erosion volume. For deposition 30 % of pore volume is considered. It is assumed that the suspended sediment and washload are transported farther downstream. The accumulated erosion and deposition volumes including fine sediments and pore volume for one of the case study streams are shown in Figure 13.2, whereas the corrected bedload volumes are shown in Figure 13.3 for the same flood event.

All erosion and deposition zones presented in this study were measured by a laser distance device and the depths/heights were estimated in the field (except for the cases with LiDAR based sediment budgets). The accuracy of this investigation method is about +/-10 % for the area and +/-50 % for the depth/height. If the main deposition occurred on the channel fan, a more detailed survey was made. If the fan is covered with buildings, the deposition heights were measured and the area was calculated from areal photos. Therefore the deposition volume estimated on the fan is more accurate than the sediment budget along the stream channel.

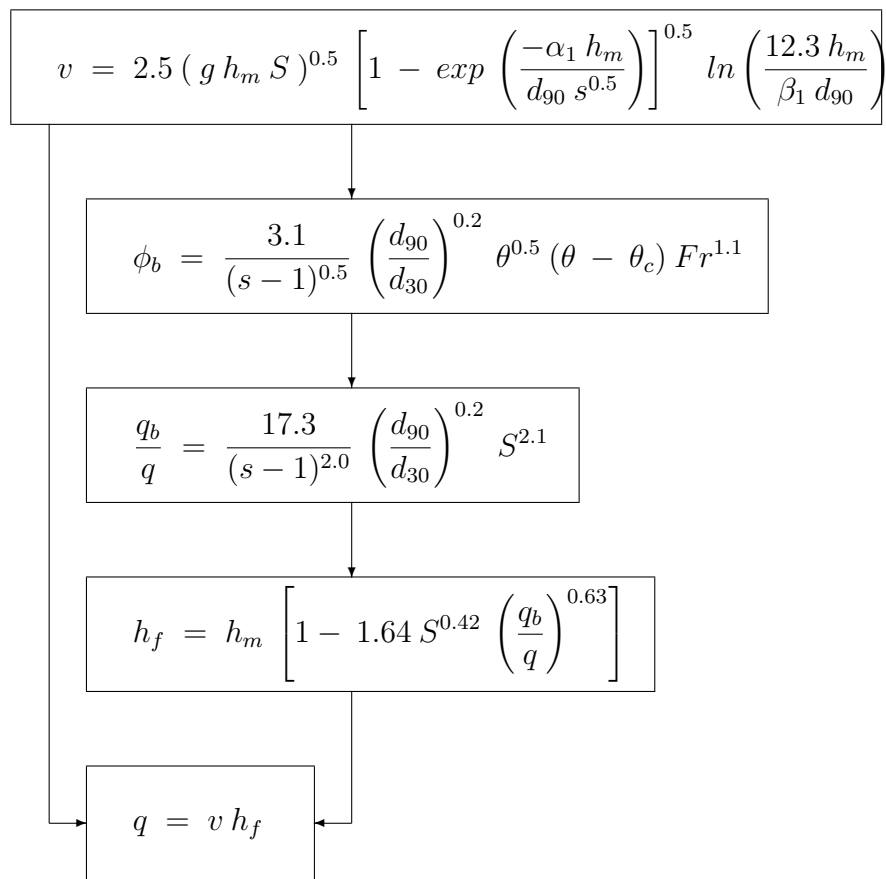


Figure 13.1: Calculation procedure for the back calculation of the peak discharge after Rickenmann (1990)

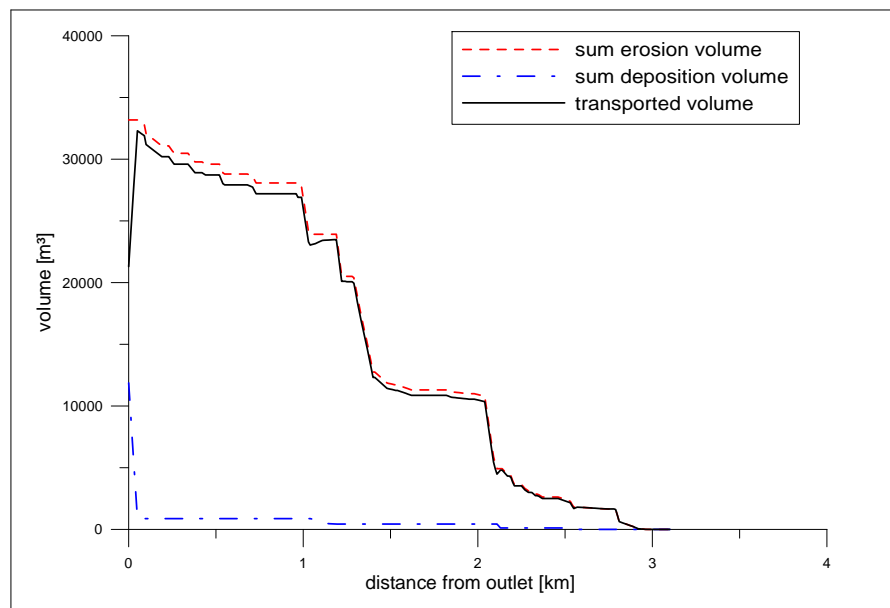


Figure 13.2: Example of the erosion and deposition volumes for one of the case study torrents (including fibre material for erosion, and pore space)

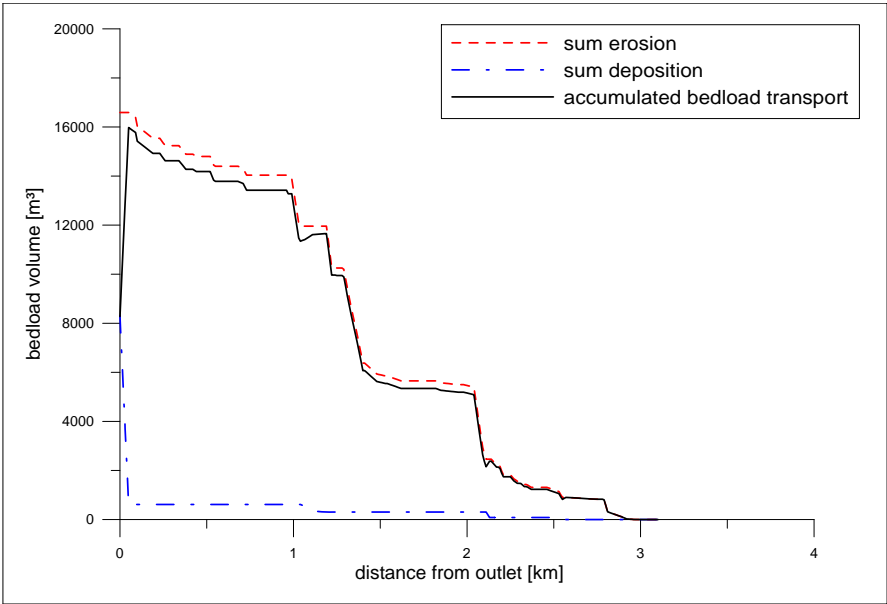


Figure 13.3: Example of the accumulated bedload transport for one of the case study torrents (excluding fine material and pore space)

13.2.2 Airborn LiDAR Data

Airborn LiDAR (Light Detection And Ranging) technology is a relatively new technology to generate high resolution elevation models. LiDAR is an active sensor system that uses laser light to measure distance. Airborn LiDAR systems rely on the Global Positioning System (GPS) and an internal reference system in the aircraft. The LiDAR device mounted on an aircraft emits laser pulses. These pulses are reflected from the ground, vegetation or structures. The time of flight is used to calculate the distance. A laser beam can be reflected several times. The first reflection (first echo) can be reflected by the vegetation cover, whereas the last reflection (last echo) should be reflected by the ground. The position of the aircraft is registered by a GPS unit and an internal measurement unit records the pitch, roll and heading of the aircraft. The reflection of surfaces with different slopes as well as the multiple reflection of vegetation (e.g. by a tree) are shown in Figure (13.4).

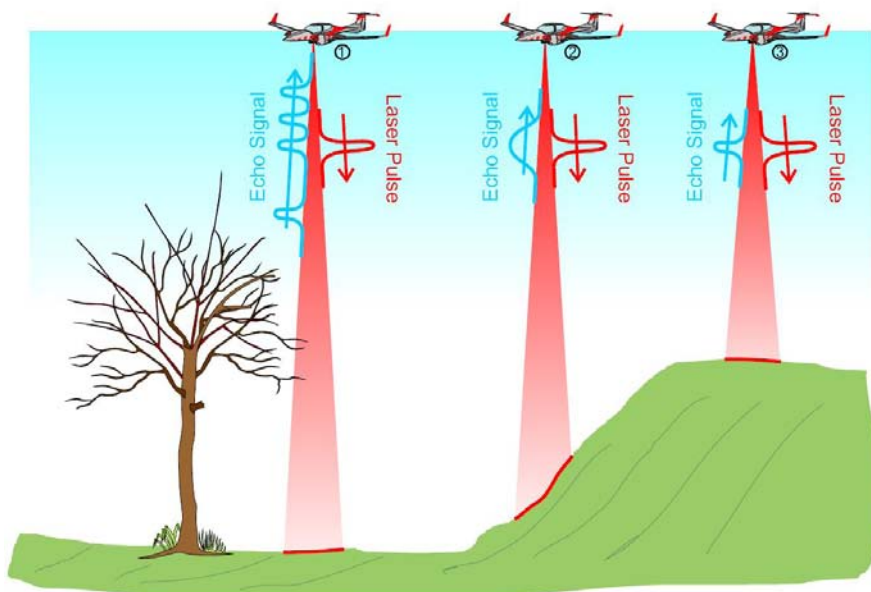
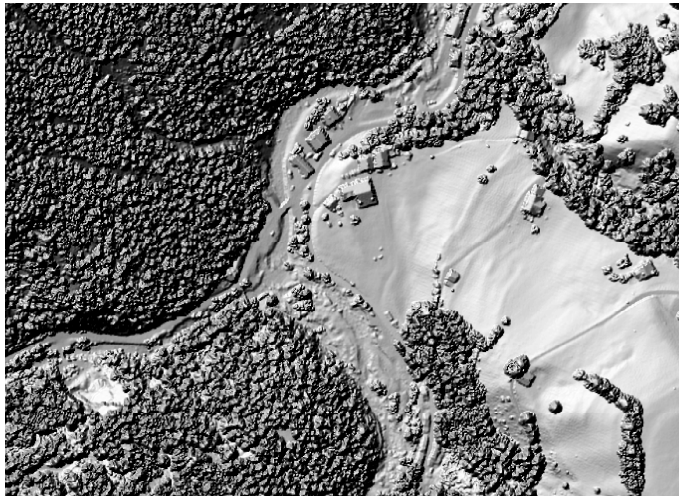
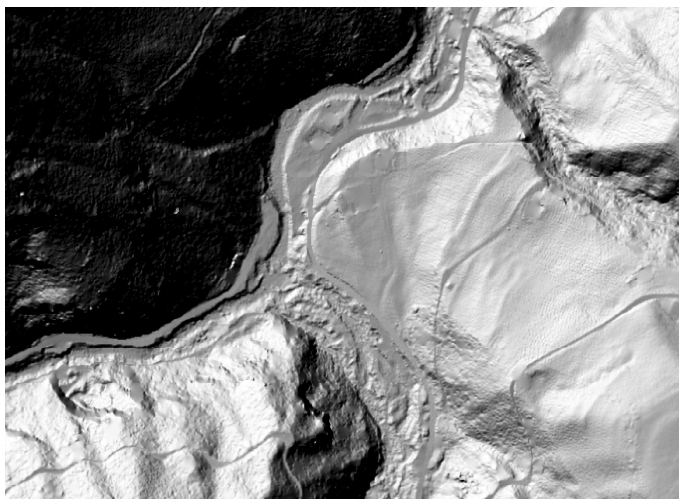


Figure 13.4: Reflection depending on the target (source: www.riegl.com)

The first echo signals can be used for generating digital surface models (DSM). After applying filter algorithms the last echo signals are used for generating digital terrain models (DTM). An example of a DSM is shown in Figure 13.5(a). The related DTM for the same area is shown in Figure 13.5(b) for comparison. Vegetation and buildings are removed by filter algorithms.



(a) Digital surface model (DSM), (DOM-AV ©2008 BAFU)



(b) digital terrain model (DTM), (DTM-AV ©2008 BAFU)

Figure 13.5: River reach with confluence of the Chirel mountain stream. Hill shades were generated with DSM and DTM.

Calculation of morphologic changes and sediment budget

A digital elevation model represents the morphology of an area at a certain time. High resolution digital elevation models can be used for the calculation of morphologic changes. If there are several (at least two) elevation models available for the same region, morphologic changes can be calculated by subtracting one elevation model from the other. The advantage of this method is the coverage of the whole area. Woolard and Colby (2002) and White and Wang (2003) analyzed morphologic changes of the coastline by subtracting one elevation model from the other. Applying the same technique Scheidl et al. (2008) calculated deposition and erosion volumes of debris flows in Switzerland. In the same way, morphologic changes can be calculated for fluvial sediment transport events in order to obtain a sediment budget for a torrent or mountain stream. Figure 13.6(a) shows a digital surface model (DSM) with an aerial photograph before a flood event occurred for one reach of a case study streams. The same area after a flood event (again DSM with aerial photograph) is shown in Figure 13.6(b). The morphologic change has been calculated with the digital terrain model (DTM) before and after a flood event (Figure 13.6(c)). Red indicates erosion and blue deposition.

One has to consider the time span between the generation of the two elevation models. For torrents and mountain streams it is generally assumed, that major morphologic changes are only caused by major flood events. If this method is used for the calibration or back-calculation of several extreme events, all flood events that occurred between the generation of the elevation models have to be considered.

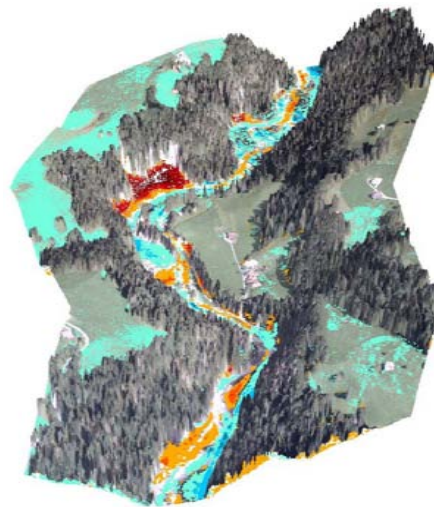
For the comparison of the two-dimensional volumetric change of the channel with results obtained by a one-dimensional simulation software like SETRAC the following method has been developed. The active channel has been separated into reaches with 50 *m* length. The net erosion or deposition is calculated with GIS software. The calculated erosion and deposition heights within the active channel reaches are shown in Figure 13.7 for a case study reach. The calculated volumes contain pore volume and fine sediments. For this study it is assumed, that the pore volume and the content of fine sediment is about 50 % of the erosion volume. For deposition 30 % of pore volume is considered. The fine sediment fractions are considered to be transported further downstream as suspended load. The same assumptions were considered for the field based assessment of the morphologic changes (Chapter 13.2.1).



(a) Aerial photograph with DSM before the flood event (DOM-AV ©swisstopo; DV033492.2)



(b) Aerial photograph with DSM after the flood event (DOM-AV ©2008 BAFU)



(c) Calculated morphologic change after the flood event (DTM-AV ©2008 BAFU; DTM-AV ©swisstopo; DV033492.2)

Figure 13.6: River reach of the Chirel mountain stream before and after the August 2005 flood event

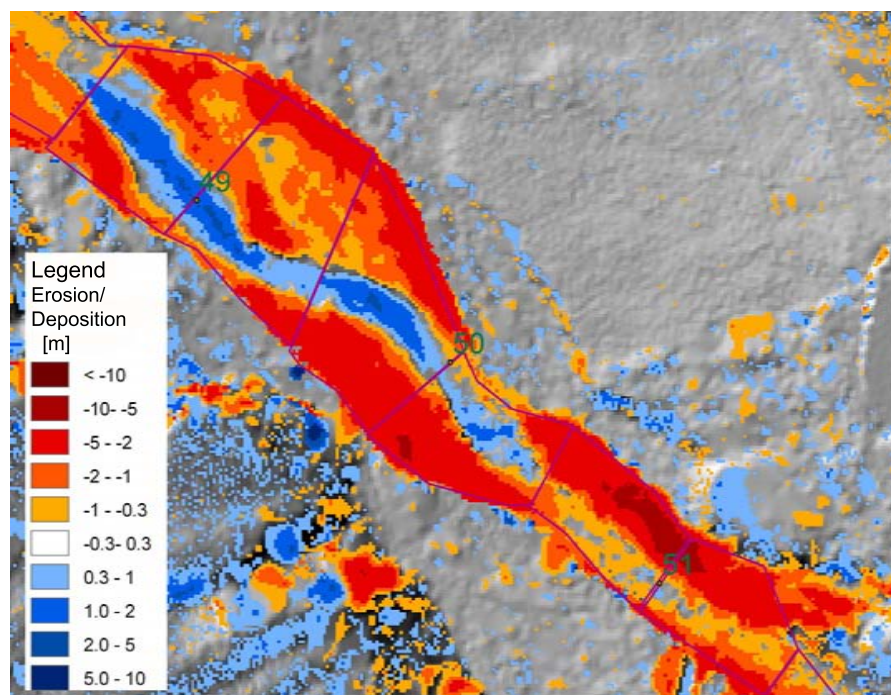


Figure 13.7: Calculated erosion and deposition heights with discretisation of the active channel reaches

Accuracy of Volumes calculated with LiDAR data

It has to be considered, that water levels cannot be measured by LiDAR techniques, because there is no reflection of the laser beam from the water surface. However, for torrents and mountain streams with low relative submergence and protruding boulders the elevation of the channel bed can be estimated. If the original scan data are available, the point density for the reaches of interest indicates whether there is enough information available for the interpolation of the channel bed. For torrents and mountain streams the water level influences the accuracy of the scan. Therefore LiDAR flights should be generated at low flow rates for more accurate reproduction of the rough channel bed. An example of the effect of the point density and the filter algorithm used to generate the DTM is shown in Figure 13.8. The points are plotted over a hill shade of a reach of the Lütschine mountain stream. The point density before the flood event was much lower compared to the DTM generated with the data from the later LiDAR flight. Comparing the cross-sections (Figure 13.8(c)) one could conclude that there were massive depositions on the channel banks. In reality this is an effect caused by the lack of scanned elevation points on the left river bank before the flood event. In the meantime scans the LiDAR technology improved. Therefore LiDAR based analysis can be problematic if they are applied exclusively. For the back-calculations of the morphologic changes the point density along the active channel has been considered. Noticeable is, that for the more recent DTMs, there is a higher point density for the same regions. Table 13.1 shows average point densities for the DTMs before and after the August 2005 flood for all investigated active channels in Switzerland, namely the Chirel mountain stream, the Chiene mountain stream and the Schwarze Lütschine mountain stream. The different point densities can be explained by the improvement of the LiDAR applications between the years 2002 and 2005.

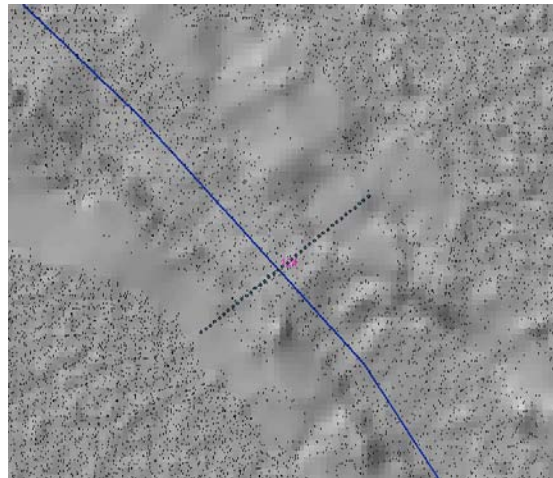
location	DTM before	DTM after
active channel	0.85 <i>Points/m²</i>	1.29 <i>Points/m²</i>

Table 13.1: Point density for the active channels before and after the August 2005 flood event in Switzerland.

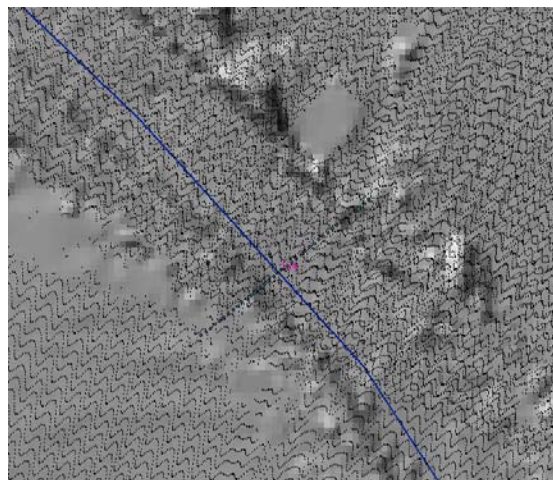
The reliability of the result can be improved in combination with other remote sensing techniques. Aerial photographs generated simultaneously help interpreting the morphologic changes caused by flood events. All calculated morphologic changes have been checked with the help of aerial photographs before and after the event to avoid unrealistic estimates of erosion and deposition.

Scheidl et al. (2008) investigated the use of airborne LiDAR data of Swiss debris flow events. They found that the accuracy of volumes determined by digital elevation models is not only dependent on the the point density, but on the hillslope angle, too.

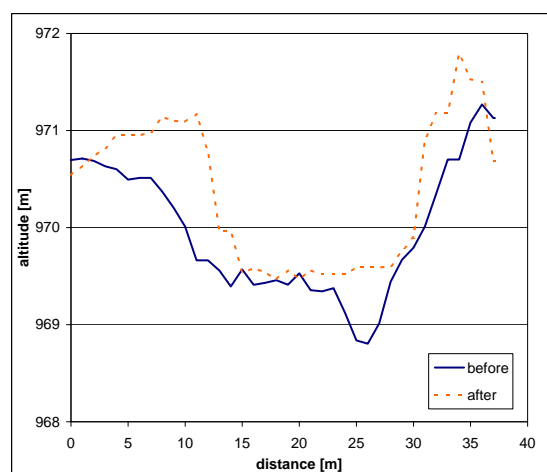
Rickenmann et al. (2008) compared the sediment budget derived by LiDAR generated differential grids and conventional event documentation and found a good agreement for the August 2005 flood event for the Chirel mountain stream.



(a) Hillshade with points before (DTM-AV ©swisstopo; DV033492.2)



(b) Hillshade with points after (DTM-AV ©2008 BAFU)



(c) Cross-section before and after the flood event

Figure 13.8: River reach of the Lütshine mountain stream before and after the August 2005 flood event

Part VII

Application of SETRAC to Case Study Streams

14 Simulation design

For a systematic comparison of different case studies a simulation design is used for all field data. Two different flow resistance approaches are combined with different bedload transport capacity formulas. The well known Strickler (1923) formula and a flow resistance equation developed for steep sediment transporting channels (Smart and Jäggi, 1983) are applied. For steep streams bedload transport equations from the type developed by Schoklitsch (1950) are recommended (Bathurst et al., 1987). Therefore a Schoklitsch type equation (Equation 6.35) and a bedload transport equation considering shear stress (Equation 6.33) are applied for comparison. Several criteria for the initiation of bedload transport as well as armouring conditions are considered to investigate their influence on the transported bedload volumes. Losses due to form roughness are neglected or considered with different extend. Simulations with consideration of form roughness losses are performed with constant exponent a in Equation 6.27 for the whole channels system, as well as varying exponents defined by the characteristic of the reaches in order to achieve a best fit simulation. The formula combinations used for the different simulation scenarios are shown in Table 14.1.

All simulations consider supply limited conditions. Possible erosion depths are estimated in the field and range from 0.05 m in channel reaches mainly in bedrock to 10.0 m for reaches in alluvial bed sediment. A constant fluid density of 1100 kg/m^3 and a value of $\theta_{cr} = 0.046$ were considered for all simulations if not explicitly mentioned otherwise for the case studies. Sediment transport is calculated as one-grain model. Morphologic changes due to erosion and deposition are considered as non negligible. Therefore the erosion module is activated within SETRAC.

Due to the sensitivity concerning the spatial discretisation, the reach length has been refined for each case study until there was no more significant change in the total transport over the whole length of the main channel. Then the coarsest discretisation without loss of accuracy has been chosen for the different simulation runs. The sensitivity concerning the spatial discretisation is discussed in Chapter 10 and the final spatial discretisation is shown in Table 10.1.

Table 14.1: Formulas used for the simulations

Simulation	flow resistance	bedload transport	incipient motion	armour layer	form roughness	Exponent γ
S1	(6.15)	(6.35)	(6.36)	-	-	-
S2	(6.15)	(6.35)	(6.37)	-	-	-
S3	(6.15)	(6.35)	(6.36)	(6.39)	-	-
S4	(6.15)	(6.35)	(6.36)	-	(6.27)	1
S5	(6.15)	(6.35)	(6.36)	-	(6.27)	1.5
S6	(6.15)	(6.35)	(6.36)	-	(6.27)	variable
S7	(6.19)	(6.33)	(6.32)	-	-	-
S8	(6.19)	(6.33)	(6.32)	(6.38)	-	-
S9	(6.19)	(6.33)	(6.32)	-	(6.27)	1
S10	(6.19)	(6.33)	(6.32)	-	(6.27)	1.5
S11	(6.19)	(6.33)	(6.32)	-	(6.27)	variable

Formula	Reference	Equation
(6.15)	Strickler (1923)	$v = k_{St} R^{0.67} S^{0.5}$
(6.19)	Smart and Jäggi (1983)	$v = 2.5v^* \left(1 - e^{\frac{-0.05h_m}{S^{0.5}d_{90}}}\right)^{0.5} \ln \left[\frac{12.3h_m}{1.5d_{90}}\right]$
(6.35)	Rickenmann (2001)	$q_b = 3.1 \left(\frac{d_{90}}{d_{30}}\right)^{0.2} (q - q_c) S^{1.5} (s - 1)^{-1.5}$
(6.33)	Rickenmann (1991)	$\Phi_b = \frac{3.1}{(s-1)^{0.5}} \left(\frac{d_{90}}{d_{30}}\right)^{0.2} \theta^{0.5} (\theta - \theta_{cr}) Fr^{1.1}$
(6.36)	after Bathurst (1985)	$q_c = 0.065(s - 1)^{1.67} g^{0.5} d_{50}^{1.5} S^{-1.12}$
(6.37)	after Whittacker and Jäggi (1986)	$q_c = 0.143(s - 1)^{1.67} g^{0.5} d_{90}^{1.5} S^{-1.167}$
(6.32)	Stevens et al. (1976)	$\theta_{crI} = \theta_{cr} \cos \arctan S \left(1 - \frac{S}{\varphi}\right)$
(6.39)	Jäggi (1992)	$q_{c,D} = q_c \left[\frac{d_{90}}{d_m}\right]^{10/9}$
(6.38)	Jäggi (1992)	$\theta_{c,D} = \theta_c \left[\frac{d_{90}}{d_m}\right]^{2/3}$
(6.27)	after Rickenmann (2005)	$\frac{n_r}{n_{tot}} = 0.092 S^{-0.35} \left(\frac{h}{d_{90}}\right)^{0.33}$

15 Extreme events August 2005

Many regions in Austria, Switzerland and Germany were affected by the flood events from August 2005 (MeteoSchweiz, 2006). A massive cyclone over the northern part of Italy caused particularly from 21. - 22. of August 2005 heavy rainfall. The period of relevant precipitation was about 4 days, whereas thunderstorms were not of major importance. Most events in Austria occurred in the western provinces Vorarlberg and Tyrol. In Switzerland the whole north-alpine region was affected. But also the southern parts of Bavaria in Germany were affected by heavy rainfall that triggered flood events. The area of heavy rainfall stretches across the whole northern Alps from Freiburg to Kufstein. The highest precipitation sums for a 72 - hours period were measured in Switzerland (more than 250 mm: in Gadmen 320 mm, Rotschalp 283 mm, Weesen 277 mm and Amden 267 mm) (MeteoSchweiz, 2006). Also in Austria higher values than 250 mm were measured (Innerlaterns 269 mm, Ebnet 268 mm and Au 257 mm). In Germany the station Balderschwang measured 257 mm. The 72-hours precipitation from 21. - 24. August 2005 is shown in Figure 15.1.

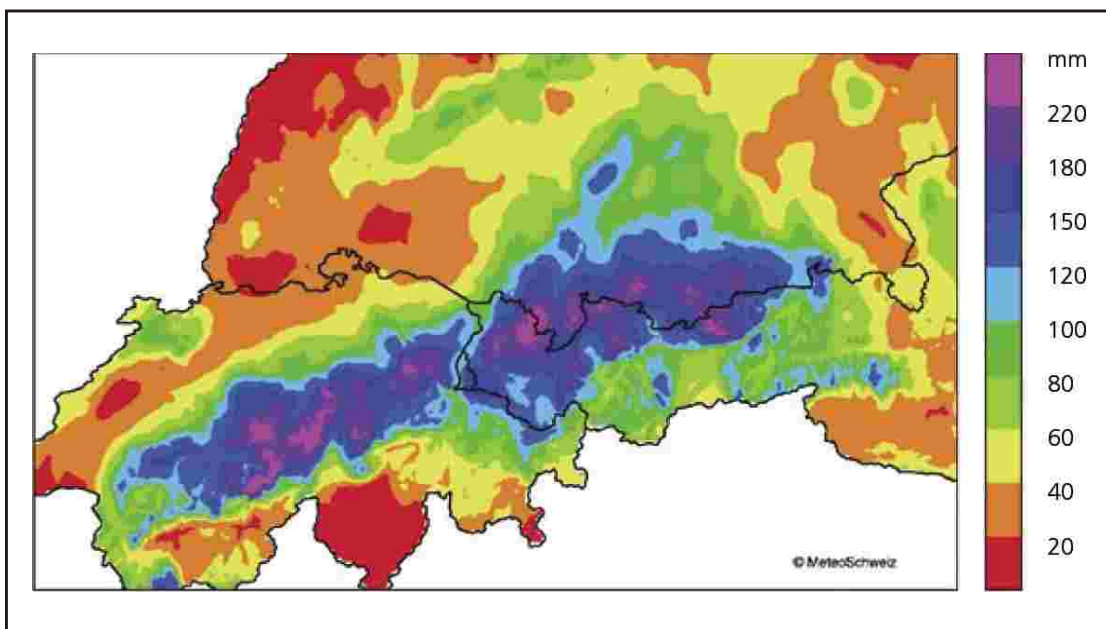


Figure 15.1: 72-hours precipitation from 21. - 24. August 2005 (source: MeteoSchweiz (2006))

After the extreme events of August 2005 a general event documentation was made for Austria (Hochwasser, 2006). Several torrents were documented by the Institute of Mountain Risk Engineering at the University of Natural Resources and Applied Life Sciences, Vienna (Hübl et al., 2005). Detailed investigations including a reconstruction

of the flood hydrograph and the sediment budget along the whole channel were made for the Sesslabach and Schnannerbach in Tyrol and for the Suggadinbach in Vorarlberg. All these torrents produced severe damages, because of massive bedload transport during the flood event. In Switzerland detailed investigations for the Chirel mountain stream (LLE-Diemtingtal, 2006), the Chiene mountain stream (LLE-Reichenbach, 2006) and the Schwarze Lutschine mountain stream (LLE-Lutschine, 2007) are available, and a general documentation of the flood events was prepared (Bezzola and Hegg, 2007, 2008).

15.1 Sesslabach

The torrent Sesslabach is a tributary to the river Trisanna in the valley Paznauntal in Tyrol. The catchment area is about 9.9 km^2 and the main channel is about 4 km long. The mean slope is 0.25 and the steepest parts are the middle reaches with channel gradients up to 0.4. The slope of the fan is 0.18. An overview of the catchment area is shown in Figure 15.2. The grain size distribution was estimated with line by number analysis and evaluated after Fehr (1987). The grain size distributions of different river reaches are shown in Figure 15.3. For the spatial discretisation every cross section in homogeneous regions was measured in the field.

The precipitation gauge recorded 125 mm for the 22. of August with intensities up to $0.4 \text{ mm}/\text{min}$. During 3 days before the event 40.8 mm of rain were measured in the catchment. According to the geostatistical analysis including all surrounding precipitation gauges the mean precipitation for the whole catchment was 119 mm for the day of the event. No streamflow measurements are available for this channel. Therefore the input hydrographs needed for SETRAC were generated with the Hydrologic Modelling System HEC-HMS. Data from a precipitation gauge situated in the catchment, which delivers data in one minute resolution, were used. The simulated peak discharge was calibrated with reconstructed values of the peak discharge at several appropriate cross sections. The catchment was separated into four sub catchments. The time evolution was calibrated with observations from the local habitants. The resulting hydrographs were attached to the related nodes in the SETRAC model. The duration of the whole event was 24 hours with a peak discharge of about $25 \text{ m}^3/\text{s}$ at the fan apex. Parameters for the precipitation discharge simulation are given in Appendix B.

About $16\,000 \text{ m}^3$ of bedload (without pore volume and fine sediment transported as wash load, see Chapter 13.2.1) were mobilized. The sediment transport was surveyed in the field (Hochwasser, 2006) in order to be compared with SETRAC calculations. The accumulated erosion and deposition volumes are shown in Figure 15.4. On the fan $8\,000 \text{ m}^3$ of bedload were deposited. Notwithstanding the steep slope of the channel no signs of debris flow occurrence were found in the catchment. Nevertheless high sediment concentrations comparable to a debris flood (Hungr, 2005) can have developed during the event in the steep middle reaches.

A public school, two bridges and a road were destroyed by the flood event. Several other buildings and two more bridges were damaged. In the channel there were no constructions like check dams built by the Austrian Forrest Technical Service for Torrent and Avalanche Control before the event. There are no recorded historical events for this

catchment.

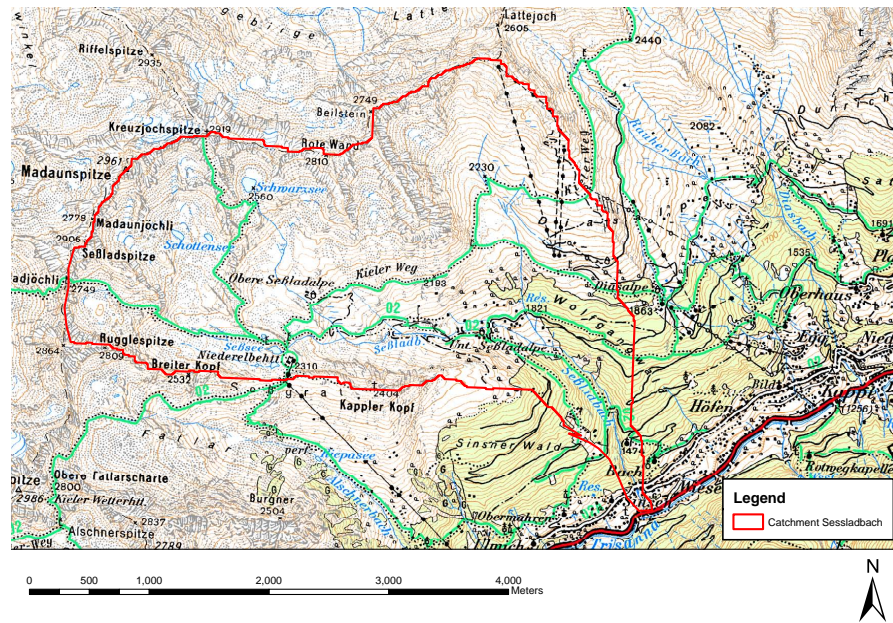


Figure 15.2: Overview Sessladbach project area

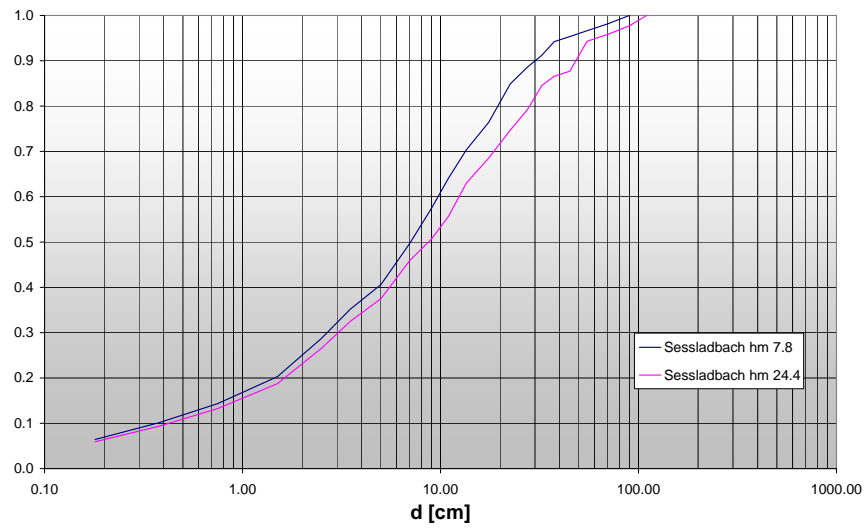


Figure 15.3: Grain size distribution for the Sesslabach project

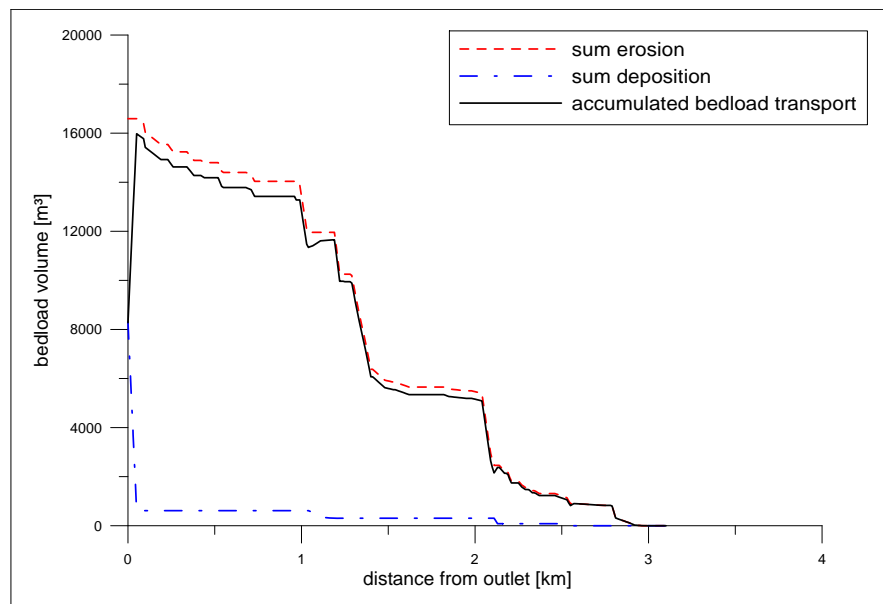


Figure 15.4: Accumulated bedload transport for the Sesslabach case study

15.1.1 Simulations of the Sesslabach extreme event

For the simulations the main channel of the Sesslabach was considered. The total modelled length is 3.0 *km*. The input hydrographs were located according the sub-catchments. A total event duration of 47 hours was modelled for the different simulation design cases.

The longitudinal profile and the related slope in the sections as well as the possible erosion depth is shown in Figure 15.5. Figure 15.6 shows the hydrograph at at the fan apex. The critical discharge is calculated with Equation 6.36 and the increased incipient motion condition due to armouring is calculated with Equation 6.39. The critical discharge is also calculated with Equation 6.37 for comparison. The slope of the considered cross-section is 0.20 and the active channel width is 5.5 *m*.

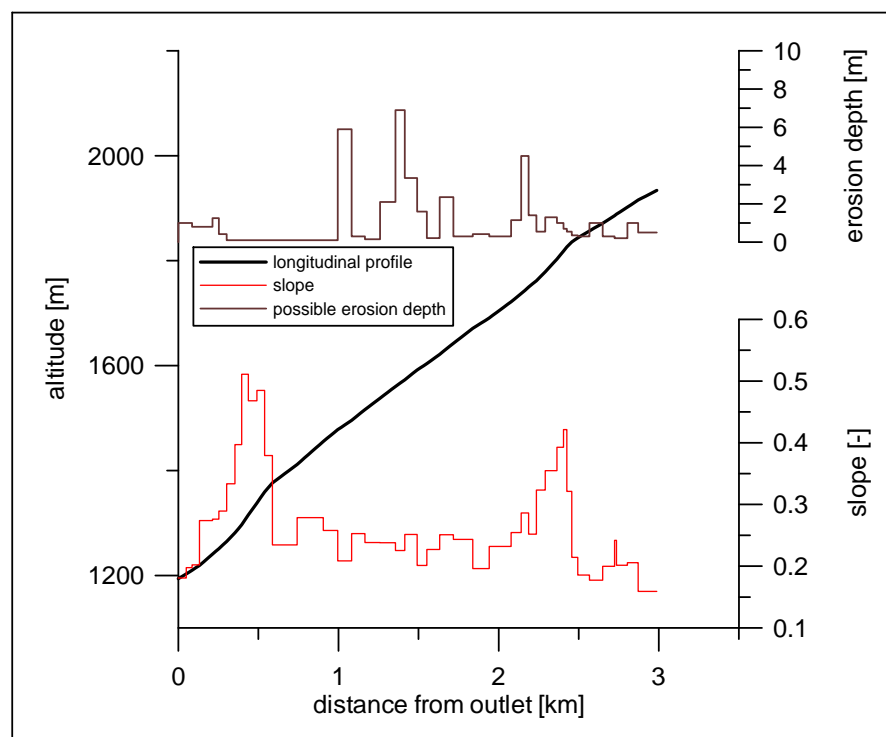


Figure 15.5: Longitudinal profile of the Sesslabach with slope and possible erosion depth for each section

Figures 15.7 to 15.11 show comparisons of SETRAC simulations with accumulated bedload transport recalculated from the field investigation. The time integrated bedload transport volumes are shown for the main channel.

The simulations without consideration of form roughness losses are shown in Figure 15.7. The simulations S1 and S7 give the same results and overestimate the recalculated bedload transport. All the sediment stock is depleted. The simulation S2 with the higher critical discharge compared to S1 and S7 is slightly lower, but still overestimates the total amount of bedload transported during the extreme event. In some reaches in the upper catchment no bedload transport is calculated, where bedload transport was observed. For the upstream reaches the initiation of motion criteria appears to be too

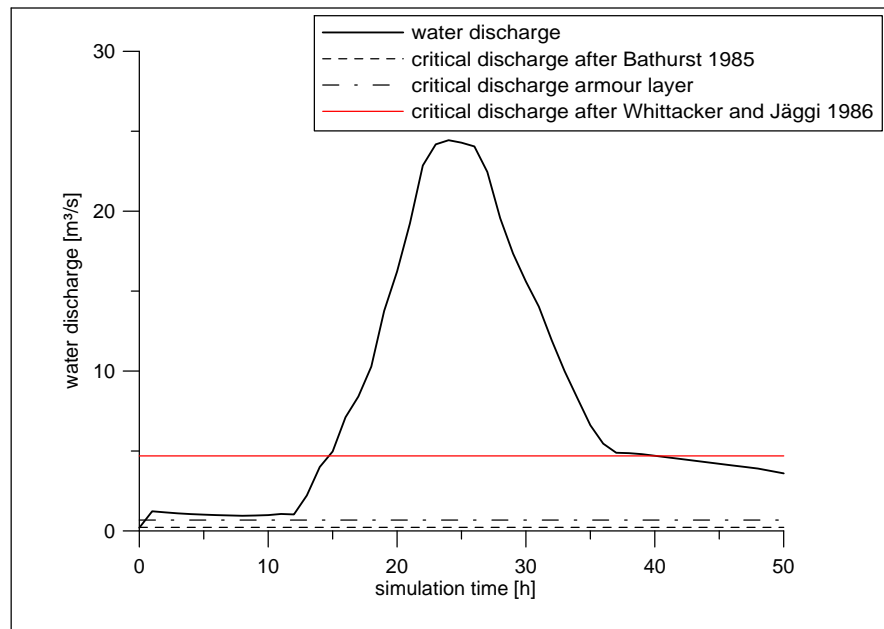


Figure 15.6: Hydrograph and related critical discharge values for a cross-section at fan apex of the Sesslabach ($S = 0.20$ and $W = 5.5$ m).

high.

Considering an armour layer criteria (Figure 15.8) The simulations S3 and S8 overestimate the total bedload transport. All sediment stock is depleted during the simulation, except at some milder downstream reaches in simulation S8.

The simulations S4 and S9 (Figure 15.9) consider a moderate reduction of the energy slope due to form roughness losses and still overestimate the reconstructed bedload transport. Again, nearly all the stock in the reaches is depleted. With a higher general reduction the modelled bedload transport is comparable with the observed amount of bedload transported by the extreme event, as shown by the simulations S5 and S10 in Figure 15.20. Both simulations underestimate the bedload transport in the downstream reaches.

A variable reduction of the energy slope available for bedload transport is applied for the simulations S6 and S11 (Figure 15.11). The exponent a was optimized to find best agreement between observed and reconstructed bedload volumes, resulting in values $1.3 < a < 1.7$. Thereby the total amount of transported bedload material for the simulation S6 is comparable to the reconstructed bedload transport caused by the August 2005 flood event. With the same reduction the simulation S11 results in slightly lower bedload transport.

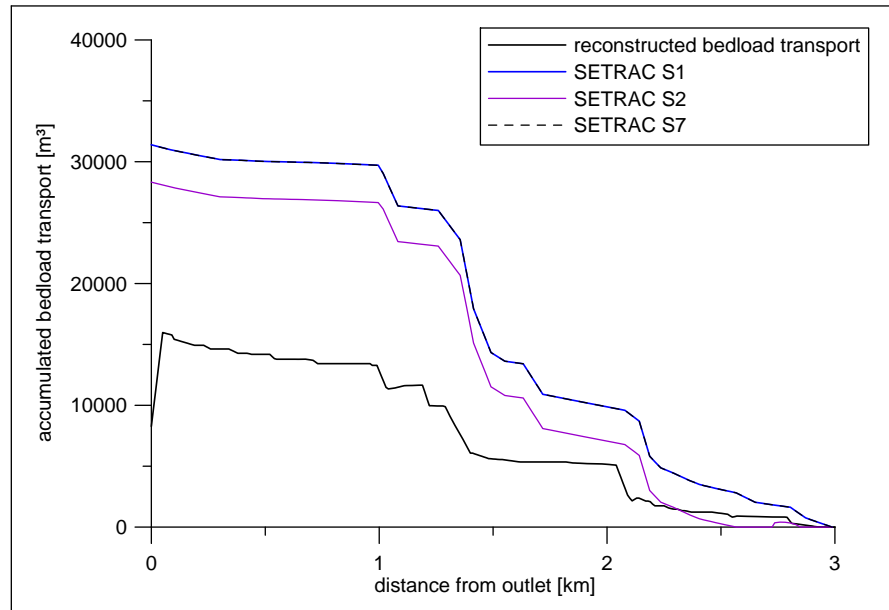


Figure 15.7: Comparison of the reconstructed bedload transport and SETRAC simulations for the cases Sesslabach S1, S2 and S7

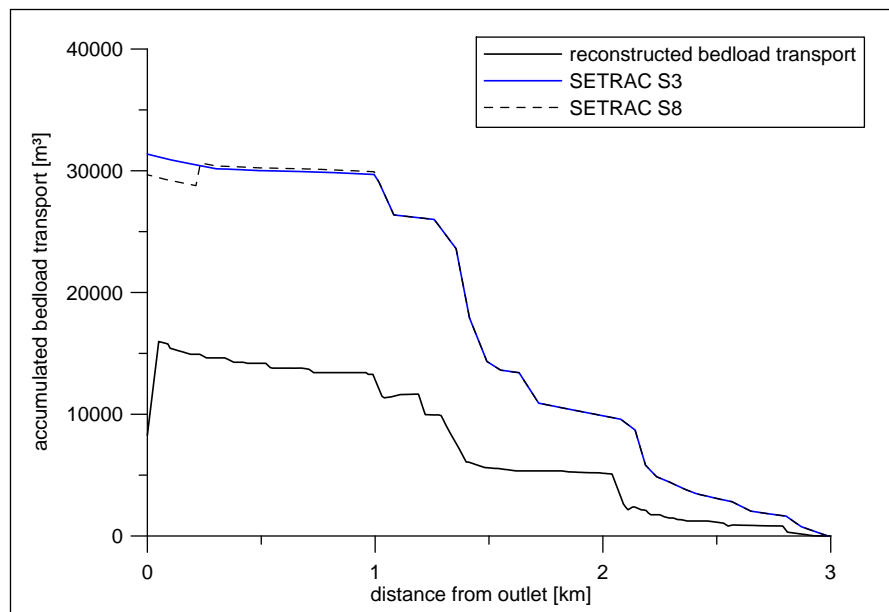


Figure 15.8: Comparison of the reconstructed bedload transport and SETRAC simulations for the cases Sesslabach S3 and S8

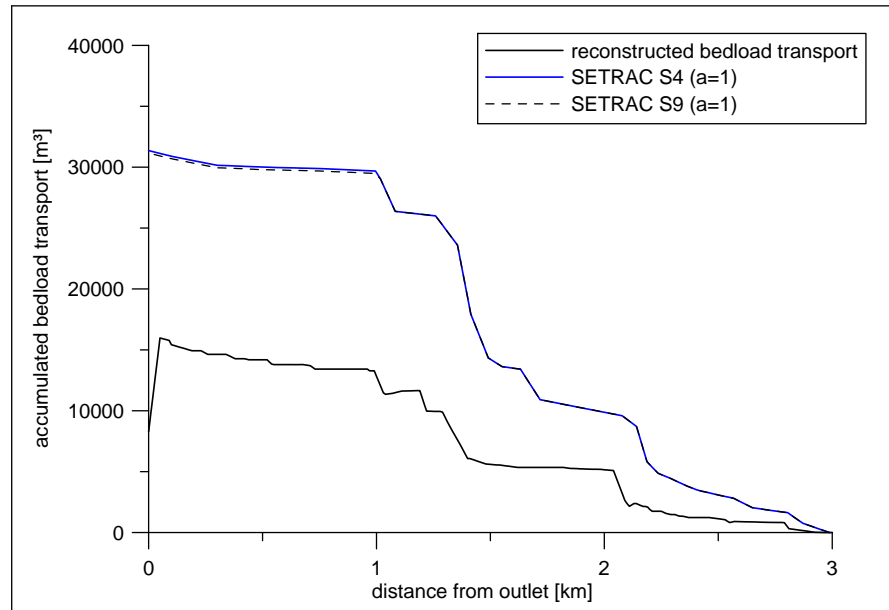


Figure 15.9: Comparison of the reconstructed bedload transport and SETRAC simulations for the cases Sessladbach S4 and S9

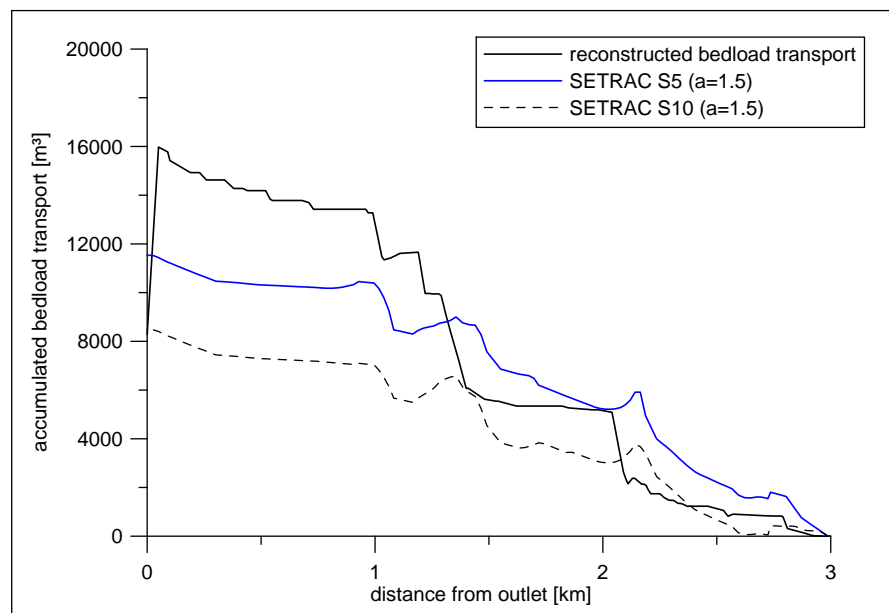


Figure 15.10: Comparison of the reconstructed bedload transport and SETRAC simulations for the cases Sessladbach S5 and S10

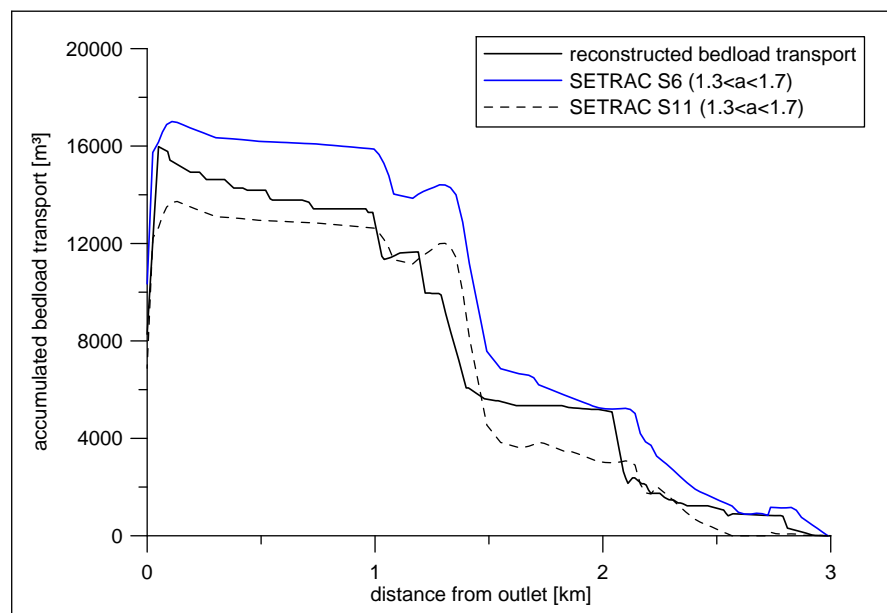


Figure 15.11: Comparison of the reconstructed bedload transport and SETRAC simulations for the cases Sesslabach S6 and S11

15.2 Schnannerbach

The second well documented torrent presented in this study is the Schnannerbach in Tyrol. The Schnannerbach is a tributary of the river Rosanna in the valley Stanzertal and has a catchment area of 6.3 km^2 and a mean channel gradient of 0.24. The steepest reaches are 0.37 and the slope on the fan is 0.10. The main channel is about 3 km long with several sources in the upstream reaches. An overview of the catchment area is shown in Figure 15.12.

The closest precipitation gauge (Flirsch) recorded 120 mm for the 22. of August. During 3 days before the event 40.8 mm of rain were measured at this station. According to the geostatistical analysis including all surrounding precipitation gauges the mean precipitation for the whole catchment was 125 mm for the day of the event. No streamflow measurements are available for Schnannerbach. That is why the input hydrographs needed for SETRAC were generated with the Hydrologic Modelling System HEC-HMS. Data from precipitation gauges situated around the catchment were used. The simulated peak discharge was calibrated with reconstructed values of the peak discharge at several appropriate cross sections. The catchment was separated into seven sub catchments. The time evolution was calibrated with observations from the local habitants and records from the fire brigade. The resulting hydrographs were attached to the related nodes in the SETRAC model. The duration of the whole event was 24 hours with a peak discharge of about $24 \text{ m}^3/\text{s}$ at the fan apex. Parameters for the precipitation discharge simulation are given in Appendix B. No stream flow measurements are available for this torrent.

About $30\,000 \text{ m}^3$ of bedload were mobilized during the extreme event. In the upstream catchment sediment supply from the hill slopes is nearly unlimited. The middle reaches are mainly in bedrock with sediment supply from side erosion. The last 200 m upstream the fan are formed by an impressive gorge. About $18\,000 \text{ m}^3$ of bedload were deposited on the inhabited fan (Hochwasser, 2006).

A business enterprise was destroyed by the flood event. Several other buildings were damaged. The channel was regulated on the fan by the Austrian Forrest Technical Service for Torrent and Avalanche Controll. In the catchment there is a big check dam which retained $9\,000 \text{ m}^3$. The sediment erosion and deposition was mapped in the field after the event in order to be compared with SETRAC calculations. Notwithstanding the steep slope of the channel no signs of debris flow occurrence were found in the catchment. Nevertheless high sediment concentrations comparable to a debris flood (Hungry, 2005) can have developed during the event in certain reaches.

The longitudinal profile and representative cross-sections were also surveyed. For the spatial discretisation every cross section in homogeneous regions was measured in the field. Grain size analysis were made with line by number sampling and evaluated after Fehr (1987) and are shown in Figure 15.13. The accumulated erosion and deposition volumes are shown in Figure 15.14 (without pore volume and fine sediment transported as washload, see Chapter 13.2.1).

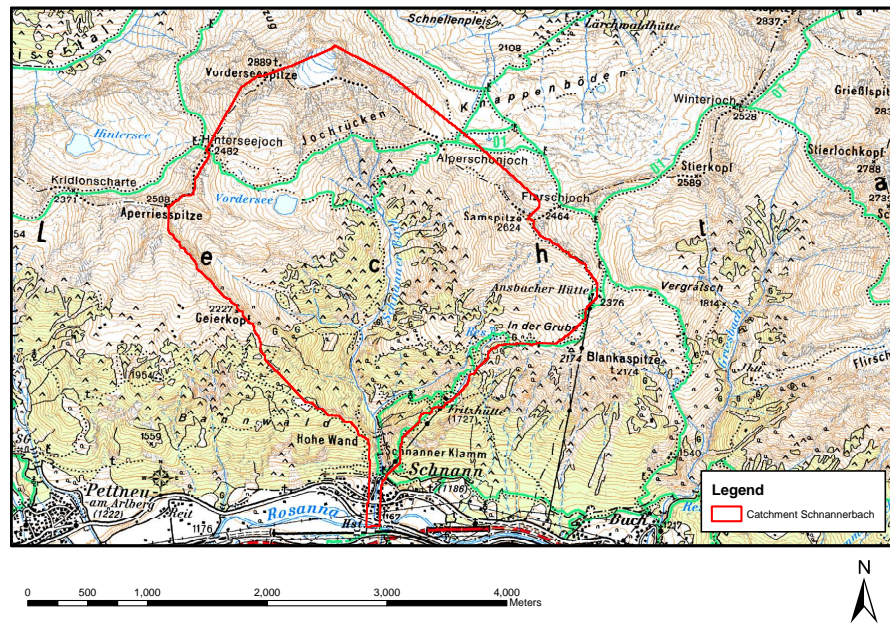


Figure 15.12: Overview Schnannerbach project area

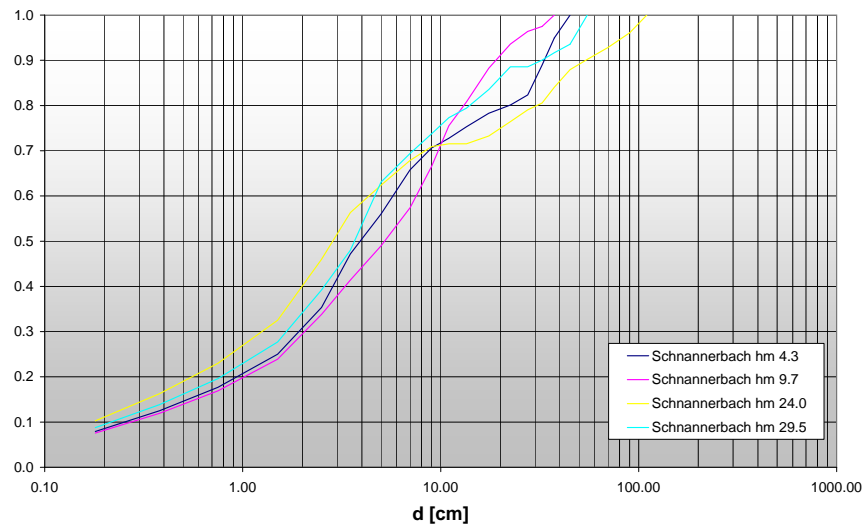


Figure 15.13: Grain size distribution for the Schnannerbach project

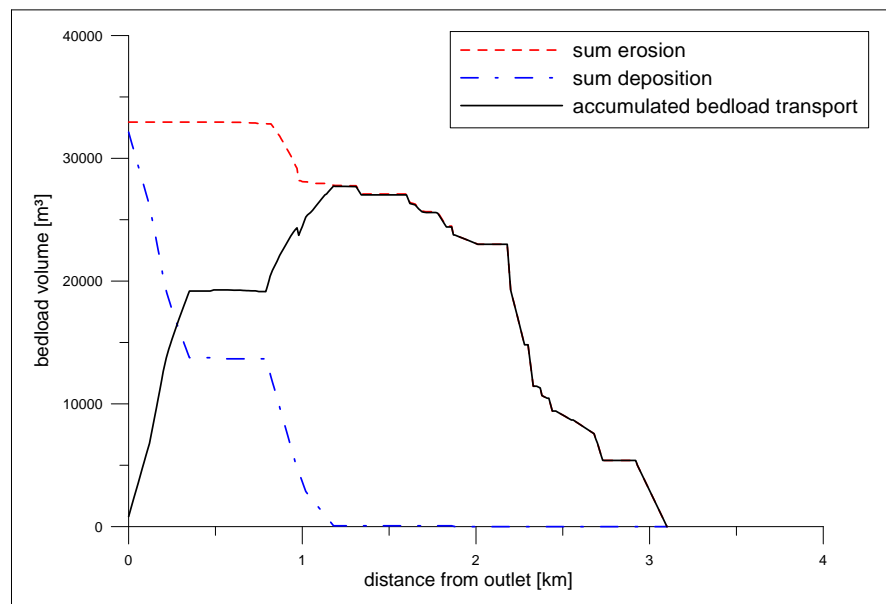


Figure 15.14: Accumulated bedload transport for the Schnannerbach case study

15.2.1 Simulations of the Schnannerbach extreme event

For the simulations the main channel of the Schnannerbach was considered. The total modelled length is 3.1 *km*. The input hydrographs were located according the sub-catchments. A total event duration of 35 hours was modelled for the different simulation design cases.

The longitudinal profile and the related slope in the sections as well as the possible erosion depth is shown in Figure 15.15. Figure 15.16 shows the hydrograph at at the fan apex. The critical discharge is calculated with Equation 6.36 and the increased incipient motion condition due to armouring is calculated with Equation 6.39. The critical discharge is also calculated with Equation 6.37 for comparison. The slope of the considered cross-section is 0.12 and the active channel width is about 5 *m*.

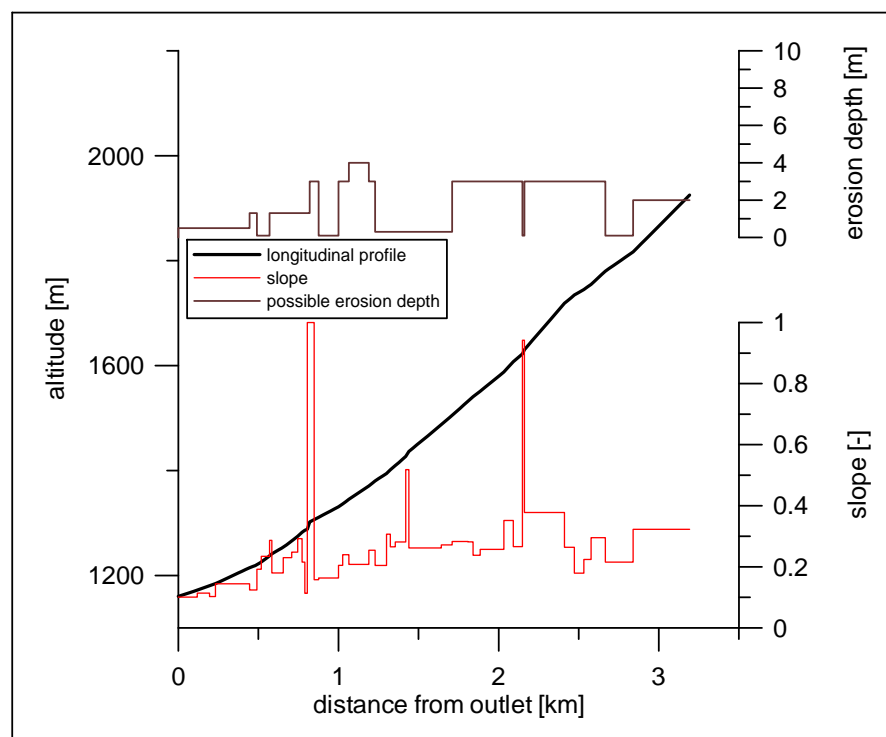


Figure 15.15: Longitudinal profile of the Schnannerbach with slope and possible erosion depth for each section

Figures 15.17 to 15.21 show comparisons of SETRAC simulations with accumulated bedload transport recalculated from the field investigation. The time integrated bedload transport volumes are shown for the main channel.

The simulations without consideration of form roughness losses are shown in Figure 15.17. The simulations S1 and S7 show comparable results and overestimate the recalculated bedload transport. All the sediment stock is depleted with simulation S7. The simulation S2 with the higher critical discharge compared to S1 partly overestimates the observed bedload transport, but in several reaches the initiation of motion criteria appears to be too high and therefore the observed accumulated of bedload transport is underestimated.

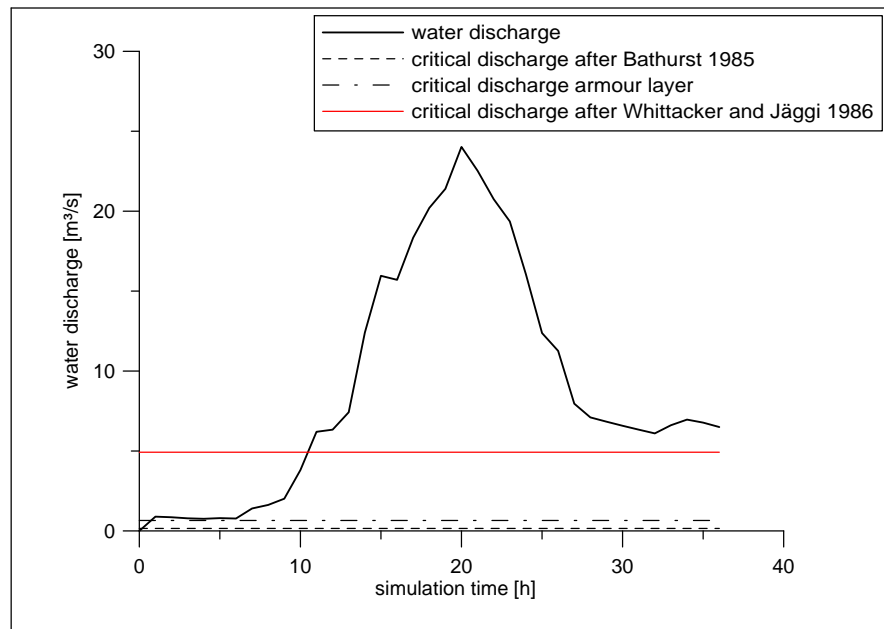


Figure 15.16: Hydrograph and related critical discharge values for a cross-section at fan apex of the Schnannerbach ($S = 0.20$ and $W = 5.5$ m).

Considering an armour layer criteria (Figure 15.18) the simulations S3 and S8 overestimate the total bedload transport. All sediment stock is depleted during the simulation and the results are comparable to simulation S1 and S3. The only difference is that the sediment stock is depleted a bit earlier without consideration of the armour layer criteria.

The simulations S4 and S9 (Figure 15.19) consider a moderate reduction of the energy slope due to form roughness losses and are in the same order of magnitude as the observed badload transport. With a higher general reduction the modelled bedload transport is underestimated, as shown by the simulations S5 and S10 in Figure 15.20.

A variable reduction of the energy slope available for bedload transport is applied for the simulations S6 and S11 (Figure 15.21). The exponent a was optimized to find best agreement between observed and reconstructed bedload volumes, resulting in values $1.0 < a < 1.2$. Thereby the total amount of transported bedload material for the simulation S6 is comparable to the reconstructed bedload transport caused by the August 2005 flood event. With the same reduction the simulation S11 slightly underestimates the total bedload transport.

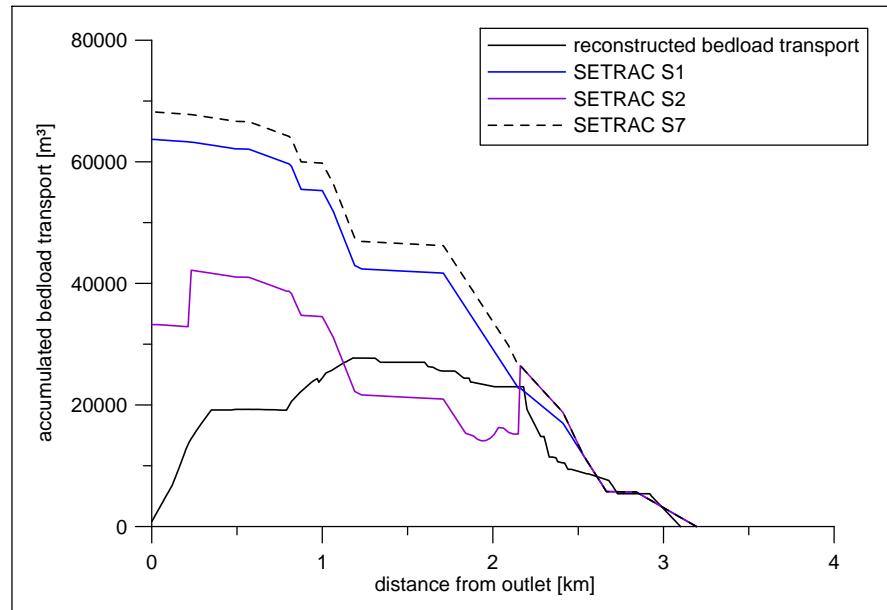


Figure 15.17: Comparison of the reconstructed bedload transport and SETRAC simulations for the cases Schnannerbach S1, S2 and S7

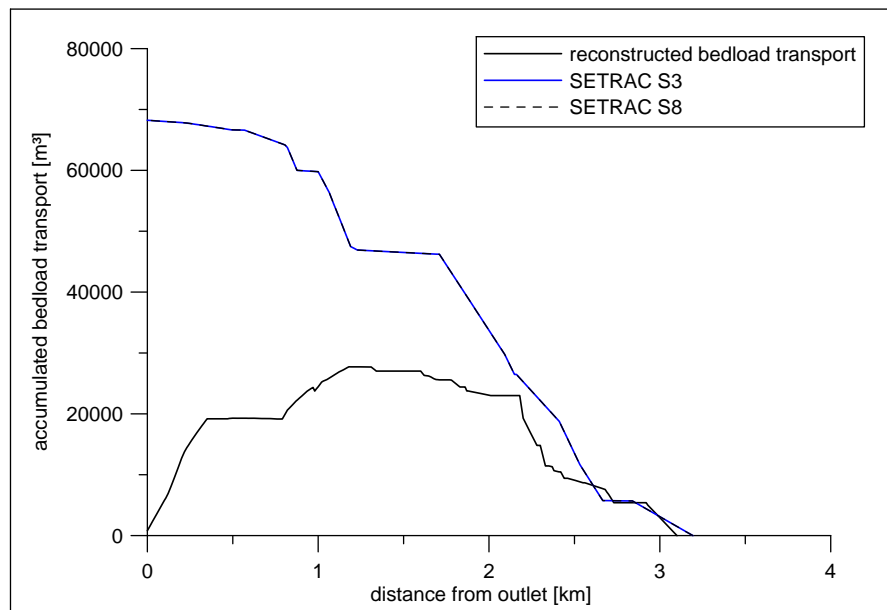


Figure 15.18: Comparison of the reconstructed bedload transport and SETRAC simulations for the cases Schnannerbach S3 and S8

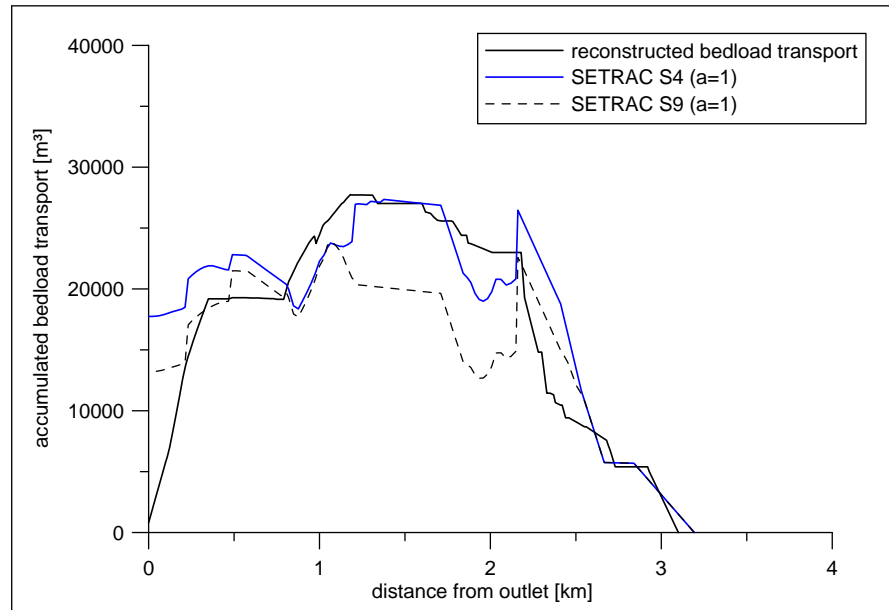


Figure 15.19: Comparison of the reconstructed bedload transport and SETRAC simulations for the cases Schnannerbach S4 and S9

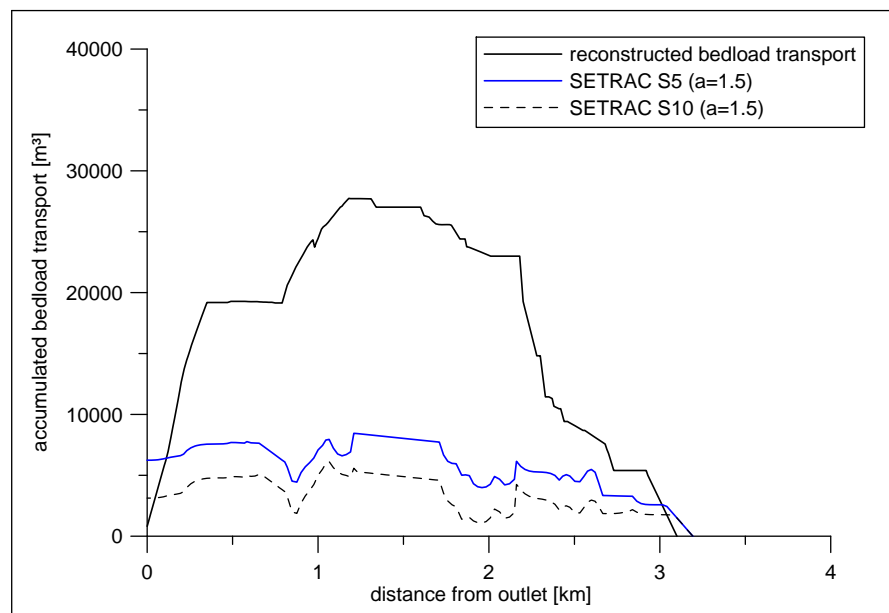


Figure 15.20: Comparison of the reconstructed bedload transport and SETRAC simulations for the cases Schnannerbach S5 and S10

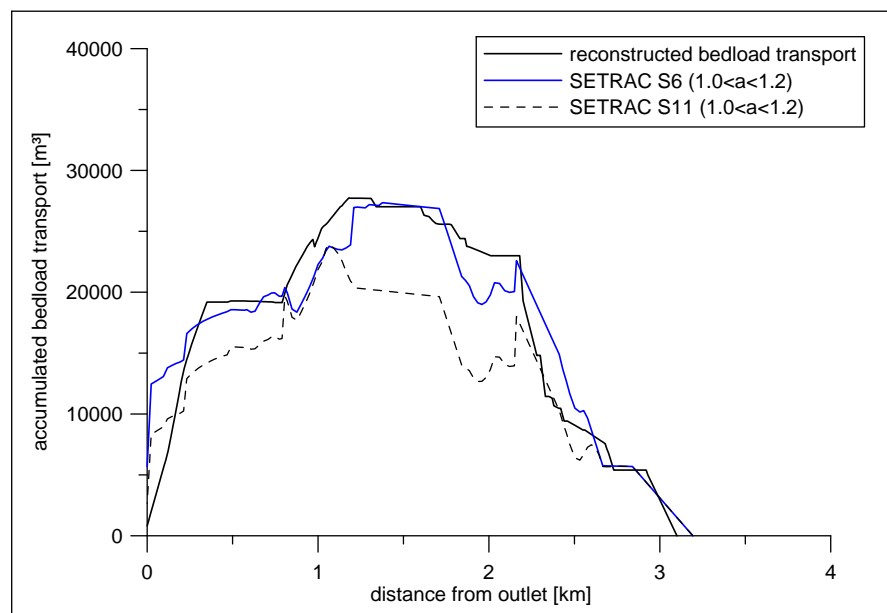


Figure 15.21: Comparison of the reconstructed bedload transport and SETRAC simulations for the cases Schnannerbach S6 and S11

15.3 Suggadinbach

The catchment of the Suggadin mountain stream was also affected by the severe flood events of August 2005. The catchment is situated in the western part of Vorarlberg with an catchment area of about 75 km^2 . The main channel in the catchment is the Suggadin mountain stream. Figure 15.22 shows the catchment area. The length of the main channel is about 8.7 km . The mean channel gradient is 0.075. The channel slope varies from 0.01 to 0.20.

For the Suggadin mountain stream, there are two stream flow gauges available, but the measurements are not reliable for the August 2005 event. Therefore a back calculation of the discharge was made (Chiari et al., 2008). The peak discharge was recalculated for cross-sections with minor morphologic changes and the time evolution of the flood event was taken from the discharge measurements. The back calculated peak discharge was about $100 \text{ m}^3/\text{s}$ for the channel outlet. The precipitation gauges in the catchment failed during the August 2005 flood, Therefore two gauges close to the catchment had to be used for the precipitation discharge simulation. The gauges Vermunt and Tschagguns were attached to the subcatchments according their altitude Mair (2008). The precipitation gauge Vermunt (altitude: 1733 m) recorded 115 mm for the time period from 22. to 23. of August, whereas the precipitation gauge Tschagguns (altitude: 680 m) recorded 100 mm for the same period. During 3 days before the event 40 mm of rain were measured at the station Vermunt and 35 mm at Tschagguns. To relate the back calculated discharge to subcatchments for better representation, the event was modelled with the hydrological simulation system HEC-HMS. Therefore the catchment has been subdivided into 13 subcatchments. Parameters for the precipitation discharge simulation are given in Appendix B.

In order to reconstruct the bedload transport during the extreme event airborne LiDAR data were used to determine the morphologic changes. Two high resolution elevation models for the Suggadin stream catchment were available. The first was from the year 2003 and the second was obtained shortly after the extreme event. Areas of erosion and deposition were verified with aerial photos. For each channel reach the amount of sediment eroded or deposited was calculated. These data were completed with records from Sediment dredging after the flood. It is estimated that about $50\,000 \text{ m}^3$ of bedload (without pore volume and fine sediment transported as washload, see Chapter 13.2.2) were mobilized during the flood event of August 2005 (Mair, 2008). Figure 15.24 shows the accumulated erosion and deposition volumes as well as the accumulated bedload transport for the August 2005 event. Grain size analysis were made by line by number analysis and evaluated after Fehr (1987). The grainsize distribution for the Suggadinbach is presented in Figure 15.23.

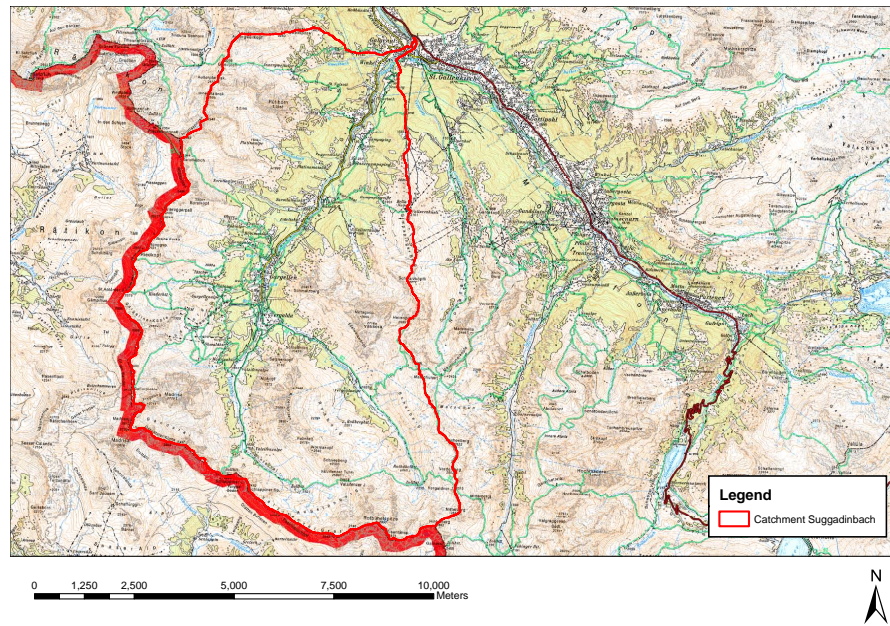


Figure 15.22: Overview Suggadin project area

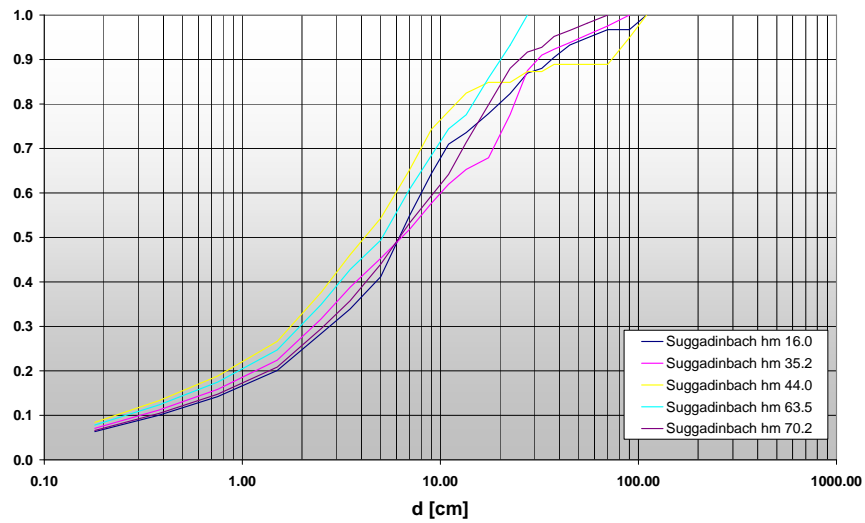


Figure 15.23: Grain size distribution for the Suggadinbach project

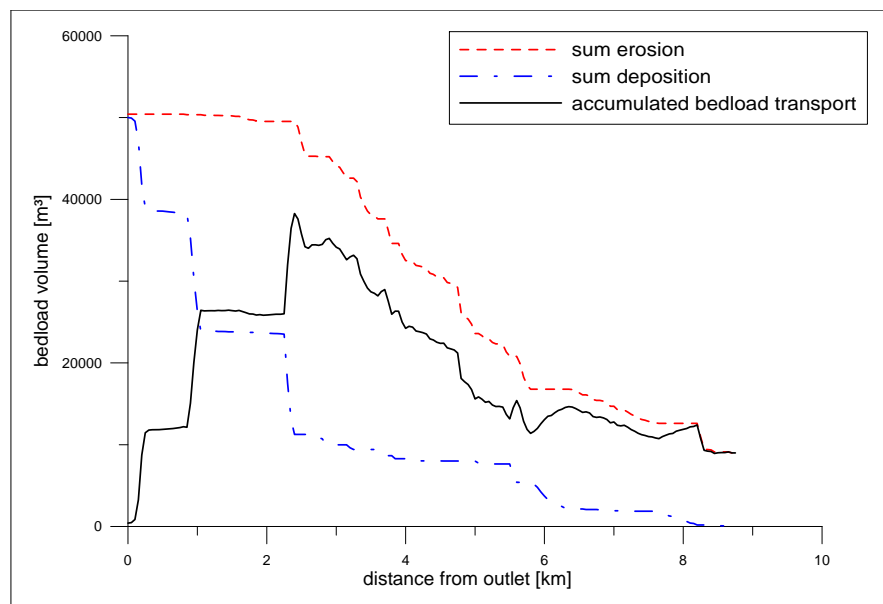


Figure 15.24: Accumulated bedload transport for the Suggadinbach case study

15.3.1 Simulations of the Suggadinbach extreme event

For the simulations the main channel of the Suggadin mountain stream was considered. For the spatial discretisation all cross sections in homogenous reeches were measured from the digital elevation model which was generated by airborne LiDAR before the extreme event occurred. The total modelled length is 8.8 km. The input hydrographs were located according the subcatchments. A total event duration of 43 hours was modelled for the different simulation design cases. The longitudinal profile and the related slope in the sections as well as the possible erosion depth is shown in Figure 15.25. Figure 15.26 shows the hydrograph at km 0.46. The critical discharge is calculated with Equation 6.36 and the increased incipient motion condition due to armouring is calculated with Equation 6.39. The slope of the considered cross-section is 0.06 and the active channel width is about 12 m.

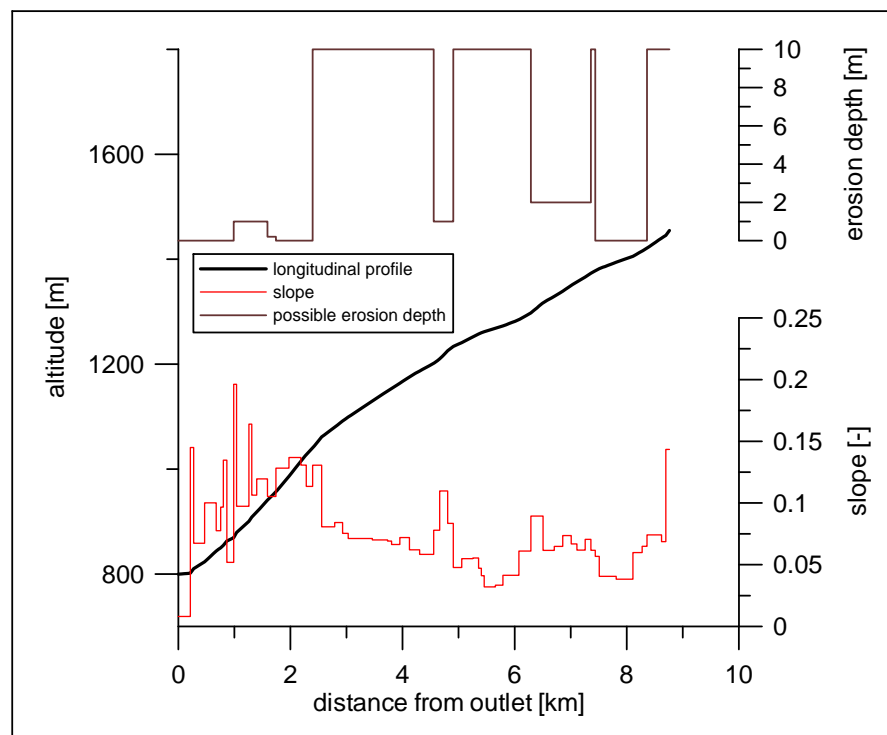


Figure 15.25: Longitudinal profile of the Suggadin mountain stream with slope and possible erosion depth for each section

Figures 15.27 to 15.31 show comparisons of SETRAC simulations with accumulated bedload transport recalculated from the morphologic changes. The time integrated bedload transport volumes are shown for the main channel.

The simulations without consideration of form roughness losses are shown in Figure 15.27. The simulations S1 and S7 show comparable results and overestimate the recalculated bedload transport. The simulation S2 with the higher critical discharge compared to S1 overestimates the observed bedload transport in most reaches, but in several reaches the initiation of motion criteria appears to be too high to allow for bedload transport and therefore the accumulated bedload transport cannot be reproduced.

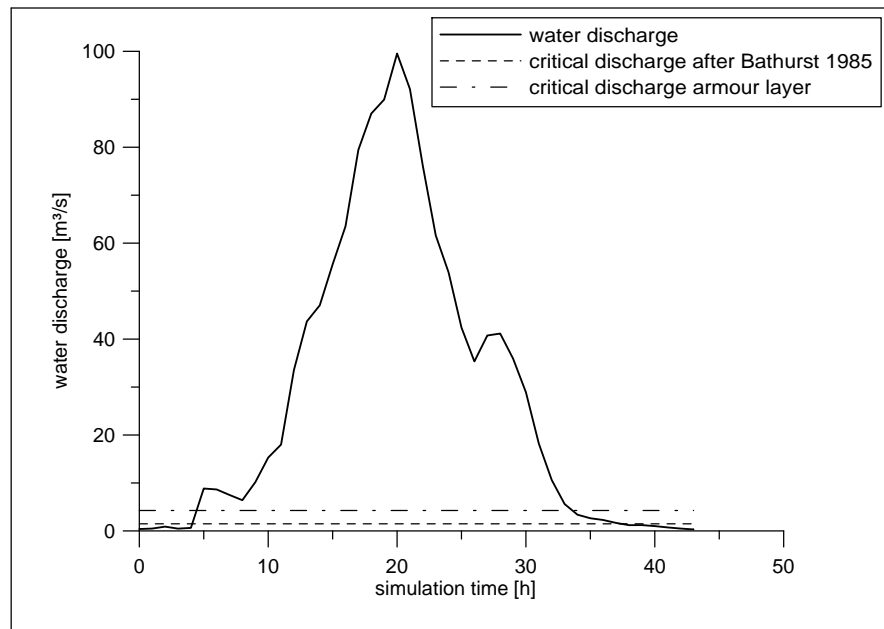


Figure 15.26: Hydrograph and related critical discharge values for a cross-section at *km* 0.5 of the Suggadinbach ($S = 0.06$ and $W = 12\text{ m}$).

Considering an armour layer criteria (Figure 15.18) the simulations S3 and S8 overestimate the total bedload transport. Compared to simulations S1 and S7 there is only a small reduction of the total amount of bedload transported during the flood event.

The simulations S4 and S9 (Figure 15.29) consider a moderate reduction of the energy slope due to form roughness losses but still overestimate the total amount of transported bedload material. With a higher general reduction the modelled bedload transport is comparable with the observed transport. The simulations S5 and S10 are shown in Figure 15.30.

A variable reduction of the energy slope available for bedload transport is applied by the simulations S6 and S11 (Figure 15.31). The exponent a was optimized to find best agreement between observed and reconstructed bedload volumes, resulting in values $1.3 < a < 1.5$. Thereby the total amount of transported bedload material for the simulation S6 is comparable to the reconstructed bedload transport caused by the August 2005 flood event. With the same reduction the simulation S11 slightly underestimates the total bedload transport.

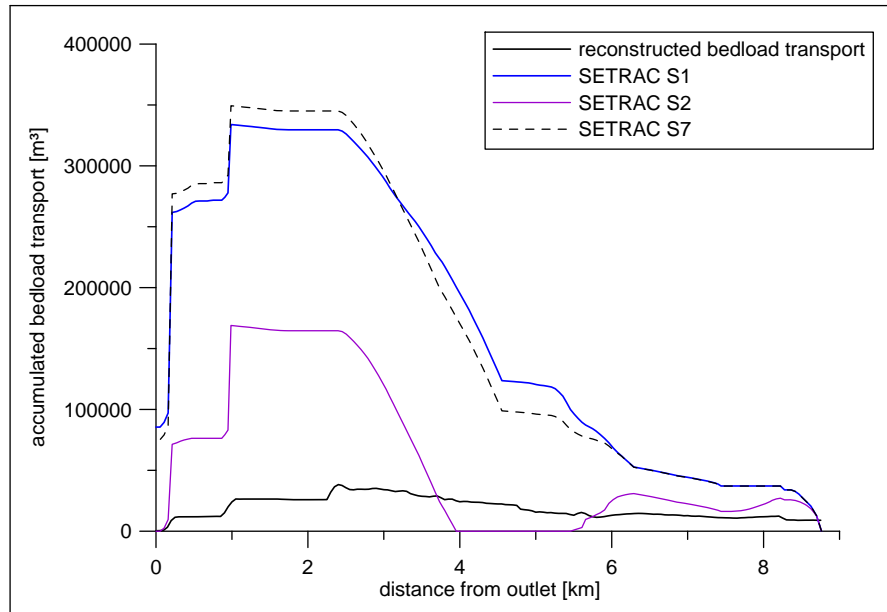


Figure 15.27: Comparison of the reconstructed bedload transport and SETRAC simulations for the cases Suggadinbach S1, S2 and S7

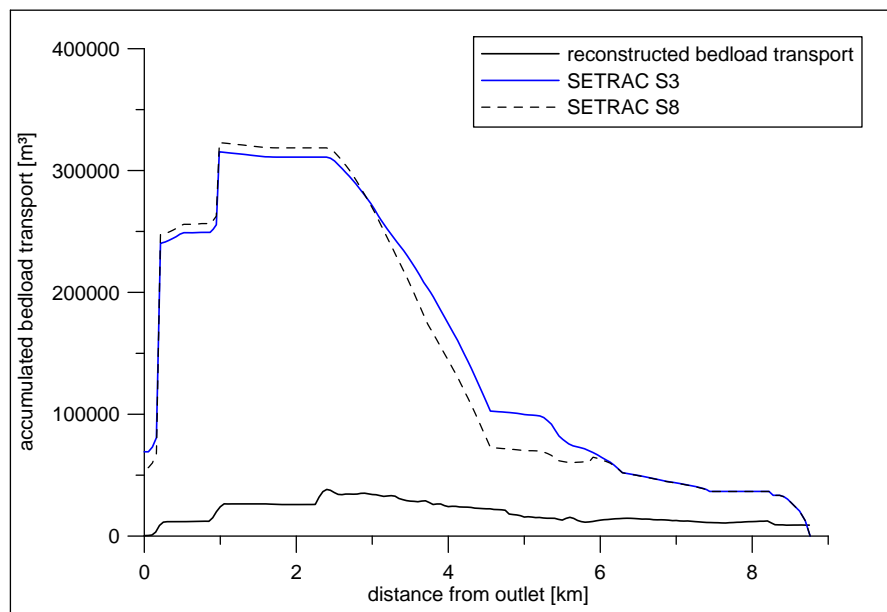


Figure 15.28: Comparison of the reconstructed bedload transport and SETRAC simulations for the cases Suggadinbach S3 and S8

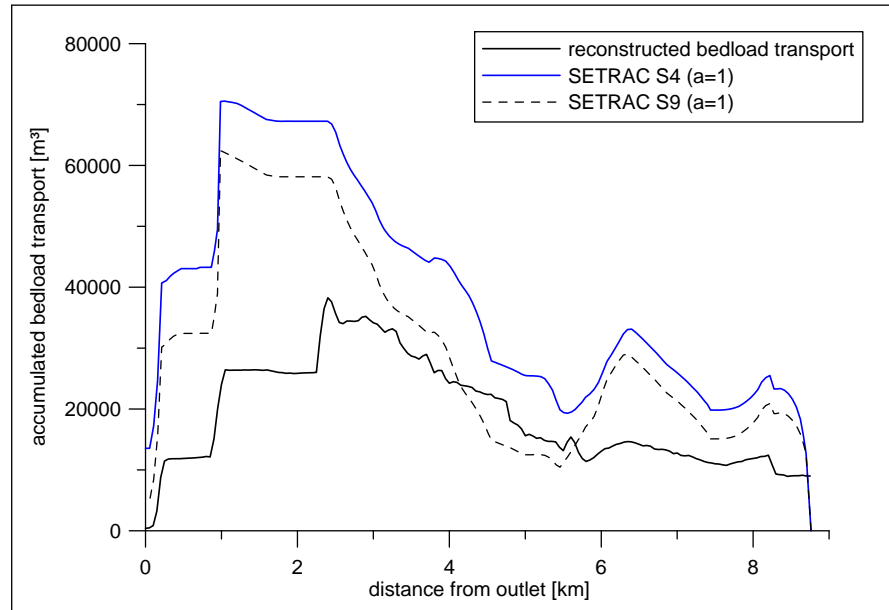


Figure 15.29: Comparison of the reconstructed bedload transport and SETRAC simulations for the cases Suggadinbach S4 and S9

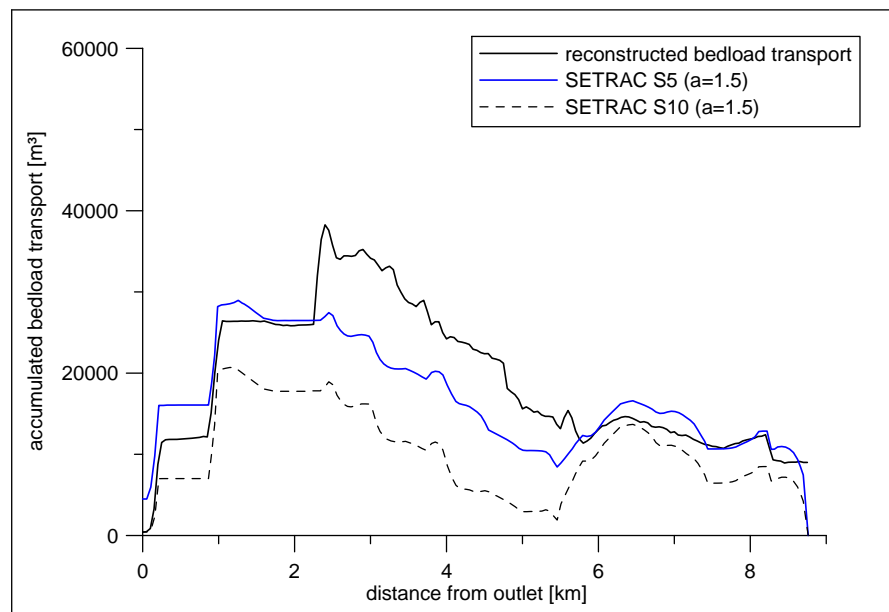


Figure 15.30: Comparison of the reconstructed bedload transport and SETRAC simulations for the cases Suggadinbach S5 and S10

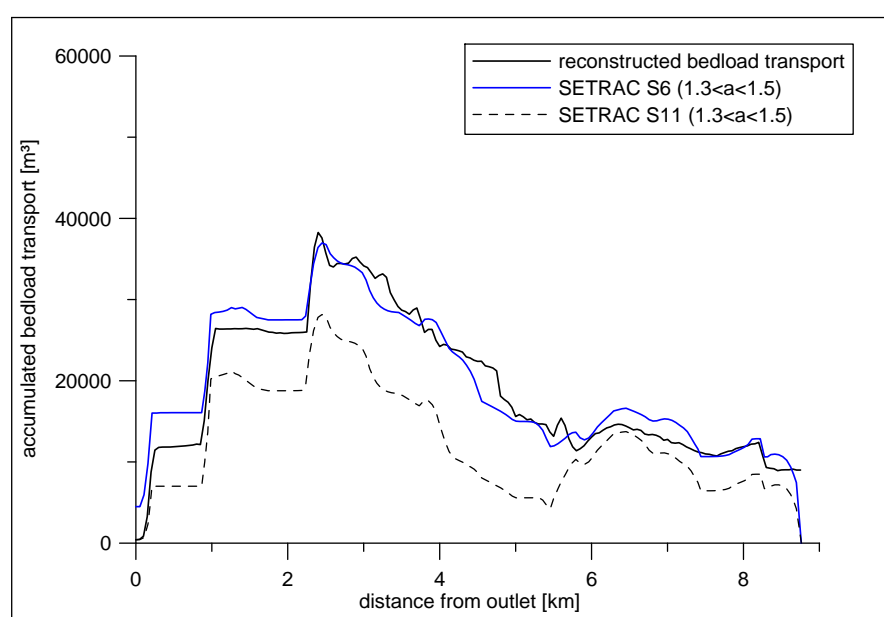


Figure 15.31: Comparison of the reconstructed bedload transport and SETRAC simulations for the cases Suggadinbach S6 and S11

15.4 Chirel

The catchment of is situated in the Canton Bern and the catchment area is 130.5 km^2 . Figure 15.32 shows the catchment area of the Chirel mountain stream. The Chirel is a mountain stream with a mean channel gradient of 0.06. The slope is ranging from 0.015 at the flattest reaches up to 0.14 in the steepest reaches. The grain size distribution was estimated with line by number analysis and evaluated after Fehr (1987). The grain size distribution of different river reaches are shown in Figure 15.33.

There are no streamflow measurements for the Chirel mountain stream, but the discharge has been reconstructed with streamflow measurements upstream and downstream of the confluence with the river Simme (LLE-Diemtital, 2006). There is one gauging station upstream (Oey) and one downstream (Latterbach) at the River Simme. The duration of the whole event was about 48 hours with a recalculated peak discharge of about $100 \text{ m}^3/\text{s}$. The catchment is surrounded by 9 precipitation gauges, but none is situated in the catchment. Therefore radar precipitation data were used in order to generate the input hydrographs needed for the SETRAC simulations. For better representation of the catchment, the area was separated into 7 subcatchments. The three days precipitation for the subcatchments of the Chirelbach varied from 149 to 172 mm . The hydrologic model HEC-HMS has been calibrated to match the reconstructed hydrograph (LLE-Diemtital, 2006). Parameters for the precipitation discharge simulation are given in Appendix B.

Airborne LiDAR data were used to determine the morphologic changes during the extreme flood event that occurred in August 2005. Two high resolution elevation models for the Chirel stream watershed were available. The first was from the year 2001 and the second was generated shortly after the extreme event. Areas of erosion and deposition were verified with aerial photos. For torrents it is generally assumed that major morphologic changes occur only during flood events. During the considered time period no other major floods occurred in the catchment. It is estimated that about $150\,000 \text{ m}^3$ of bedload (without pore volume and fine sediment transported as washload, see Chapter 13.2.2) were mobilized during the flood event of August 2005. There were several debris flow events supplying material from tributaries to the Chirel mountain stream. The reconstructed accumulated bedload transport is shown in Figure 15.34.

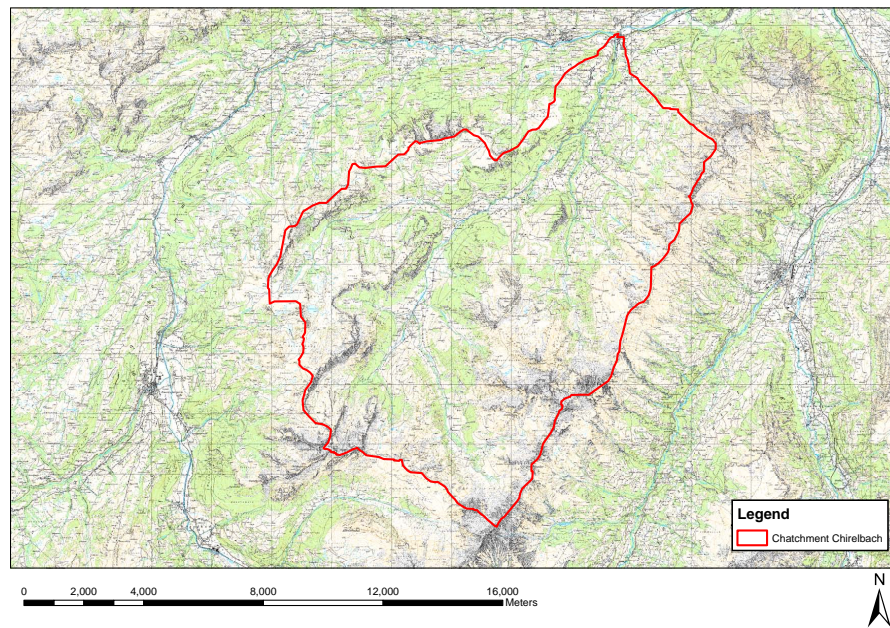


Figure 15.32: Overview Chirelbach project area

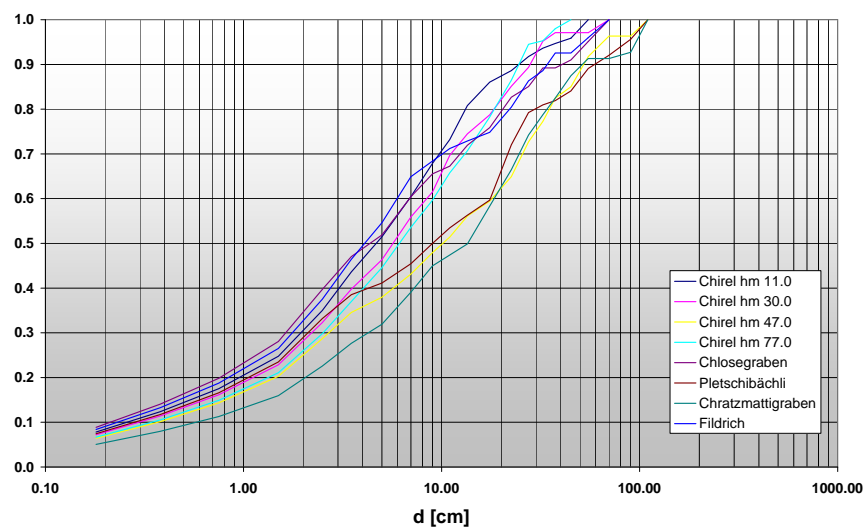


Figure 15.33: Grain size distribution for the Chirel project

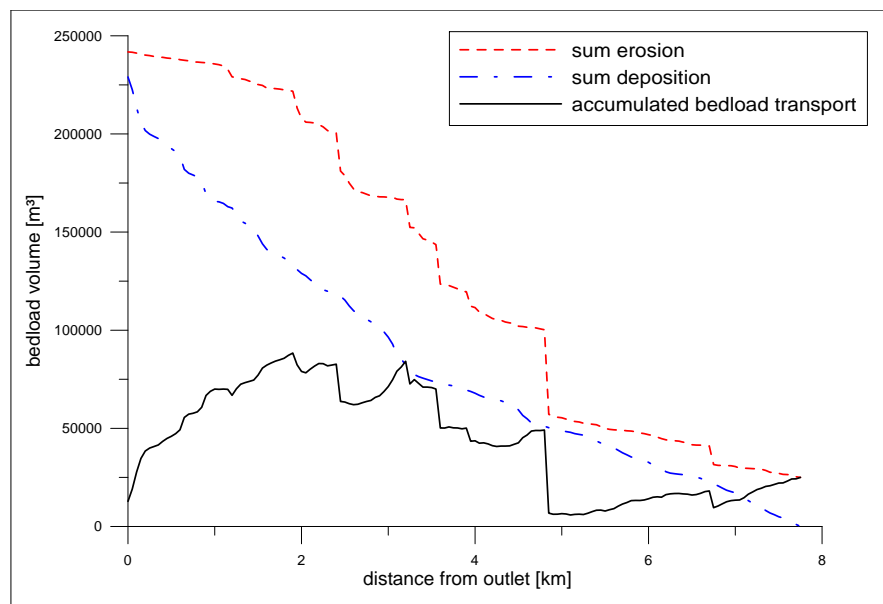


Figure 15.34: Accumulated bedload transport for the Chirelbach case study

15.4.1 Simulations of the Chirel extreme event

For the simulations the Chirel mountain stream as well as sediment input from side channels were considered. The sediment input from the tributaries was in the form of debris flow events. The debris flow volumes were considered as sedigraphs in the affected channel reaches. The volumes of the debris flows were determined by analysis of the morphologic changes in the tributaries. They were considered as triangular shaped sedigraphs with a duration of 15 minutes, triggered by the highest rainfall intensities in the catchment. More information about these debris flow sediment inputs is not available. For the spatial discretisation every 50 m a cross section was measured from the digital elevation model obtained from airborne LiDAR data for the simulation before the extreme event occurred. The total modelled length is 7.8 km. The input hydrographs were located according to the subcatchments. A total event duration of 59 hours was modelled for the different simulation design cases. The longitudinal profile and the related slope in the sections as well as the possible erosion depth is shown in Figure 15.35. Figure 15.36 shows the hydrograph at km 1.2 where the main deposition started. The critical discharge is calculated with Equation 6.36 and the increased incipient motion condition due to armoring is calculated with Equation 6.39. The slope of the considered cross-section is 0.024 and the active channel width is about 15 m.

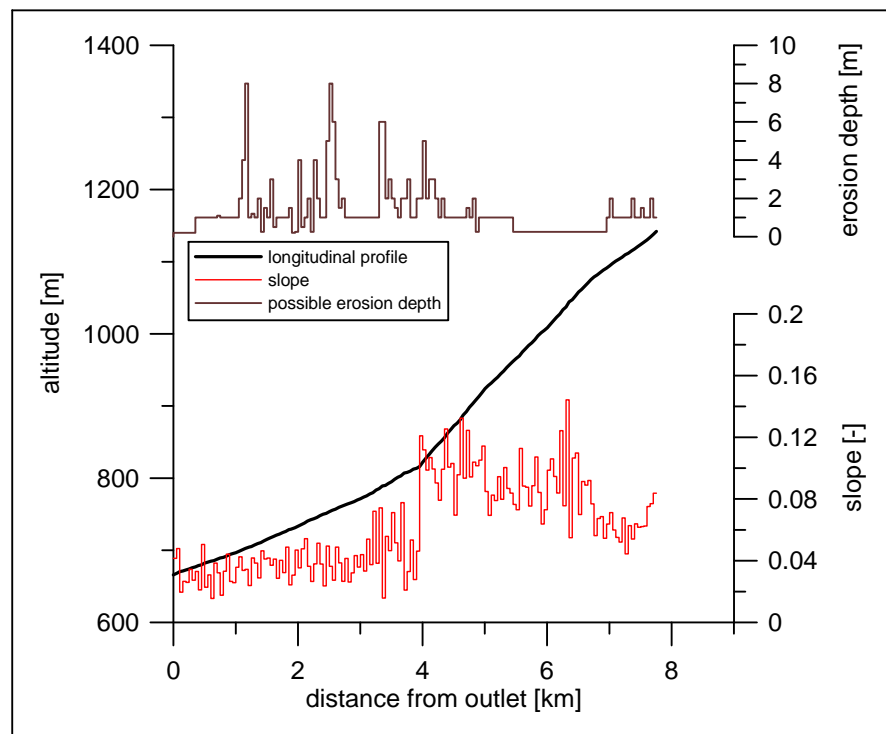


Figure 15.35: Longitudinal profile of the Chirel mountain stream with slope and possible erosion depth for each section

Figures 15.37 to 15.49 show comparisons of SETRAC simulations with accumulated bedload transport recalculated from the morphologic changes. The time integrated bedload transport volumes are shown for the main channel.

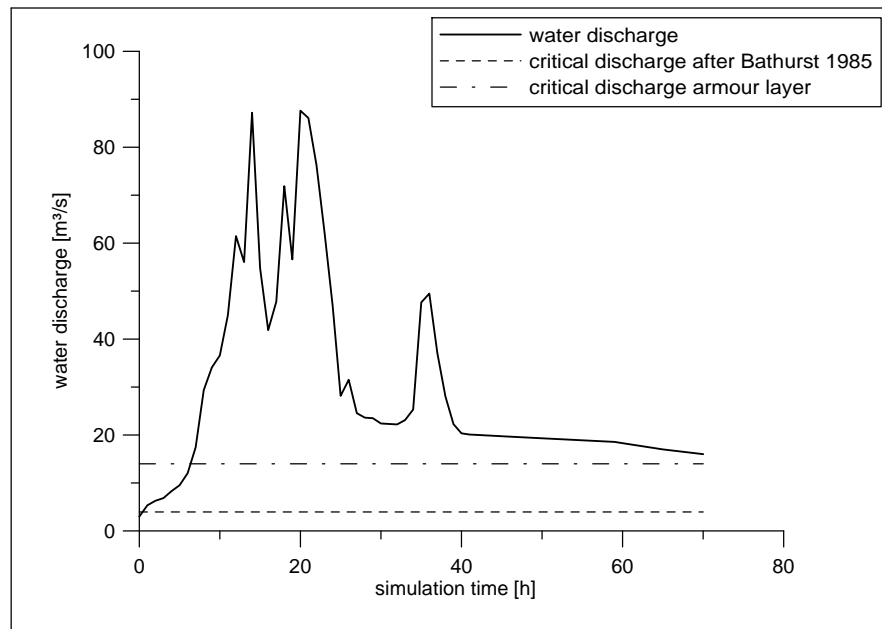


Figure 15.36: Hydrograph and related critical discharge values for a cross-section at *km* 1.2 of the Chirel mountain stream ($S = 0.026$ and $W = 15\text{ m}$).

The simulations without consideration of form roughness losses are shown in Figure 15.37. The simulations S1 and S7 show comparable results and overestimate the recalculated bedload transport. The simulation S2 with the higher critical discharge compared to S1 underestimates the bedload transport and in several reaches the incipient of motion criteria appears to be too high to allow for bedload transport at all.

Considering an armour layer criteria (Figure 15.38) The simulations S3 and S8 are in good accordance with the reconstructed bedload transport. The increase of the critical discharge (S3) or the critical shear stress (S8) reduces the transported bedload volumes compared to simulation S1 and S7 (Figure 15.37) and can be regarded as best fit simulations for the Chirel mountain stream.

The simulations S4 and S9 (Figure 15.39) consider a moderate reduction of the energy slope due to form roughness losses and underestimate the total amount of transported bedload material. With a higher general reduction the modelled bedload transport is even more underestimated, as shown by the simulations S5 and S10 in Figure 15.40.

A variable reduction of the energy slope available for bedload transport has not been considered because the simulations S4 and S9 (minimum reduction with $a = 1.0$) already underestimate the back calculated bedload transport.

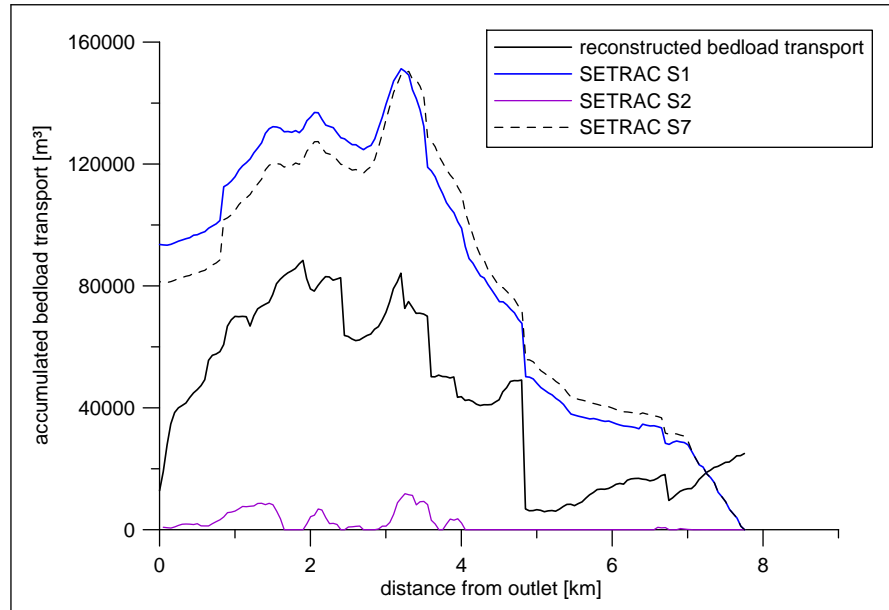


Figure 15.37: Comparison of the reconstructed bedload transport and SETRAC simulations for the cases Chirelbach S1, S2 and S7

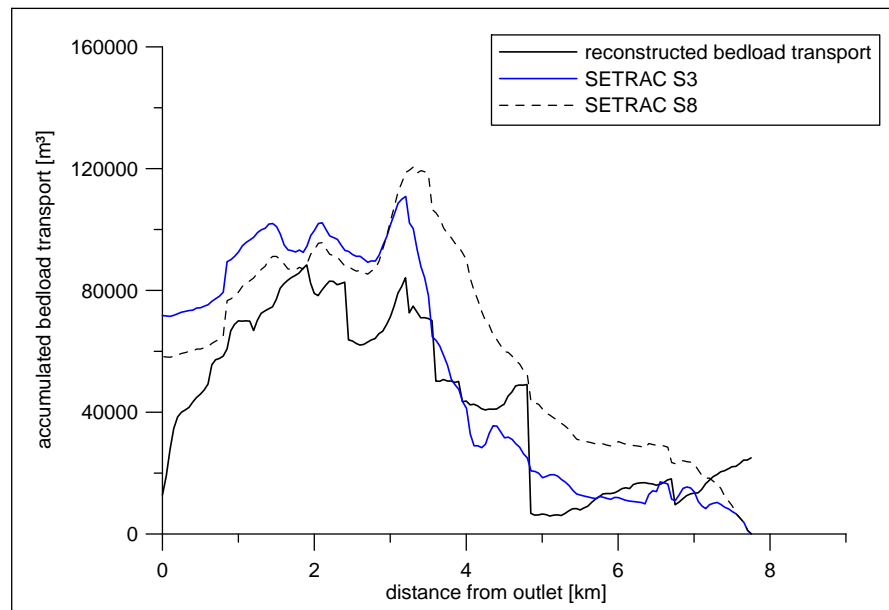


Figure 15.38: Comparison of the reconstructed bedload transport and SETRAC simulations for the cases Chirelbach S3 and S8

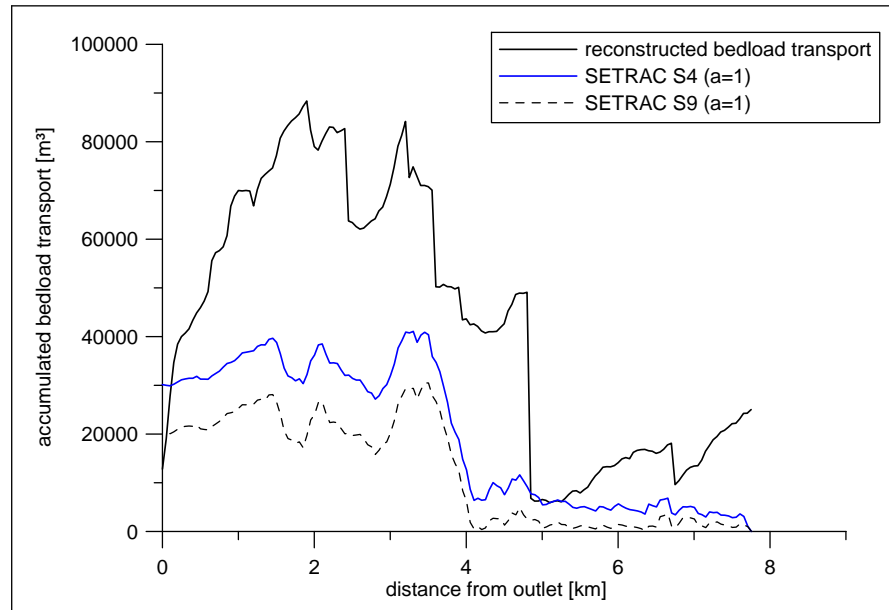


Figure 15.39: Comparison of the reconstructed bedload transport and SETRAC simulations for the cases Chirelback S4 and S9

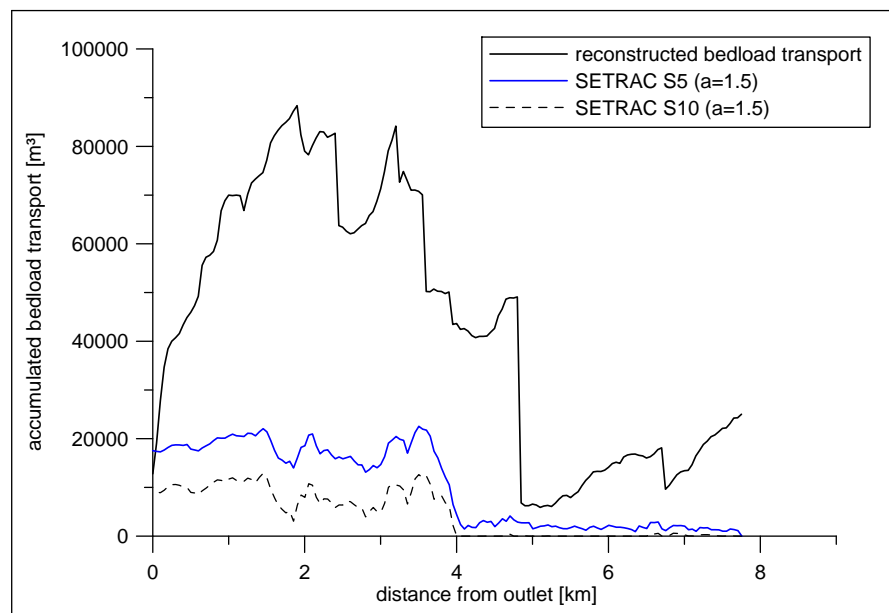


Figure 15.40: Comparison of the reconstructed bedload transport and SETRAC simulations for the cases Chirelback S5 and S10

15.5 Chiene

Another affected catchments of the August 2005 events is the Chiene mountain stream. The catchment is situated in the Canton Bern and the catchment area is 90.5 km^2 . Figure 15.41 shows the catchment area of the Chiene mountain stream. The Chiene is a steep mountain stream with a mean channel gradient of 0.05. The slope is ranging from 0.004 at the flat middle reaches up to 0.17 in the steepest reaches. The grain size distribution was estimated with line by number analysis and evaluated after Fehr (1987). The grain size distribution of different river reaches are shown in Figure 15.42.

Airborne LiDAR data before and after the flood event are available for the catchment and were used for the reconstruction of the morphologic changes. The reconstructed accumulated bedload transport is shown in Figure 15.43. During the event about $120\,000 \text{ m}^3$ of bedload (without pore volume and fine sediment transported as washload, see Chapter 13.2.2) were mobilised. Most of the material was deposited in the flat middle reaches and in the village of Kien.

There are no streamflow measurements for the Chiene mountain stream available, but the discharge has been reconstructed with streamflow measurements upstream and downstream of the confluence with the river Kander (LLE-Reichenbach, 2006). There is one gauging station 6 km upstream (Hondrich) and one 6 km downstream (Rybrügg Frutigen) at the River Kander. Radar precipitation data were used in order to generate the input hydrographs needed for the SETRAC simulations. The hydrologic model HEC-HMS has been calibrated to match the reconstructed hydrograph (LLE-Reichenbach, 2006). For better representation of the catchment, the area was separated into 9 subcatchments. Parameters for the precipitation discharge simulation are given in Appendix B.

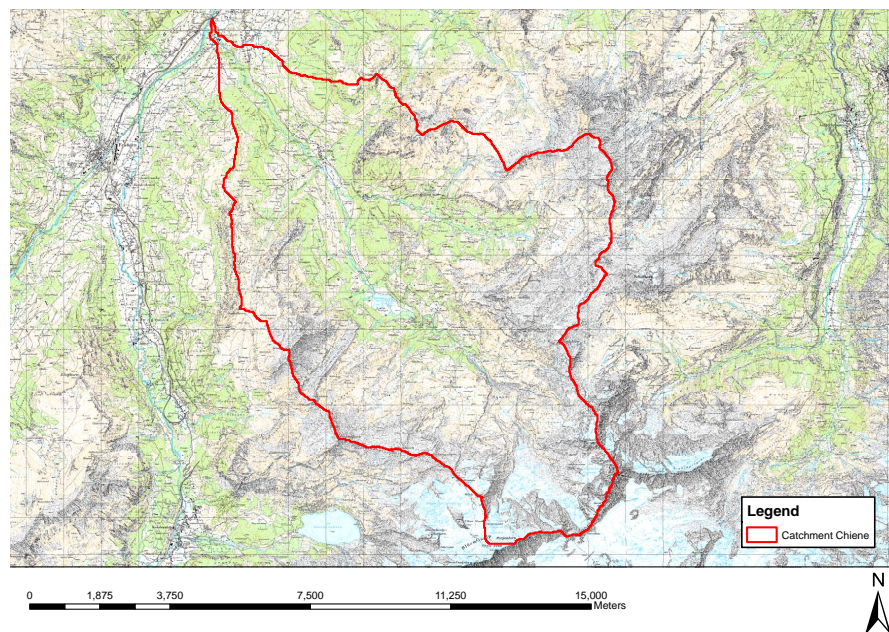


Figure 15.41: Overview Chiene project area

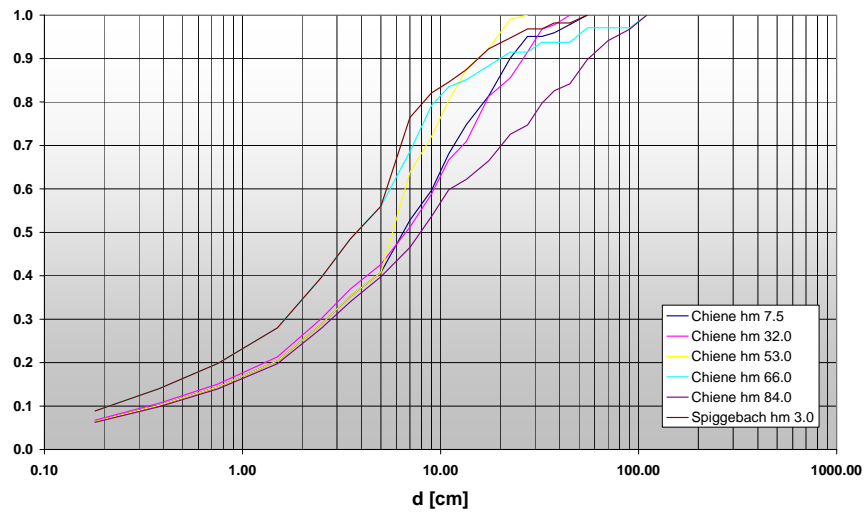


Figure 15.42: Grain size distribution for the Chiene project

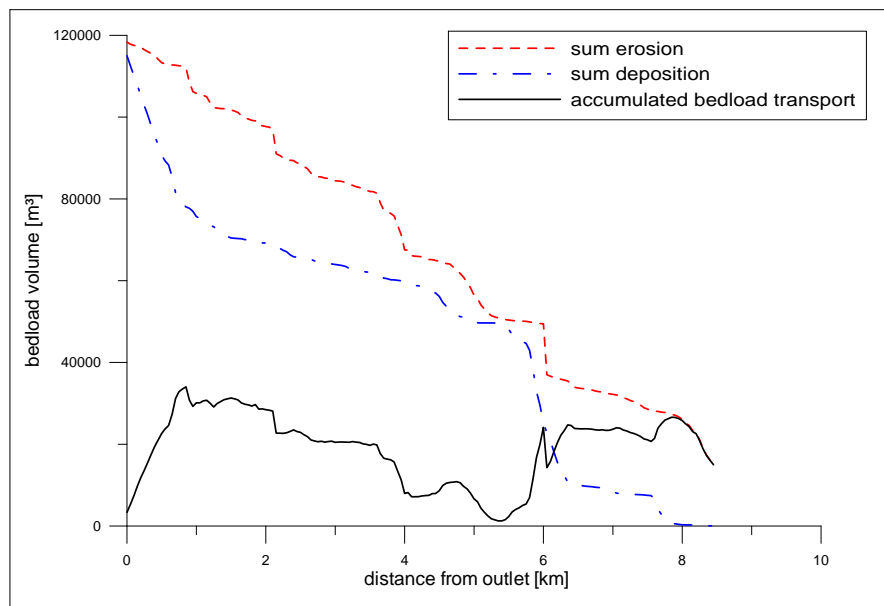


Figure 15.43: Accumulated bedload transport for the Chiene case study

15.5.1 Simulations of the Chiene extreme event

For the simulations the Chiene mountain stream as well as the most important tributary (Spiggebach) were considered. For the spatial discretisation every 50 m a cross section was measured from the digital elevation model which was generated by airborne LiDAR before the extreme event occurred. The total modelled length is 9.77 km (8.24 km Chiene and 1.44 km Spiggebach). The input hydrographs were located according to the subcatchments. A total event duration of 58 hours was modelled for the different simulation design cases. The longitudinal profile and the related slope in the sections as well as the possible erosion depth is shown in Figure 15.44. Figure 15.45 shows the hydrograph at the fan apex (km 0.75). The critical discharge is calculated with Equation 6.36 and the increased incipient motion conditions due to armoring are calculated with Equation 6.39. The slope of the considered cross-section is 0.022 and the active channel width is about 18 m.

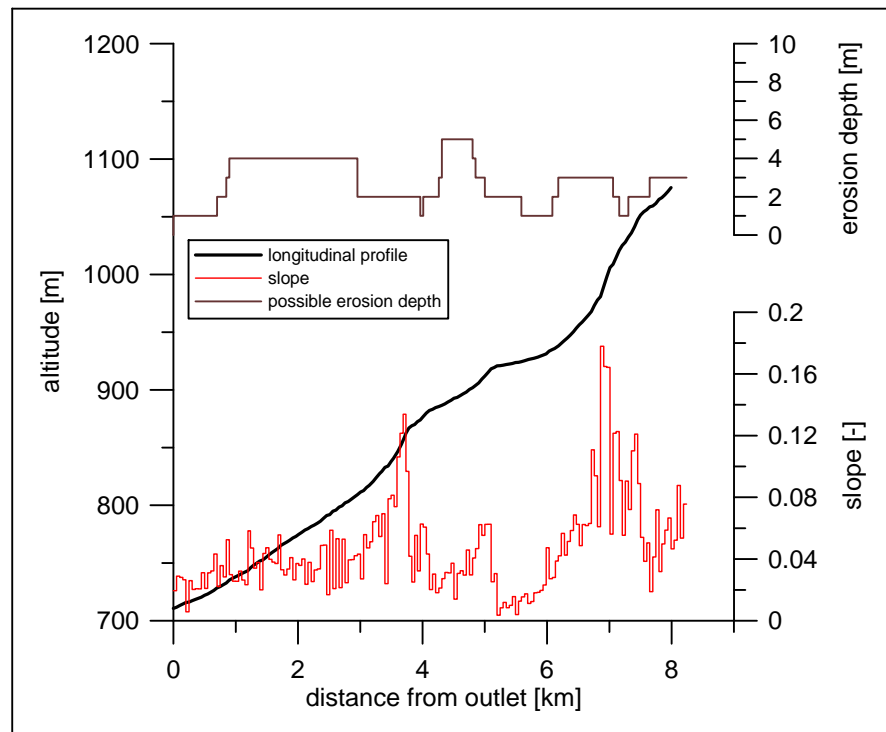


Figure 15.44: Longitudinal profile of the Chiene mountain stream with slope and possible erosion depth for each section

Figures 15.46 to 15.50 show comparisons of SETRAC simulations with the accumulated bedload transport recalculated from the morphologic changes. The time integrated bedload transport volumes are shown for the main channel. The sediment input from the Spiggebach tributary can be noticed at km 6.

The simulations without consideration of form roughness losses are shown in Figure 15.46. The simulations S1 and S7 show comparable results and overestimate the recalculated bedload transport. The simulation S2 with the higher critical discharge compared to S1 is closer to the observed bedload transport, but in several reaches the

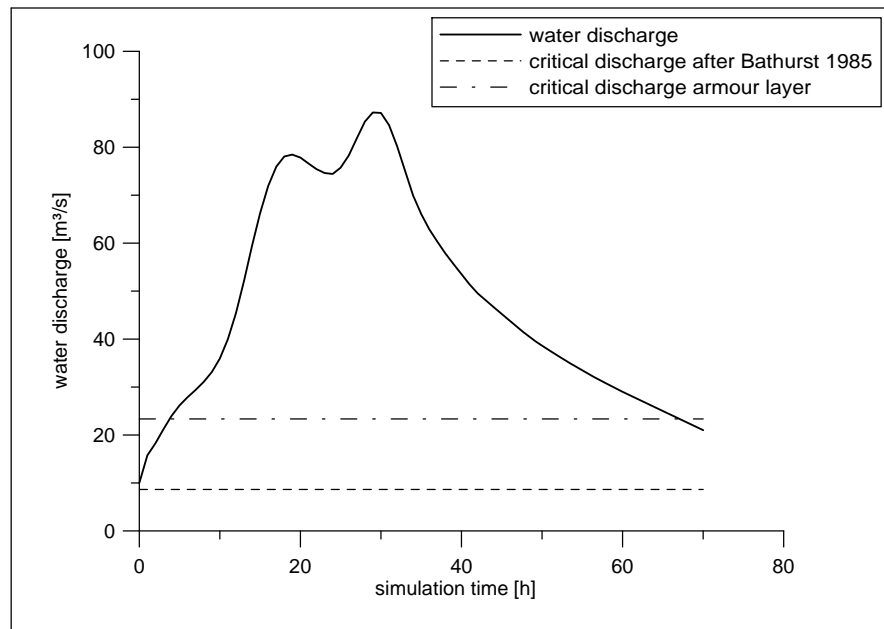


Figure 15.45: Hydrograph and related critical discharge values for a cross-section at *km* 0.75 of the Chiene mountain stream ($S = 0.022$ and $W = 18$ m).

incipient of motion criteria appears to be too high to allow for bedload transport and therefore the observed accumulated bedload transport can not be reproduced.

Considering an armour layer criteria (Figure 15.47) the simulations S3 and S8 overestimate the total bedload transport. Compared to simulations S1 and S7 there is only a small reduction of the total amount of bedload transported during the flood event.

The simulations S4 and S9 (Figure 15.48) consider a moderate reduction of the energy slope due to roughness losses but still overestimate the total amount of transported bedload material. With a higher general reduction the modelled bedload transport is comparable with the observed transport, as shown by the simulations S5 and S10 in Figure 15.49.

A variable reduction of the energy slope available for bedload transport is applied by the simulations S6 and S11 (Figure 15.50). The exponent a was optimized to find best agreement between observed and reconstructed bedload volumes, resulting in values $1.1 < a < 2.0$. Thereby the total amount of transported bedload material is comparable to the reconstructed bedload transport caused by the August 2005 flood event.

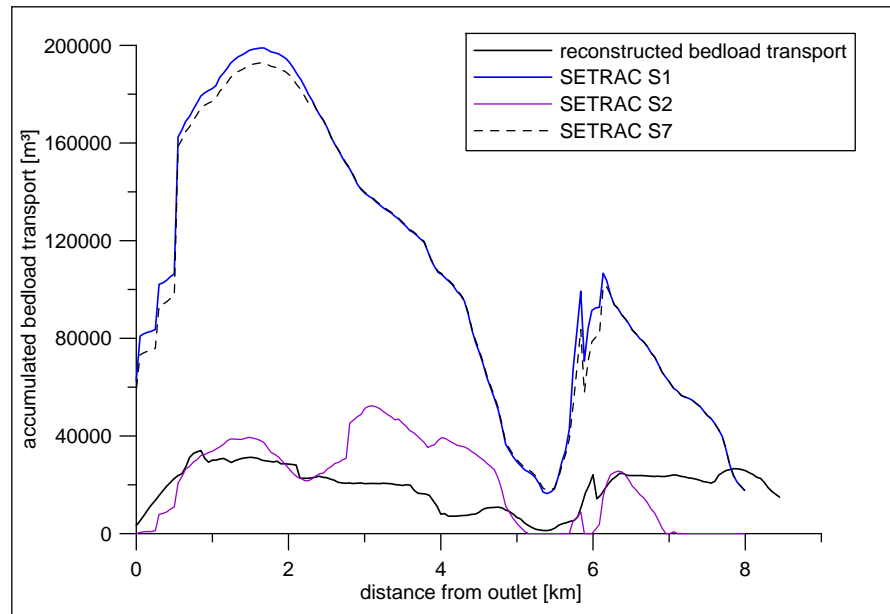


Figure 15.46: Comparison of the reconstructed bedload transport and SETRAC simulations for the cases Chiene S1, S2 and S7

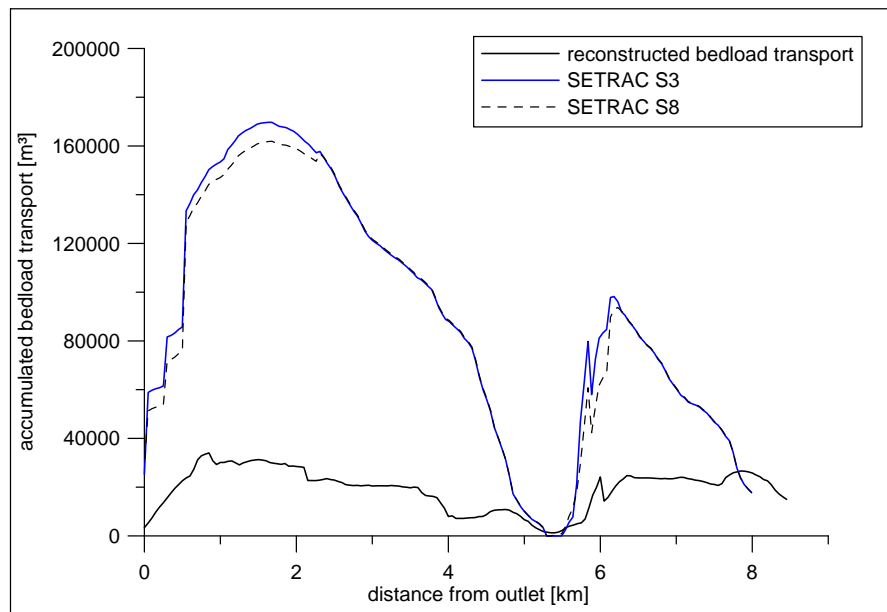


Figure 15.47: Comparison of the reconstructed bedload transport and SETRAC simulations for the cases Chiene S3 and S8

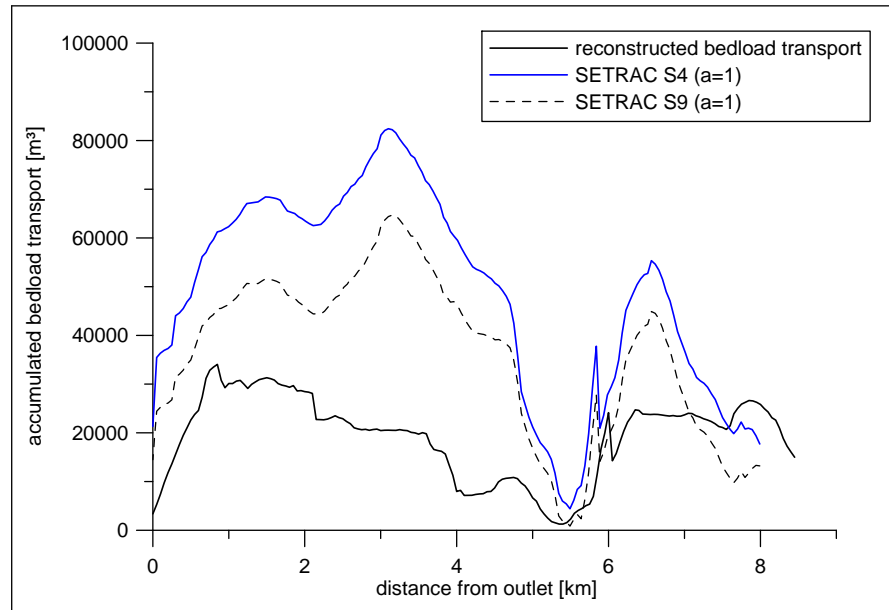


Figure 15.48: Comparison of the reconstructed bedload transport and SETRAC simulations for the cases Chiene S4 and S9

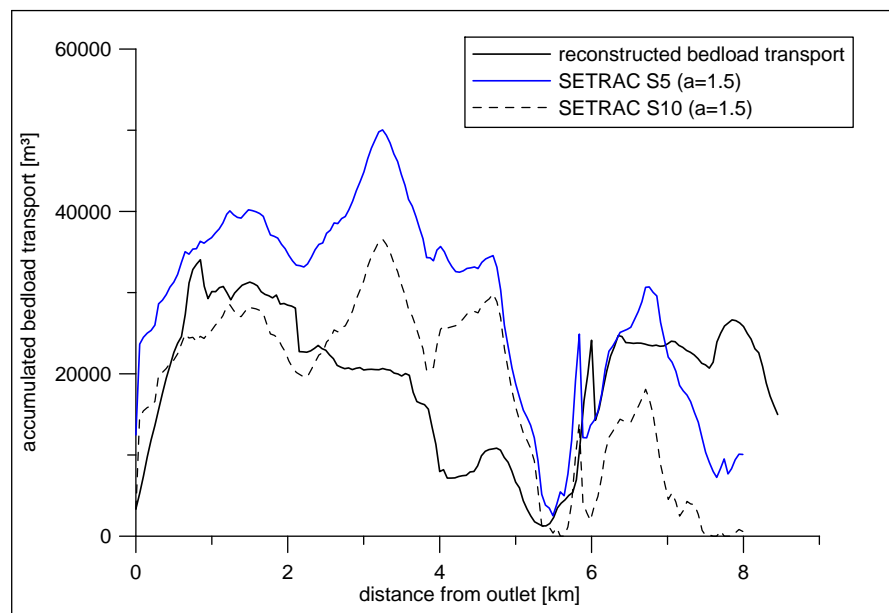


Figure 15.49: Comparison of the reconstructed bedload transport and SETRAC simulations for the cases Chiene S5 and S10

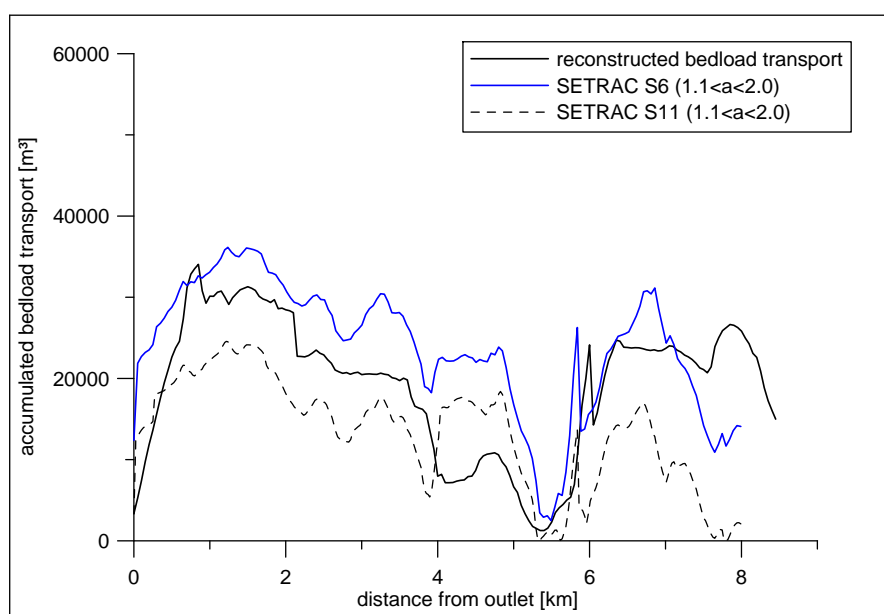


Figure 15.50: Comparison of the reconstructed bedload transport and SETRAC simulations for the cases Chiene S6 and S11

15.6 Schwarze Lütschine

The catchment of the Schwarze Lütschine mountain stream in the Canton Bern was affected by the August 2005 flood event (LLE-Lütschine, 2007). The catchment area is 180 km^2 . The catchment area is shown in Figure 15.51. The Schwarze Lütschine is a steep mountain stream with a mean channel gradient of 0.034. The slope ranges from 0.003 at the flat lower reaches up to 0.19 in the steepest reaches. There are several precipitation gauges in the catchment. The precipitation gauge Grindelwald is situated in the catchment and recorded 171 mm during the time period of the event from 20. to 22. August. Radar precipitation data are also available for this area. A reconstruction of the area integrated rainfall for several sub catchments of the Schwarze Lütschine was made (LLE-Lütschine, 2007). The average rainfall height for the total event was about 210 mm during the whole duration of 3 days.

No streamflow measurements are available for the Schwarze Lütschine mountain stream, but further downstream streamflow measurements are available for the raising and the falling limb of the flood event. During the peak flow no measurements are available. The input hydrographs needed for SETRAC were generated with the Hydrologic Modelling System HEC-HMS and calibrated according to the available streamflow data. As both gauging stations are further downstream, the whole catchment of the Lütschine has been modelled in order to achieve a more reliable calibration for the August 2005 flood event. Corrected values of the radar precipitation data were used for the precipitation-discharge simulation (MeteoSchweiz, 2006). The simulated peak discharge was calibrated with reconstructed values of the peak discharge (LLE-Lütschine, 2007). The duration of the whole event was 48 hours with a peak discharge of about $140 \text{ m}^3/\text{s}$. Parameters for the precipitation discharge simulation are given in Appendix B.

The grain size distribution was estimated with line by number analysis and evaluated after Fehr (1987). The grain size distributions of different river reaches are shown in Figure 15.52. Airborne LiDAR data before and after the flood event are available for the catchment and were used for the reconstruction of the morphologic changes. The reconstructed accumulated bedload transport is shown in Figure 15.53. During the event about $80\,000 \text{ m}^3$ of bedload (without pore volume and fine sediment transported as washload, see Chapter 13.2.2) were mobilized. Most of the material was deposited in the flat lower reaches.

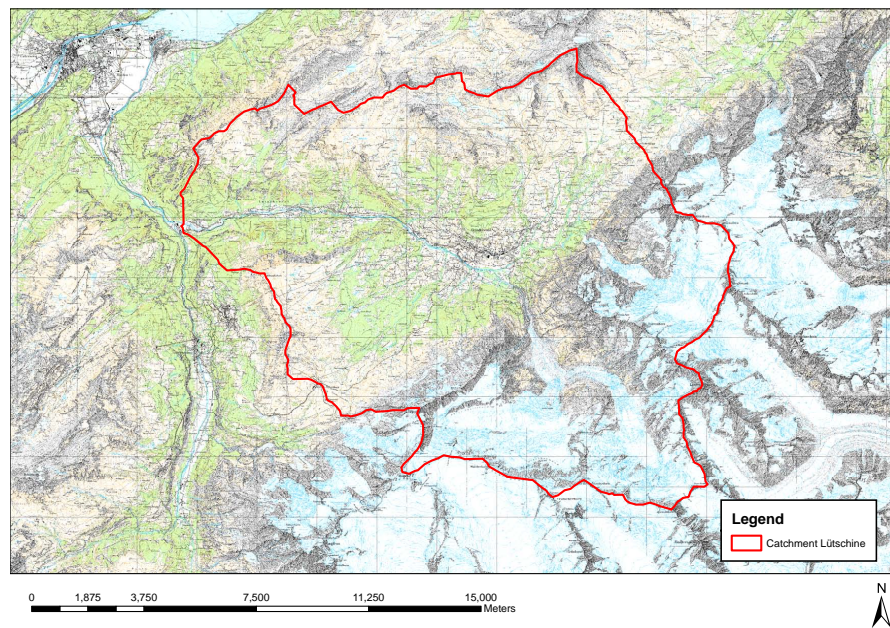


Figure 15.51: Overview Lütschine project area

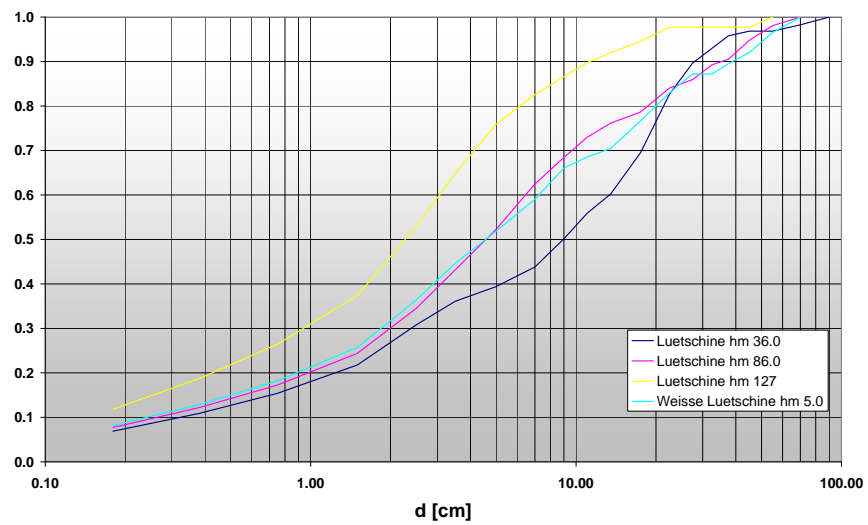


Figure 15.52: Grain size distribution for the Lütschine project

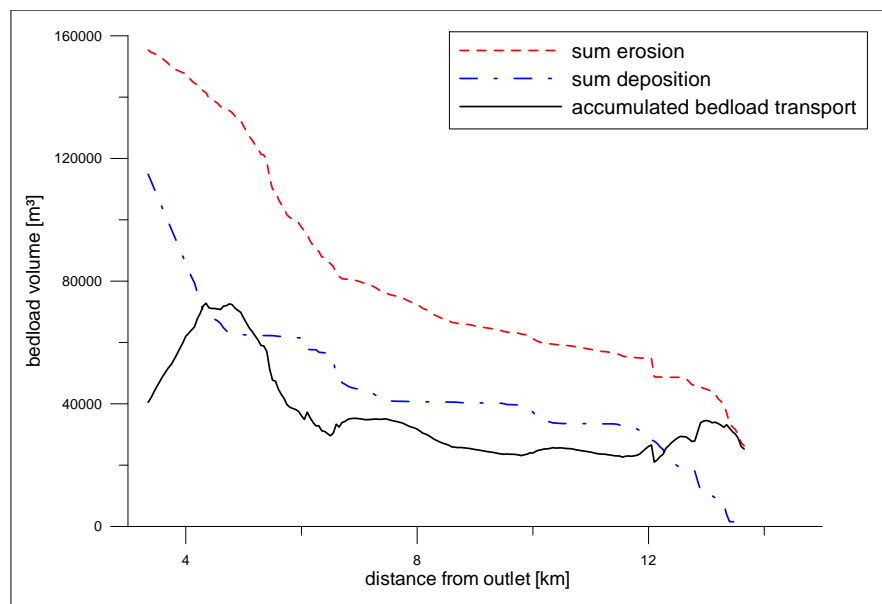


Figure 15.53: Accumulated bedload transport for the Lütschine case study

15.6.1 Simulations of the Schwarze Lüttschine extreme event

For the simulations the Lüttschine mountain stream as well as the most important tributary (Weisse Lüttschine) were considered. For the spatial discretisation every 50 m a cross section was measured from the digital elevation model which was generated by airborne LiDAR before the extreme event occurred. The total modelled length is 10.55 km (9.95 km Lüttschine and 0.60 km tributary Weisse Lüttschine). The input hydrographs were located according the subcatchments. A total event duration of 59 hours was modelled for the different simulation design cases. The longitudinal profile and the related slope in the sections as well as the possible erosion depth is shown in Figure 15.54. Figure 15.55 shows the hydrograph at km 4.0 where the main deposition started. The critical discharge is calculated with Equation 6.36 and the increased incipient motion condition due to armouring is calculated with Equation 6.39. The slope of the considered cross-section is 0.022 and the active channel width is about 20 m.

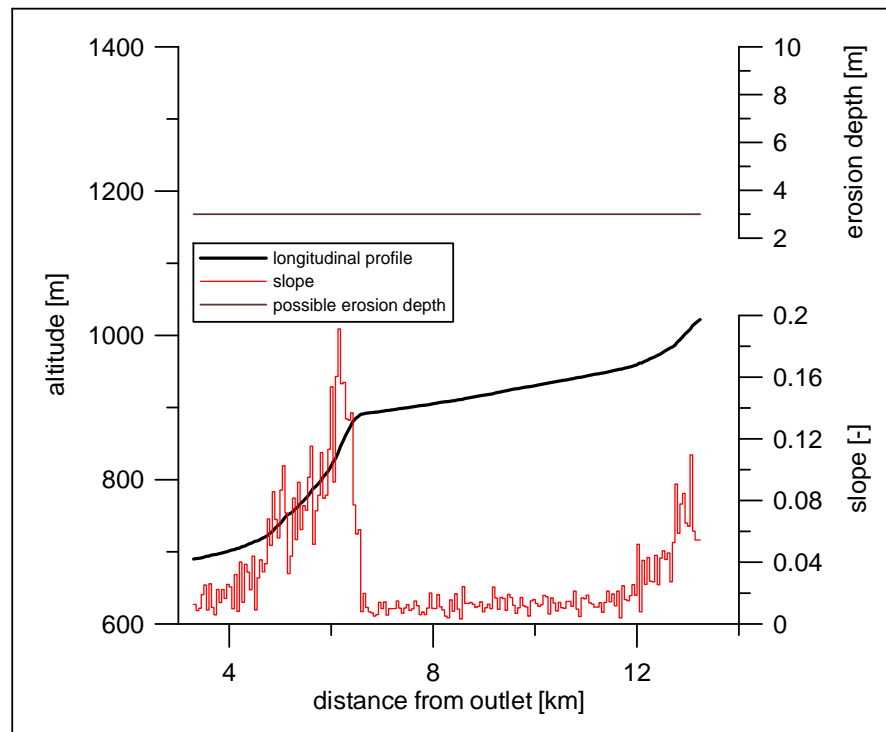


Figure 15.54: Longitudinal profile of the Lüttschine mountain stream with slope and possible erosion depth for each section

Figures 15.56 to 15.60 show comparisons of SETRAC simulations with the accumulated bedload transport recalculated from the morphologic changes. The time integrated bedload transport volumes are shown for the main channel. The sediment input from the tributary Weisse Lüttschine can be noticed at km 12.

The simulations without consideration of form roughness losses are shown in Figure 15.56. The simulations S1 and S7 show comparable results and overestimate the recalculated bedload transport. The simulation S2 with the higher critical discharge compared to S1 is closer to the observed bedload transport, but in most reaches the

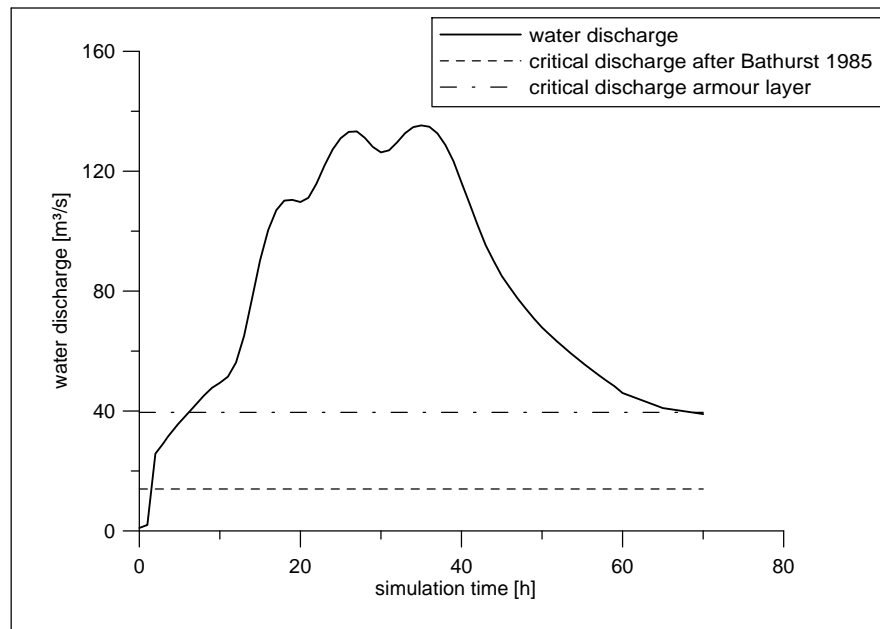


Figure 15.55: Hydrograph and related critical discharge values for a cross-section at *km* 4.0 of the Schwarze Lutschine mountain stream ($S = 0.022$ and $W = 20\text{ m}$).

ignition of motion criteria is too high to allow for bedload transport and therefore the observed behavior can not be reproduced.

Considering an armour layer criteria (Figure 15.57) the simulations S3 and S8 overestimate the total bedload transport in the steep channel reaches. For the flatter reaches simulation S3 slightly overestimates the reconstructed bedload transport, whereas simulation S(underestimates the accumulated bedload transport. Compared to simulations S1 and S7 there is only a small reduction of the total amount of bedload transported during the flood event.

The simulations S4 and S9 (Figure 15.58) consider a moderate reduction of the energy slope due to form roughness losses but still overestimate the total amount of transported bedload material in the steeper reaches. With a higher general reduction the modelled bedload transport is underestimated in the flatter reaches, but the channel erosion in the steep part from *km* 4.6 to *km* 6.2 is still overestimated, as shown by the simulations S5 and S10 in Figure 15.59.

A variable reduction of the energy slope available for bedload transport is applied by the simulations S6 and S11 (Figure 15.60). The exponent a was optimized to find best agreement between observed and reconstructed bedload volumes, resulting in values $1.1 < a < 2.0$. Thereby the total amount of transported bedload material is comparable to the reconstructed bedload transport caused by the August 2005 flood event. Simulation S6 slightly overestimates the reconstructed bedload transport, whereas simulation S11 underestimates. For these two simulations the same exponents were used to account for form drag.

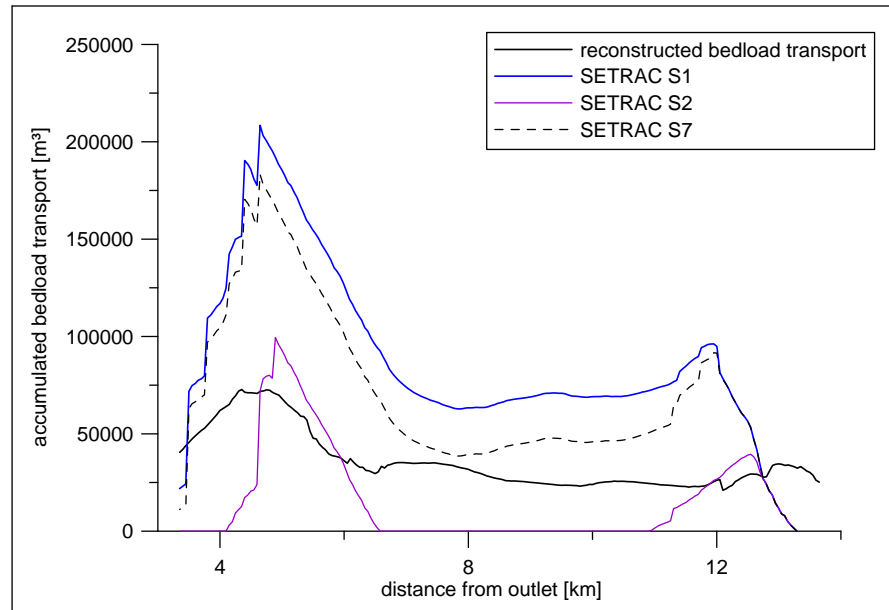


Figure 15.56: Comparison of the reconstructed bedload transport and SETRAC simulations for the cases Lütshine S1, S2 and S7

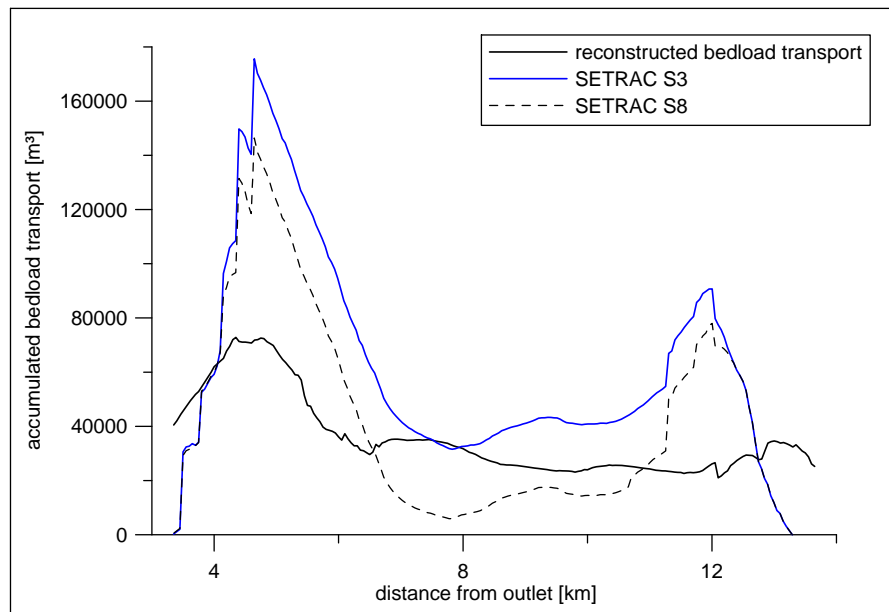


Figure 15.57: Comparison of the reconstructed bedload transport and SETRAC simulations for the cases Lütshine S3 and S8

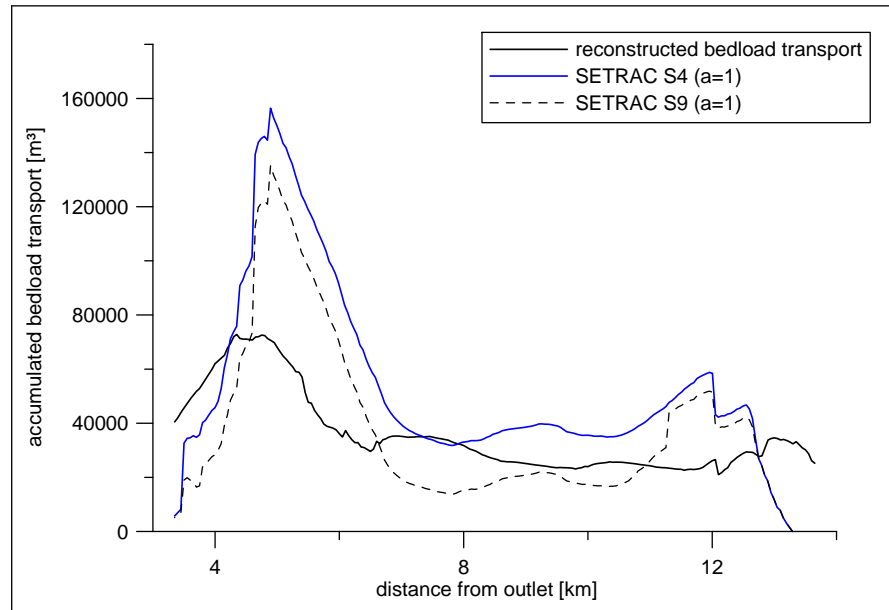


Figure 15.58: Comparison of the reconstructed bedload transport and SETRAC simulations for the cases Lütshine S4 and S9

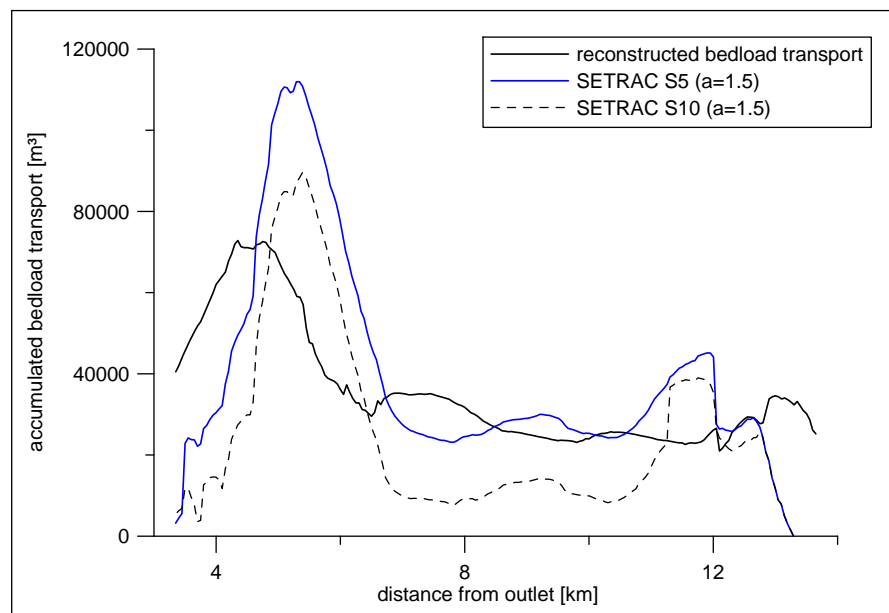


Figure 15.59: Comparison of the reconstructed bedload transport and SETRAC simulations for the cases Lütshine S5 and S10

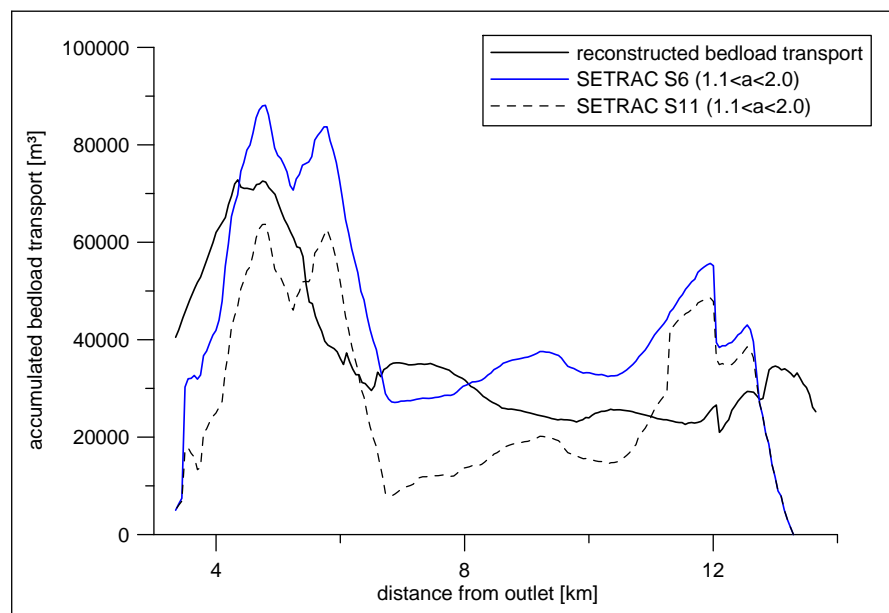


Figure 15.60: Comparison of the reconstructed bedload transport and SETRAC simulations for the cases Luetschine S6 and S11

16 Case study in France

16.1 Draix

The Draix experimental catchments are a field laboratory for mountain erosion studies. They are situated in the Southern French Alps close to the villages of Draix and Le Brusquet. The investigated catchment is called Laval and has a catchment area of 0.86 km^2 . It is located on black marls, which is a very erodible outcrop. 68 % of the catchment are classified as badlands with a mean slope of 58 %. An overview over the project area is given in Figure 16.1. Floods in this catchment generate high levels of solid transport. The basin is equipped for measuring rainfall, runoff, bedload and suspended sediment transport. Sediment traps upstream of the measuring station are used to measure the sediment yield from the catchment. These traps are surveyed after each flood event to calculate the deposited bedload volumes.

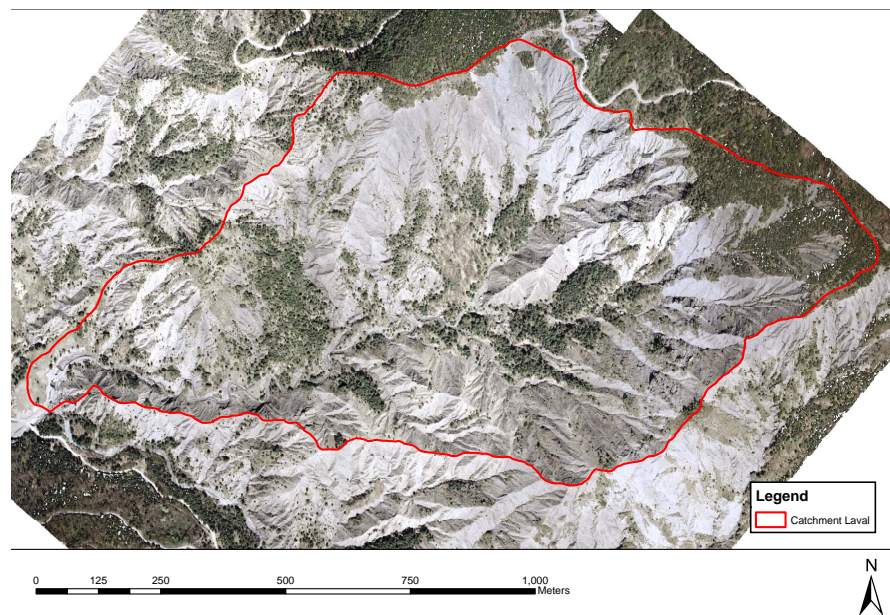


Figure 16.1: Overview Laval project area

Data for a flood event that occurred in July 2006 were provided by Cemagref Grenoble. During the event of July 6, 2006, 410 m^3 of sediment with a bulk density of 1.7 t/m^3 were trapped in the bedload deposition basin. Due to the high fine sediment concentration the average fluid density was very high (1250 kg/m^3). Rainfall and runoff data are shown in Figure 16.2. Two precipitation gauges are situated in the catchment.

The discharge as well as the fine sediment concentration were measured at the deposition basin. The hydrographs for the subcatchments were generated with the ETC model (Mathys et al., 2003) and calibrated with the measured discharge at the outlet of the catchment. These hydrographs were used for the SETRAC simulations. In ETC it is also possible to estimate the sediment input from the hillslopes. These sediment inputs were also considered as sedigraphs in SETRAC.

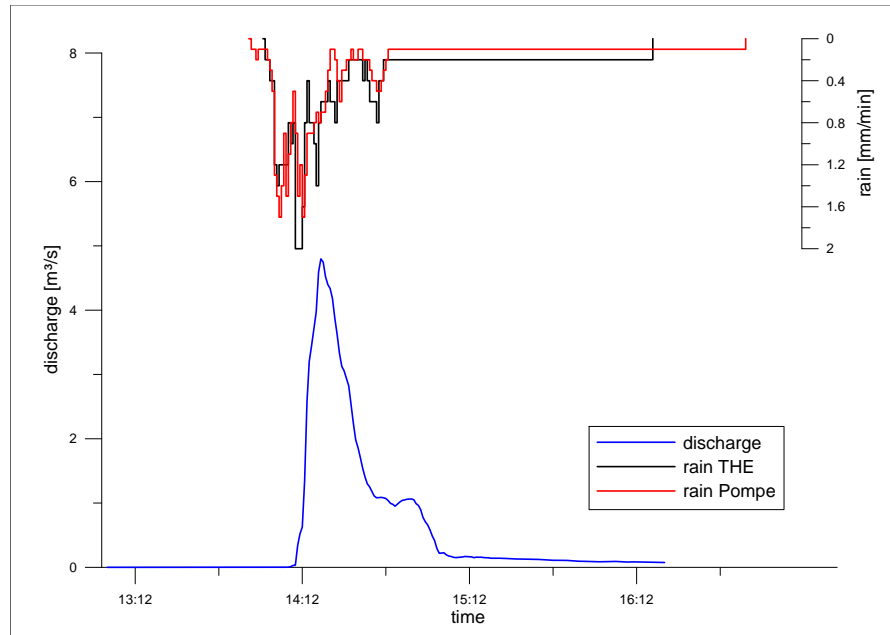


Figure 16.2: Rainfall and runoff measurements for the Laval case study

The longitudinal profile and the related slope in the sections as well as the possible erosion depth is shown in Figure 16.3.

16.1.1 Model comparison

A model comparison has been performed for the Laval field study. The same formulas were used in SETRAC and ETC (see Table 16.1). For direct comparison the simplified cross-section geometry required for ETC was also used for the SETRAC simulation. The simulation has been performed under fix bed conditions. Morphologic changes due to erosion and deposition were not considered, because this is not possible in ETC. No form roughness losses were considered due to the plane bed and fine sediment found in the Laval catchment (Figure 16.4). Sediment stock in reaches were defined, according to field investigations done before the event. The spatial discretisation length for SETRAC was set as the longest distance between two cross-sections, because no refined spatial discretisation can be defined in ETC. A comparison between the results obtained by SETRAC and ETC simulations is made in Figure 16.5. Both models show nearly similar results, but the total bedload delivered to the bedload deposition basin is underestimated with 183 m^3 compared to 260 m^3 solid volume in the sediment trap.

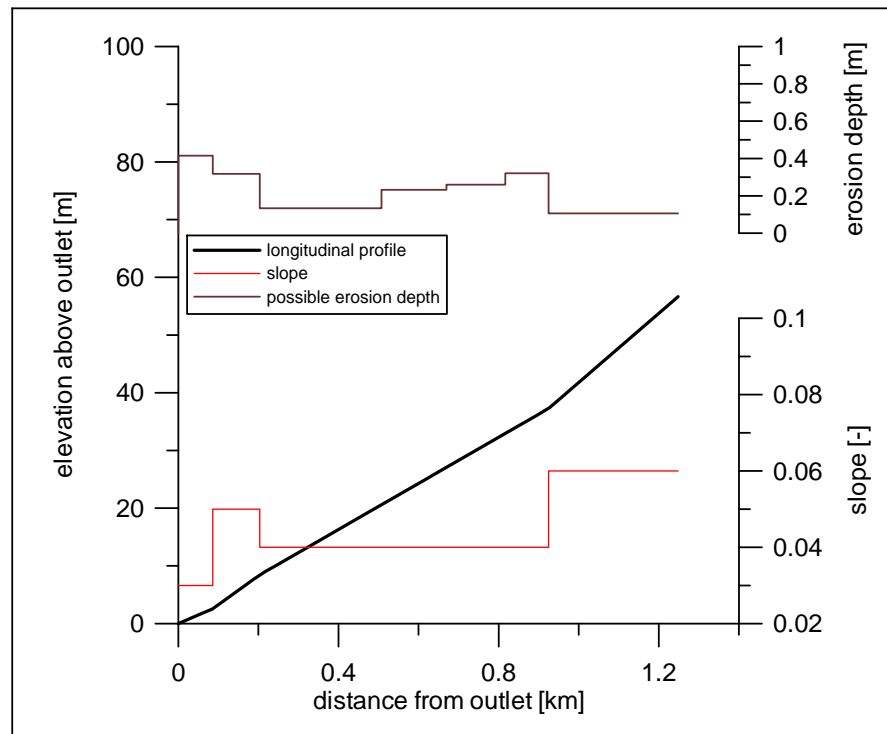


Figure 16.3: Longitudinal profile of the Laval torrent with slope and possible erosion depth for each section

In the same figure a SETRAC simulation with mobile bed and finer discretisation (10 m) is shown for comparison. The sediment output obtained by this simulation is 222 m^3 at the channel outlet. This value is much closer to the measured volume in the sediment trap. Changes of the slope are rounded and do not affect the transport as much as the geometry changes when neglecting the movable bed conditions. Therefore morphologic changes should be considered in small torrential catchments, as well as in mountain streams.

Table 16.1: Formulas used for the model comparison

flow resistance	bedload transport	incipient of motion
(6.15)	(6.34)	(6.36)



Figure 16.4: Channel bed with fine sediment in the Laval catchment

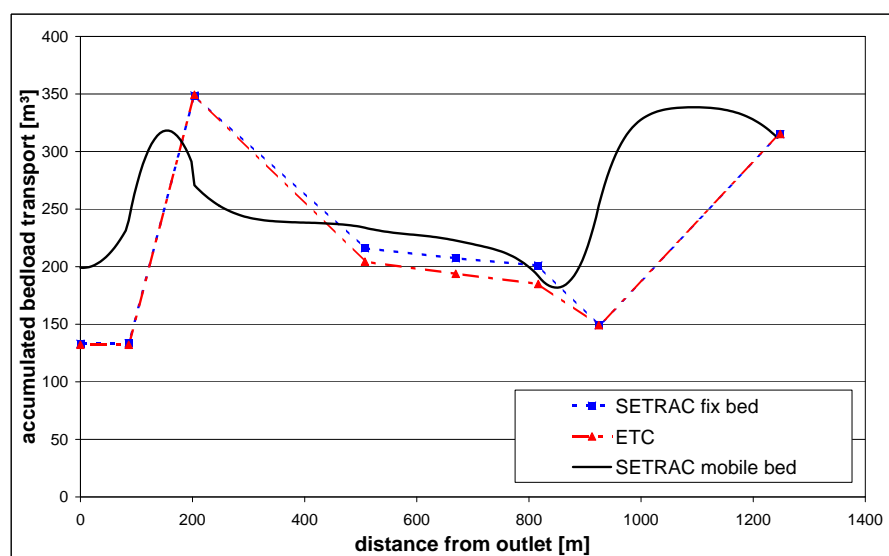


Figure 16.5: Comparison of simulation results obtained with the SETRAC and ETC models for the Laval case study

Part VIII
Discussion

17 Discussion of simulation results

17.1 Agreement of predicted and observed loads and likely influence of form resistance

Modelling bedload transport in steep headwater catchments is a challenging task. High sediment transport rates during flood events result in fast changes of the cross-section geometry. For the simulation of bedload transport in torrents and mountain streams, observations on bedload transport in steep experimental flumes are taken as reference conditions. These conditions define maximum transport rates for the idealized case of rather uniform bed material. Essentially no morphological features and hence no significant form roughness effects were present in the experiments. The simulation results show that the application of sediment transport equations derived from laboratory experiments in steep rough channels results in an average overestimation of the bedload transport of one orders of magnitude (factor of 10) for flood events with generally high flow intensities. Rickenmann (2001) found that observed sediment transport in the steep and small streams was one to three orders of magnitude smaller than values predicted by a sediment transport capacity formula, where the flows are mostly of small or intermediate intensity. The discrepancy between observed and calculated bedload volumes appears to be lower for higher flow intensities, because the discharge is much higher than the critical discharge for incipient motion. Apart from limited sediment supply (Bathurst, 2007), this discrepancy may be partly due to substantial bedform roughness reducing bedload transport efficiencies. Applying two sediment transport models to a river reach with a channel gradient of about 0.02, Rathburn and Wohl (2001) found that predicted bedload discharges overestimated observed ones by up to several orders of magnitude.

Lamb et al. (2008) indicated an increase in threshold shear stress for initiation of particle motion with increasing channel slopes. A higher threshold will reduce transport rates, and this effect may be important at low and medium flow intensities (unfortunately not yet implemented in SETRAC). Apart from limited sediment supply form roughness losses can be regarded as an important reason why transport formulas often overestimate bedload transport when they are applied to channels where the effect of bed forms on flow resistance and sediment transport can not be neglected. Palt (2001) accounted for form losses and found in this case much better agreement between his bedload measurements in Himalayan rivers and the bedload transport formulas of Meyer-Peter and Mueller (1948), Smart and Jäggi (1983) and Rickenmann (2001). Millar (1999) showed that form resistance in gravel bed rivers is highly variable and may range between 0 % and 90 % of the total flow resistance. Petit et al. (2005) concluded that losses due to

the resistance of bed forms in smaller and steeper catchments are higher, resulting in a higher critical specific stream power for the mobilization of bedload material. Other authors report that grain roughness contributes only about 20-40 % of the total roughness in boulder-dominated streams (e.g. Zimmermann and Church, 2001; Canovaro et al., 2007; Church and Zimmerman, 2007).

The back-calculations of the August 2005 extreme events with the SETRAC model indicate that form roughness losses are non negligible when modelling bedload transport in steep headwater streams. The exponent a serves as calibration parameter for form roughness losses, to obtain a better agreement between observed and simulated bedload transport in steep streams. If only a limitation of the sediment stock in reaches to model "supply limited" conditions is considered, this cannot reproduce the time evolution of the recalculated extreme events and results in a clear overestimation of the total sediment load. The extreme flood events in the Swiss Alps in August 2005 resulted in high bedload transport volumes in many streams. For channel slopes steeper than about 0.05, bedload volumes calculated with the bedload transport Equation 5.23 are about an order of magnitude larger on average than the observed volumes, suggesting that a correction for form resistance losses may be important (Rickenmann et al., 2008).

17.2 Effect of armour layer criteria in combination with one grain model

For sediment routing calculations in gravel-bed rivers armouring has to be considered (Hunziker and Jäggi, 2002). An armour criteria as implemented in SETRAC may be regarded as upper boundary (resulting in a lower limit for bedload transport volume estimates), because the incipient motion criteria is increased for the whole simulation time. The relation between discharge and the bedload effective water volume V_{re} is illustrated in Figure 17.1. Where $V_{re,1}$ is the effective water volume considering a critical discharge and $V_{re,2}$ is the effective water volume considering a critical discharge in combination with an armour layer criteria. In natural rivers, once the armour layer is broken the incipient motion may be reduced because of the destroyed armour layer (shown by the dashed line in Figure 17.1), or effectively a mobile armour layer may form.

The simulation results of the mountain streams modelled within this study show that considering armouring, the total bedload transport is reduced. About 10 % to 20 % less bedload is transported compared to simulations neglecting armouring in mountain streams. For the Chirel mountain stream (Chapter 15.4) this reduction of the transport capacity is sufficient to reconstruct the accumulated bedload transport for the August 2005 flood event. For the other mountain streams (Suggadinbach Chapter 15.3, Chiene Chapter 15.5 and Schwarze Lütschine Chapter 15.6) the total bedload transport is overestimated. Thus form drag has to be considered for the recalculation of the August 2005 events in these mountain streams.

For steep torrents, the application of the incipient motion criteria due to armouring still results in an overestimation of observed bedload transport volumes. For the Sesslabach (Chapter 15.1) and the Schnannerbach (Chapter 15.2) no reduction of the accumulated bedload transport is achieved, because all the sediment stock is depleted.

Therefore the consideration of a simple armour criteria in combination with a one grain-size model cannot reproduce the recalculated bedload transport. Form roughness losses appear to be more important at very steep slopes. For torrents, where also colluvial sediment makes up the channel bed, the concept of armouring is questionable. Stable bed-forms like step-pool systems are more likely to develop.

17.3 Importance of form roughness losses

Our simulation results confirm observations on bedload transport in steep mountain streams and torrents. As reported by other authors the application of theoretical sediment transport equations derived from laboratory experiments in steep rough channels results in an overestimation of the bedload transport up to three orders of magnitude (e.g. Gomi and Sidle, 2003; Bathurst et al., 1987; Gomez and Church, 1989; Reid and Laronne, 1995; Hegg and Rickenmann, 1999; Rickenmann, 2001).

A limitation of the sediment stock available to model "supply limited" conditions cannot reproduce the time evolution of observed bedload transport for two steep torrents modeled in this study. The hydrograph as well as the sedigraphs of the simulation without form roughness losses (S1) as well as for the simulation with the varying exponent (S6) are shown in Figure 17.2 for the Schnannerbach field study (see Chapter 15.2). The temporal evolution of bedload transport on the fan can not be reconstructed in agreement with the observations of the inhabitants of the fan without consideration of form drag. After 21 hours of simulation time all the sediment stock is depleted. Considering form drag, the accumulated transported bedload volumes are in better agreement with the reconstruction of the temporal sequence of the extreme event.

The hydrograph as well as the sedigraphs of the simulation without form roughness losses (S1) as well as for the simulation with the varying exponent (S6) are shown in Figure 17.3 for the Sesslabach field study (see Chapter 15.1). The sedigraph peaks before the hydrograph, because sediment delivery is limited from the upstream reaches. Again, the temporal evolution of the bedload transport can not be reconstructed in agreement with the observations of the inhabitants of the fan without consideration of form drag. After 17 hours of simulation time all the sediment stock is depleted. Considering form drag the temporal sequence of the event with simultaneously peaking hydro- and sedigraph and the total transported volume can be much better reproduced.

The quantification of form roughness losses is rather difficult. Approaches derived from natural data are rarely available. The dataset used by Rickenmann (1996) for the estimation of total roughness has been used for the quantification of the contribution of grain roughness to total roughness (see Figure 4.2 in Chapter 4.2). Even approaches derived from the same dataset show quite a range of possible proportions of form resistance losses (Equations 4.11 to 4.17), depending on whether the influence of the relative submergence is considered or neglected and with which approach the total roughness is estimated. Other approaches presented in this study are based on laboratory measurements with stable structures (e.g. Pagliara and Chiavaccini, 2006). The arrangement and the density of the immobile roughness elements are responsible for the losses due to form roughness (Pagliara and Chiavaccini, 2006; Canovaro and Solari, 2007a). Equation 4.14 and Equation 4.16 may be regarded as upper boundary for the contribution of

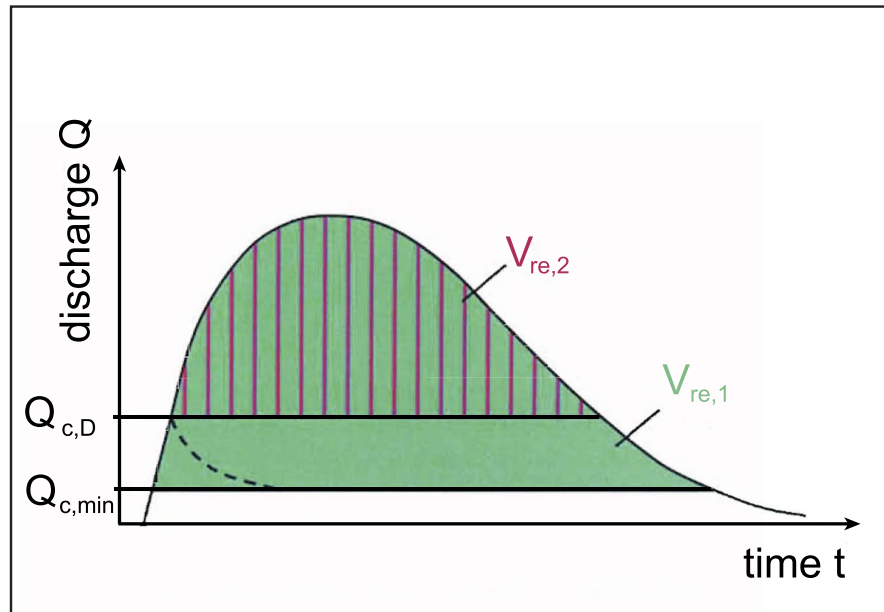


Figure 17.1: Relation between discharge and effective water volume after Badoux and Rickenmann (2008)

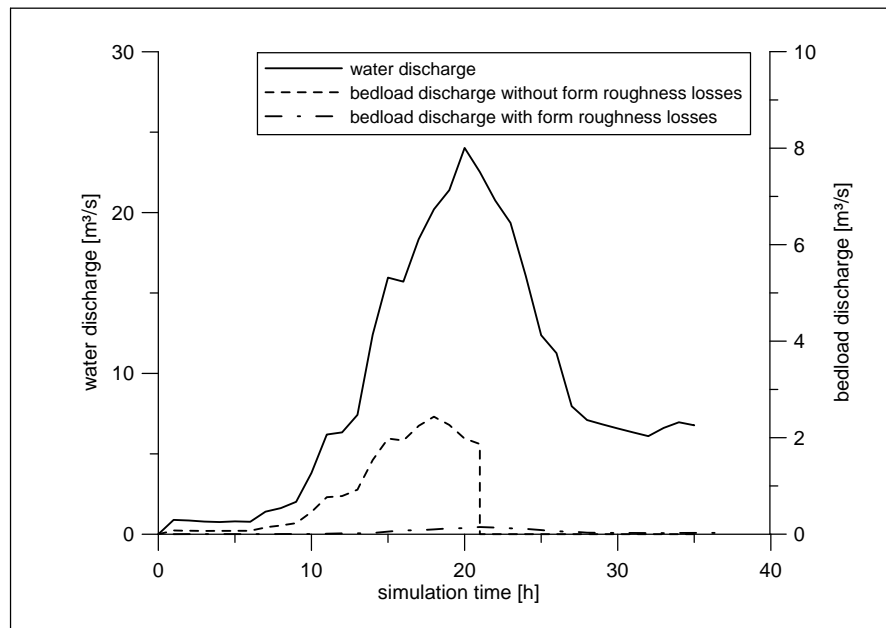


Figure 17.2: Hydrograph and sedi-graphs for the channel outlet of the Schnannerbach

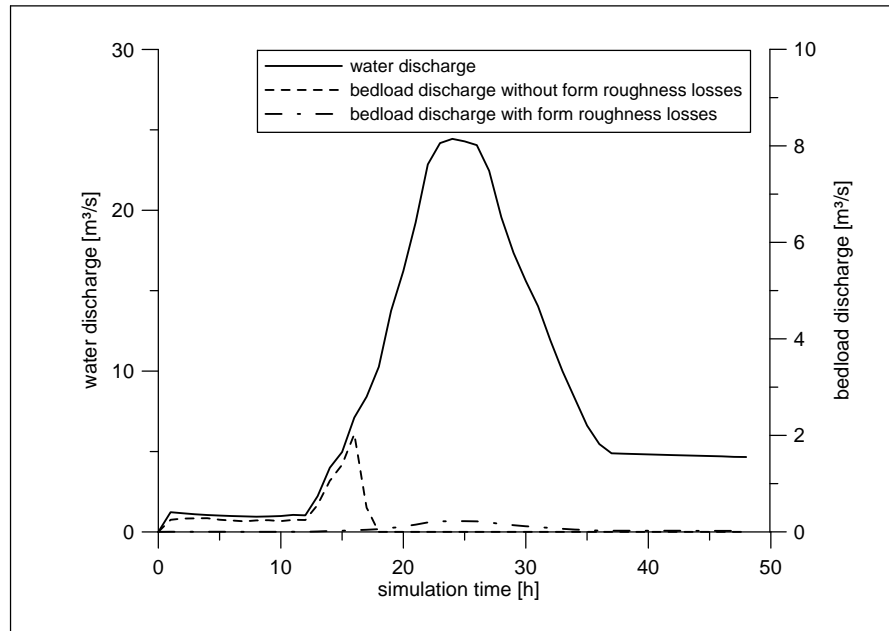


Figure 17.3: Hydrograph and sedi-graphs for the channel outlet of the Sesslabach

form roughness losses, whereas Equation 4.28 appears to be a lower boundary. According to the limited data available, the contribution of form roughness to total roughness appears to be in the range from 40 to 90 % of the total roughness and may decrease when the channel bed becomes mobile (Hu and Abrahams, 2006).

Form roughness losses calculated in SETRAC can be regarded as upper boundary, because if considered, they are calculated for the whole simulation time. Steep torrents with stable bed structures may show a different behavior concerning form roughness once the stable structures are partly or completely destroyed. Then form resistance may become less important, but may still be present due to big boulders and other roughness structures.

In this study the exponent a in Equation 6.30 has been used as calibration parameter in combination with the form roughness losses calculated with Equation (6.27). Possible values for a are in the range $1.0 < a < 2.0$ and were calibrated for a best fit with the back-calculated amount of bedload transported in the reaches during the flood event. Now the question arises whether or not it is possible to relate the amount of reduction to different roughness structures. For this purpose characteristic cross-sections and their calibrated exponent are compared. Figures 17.4 to 17.7 show selected river reaches of several case study streams and their calibrated exponent a . As the pictures show, the calibrated exponent a can vary for similar looking reaches which gives the impression of having similar degrees of roughness due to large particles or bed form structures. Therefore it is difficult to estimate the exponent a before a simulation. However, it should be noticed, that such a rough and qualitative assessment based on (often) one single photograph per reach is not sufficient to rule out any correlation between back-calculated a values and quantitative measures of roughness that could be made for the studied reaches.

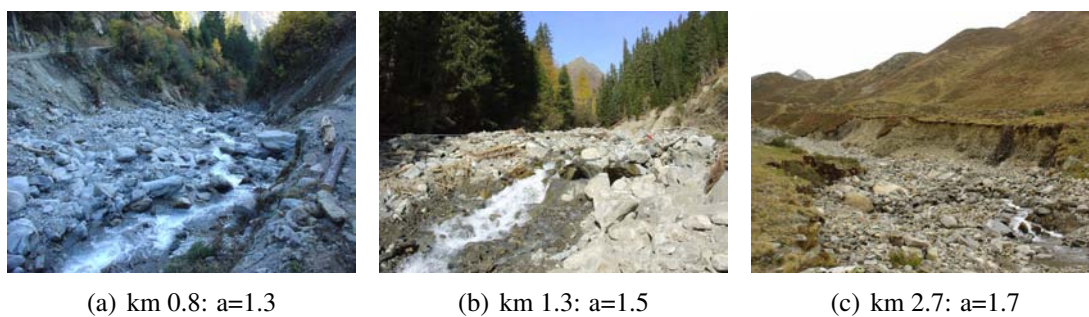


Figure 17.4: The calibrated exponent a for the Sesslabach

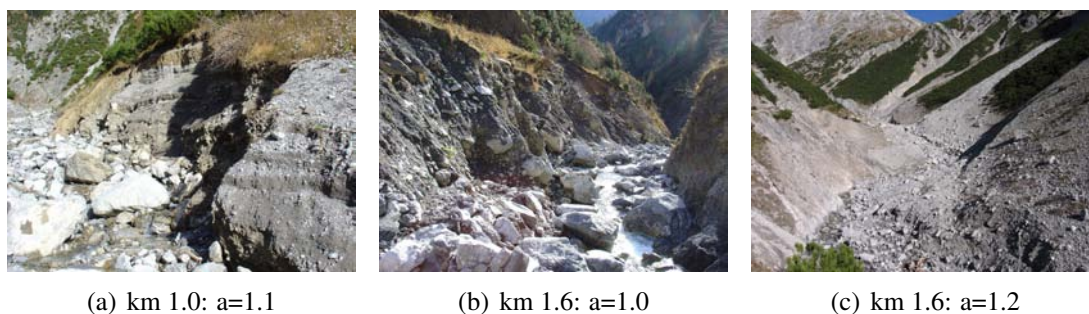


Figure 17.5: The calibrated exponent a for the Schnannerbach



Figure 17.6: The calibrated exponent a for the Chiene mountain stream

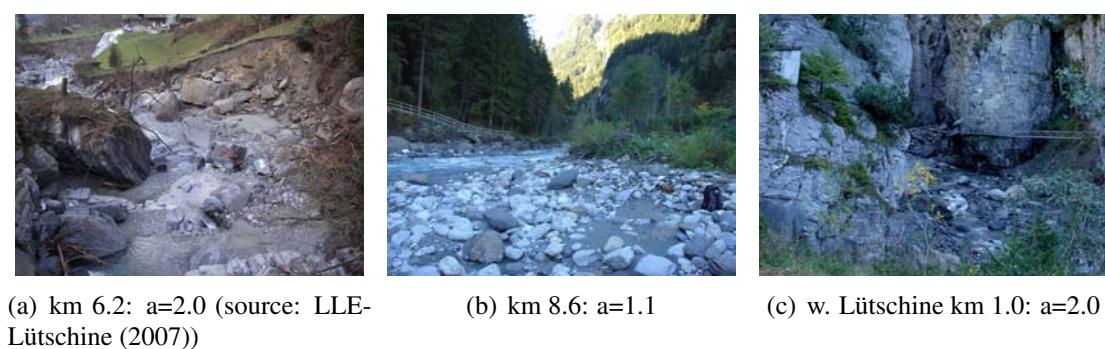


Figure 17.7: The calibrated exponent a for the Lüttschine mountain stream

17.4 Comparison between transport capacity and observed transport on a channel reach basis

For the presented case studies of the August 2005 extreme events the transport capacity of each cross-section was calculated. For this comparison morphologic changes of the cross-section geometry and of the channel slope between the cross-sections were neglected. To model unlimited supply conditions, the possible erosion depth was set to the high value of 100 *m*. For comparison with the reconstructed bedload volumes time integrated bedload volumes are calculated with SETRAC. For further analysis the ratio of the simulated versus the reconstructed (observed) bedload transport is plotted in Figure 17.8 for the field cases for each channel reach. This comparison of the transport capacity and the recalculated bedload transport can not distinguish between limited sediment supply and reduced transport capacity due to form roughness losses. For steeper torrents (Sessladbach and Schnannerbach) limited sediment supply may be more important than for mountain streams, where generally more sediment is stored in the channel bed. Figure 17.8 shows different patterns, but the same trend for all field cases. With the exception of some reaches, the observed bedload transport is overestimated by one to three orders of magnitude. A potential fit trend line for all data is shown in Figure 17.9. In several reaches flatter than 0.01 the actual bedload transport is underestimated. This can be an effect of the non mobile bed approach used in the SETRAC calculations for this comparison and may not be representative. For the above mentioned reason data with a ratio *simulated/observed* < 1 were excluded in Figure 17.10. To focus on the sections with steeper slope range, in Figure 17.11 only data with $S > 0.02$ are presented.

For this analysis one has to consider the possibility of different uncertainties of the observed loads within the same case study. For the field investigations (see Chapter 13.2.1) depositions on the fan may be more accurate to measure than channel or side erosion in steep reaches. Also for airborne LiDAR generated differential elevation models, the accuracy depends on the slope (see Chapter 13.2.2).

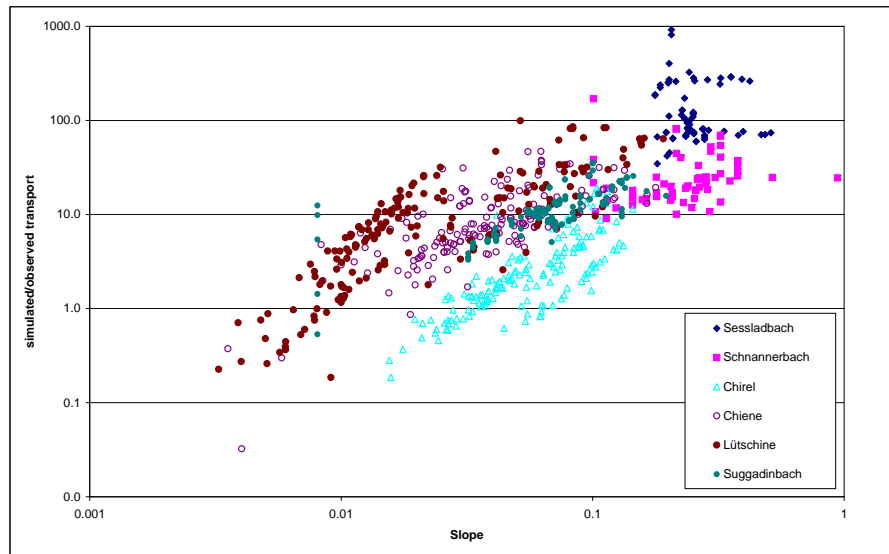


Figure 17.8: Ratio of transport capacity and reconstructed bedload transport for all field data

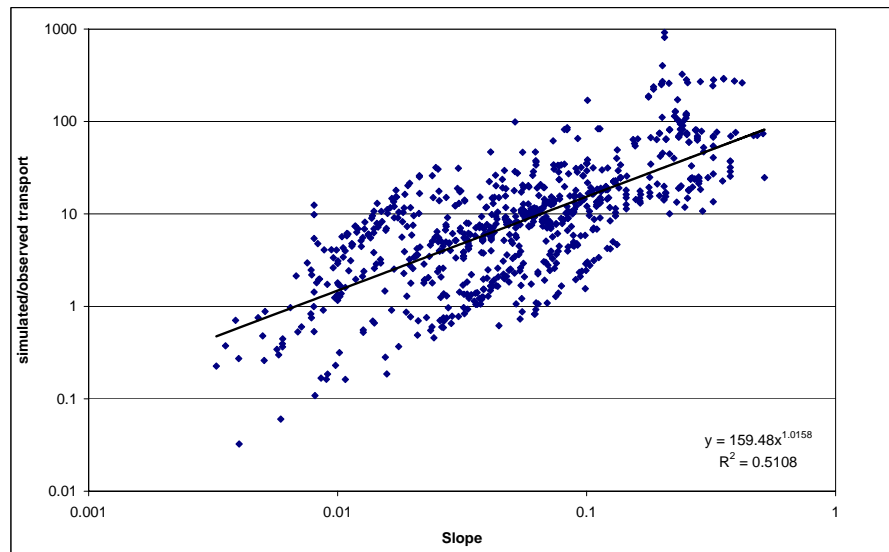


Figure 17.9: Ratio of transport capacity and reconstructed bedload transport for all torrents and mountain streams

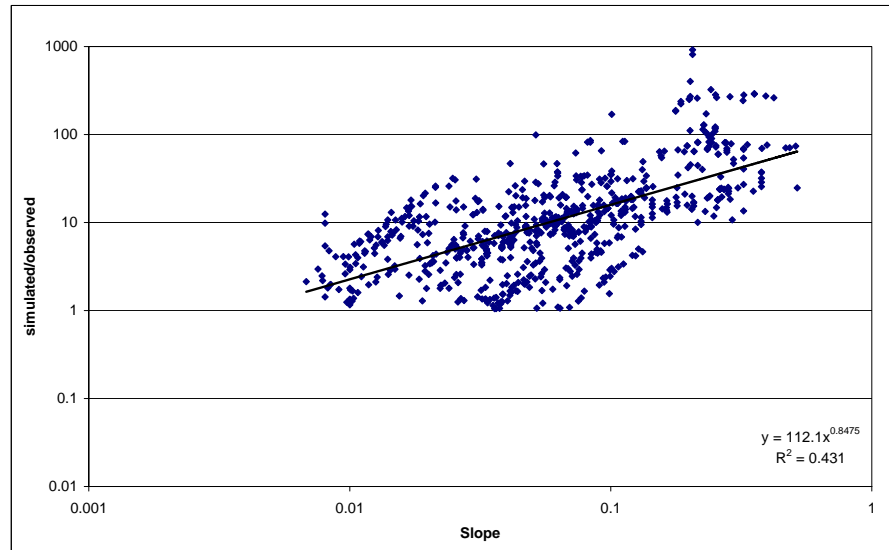


Figure 17.10: Ratio of transport capacity and reconstructed bedload transport for all field data where the ratio is >1

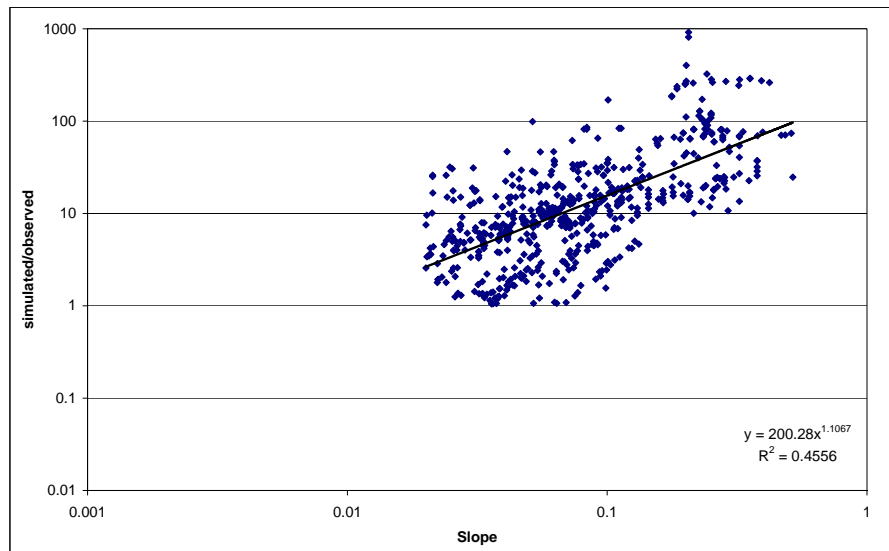


Figure 17.11: Ratio of transport capacity and reconstructed bedload transport for all field data where the ratio is >1 and the slope is steeper than 0.02

17.5 Back calculated form roughness losses on a channel reach basis

Palt (2001) derived an approach from natural data for the slope range $0.002 < S < 0.12$ (Equation 17.1).

$$\frac{n_r}{n_{tot}} = 0.1S^{-0.36} \quad (17.1)$$

Fitting a power law regression for n_r/n_{tot} as a function of slope to the data calculated with Equation 4.17 after Rickenmann et al. (2006) (see also Figure 4.1), similar to Equation 17.1 results in an equation:

$$\frac{n_r}{n_{tot}} = 0.12S^{-0.34} \quad (17.2)$$

A similar expression can be derived from the presented field and SETRAC simulation data. Considering only data where the ratio of simulated transport and reconstructed bedload transport is $V_{b,sim}/V_{b,observed} > 1$ (see Figure 17.10), it is possible to express the contribution of form roughness to total roughness (n_r/n_{tot}) as a function of the channel slope by considering Equation 5.19:

$$\frac{V_{b,sim}}{V_{b,obs}} \approx \left(\frac{A(Q - Q_c)S^{1.5}}{A(Q - Q_c)S_{red}^{1.5}} \right) \approx \left(\frac{S}{S_{red}} \right)^{1.5} \quad (17.3)$$

$$S_{red} = S \left(\frac{n_r}{n_{tot}} \right)^a \quad (17.4)$$

$$\frac{n_r}{n_{tot}} = \left(\frac{V_{b,sim}}{V_{b,obs}} \right)^{\left(-\frac{1}{1.5a}\right)} \quad (17.5)$$

According to the Manning-Strickler equation an appropriate value of a in Equation 17.4 should be $a = 2$. Using this value, the corresponding data of Equation 17.5 is plotted in Figure 17.12. Fitting an power law regression to the data in Figure 17.12 results in:

$$\frac{n_r}{n_{tot}} = 0.21S^{-0.28} \quad (17.6)$$

Equation 17.6 is valid for the slope range $0.007 < S < 0.52$ and the coefficient of correlation is $R^2 = 0.43$. A comparison between Equation 17.1 and Equation 17.6 is made in Figure 17.12. With $a = 2$ form roughness losses appear to be lower than predicted with Equation 17.1 and Equation 17.2.

Meyer-Peter and Mueller (1948) argued that the exponent in the Equation 4.24 may be different from 2, and from their experiments they empirically determined a value of 1.5. Therefore the exponent a has been varied to bring the field data from this study in better agreement with Equation 17.1 and 17.2. The best fit was found for $a = 1.35$ (Figure 17.13). For this condition, the trend line is:

$$\frac{n_r}{n_{tot}} = 0.10S^{-0.42} \quad (17.7)$$

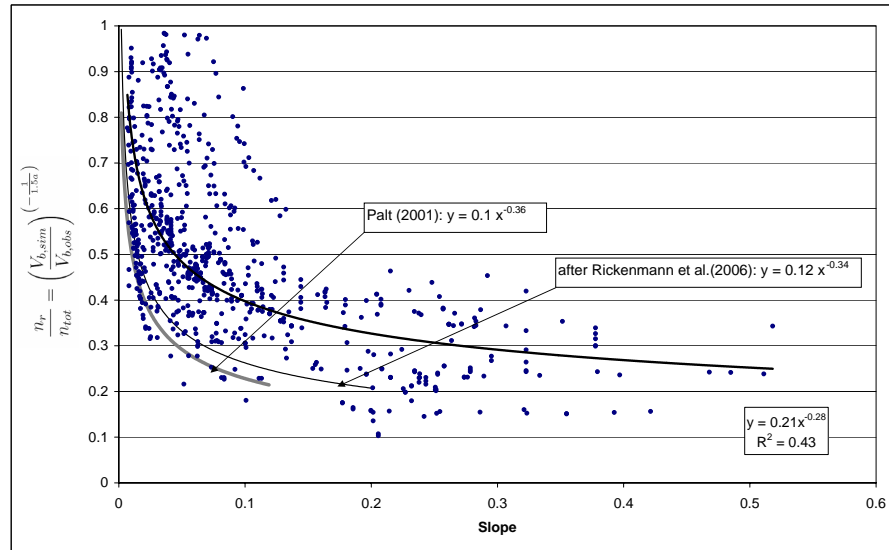


Figure 17.12: Contribution of form roughness to total roughness as a function of slope if $a = 2$ is used in Equation 17.5.

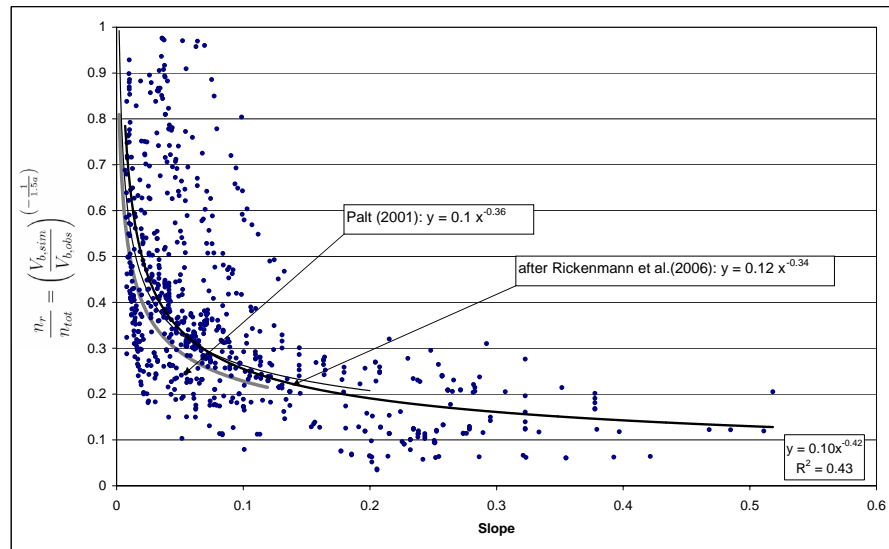


Figure 17.13: Contribution of form roughness to total roughness as a function of slope if $a = 1.35$ is used in Equation 17.5.

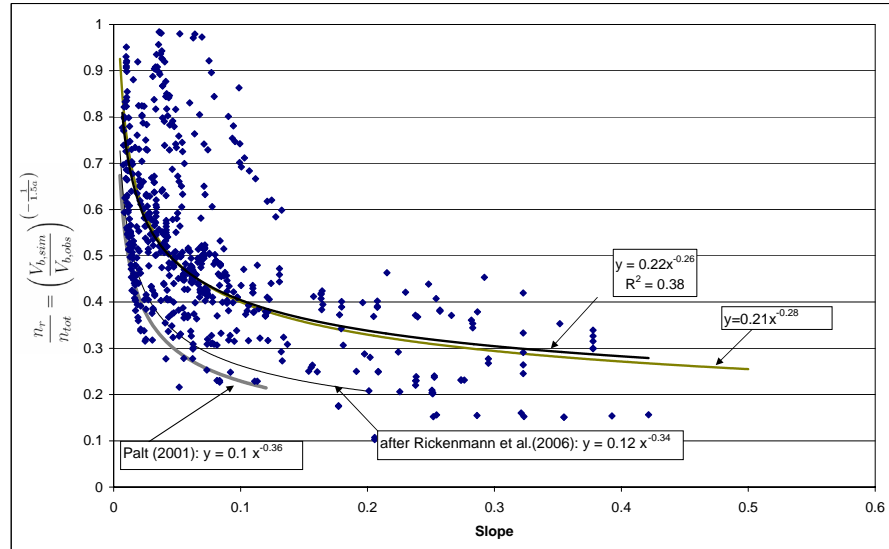


Figure 17.14: Contribution of form roughness to total roughness as a function of slope for channel reaches in alluvium if $a = 2$ is used in Equation 17.5.

A comparison of Equation 17.1, 17.2 and 17.7 is shown in Figure 17.13.

In the case study simulations described in Chapter VII, Equation 4.17 has been applied for the simulation of the field studies and the exponent a has been used as calibration parameter. For the best fit simulations the calibrated exponent a was in the range from 1.0 to 2.0 for the single reaches with an average value of 1.35 as shown in Figure 17.13. According to the field data, form roughness losses calculated with Equation 17.6 would allow for an average exponent $a = 2.0$ as derived from the Manning-Strickler equation.

Data shown in Figures 17.12 and 17.13 include all modelled channel reaches with $V_{b,sim}/V_{b,observed} > 1$. The presented data include all modelled reaches neglecting sediment availability. Therefore Equation 17.6 represents a mixture of form roughness losses and underestimation of the transported sediment due to limited sediment supply.

Considering only reaches in alluvium with no supply-limitation results in Equation 17.8. All reaches with possible erosion depth smaller than 0.5 m (e.g. bedrock or heavy river regulation) were excluded. Similar to Equation 17.6 a power law regression has been fitted:

$$\frac{n_r}{n_{tot}} = 0.22S^{-0.26} \quad (17.8)$$

Equation 17.8 is valid for the slope range $0.007 < S < 0.42$ and the coefficient of correlation is $R^2 = 0.37$. The data used for this analysis are shown in Figure 17.14. For comparison Equation 17.1, 17.2 and 17.6 are also shown. For the steep slope range ($S > 0.07$) Equation 17.8 delivers slightly higher values of n_r/n_{tot} .

17.6 One grain-size model versus fractional bedload transport

Considering the main purpose of SETRAC, developing the SETRAC model and its potential application, namely torrential extreme events, the one grain-size model appears to be adequate to describe the transport processes in steep headwater catchments. For mountain rivers the effect of armouring at low flow rates seems to be non negligible, but further research is necessary to understand the processes of downstream fining or even downstream coarsening (Solari and Parker, 2000; Brummer and Montgomery, 2003) of the active layer at steeper slopes. Parker et al. (2007) discussed the behavior of the grain size distribution of gravel-bed rivers during floods and concludes that the surface size distribution present during floods may differ little from that prevailing at low flow. The main problem is that the grain size distribution during high floods can not be sampled easily. Once the armour layer is broken essentially all sizes are roughly equal mobile and therefore not much extra accuracy can be gained by calculating bedload transport for each size fraction separately and summing (Parker et al., 1982a). Computing fractional bedload transport at steep slopes requires more data for calibration. The change of the grain size distribution due to selective transport is dependent on the hiding function and the active layer thickness. Hassan and Church (1994) investigated vertical mixing in gravel bed rivers and found that the burial depth of particles is dependent on the magnitude and duration of the flow event. In addition the number of events and the surface structure and texture influence vertical mixing. Hence the determination of the active layer thickness is not a priori known and can be used as a calibration parameter to adopt the rate of change in the grain size distribution in combination with the exponent of the hiding function. Concerning lowland rivers, more data on selective transport are available. Therefore a calibration of a fractional bedload transport computation seems more reasonable than for torrents and steep mountain streams. For example Wright and Parker (2005b) developed and applied (Wright and Parker, 2005a) a model for downstream fining in sand-bed rivers. The characteristic of two large lowland sand bed rivers were studied. The development of a downstream decrease in bed slope and a downstream decrease in characteristic bed sediment diameter were obtained. Also for gravel-bed rivers a better performance can be expected using fraction wise bedload transport equations (Hunziker and Jäggi, 2002). Hunziker and Jäggi (1997) applied such a calculation to strongly aggrading river reaches and found a better agreement with the observed behavior when using fractional transport. For the application of fractional bedload transport equations to steep mountain streams and torrents further research is required, to understand selective transport mechanisms at steep slopes.

18 Application of other simulation models

One of the objectives of this study was the evaluation of different available one- and two-dimensional sediment transport models at steep slopes. Beside SETRAC the following one-dimensional models have been considered:

- BASEMENT - module BASECHAIN (Vetsch et al., 2005)
- G-STAR-1D (Huang and Greimann, 2006)
- CCHE1D (Version 3.0) (Vieira and Wu, 2002)
- ETC (Version 2.5) (Mathys et al., 2003)

And the following two-dimensional models were evaluated:

- FLUMEN (Version 1.3) (Beffa, 2005)
- CCHE2D (Version 2.2) (Wu, 2001)

For direct comparison with SETRAC Equation 6.33 (Rickenmann, 1991) has been implemented to the BASEMENT-BASECHAIN model by the developers. The model has been applied to downstream reaches of the Chirel mountain stream and to the middle reaches of the Suggadinbach. The hydrodynamic part of the model performed well, whereas the sediment transport module failed at reaches steeper than 0.04. The problems could not be solved in cooperation with the model developers within this study. Fast changes of the cross-section geometry may cause the problems.

The GSTAR-1D model has been applied to the same river reaches as the BASEMENT model and failed at reaches steeper than 0.04. No special bedload transport equations for steep slopes are available, therefore the Meyer-Peter and Mueller (1948) formula had been used for the simulations. Again, fast changes of the cross-section geometry may have caused numerical instabilities.

The CCHE1D model has been applied to mountain streams and steep torrents. There is no special sediment transport formula for steep slopes available in CCHE1D model, therefore the Meyer-Peter and Mueller (1948) (SEDTRA module) formula has been used for the simulations. The model performed well, but the total transport was overestimated, because form roughness losses cannot be considered. For steep slopes the results were comparable with SETRAC simulations neglecting form drag, because all

the sediment stock is depleted.

The ETC model has been applied to torrents and mountain streams. For a direct comparison the same transport formulas can be selected in SETRAC and in ETC (Equation 6.34 of Rickenmann, 1990). Neglecting changes due to erosion and deposition by deactivating the mobile bed module in SETRAC and applying the one-grain model, both models deliver nearly identical results (see Chapter 16.1.1). Differences are caused by the different degree of abstraction of the cross-section geometry. In ETC, a cross-section is defined by the width and the side slope, whereas SETRAC can handle complex cross-section geometries.

The FLUMEN model is a two dimensional simulation model calculating morphologic changes on triangulated irregular networks. FLUMEN has been applied for the whole length of the Chiene, Chirelbach and Suggadinbach (Mair, 2008) mountain streams. The model is stable for all channel slopes. For direct comparison with SETRAC the bedload transport Equation 6.31 (Smart and Jäggi, 1983) can be selected. Armouring can be considered or neglected. Problems occurred with the bedload transport module of FLUMEN. The total amount of transported sediment has been underestimated compared to the back-calculated transport during the August 2005 flood events. The Simulation results were in the same order of magnitude as SETRAC simulations considering form roughness losses with $a = 1.0$ in Equation 6.27. This discrepancy could not be solved in cooperation with the developer of the model within this study.

The CCHE2D model has been applied for back-calculation of laboratory experiments to optimize a bedload retention basin (Kaitna et al., 2007). The slope of the inlet section is 0.04 and 0.01 at the deposition basin. As there is no special sediment transport formula for steep slopes available the Meyer-Peter and Mueller (1948) (SEDTRA module) formula has been used for the model test. Experimenting with different mesh sizes, the model could be calibrated to describe the observed deposition behavior. CCHE2D has not been applied for the back-calculation of natural extreme events at steep slopes within this study.

Part IX
Conclusions

Conclusions

The SETRAC model is a one-dimensional simulation program for modelling bedload transport in torrents and mountain stream. A graphical user interfaces simplifies the application of the model and the visualization of the results. Three flow resistance approaches and four bedload transport equations appropriate for steep channel gradients have been implemented. Several formulas are established to take into account the effect of flow resistance due to form roughness on sediment transport in channels with stable structures by modifying the energy slope. The degree of the reduction of the energy slope can be used as calibration parameter. These formulas can be combined dependent on the users needs. As a result of the modular structure of SETRAC the model can consider morphologic changes due to erosion and deposition as well as sediment transport by size fractions. Armouring effects can also be considered in combination with the one gain model. For simplified applications the bedload transport can also be calculated for the one grain-size model without morphologic changes resulting in shorter computation time.

Back-calculations of flume experiments have been used for model validation. Experiments to optimize a bedload retention basin show the models ability to simulate morphologic changes. Another flume study is used to test the fractional bedload transport module by modelling the development of an armor layer and a rotation of the channel slope.

The back calculations of well documented extreme events in Austria and Switzerland stress the importance of the consideration of form roughness losses. Neglecting form roughness at steep slopes results in overestimation of the observed bedload transport by about a factor of 10 on average. Pure limitation of the sediment stock in reaches to model supply limited conditions can not reproduce the time evolution of some extreme events, because all the sediment stock would be depleted with the raising limb of the hydrograph, which is contrary to observations. A simple armour criteria in combination with the one grain model is not sufficient in many case studies to reduce the transport capacity during flood events, particularly at steep channel slopes. Form roughness losses appear to be important to describe transport processes during flood events in steep channel systems. The quantification of losses due to form drag is not trivial. Depending on the channel slope, the contribution of form roughness to total roughness may be in the range from 50 to 90 % for natural streams. Further investigations are required to develop more reliable approaches to estimate form roughness losses for the calculation of bedload transport at steep slopes during extreme events.

The SETRAC model has been developed for the simulation of bedload transport at steep slopes with a focus on extreme flood events. The application of the one grain-size

model appears to be adequate to describe the erosion and deposition behavior during intense flood events.

The kinematic wave assumption used in the SETRAC model appears sufficiently accurate for the application in steep headwater torrents and mountain streams, especially in combination with a Schoklitsch type bedload transport equation recommended for streams steeper than 2 %. Nevertheless the user has to keep in mind the limitation of this approach concerning backwater effects caused by check dams or bridge passages. Further developments of the SETRAC model should include a consideration of the full dynamic wave routing. The main improvement would be the possibility to calculate the waterlevel for channel reaches with backwater effects and a better representation of the effects of hydraulic structures concerning the bedload transport. Modelling reaches with counter slope, that can even occur at steep channels when the spatial discretisation is very fine (e.g. step-pool systems), would then also be possible.

Nomenclature

α	variable	—
β	variable	—
Δt	time step	<i>s</i>
Δx	discretisation length	<i>m</i>
δz	enhancement or lowering of the cross-section	<i>m</i>
η_1	application criteria 1 for the kinematic wave	—
η_2	application criteria 2 for the kinematic wave	—
$\frac{1}{g} \frac{\partial v}{\partial t}$	local acceleration	—
$\frac{\partial h}{\partial x}$	pressure term	—
$\frac{v}{g} \frac{\partial v}{\partial x}$	convective acceleration	—
Γ	boulder concentration	—
γ	exponent in the hiding function	—
ν	kinematic viscosity of the water	<i>m</i> ² / <i>s</i>
ω	variable	—
$\bar{\tau}$	bed shear stress	<i>N/m</i> ²
Φ_{bi}	dimensionless transport rate per size fraction	—
Φ_b	dimensionless bedload transport rate	—
ρ_f	density of fluid	<i>kg/m</i> ³
ρ_s	density of sediment	<i>kg/m</i> ³
τ_c	critical shear stress at beginning of motion	<i>N/m</i> ²
θ	dimensionless shear stress	—
$\theta_{c,D}$	dimensionless critical shear stress for an armour layer	—
θ_{c50}	dimensionless critical shear stress of the surface median grain size	—

θ_{ci}	dimensionless critical shear stress for a size fraction	—
θ_{ci}	dimensionless critical shear stress per size fraction	—
θ_{crS}	critical dimensionless shear stress at beginning of motion corrected for steep slopes	—
θ_c	critical dimensionless shear stress at beginning of motion	—
θ_i	dimensionless shear stress per size fraction	—
A	wetted area of the cross-section	m^2
a	a variable exponent	—
c	parameter	—
C_{bc}	volumetric bedload concentration at capacity	—
C_b	volumetric bedload concentration	—
C_D	coefficient of drag force	—
c_k	velocity of propagation of the kinematic wave	m/s
C_L	coefficient of lift force	—
d	uniform grain diameter	m
d_*	dimensionless grain diameter	—
d_{30}	characteristic grain size , 30 % of the material by weight is finer	m
d_{40}	characteristic grain size , 40 % of the material by weight is finer	m
d_{50s}	subsurface median particle size	m
d_{50}	characteristic grain size , 50 % of the material by weight is finer	m
d_{65}	characteristic grain size , 65 % of the material by weight is finer	m
d_{84}	characteristic grain size , 84 % of the material by weight is finer	m
d_{90}	characteristic grain size , 90 % of the material by weight is finer	m
d_{gi}	geometric mean diameter of the size fraction	m
d_i	characteristic grain diameter for a size fraction	m
$d_{m,D}$	mean diameter of the armour layer	m
$d_{m,S}$	mean diameter of the subsurface layer	m
d_{max}	maximum particle size	m

d_m	mean grain size	m
E	empirical coefficient	—
e	parameter	—
e	resistance factor defined by the ratio $e = v_m/v^*$	—
f	Darcy-Weisbach friction factor	—
f_{bt}	Darcy-Weisbach friction factor for bedload transport resistance	—
F_i	proportion of the grain size distribution	—
Fr	Froude number equal to $v/(gh)^{0.5}$	—
g	acceleration due to gravity	m/s^2
G_E	total bedload volume	m^3
g_s	bedload mass discharge per unit width	kg/sm
h	water depth	m
h_f	fluid flow depth	m
h_m	mixture flow depth	m
i	index for the length step	—
j	index for the time step	—
$k_{i,z}$	a weighting factor	—
k_{St}	Strickler's coefficient of total roughness	$m^{1/3}/s$
L_d	length of the (sub-) section down stream	m
L_u	length of the (sub-) section up stream	m
n_r	Manning's roughness coefficient associated with skin friction only	$s/m^{1/3}$
n_{tot}	Manning's coefficient of total roughness	$s/m^{1/3}$
p	lateral inflow per unit width	m^3/sm
Q	water discharge	m^3/s
q	specific water discharge per unit width	m^3/sm
$Q_{B,i}$	volumetric sediment input	m^3
q_{bi}	specific bedload transport rate per unit width and size fraction	m^3/sm
Q_b	average bedload transport rate	m^3/s

q_b	specific bedload discharge per unit width	m^3/sm
$q_{c,D}$	critical specific discharge $q_{c,D}$ to break up an armor layer	m
q_{c2}	critical discharge for the Phase 2 transport	m^3/sm
Q_c	critical discharge	m^3/s
q_c	critical discharge at beginning of bedload transport	m
Q_m	average flow rate	m^3/s
R	hydraulic radius	m
r	is the rate of change of bedload discharge with water mass discharge	—
S	energy slope	m/m
s	ratio between sediment to fluid density	—
S_0	channel slope	m/m
S_f	friction slope	m/m
S_{red}	component of the energy line related with skin friction	m/m
t	time	s
v	flow velocity	m/s
v^*	shear velocity	m/s
v_m	mean flow velocity	m/s
V_{re}	bedload effective runoff	m^3
V_{tot}	total bedload volume	m^3
W	submerged weight	kg
W_d	width of the main channel down stream	m
W_u	width of the main channel up stream	m
x	coordinate in x direction	m
y	variable	—

Bibliography

- Aberle, J. and G. Smart (2003). The influence of roughness structure on flow resistance on steep slopes. *Journal of Hydraulic Research* 41(3), 259–269.
- Armanini, A. (1995). Non-uniform sediment transport dynamics of the active layer. *Journal of Hydraulic Research* 33(5), 611–622.
- Armanini, A. and G. Di Silvio (1988). A one-dimensional model for the transport of a sediment mixture in non-equilibrium conditions. *Journal of Hydraulic Research* 26(3), 275–292.
- Armanini, A. and C. Gregoretti (2005). Incipient sediment motion at high slopes in uniform flow condition. *Water Resources Research* 41, 8.
- Badoux, A. and D. Rickenmann (2008). Berechnung zum Geschiebetransport während der Hochwasser 1993 und 2000 im Wallis. *Wasser Energie Luft* 3, 217–226. 100.Jahrgang.
- Bagnold, R. A. (1956). The flow of cohesionless grains in fluids. *Royal Society of London Philosophical Transactions Series A* 249, 235–297.
- Bahadori, F., A. Ardeshtir, and A. Tahershamsi (2006). Prediction of alluvial river bed variation by SDAR model. *Journal of Hydraulic Research* 44(5), 614–623.
- Barry, J., J. M. Buffington, and J. G. King (2004). A general power equation for predicting bed load transport rates in gravel bed rivers. *Water Resources Research* 40, W10401.
- Bathurst, J. (2002). At-a-site variation and minimum flow resistance for mountain rivers. *Journal of Hydrology* 269(1-2), 11–26.
- Bathurst, J. (2007). Effect of coarse surface layer on bed-load transport. *Journal of Hydraulic Engineering* 133(11), 1192–1205.
- Bathurst, J., W. Graf, and H. Cao (1987). Bed load discharge equations for steep mountain rivers. In C. R. T. and J. C. Bathurst and R. D. Hey (Eds.), *Sediment Transport in Gravel-Bed Rivers*, New York, pp. 453–477. John Wiley.
- Bathurst, J. C. (1985). Flow resistance estimation in mountain rivers. *Journal Of Hydraulic Engineering-ASCE* 111(4), 625–643.
- Beffa, C. (2005). 2D-Simulation der Sohlenreaktion in einer Flussverzweigung. *Österreichische Wasser- und Abfallwirtschaft* 42(1-2), 1–6.

-
- Bezzola, G., N. Semadeni, and T. Janisch (2005). *Mitteilung VAW 190*, Chapter Rampen und Schwellen - künstliche Schnellen, pp. 241–254.
- Bezzola, G. R. and C. Hegg (2007). Ereignisanalyse Hochwasser 2005, Teil 1- Prozesse, Schäden und erste Einordnung. Umwelt-Wissen 0707, Bundesamt für Umwelt BAFU, Eidgenössische Forschungsanstalt WSL. 215 p.
- Bezzola, G. R. and C. Hegg (2008). Ereignisanalyse Hochwasser 2005, Teil 2 - Analyse von Prozessen, Massnahmen und Gefahregrundlagen. Umwelt-Wissen 0825, Bundesamt für Umwelt BAFU, Eidgenössische Forschungsanstalt WSL. 429 p.
- Brummer, C. J. and D. R. Montgomery (2003). Downstream coarsening in headwater channels. *Water Resources Research* 39(10). 1294.
- Buffington, J. and D. Montgomery (1997). A systematic analysis of eight decades of incipient motion studies, with special reference to gravel-bedded rivers. *Water Resources Research* 33(8), 1993–2029.
- Canovaro, F., E. P. and L. Solari (2007a). Effects of macro-scale bed roughness geometry on flow resistance. *Water Resources Research* 43, 17.
- Canovaro, F., E. Paris, and L. Solari (2007). Effects of macro-scale bed roughness geometry on flow resistance. *Water Resources Research* 43(10), W10414.
- Canovaro, F. and L. Solari (2006). Flow resistance associated to a schematic step-pool pattern. In L. Ferreira, Alves and Cardoso (Eds.), *River Flow 2006*, Volume 1, pp. 1005–1011.
- Canovaro, F. and L. Solari (2007b). Dissipative analogies between a schematic macro-roughness arrangement and step-pool morphology. *Earth Surface Processes and Landforms* 32(11), 1628–1640.
- Chiari, M., K. Friedl, and D. Rickenmann (2007). Geschiebetransport in Wildbächen. *Forstzeitung* 5, 16–17.
- Chiari, M., E. Mair, and D. Rickenmann (2008). Geschiebetransportmodellierung in Wildbächen und Vergleich der morphologischen Veränderung mit LiDAR Daten. In *Schutz des Lebensraumes vor Hochwasser, Muren, Massenbewegungen und Lawinen. Interpraevent , Dornbirn, Vorarlberg, Austria. Conference Proceedings,* Volume 1, pp. 295–306.
- Chiari, M. and D. Rickenmann (2007). The influence of form roughness on modelling of sediment transport at steep slopes. In S. Kostadinov, S. Bruk, and D. Walling (Eds.), *Making 100 years of experience with erosion and torrent control in Serbia, Conference Proceedings on CD, Erosion and torrent control as a factor in sustainable river basin management.*
- Chow, V., D. Maidment, and L. Mays (1988). *Applied Hydrology*. New York: McGraw-Hill Inc.
-

-
- Church, M. and A. Zimmerman (2007). Form stability of step-pool channels: Research progress. *Water Resources Research* 43(W0341), 21.
- Colebrook, C. and C. White (1937). Experiments with fluid friction in roughened pipes. In *Proc. of the Royal Society of London*, Volume 161 of A, pp. 367–387.
- Courant, R., K. Friedrichs, and H. Lewy (1967, March). On the partial difference equations of mathematical physics. *IBM Journal*, 215–234. English translation of the 1928 German original.
- Cui, Y. and G. Parker (2005). Numerical model of sediment pulses and sediment-supply disturbances in mountain rivers. *Journal of Hydraulic Engineering* 131(8), 646–656.
- D'Agostino, V. and M. Lenzi (1999). Bedload transport in the instrumented catchment of the Rio Cordon Part II: Analysis of the bedload rate. *Catena* 36, 191–204.
- Doten, C., L. Bowling, J. Lanini, E. P. Maurer, and D. P. Lettenmaier (2006). A spatially distributed model for the dynamic prediction of sediment erosion and transport in mountainous forested watersheds. *Water Resources Research* 42, W04417.
- Fehr, R. (1987). *Geschiebeanalysen in Gebirgsflüssen*. Mitteilung 92 der Versuchsanstalt für Wasserbau, Hydrologie und Glaziologie, ETH Zurich.
- Ferguson, R. (1994). Critical discharge for entrainment of poorly sorted gravel. *Earth Surface Processes and Landforms* 19, 179–186.
- Friedl, K. (2004). *Computergestützte Modellierung von Sedimenttransport in alpinen Einzugsgebieten unter Anwendung Geographischer Informationssysteme*. Ph. D. thesis, Universität für Bodenkultur, Wien, Institut für Vermessung, Fernerkundung und Landinformation.
- Fuchs, H. and K. Friedl (1999). Sedimenttransport in alpinen Einzugsgebieten. Technical Report 1. Zwischenbericht, Universität für Bodenkultur Wien, Institut für Vermessung, Fernerkundung und Landinformation. Auftraggeber: Bundesministerium für Land- und Forstwirtschaft, Umwelt und Wasserwirtschaft.
- Fuchs, H. and K. Friedl (2000). Sedimenttransport in alpinen Einzugsgebieten. Technical Report 2. Zwischenbericht, Universität für Bodenkultur Wien, Institut für Vermessung, Fernerkundung und Landinformation. Auftraggeber: Bundesministerium für Land- und Forstwirtschaft, Umwelt und Wasserwirtschaft.
- Fuchs, H. and K. Friedl (2002). Ermittlung des Naturraumrisikos in ausgewählten Einzugsgebieten - Entwicklung und Anwendung des Modells SETRAC als Grundlage einer flächendeckenden, dynamisierten, gefahrenorientierten regionalen Raumplanung. Technical Report Endbericht, Universität für Bodenkultur Wien, Institut für Vermessung, Fernerkundung und Landinformation. Auftraggeber: Bundesministerium für Land- und Forstwirtschaft, Umwelt und Wasserwirtschaft.
- Gao, P. and A. D. Abrahams (2004). Bedload transport resistance in rough open-channel flows. *Earth Surface Processes and Landforms* 29(4), 423–435.
-

- Gessler, J. (1965). *Der Geschiebetriebbeginn bei Mischungen untersucht an natürlichen Abpflästerungserscheinungen in Kanälen*. Mitteilung No. 60 der Versuchsanstalt für Wasserbau und Erdbau, ETH, Zürich.
- Günter, A. (1971). *Die kritische mittlere Sohlenschubspannung bei Geschiebemischungen unter Berücksichtigung des Deckschichtbildung und der turbulenzbedingten Sohlenschubspannungsschwankungen*. Mitteilung der Versuchsanstalt für Wasserbau, Hydrologie und Glaziologie (VAW) Nr. 3, ETH, Zürich.
- Gomez, B. (1987). *Glacio-fluvial Sediment Transfer*, Chapter Bedload, pp. 355–376. New York: John Wiley.
- Gomez, B. and M. Church (1989). An assessment of bedload sediment transport formulae for gravel bed rivers. *Journal of Water Resources Research* 25(6), 1161–1186.
- Gomi, T. and R. Sidle (2003). Bed load transport in managed steep-gradient headwater streams of southeastern alaska. *Water Resources Research* 39(12), 1336.
- Habersack, H., M. Hengl, H. Knoblauch, G. Reichel, P. Rutschmann, B. Sackl, and M. Tritthart (2007). *Fließgewässersmodellierung - Arbeitsbehelf Hydrodynamik*, Volume 37. Bundesministerium für Land- und Forstwirtschaft, Umwelt und Wasserwirtschaft; Österreichischer Wasser- und Abfallwirtschaftsverband (ÖWAV).
- Hager, W. and K. Hager (1985). Application limits for the kinematic wave approximation. *Nordic Hydrology* 16, 203–212.
- Hassan, M. and M. Church (1994). Vertical mixing of coarse particles in gravel bed rivers: A kinematic model. *Water Resources Research* 30(4), 1173–1185.
- Hassan, M. A., M. Church, T. E. Lisle, F. Brardinoni, L. Benda, and G. E. Grant (2005). Sediment transport and channel morphology of small, forested streams. *Journal of the American Water Resources Association* 41(4), 853–876.
- Hübl, J., E. Ganahl, M. Bacher, M. Chiari, M. Holub, R. Kaitna, A. Prokop, G. Dunwoody, A. Forster, M. Kerschbaumer, and S. Schneiderbauer (2005). Ereignisdokumentation 22./23. August 2005, Tirol, Band 1: Generelle Aufnahme (5W-Standard). IAN Report 109, Institut für Alpine Naturgefahren. im Auftrag von: BMLFUW, Abt. IV/5 (unpublished).
- Hegg, C. and D. Rickenmann (1999). Comparison of bedload transport in a steep mountain torrent with a bedload transport formula. In *Hydraulic Engineering for Sustainable Water Resources Management at the Turn of the Millenium; Proceedings 28th IAHR Congress, 22-27 August 1999, Graz, Austria. [CD-ROM]*, Technical University, pp. 7.
- Hirano, M. (1971). Studies on variation and equilibrium state of a river bed composed of non-uniform material. *Trans. of JSCE* 4, 128–129.
-

-
- Hochwasser (2006). Hochwasser 2005 - Ereignisdokumentation. Technical report, der Bundeswasserbauverwaltung, des Forsttechnischen Dienstes für Wildbach- und Lawinnenverbauung und des Hydrographischen Dienstes; Bundesministerium für Land- und Forstwirtschaft, Umwelt- und Wasserwirtschaft.
- Hu, S. and A. D. Abrahams (2004). Resistance to overland flow due to bed-load transport on plane mobile beds. *Earth Surface Processes and Landforms* 29(13), 1691–1701.
- Hu, S. and A. D. Abrahams (2005). The effect of bed mobility on resistance to overland flow. *Earth Surface Processes and Landforms* 30(11), 1461–1470.
- Hu, S. and A. D. Abrahams (2006). Partitioning resistance to overland flow on rough mobile beds. *Earth Surface Processes and Landforms* 31(10), 1280–1291.
- Huang, J. and B. Greimann (2006). User's Manual for GSTAR-1D 1.1. Report rr-2006-xx, US Department of Interior, Bureau of Reclamation, Technical Service Center, Sedimentation and River Hydraulics Group. 247p.
- Hungr, O. (2005). *Debris-flow Hazard and Related Phenomena*, Chapter Classification and terminology, pp. 9–23. Springer.
- Hunziker, R. and M. Jäggi (1997). Fractionwise sediment calculation in case of erosion and aggradation. In *Proceedings of the 27th Congress, Int Association of Hydraulic Research*, Volume 2, pp. 1475–1480.
- Hunziker, R. and M. N. R. Jäggi (2002). Grain sorting processes. *Journal of Hydraulic Engineering* 128(12), 1060–1068.
- Jäggi, M. (1992). *Sedimenthaushalt und Stabilität von Flussbauten*. Mitteilungen der Versuchsanstalt für Wasserbau, Hydrologie und Glaziologie der ETH Zürich Nr. 119.
- Kaitna, R., M. Chiari, J. Zlatic-Jugovic, M. Kerschbaumer, J. Kapeller, F. Zott, R. Totschnig, and J. Hübl (2007). Optimisation of a bedload retention basin using a physical scale model and numerical simulation. In S. Kostadinov, S. Bru, and D. Walling (Eds.), *Erosion and torrent control as a factor in sustainable river basin management, Making 100 years of experience with erosion and torrent control in Serbia*, Belgrade. Proceedings on CD.
- Kidson, R. L., K. S. Richards, and P. A. Carling (2006). Hydraulic model calibration for extreme floods in bedrock-confined channels: case study from northern thailand. *Hydrological Processes* 20(2), 329–344.
- Kirchner, J., W. Dietrich, F. Iseya, and H. Ikeda (1990). The variability of critical shear stress, friction angle, and grain protrusion in water worked sediments. *Journal of Sedimentology* 37, 647–672.
- Lamb, M., W. Dietrich, and J. Venditti (2008). Is the critical shields stress for incipient sediment motion dependent on channel-bed slope? *Journal of Geophysical Research* 113, F02008.
-

-
- Lee, A. and R. Ferguson (2002). Velocity and flow resistance in step-pool streams. *Geomorphology* 46(1-2), 59–71.
- Lenzi, M., L.Mao, and F. Comiti (2006). When does bedload transport begin in steep boulder-bed streams? *Hydrological Processes* 20, 3517–3533.
- LLE-Diemtigtal (2006). Lokale lösungsorientierte Ereignisanalyse (LLE) Hochwasser 2005 im Diemtigtal. Technischer Bericht, Schälchli, Abegg + Hunzinger, Bern; geo7 AG, Bern, Kissling + Zbinden AG, Spiez. im Auftrag des Tiefbauamtes des Kantons Bern, 53 S. + Anhang.
- LLE-Lütschine (2007). Lokale Lösungsorientierte Ereignisanalyse (LLE) Lütschine. Technischer Bericht, PD Dr. Martin Jäggi, Ebmatingen; Geotest AG, Zollikofen; Dr. Christoph Lehmann, Schönbühl; Mätzener & Wyss AG Interlaken; Dr. Felix Naef, ETH Zürich; Bettschen + Blumer AG, Unterseen. im Auftrag des Tiefbauamtes des Kantons Bern, 124 S.
- LLE-Reichenbach (2006). Lokale Lösungsorientierte Ereignisanalyse (LLE) Reichenbach. Technischer Bericht, Emch+Berger AG, Spiez; Hunziker, Zarn & Partner AG, Aarau; Geotest AG, Zollikofen. im Auftrag des Tiefbauamtes des Kantons Bern, 62 S.
- Mair, E. (2008). Geschiebetransportsimulationen am Beispiel des Suggadinbaches in Vorarlberg. Master's thesis, University of Natural Resources and Applied Life Science, Vienna. 109 p.
- Maniak, U. (2005). *Hydrologie und Wasserwirtschaft: eine Einführung für Ingenieure* (5., bearb. u. erw. Aufl. ed.). Springer-Verlag, Berlin.
- Mao, L., G. U. A. Iroumé, and M. Lenzi (2008). Field based analysis of sediment entrainment in two high gradient streams located in alpine and andine environments. *Geomorphology* 93, 368–383.
- Mathys, N., S. Brochot, M. Meunier, and D. Richard. (2003). Erosion quantification in the small marly experimental catchments of Draix (Alpes de Haute Provence, France). Calibration of the ETC rainfall-runoff-erosion model. *Catena* 50, 527–548.
- MeteoSchweiz (2006). Starkniederschlagsereignis August 2005. Arbeitsberichte der MeteoSchweiz 211, Bundesamt für Meteorologie und Klimatologie. 63pp.
- Meyer-Peter, E. and R. Mueller (1948). Formulas for bedload transport. In *Proc. 2nd meeting Int. Assoc. Hydraulic Structures Research, Stockholm, Sweden*, pp. 39–64. Appendix 2.
- Millar, R. (1999). Grain and form resistance in gravel-bed rivers. *Journal of Hydraulic Research* 37(3), 303–312.
- Morvan, H., D. Knight, N. Wright, X. Tang, and A. Crossley (2008). The concept of roughness in fluvial hydraulic and its formulation in 1D, 2D and 3D numerical simulation models. *Journal of Hydraulic Engineering* 46(2), 191–208.
-

-
- Pagliara, S. and P. Chiavaccini (2006). Flow resistance of rock chutes with protruding boulders. *Journal of Hydraulic Engineering* 132(6), 545–552. doi:10.1061/(ASCE)0733-9429(2006)132:6(545).
- Palt, S. (2001). *Sedimenttransporte im Himalaya-Karakorum und ihre Bedeutung für Wasserkraftanlagen*. Mitteilung 209 des Instituts für Wasserwirtschaft und Kulturtechnik, Universität Karlsruhe.
- Papanicolaou, A., A. Bdour, and E. Wicklein (2004). One-dimensional hydrodynamic/sediment transport model applicable to steep mountain streams. *Journal of Hydraulic Research* 42(4), 357–375.
- Parker, G. (2008). *Sedimentation Engineering: Theories, Measurements, Modeling, and Practice, ASCE Manuals and Reports on Engineering Practice No. 110*, Chapter 3: Transport of gravel and sediment mixtures, pp. 165–252.
- Parker, G., M. Hassan, and P. Wilcock (2007). Adjustment of the bed surface size distribution of gravel-bed rivers in response to cycled hydrographs. In *Gravel Bed River 2005*.
- Parker, G., P. Klingeman, and D. McLean (1982a). Bedload and size distribution in paved gravel-bed streams. *Journal of Hydraulic Engineering* 108(4), 544–571.
- Parker, G., P. Klingeman, and D. McLean (1982b). On why gravel bed streams are paved. *Water Resources Research* 18(5), 1409–1423.
- Parker, G., C. Paola, and S. Leclair (2000). Probabilistic Exner sediment continuity equation for mixtures with no active layer. *Journal of Hydraulic Engineering* 126(11), 818–826.
- Parker, G. and C. Toro-Escobar (2002). Equal mobility of gravel in streams: The remains of the day. *Water Resources Research* 38(11), 1264.
- Petit, F., F. Gob, G. Houbrechts, and A. Assani (2005). Critical specific stream power in gravel-bed rivers. *Geomorphology* 69, 92–101.
- Rathburn, S. and E. Wohl (2001). One-dimensional sediment transport modeling of pool recovery along a mountain channel after a reservoir sediment release. *Regulated Rivers: Research & Management* 17(3), 251–273.
- Recking, A., P. Frey, A. Paquier, P. Belleudy, and J. Y. Champagne (2008a). Bedload transport flume experiments on steep slopes. *Journal of Hydraulic Engineering* 134(9), 1302–1310.
- Recking, A., P. Frey, A. Paquier, P. Belleudy, and J. Y. Champagne (2008b). Feedback between bed load transport and flow resistance in gravel and cobble bed rivers. *Water Resources Research* 44(5), W05412.
-

-
- Reichel, G., R. Fäh, and G. Baumhackl (2000). FLORIS-2000: Ansätze zur 1.5D-Simulation des Sedimenttransportes im Rahmen der mathematischen Modellierung von Fließvorgängen. In *Internat. Symposium 'Betrieb und Überwachung wasserbaulicher Anlagen'*.
- Reid, I. and J. Laronne (1995). Bedload sediment transport in an ephemeral stream and comparison with seasonal and perennial counterparts. *Water Resources Research* 31(3), 773–781.
- Rice, C., K. Kadavy, and K. Robinson (1998). Roughness of loose rock riprap on steep slopes. *Journal of Hydraulic Engineering* 124(2), 179–184.
- Rickenmann, D. (1990). *Bedload transport capacity of slurry flows at steep slopes*. Mitteilung 103 der Versuchsanstalt für Wasserbau, Hydrologie Glaziologie, ETH Zürich.
- Rickenmann, D. (1991). Hyperconcentrated flow and sediment transport at steep slopes. *Journal of Hydraulic Engineering Vol. 117*(11), 1419–1439.
- Rickenmann, D. (1994). An alternative equation for the mean velocity in gravel-bed rivers and mountain torrents. In G. C. . R. Rumer (Ed.), *Proceedings ASCE 1994 National Conference on Hydraulic Engineering, Buffalo N.Y., USA*, pp. 672–676, Volume 1. ASCE.
- Rickenmann, D. (1996). Fließgeschwindigkeit in Wildbächen und Gebirgsflüssen. *Wasser, Energie, Luft* 88(11/12), 298–304.
- Rickenmann, D. (2001). Comparison of bed load transport in torrents and gravel bed streams. *Water Resources Research* 37(12), 3295–3305.
- Rickenmann, D. (2005). *Geschiebetransport bei steilen Gefällen*. Mitteilung 190 der Versuchsanstalt für Wasserbau, Hydrologie und Glaziologie, ETH Zurich: 107-119.
- Rickenmann, D., M. Chiari, and K. Friedl (2006). SETRAC - A sediment routing model for steep torrent channels. In R. Ferreira, E. A. J. Leal, and A. Cardoso (Eds.), *River Flow 2006*, Volume 1, London, pp. 843–852. Taylor & Francis.
- Rickenmann, D., L. Hunzinger, and A. Koschni (2008). Hochwasser und Sedimenttransport während des Unwetters vom August 2005 in der Schweiz. In H. J. K. G. Mikos, M. (Ed.), *Schutz des Lebensraumes vor Hochwasser, Muren, Massenbewegungen und Lawinen. Interpraevent , Dornbirn, Vorarlberg, Austria. Conference Proceedings*, Volume 1, pp. 465–476.
- Rickenmann, D., A. Koschni, M. Chiari, C. Scheidl, and N. Canuto (2008). *Ereignisanalyse Hochwasser 2005, Teil2 - Analyse von Prozessen, Maßnahmen und Gefahrengrundlagen*, Chapter Abschätzung von Feststofffrachten in Wildbächen und Gebirgsflüssen, pp. 152–162. Bundesamt für Umwelt BAFU, Eidgen. Forschungsanstalt WSL, Bern. Umwelt-Wissen, Nr. 0825.
-

-
- Rinderer, M., S. Jenewein, S. Senfter, D. Rickenmann, F. Schöber, J. Stötter, and C. Hegg (i.p.). *Sustainability in Natural Hazard Management*, Chapter Runoff and bedload transport modelling for flood hazard assessment in small alpine catchments - the model PROMAB-GIS.
- Ryan, S., L. Porth, and C. Troendle (2002). Defining phases of bedload transport using piecewise regression. *Earth Surface Processes and Landforms* 27, 971–990.
- Ryan, S., L. Porth, and C. Troendle (2005). Coarse sediment transport in mountain streams in Colorado and Wyoming, USA. *Earth Surface Processes and Landforms* 30, 269–288.
- Scheidl, C., D. Rickenmann, and M. Chiari (2008). The use of airborne LiDAR data for the analysis of debris flow events in Switzerland. *Natural Hazards and Earth System Science* 8(5), 1113–1127.
- Schoklitsch, A. (1950). *Handbuch des Wasserbaus, 2. Auflage*. Springer Verlag, Wien.
- Schoklitsch, A. (1962). *Handbuch des Wasserbaus, 3rd edition*. Springer Verlag, Wien.
- Shields, A. (1936). *Mitteilungen der Preussischen Versuchsanstalt für Wasserbau und Schiffbau* 26, Chapter Application of similarity principles and turbulence research to bed-load movement, pp. 5–24.
- Shvidchenko, A. and G. Pender (2000). Flume study of the effect of relative depth on the incipient motion of coarse uniform sediments. *Water Resources Research* 36, 619–628. 2.
- Singh, V. (1996). *Kinematic Wave Modeling in Water Resources: Surface Water Hydrology*. Wiley, New York.
- Smart, G. (2006). The resistance of transported sediment. In Ferreira, Alves, Leal, and Cardoso (Eds.), *River Flow 2006*, Volume 1, pp. 867–875. Taylor & Francis Group, London.
- Smart, G., M. Duncanand, and M. Walsh (2002). Relatively rough flow resistance equations. *Journal of Hydraulic Engineering* 128(6), 568–578.
- Smart, G. and M. Jäggi (1983). *Sedimenttransport in steilen Gerinnen*. Mitteilung 64 der Versuchsanstalt für Wasserbau, Hydrologie und Glaziologie, ETH Zurich.
- Solari, L. and G. Parker (2000). The curious case of mobility reversal in sediment mixtures. *Journal of Hydraulic Engineering, ASCE* 12(3), 198–208.
- Song, T., Y. Chiew, and c.o. Chin (1998). Effect of bedload movement on flow friction factor. *Journal of Hydraulic Engineering*, 165–175.
- Stevens, M., G. Lewis, and D. Simons (1976). Safety factors for riprap protection. *Journal of the Hydraulics Division* 102(5), 637–655.
-

-
- Strickler, A. (1923). *Beiträge zur Frage der Geschwindigkeitsformel und der Rauheitszahlen für Ströme, Kanäle und geschlossene Leitungen*. Mitteilungen des Amtes für Wasserwirtschaft 16.
- Takahashi, T. (1987). High velocity flow in steep erodible channels. In *Proceedings 22nd IAHR Congress, Lausanne, Switzerland, Techn. Session A*, pp. 42–53. IHAR.
- Thomas, W. and H. Chang (2008). *Sedimentation Engineering: Theories, Measurements, Modeling, and Practice, ASCE Manuals and Reports on Engineering Practice No. 110*, Chapter 14: Computational Modelling of Sedimentation Processes, pp. 649–681.
- USACE (1994). Engineering and Design - Flood-Runoff Analysis. Chapter 9 Streamflow and Reservoir Routing Publication Number: EM 1110-2-1417. Technical report.
- Vetsch, D., R. Fäh, D. Farshi, and R. Müller (2005). Ein objektorientiertes Softwaresystem zur numerischen Simulation von Naturgefahren. In *Versuchsanstalt für Wasserbau, Hydrologie und Glaziologie, ETH Zürich, Mitteilung Nr. 190*, pp. 201–212. VAW.
- Vieira, D. and W. Wu (2002). One-Dimensional Channel Network Model CCHE1D Version 3.0 - User's Manual. Report rr-2006-xx, National Center for Computational Hydroscience and Engineering. 181p.
- Vollmer, S. and M. Kleinhans (2007). Predicting incipient motion, including the effect of turbulent pressure fluctuations in the bed. *Water Resources Research* 43, 1–16. W05410.
- White, S. A. and Y. Wang (2003). Utilizing DEMs derived from LiDAR data to analyze morphologic change in the North Carolina coastline. *Remote Sensing of Environment* 85, 39–47.
- Whittacker, J. and M. Jäggi (1986). *Blockschwellen*. Mitteilung 91 der Versuchsanstalt für Wasserbau, Hydrologie Glaziologie, ETH Zürich.
- Wicks, J. and J. Bathurst (1996). SHESED: a physically based, distributed erosion and sediment yield component for the SHE hydrological modelling system. *Journal of Hydrology* 175, 213–238.
- Wieberg, P. and J. Smith (1987). Initial motion of coarse sediment in streams of high gradient. In *Erosion and Sedimentation in the Pacific Pim (Proceedings of the Corvallis Symposium)*, pp. 299–308.
- Wilcox, A. and E. Wohl (2006). Flow resistance dynamics in step-pool stream channels: 1. Large woody debris and controls on total resistance. *Water Resources Research* 42, W05418.
- Wohl, E. and D. Thompson (2000). Velocity characteristics along a small step-pool channel. *Earth Surface Processes and Landforms* 25, 353–367.
-

-
- Wong, M. and G. Parker (2006). Re-analysis and correction of bedload relation of Meyer-Peter and Müller using their own database. *Journal of Hydraulic Engineering*, 31p.
- Woolard, J. W. and J. D. Colby (2002). Spatial characterization, resolution, and volumetric change of coastal dunes using airborne LIDAR: Cape Hatteras, North Carolina. *Geomorphology* 48, 269–287.
- Wright, S. and G. Parker (2005a). Modeling downstream fining in sand-bed rivers. i: formulation. *Journal of Hydraulic Research* 43(6), 612–619.
- Wright, S. and G. Parker (2005b). Modeling downstream fining in sand-bed rivers. ii: application. *Journal of Hydraulic Research* 43(6), 620–630.
- Wu, W. (2001). CCHE2D Sediment Transport Model. Report rr-2006-xx, National Center for Computational Hydroscience and Engineering. 48p.
- Yager, E. M., J. W. Kirchner, and W. E. Dietrich (2007). Calculating bed load transport in steep boulder bed channels. *Water Resources Research* 43(7), W07418.
- Yang, S., J. HU, and X. Wang (2006). Incipient motion of coarse particles in high gradient rivers. *International Journal of Sediment Research* 21(3), 220–229.
- Zimmermann, A. and M. Church (2001). Channel morphology, gradient profiles and bed stresses during flood in a step-pool channel. *Geomorphology* 40, 311–327.
-

Curriculum vitae

Curriculum vitae

Personal Details

Name	CHIARI, Michael
Address	Brunnenfeldstraße 913, A-5411 Oberalm, Austria
Tel	+43-(0)699- 81901690
E-mail	Michael.Chiari@boku.ac.at
Born	1979-11-07 in Hallein, Salzburg, Austria
Nationality	Austrian
Gender	Male
Marital Status	Married
Depentants	None

Education

1990-1998	Secondary school
1998	Matura (Austrian school leaving certificate, university entry qualification)
1998-1999	Community service in an old people's home in Großgmain
1999	University of Natural Ressources and Applied Life Sciences, Vienna Course of study: Forestry
2005-06	Degree of Diplom Ingenieur (civil engineer)
2005-2009	University of Natural Ressources and Applied Life Sciences, Vienna Course of study: PhD/Forestry, Topic of research: Numerical modelling of sediment transport in torrents

Work Experience

2003-2005	University of Natural Ressources and Applied Life Sciences, Vienna: Working for the project "Sicherheitsstudie Feuersanglawine"
2005-2009	University of Natural Ressources and Applied Life Sciences, Vienna: Project Assistant for numerical simulation of sediment transport in torrents (4 years project)

Holiday work

- 1997 Alpen-Mayr KESTAG, Salzburg: Working as a trainee for Transport logistic
- 2001 Österreichische Bundesforste AG, Forstbetrieb Abtenau: Surveying borders in steep mountain forests
- 2002 Forrest technical service for torrent and avalanche control (WLV), Bludenz: Evaluation of protection measures
- 2003 Bundesamt und Forschungszentrum für Wald: Mapping torrent catchments

Hobbies Climbing, skiing, recumbent cycling

Publications

Chiari, M. (2005): Analyse der technischen Schutzmaßnahmen am Beispiel der Feuersanglawine Diplomarbeit an der Universität für Bodenkultur, Wien, S.160; Wien

Chiari, M., Rickenmann, D.(2007): The influence of form roughness on modelling sediment transport at steep slopes In: Kostadinov, St., Bruk, St., Walling, D. (Hrsg.), International Conference, Making 100 years of experience with erosion and torrent control in Serbia, Conference Abstracts, Erosion and torrent control as a factor in sustainable river basin management, 25.-28. September 2007, Belgrad, 55-56; ISBN: 978-86-7299-132-1

Chiari, M., Friedl, K., Rickenmann, D. (2007): Geschiebetransport in Wildbächen Forstzeitung, 5, 16-17; ISSN 1012-4667

Chiari, M., Mair, E., Rickenmann, D. (2008): Geschiebetransportmodellierung in Wildbächen und Vergleich der morphologischen Veränderung mit LIDAR Daten. In: Mikos, M., Hübl, J., Koboltschnig, G. (Hrsg.), 11th Congress INTERPRAEVENT 2008, 26.-30. Mai 2008, Dornbirn Vol. 1, 295 - 306; ISBN 978-3-901164-10-1

Bacher, M., Chiari, M.(2005): Sicherheitsstudie Feuersanglawine, Winteraufnahmen 2005 Zwischenbericht, im Auftrag von: ÖBB (unpublished)

Hübl, J., Ganahl, E., Bacher, M., Chiari, M., Holub, M., Kaitna, R., Prokop, A., Dunwoody, G., Forster, A., Kerschbaumer, M., Schneiderbauer, S.. (2005): Ereignisdokumentation 22./23. August 2005, Tirol, Band 1: Generelle Aufnahme (5W-Standard) IAN Report 109, im Auftrag von: BMLFUW, Abt. IV/5 (unpublished)

Hübl, J., Ganahl, E., Bacher, M., Chiari, M., Holub, M., Kaitna, R., Prokop, A., Dunwoody, G., Forster, A., Schneiderbauer, S.. (2006): Dokumentation der Wildbachereignisse vom 22./23. August 2005 in Tirol, Band 2: Detaillierte Aufnahme (5W+ Standard) IAN Report 109, Band 2, Institut für Alpine Naturgefahren, Universität für Bodenkultur-Wien, im Auftrag des Lebensministerium, Abteilung IV/5 (unpublished)

- Hübl, J., Ganahl, E., Bacher, M., Chiari, M., Holub, M., Kaitna, R., Prokop, A., Dunwoody, G., Forster, A., Schneiderbauer, S.. (2006): Dokumentation der Wildbachereignisse vom 22./23. August 2005 in Tirol, Band 3: Zusammenstellung der Aufnahmen IAN Report 109, Band 3, Institut für Alpine Naturgefahren, Universität für Bodenkultur-Wien, im Auftrag des Lebensministerium, Abteilung IV/5 (unpublished)
- Hübl, J., Kleemayr, K., Chiari, M., Bacher, M.. (2006): Sicherheitsstudie Feueranglawine, Modul 1: Ermittlung der flächigen Schneehöhenverteilung und Wirksamkeitsbeurteilung der Verbauungsmaßnahmen; IAN Report 100 Modul 1 Österreichische Bundesbahnen (unpublished)
- Kaitna, R., Chiari, M., Zlatic-Jugovic, J., Kerschbaumer, M., Kapeller, H., Zott, F., Hübl, J. (2007): Optimisation of a bedload retention basin using a physical scale model and numerical simulation In: Kostadinov, St., Bruk, St., Walling, D. (Hrsg.), International Conference, Making 100 years of experience with erosion and torrent control in Serbia, Conference Proceedings on CD, Erosion and torrent control as a factor in sustainable river basin management, 25.-28. September 2007, Belgrade
- Kaitna, R., Zlatic-Jugovic, J., Kerschbaumer, M., Kapeller, J., Zott, F., Chiari, M., Totschnig, R., Hübl, J. (2007): Bedload Retention Basin Vorderbergerbach Austria - Physical Scale Model Study , In: Faculty of Civil Engineering, Zagreb , Proceedings on CD, 10th International Symposium on Water Management and Hydraulic Engineering, 4-9 Sept. 2007, Sibenik; ISBN: 978-953-6272-22-8
- Kaitna, R., Kerschbaumer, M., Zlatic-Jugovic, J., Chiari, M., Hübl, J.. (2008) Modellierung des Geschiebeablagerungsplatzes Vorderbergerbach Wildbach- und Lawinenverbau, H. 158, 24-31
- Rickenmann, D., Chiari, M., Friedl, K. (2006): SETRAC - A sediment routing model for steep torrent channels, In: Ferreira, R.M.L., Alves, E., Leal, J., Cardoso, A. (Eds.), River Flows 2006, proceedings of the International Conference on Fluvial Hydraulics, Lisbon, Portugal, 6-8 September 2006 1, Taylor & Francis, London, Riverflow 2006, International Conference on Fluvial Hydraulics, September 6 - 8, 2006 , Lisabon, Volume 1, 843-852; ISBN: 0-415-40815-6
- Rickenmann, D., Koschni A., Chiari M., Scheidl C., and Canuto, N. (2008): Ereignisanalyse Hochwasser 2005, Teil2 - Analyse von Prozessen, Maßnahmen und Gefahrengrundlagen, Chapter Abschätzung von Feststofffrachten in Wildbächen und Gebirgsflüssen, pp. 152-162. Bundesamt für Umwelt BAFU, Eidgen. Forschungsanstalt WSL, Bern. Umwelt-Wissen, Nr. 0825.
- Scheidl, C., Rickenmann, D., Chiari, M.(2008): The use of airborne LiDAR data for the analysis of debris flow events in Switzerland, Natural Hazards and Earth System Sciences 8(5), 1113-1127
-

Part X
Appendix

A SETRAC

A.1 Possible formula combination

All possible formula combinations for SETRAC simulations are shown in Figure A.1 to A.3. For simulations using the $q_b - q$ form possible combinations are shown in Figure A.1. Figure A.2 shows the possible combinations for the $\Phi_b - \theta$ form calculations, whereas Figure A.3 describes the combinations for fractional bedload transport. Within one figure all formulas can be combined without limitations. Flow velocity, bedload transport and incipient of motion are obligatory. The calculation of form roughness losses of the consideration of an armour layer criteria are optional modules.

flow velocity	bedload transport	incipient motion	form roughness losses (optional)	armour layer (optional)
$v = k_{st} R^{0.67} S^{0.5} \quad (6.15)$	$q_b = 3.1 \left(\frac{d_{90}}{d_{30}} \right)^{0.2} (q - q_c) S^{1.5} (s - 1)^{-1.5} \quad (6.35)$	$q_c = 0.065 (s - 1)^{1.67} g^{0.5} d_{50}^{1.5} S^{-1.12} \quad (6.36)$	$\frac{n_r}{n_{tot}} = \frac{0.0756 Q^{0.11}}{g^{0.06} d_{90}^{0.28} S^{0.33}} \quad (6.25)$	
			$\frac{n_r}{n_{tot}} = \frac{0.133 Q^{0.19}}{g^{0.096} d_{30}^{0.47} S^{0.19}} \quad (6.26)$	
			$\frac{n_r}{n_{tot}} = 0.092 S^{-0.35} \left(\frac{h}{d_{90}} \right)^{0.33} \quad (6.27)$	$q_{c,D} = q_c \left[\frac{d_{90}}{d_m} \right]^{10/9} \quad (6.39)$
$v = \frac{1.93 g^{0.5} h^{1.5} S^{0.5}}{d_{90}} \quad (6.18)$	$q_b = 12.6 \left(\frac{d_{90}}{d_{30}} \right)^{0.2} (q - q_c) S^{2.0} (s - 1)^{-1.6} \quad (6.34)$	$q_c = 0.143 (s - 1)^{1.67} g^{0.5} d_{50}^{1.5} S^{-1.167} \quad (6.37)$	$\frac{n_r}{n_{tot}} = 0.185 S^{-0.22} \left(\frac{h}{d_{90}} \right)^{0.55} \quad (6.28)$	

Figure A.1: Possible formula combinations for SETRAC simulations for sediment mixtures, using the $q_b - q$ form

flow velocity	bedload transport	incipient motion	form roughness losses (optional)	armour layer (optional)
$v = 2.5v^* \left(1 - e^{\frac{-0.005hm}{3^{0.3}d_{90}}} \right)^{0.5} \ln \left[\frac{12.3hm}{1.5d_{90}} \right]$ <p style="text-align: center;">(6.19)</p>	$q_b = \frac{4}{s-1} \left(\frac{d_{90}}{d_{30}} \right)^{0.2} q_i S^{1.6} \left(1 - \frac{\theta_{crT}}{\theta} \right)$ <p style="text-align: center;">(6.31)</p>	$\theta_{crS} = \theta_{cr} \cos \arctan S \left(1 - \frac{S}{\varphi} \right)$ <p style="text-align: center;">(6.32)</p>	$\frac{n_r}{n_{tot}} = \frac{0.0756Q^{0.11}}{g^{0.06} d_{90}^{0.28} S^{0.33}}$ <p style="text-align: center;">(6.25)</p>	$\theta_{c,D} = \theta_c \left[\frac{d_{90}}{d_m} \right]^{2/3}$ <p style="text-align: center;">(6.38)</p>
			$\frac{n_r}{n_{tot}} = \frac{0.133Q^{0.19}}{g^{0.096} d_{90}^{0.47} S^{0.19}}$ <p style="text-align: center;">(6.26)</p>	
			$\frac{n_r}{n_{tot}} = 0.092S^{-0.35} \left(\frac{h}{d_{90}} \right)^{0.33}$ <p style="text-align: center;">(6.27)</p>	
	$\Phi_b = \frac{3.1}{(s-1)^{0.5}} \left(\frac{d_{90}}{d_{30}} \right)^{0.2} \theta^{0.5} (\theta - \theta_{cr}) F_r^{1.1}$ <p style="text-align: center;">(6.33)</p>		$\frac{n_r}{n_{tot}} = 0.185S^{-0.22} \left(\frac{h}{d_{90}} \right)^{0.55}$ <p style="text-align: center;">(6.28)</p>	

Figure A.2: Possible formula combinations for SETRAC simulations for sediment mixtures, using the $\Phi_b - \theta$ form

flow velocity	bedload transport	incipient motion	form roughness losses (optional)
$v = 2.5v^* \left(1 - e^{\frac{-0.0075hm}{50.9d_{90}}} \right)^{0.5} \ln \left[\frac{12.3hm}{1.5d_{90}} \right]$ <p style="text-align: center;">(6.19)</p>	$\Phi_{bi} = \frac{3.255}{(s-1)^{0.5}} \theta^{0.5} (\theta_i - \theta_{ci}) F_r^{1.1}$ <p style="text-align: center;">(6.40)</p> $\Phi_{bi} = \frac{3.1}{(s-1)^{0.5}} \left(\frac{d_{90}}{d_{30}} \right)^{0.2} \theta^{0.5} (\theta_i - \theta_{ci}) F_r^{1.1}$ <p style="text-align: center;">(6.41)</p>	$\theta_{ci} = \left(\frac{d_i}{d_{50}} \right)^{-\gamma} \theta_{c50}$ <p style="text-align: center;">(6.44)</p>	$\frac{n_r}{n_{tot}} = \frac{0.0756Q^{0.11}}{g^{0.06} d_{90}^{0.28} S^{0.33}}$ <p style="text-align: center;">(6.25)</p> $\frac{n_r}{n_{tot}} = \frac{0.133Q^{0.19}}{g^{0.096} d_{90}^{0.47} S^{0.19}}$ <p style="text-align: center;">(6.26)</p> $\frac{n_r}{n_{tot}} = 0.092S^{-0.35} \left(\frac{h}{d_{90}} \right)^{0.33}$ <p style="text-align: center;">(6.27)</p> $\frac{n_r}{n_{tot}} = 0.185S^{-0.22} \left(\frac{h}{d_{90}} \right)^{0.55}$ <p style="text-align: center;">(6.28)</p>

Figure A.3: Possible formula combinations for SETRAC simulations for sediment mixtures for sediment transport calculations by size fractions

A.2 SETRAC file formats

A.2.1 Cross-section file format

The cross-section geometry is described by the cross-section file. The related grain size distributions for the active layer and the bedload layer are cross referenced. All tags in Table A.1 are obligatory.

Table A.1: Tags for the cross-section file

start tag	end tag	description	type	unit
<XSecFile>	</XSecFile>	cross-section file	-	-
<XSec>	</XSec>	cross-section	-	-
<Id>	</Id>	id of the cross-section	integer	-
<Name>	</Name>	name of the cross-section	string	-
GrainSizeDist_AL>	</GrainSizeDist_AL>	corresponding GSD of the active layer	string	-
<GrainSizeDist_BL>	</GrainSizeDist_BL>	corresponding GSD of the bedload layer	string	-
<Pnt>	</Pnt>	point	double	<i>m</i>

Each point in the cross-section file consists of two coordinates and a code for the type of the connection to the next cross-section point, which are separated by comma:

- distance from the left bank in *m*
- sea level in *m*
- channel type: R for riparian, B for bank and M for main channel

The axis of the channel is marked with the code A in front of the distance from the left bank. The last point of the cross-section has a blank instead of the channel type.

Example of cross-section file

```
<XSecFile>

<XSec>
<Id>0</Id>
<Name>CS hm 0.0</Name>
<GrainSizeDist_AL>LZA1</GrainSizeDist_AL>
<GrainSizeDist_BL>LZA2</GrainSizeDist_BL>
<Pnt>0, 666.349, B</Pnt>
<Pnt>5, 666.378, M</Pnt>
<Pnt>14, 667.263, M</Pnt>
<Pnt>18, 666.473, M</Pnt>
<Pnt>20, 666.353, M</Pnt>
<Pnt>A22, 665.88, M</Pnt>
<Pnt>27, 666.523, M</Pnt>
```

<Pnt>29, 666.325, M</Pnt>
<Pnt>34, 668.099, M</Pnt>
<Pnt>36, 667.968, B</Pnt>
<Pnt>40, 668.222, </Pnt>
</XSec>

<XSec>
<Id>1</Id>
<Name>CS hm 0.5</Name>
<GrainSizeDist_AL>LZA1</GrainSizeDist_AL>
<GrainSizeDist_BL>LZA2</GrainSizeDist_BL>
<Pnt>0, 669.2, B</Pnt>
<Pnt>5, 668.288, M</Pnt>
<Pnt>8, 668, M</Pnt>
<Pnt>A10, 668, M</Pnt>
<Pnt>13, 668.427, M</Pnt>
<Pnt>15, 668.658, M</Pnt>
<Pnt>19, 670.189, M</Pnt>
<Pnt>21, 669.669, B</Pnt>
<Pnt>22, 668.992, </Pnt>
</XSec>

<XSec>
<Id>2</Id>
<Name>CS hm 1.0</Name>
<GrainSizeDist_AL>LZA1</GrainSizeDist_AL>
<GrainSizeDist_BL>LZA2</GrainSizeDist_BL>
<Pnt>0, 671.215, B</Pnt>
<Pnt>3, 670.93, B</Pnt>
<Pnt>5, 671.062, M</Pnt>
<Pnt>9, 670.445, M</Pnt>
<Pnt>A12, 670.39, M</Pnt>
<Pnt>16, 670.477, M</Pnt>
<Pnt>17, 670.573, M</Pnt>
<Pnt>18, 670.659, B</Pnt>
<Pnt>21, 671.606, B</Pnt>
<Pnt>23, 671.639, </Pnt>
</XSec>

</XSecFile>

A.2.2 Point file format

In the point file the coordinates of the axis points for the cross-sections are stored. Thus the channel can be visualized geo-referenced in the GUI of SETRAC. The corresponding cross-section is cross referenced. All tags are obligatory and are described in Table A.2.

Table A.2: Tags for the point file

start tag	end tag	description	type	unit
<PntFile>	</PntFile>	point file	-	-
<Pnt>	</Pnt>	point	-	-
<Id>	</Id>	id of the point	integer	-
<x>	</x>	x-coordinate	double	<i>m</i>
<y>	</y>	y-coordinate	double	<i>m</i>
<XSecId>	</XSecId>	corresponding cross-section	integer	

Example of point file

```
<PntFile>
```

```
<Pnt>
```

```
<Id>0</Id>
```

```
<x>610546</x>
```

```
<y>167694</y>
```

```
<XSecId>0</XSecId>
```

```
</Pnt>
```

```
<Pnt>
```

```
<Id>1</Id>
```

```
<x>610521</x>
```

```
<y>167650</y>
```

```
<XSecId>1</XSecId>
```

```
</Pnt>
```

```
<Pnt>
```

```
<Id>2</Id>
```

```
<x>610493</x>
```

```
<y>167609</y>
```

```
<XSecId>2</XSecId>
```

```
</Pnt>
```

```
</PntFile>
```

A.2.3 Section file format

Information how the cross-sections have to be connected is stored in the section file. Thereby a channel network with unlimited number of branches can be modelled. Information on the real flow length between two cross-sections and possible erosion depths in the main channel are defined optionally. Sections can be defined as steps: All sediment and water is transferred through this section without calculation of bedload transport in order to model steep waterfalls or filled check dams. The elevation of cross-sections marked by the step tag is set as unchangeable. Morphologic changes can occur one subsection upstream and one subsection downstream of the step. This is a routine to avoid unrealistic extrapolations of the sediment transport capacity in short steep sections. These sections are excluded in the calculation of the required time step. Another optional tag is the definition of a specific exponent a for form roughness calculations in sections.

Table A.3: Tags for the section file

start tag	end tag	description	type	unit	obligatory/optional
<SecFile>	</SecFile>	section file	-	-	ob
<Sec>	</Sec>	section	-	-	ob
<Id>	</Id>	id of the section	integer	-	ob
<FromPnt>	</FromPnt>	start point	integer	-	ob
<ToPnt>	</ToPnt>	end point	integer	-	ob
<Length>	</Length>	section length	double	m	op
<z_Main>	</z_Main>	erosion depth	double	m	op
<Step>	</Step>	step or fall	string	-	op
<Exp_a>	</Exp_a>	exponent a for form roughness	double	-	op

Example of section file

```
<SecFile>
```

```
<Sec>
```

```
<Id>0</Id>
```

```
<FromPnt>2</FromPnt>
```

```
<ToPnt>1</ToPnt>
```

```
<Length>50</Length>
```

```
<z_Main>3</z_Main>
```

```
</Sec>
```

```
<Sec>
```

```
<Id>1</Id>
```

```
<FromPnt>1</FromPnt>
```

```
<ToPnt>0</ToPnt>
```

```
<Length>51</Length>
```

```
<z_Main>3</z_Main>
```

</Sec>

</SecFile>

A.2.4 Grain size distribution file format

Within the grain size distribution file the sediment properties for the one grain model as well as for the fractional bedload transport are defined. The number of grain classes and their range is defined by the the user. the number of grain size classes is unlimited. For sediment transport with the one-grain model at least one grain class has to be defined. All tags in Table A.4 are obligatory.

Table A.4: Tags for the grain size distribution file

start tag	end tag	description	type	unit
<GrainSizeDistFile>	</GrainSizeDistFile>	grain size distribution file	-	-
<GrainSizeDist>	</GrainSizeDist>	grain size distribution	-	-
<Name>	</Name>	name of grainsize distribution	string	-
<SedimentMixture>	</SedimentMixture>	one grain model	-	-
<d30>	</d30>	d_{30}	double	m
<d50>	</d50>	d_{50}	double	m
<d90>	</d90>	d_{90}	double	m
<dm>	</dm>	d_m	double	m
<kSt>	</kSt>	Strickler roughness value	double	$m^{1/3}/s$
<FractionalSedimentTransport>	</FractionalSedimentTransport>	fractional transport	-	-
<K1>	</K1>	grain class 1	double	-
<perc>	</perc>	fraction 1	double	%
<GrainSizeDT>	</GrainSizeDT>	grainsize definition table	-	-
<d_min>	</d_min>	minimum diameter	double	m
<dia>	</dia>	maximum diameter of grain class	double	m

Example of grain size distribution file

The example shows a grain size distribution file with two grain size distributions and 19 grain size classes.

```
<GrainSizeDistFile>

<GrainSizeDist>
<Name>LZA1</Name>
<SedimentMixture>
<d30>0.0262</d30>
<d50>0.0576</d50>
<d90>0.2804</d90>
<dm>0.061</dm>
<kSt>15</kSt>
</SedimentMixture>
<FractionalSedimentTransport>
<K1>
<perc>16.16</perc>
</K1>
<K2>
<perc>6.69</perc>
</K2>
<K3>
<perc>9.46</perc>
</K3>
<K4>
<perc>7.48</perc>
</K4>
<K5>
<perc>6.56</perc>
</K5>
<K6>
<perc>9.58</perc>
</K6>
<K7>
<perc>5.58</perc>
</K7>
<K8>
<perc>8.18</perc>
</K8>
<K9>
<perc>4.80</perc>
</K9>
<K10>
<perc>4.24</perc>
</K10>
```

```
<K11>
<perc>6.38</perc>
</K11>
<K12>
<perc>4.26</perc>
</K12>
<K13>
<perc>5.83</perc>
</K13>
<K14>
<perc>1.90</perc>
</K14>
<K15>
<perc>0</perc>
</K15>
<K16>
<perc>0</perc>
</K16>
<K17>
<perc>2.90</perc>
</K17>
<K18>
<perc>0</perc>
</K18>
<K19>
<perc>0</perc>
</K19>
</FractionalSedimentTransport>
</GrainSizeDist>

<GrainSizeDist>
<Name>LZA2</Name>
<SedimentMixture>
<d30>0.0201</d30>
<d50>0.0472</d50>
<d90>0.2469</d90>
<dm>0.051</dm>
<kSt>15</kSt>
</SedimentMixture>
<FractionalSedimentTransport>
<K1>
<perc>17.50</perc>
</K1>
<K2>
<perc>7.25</perc>
</K2>
```

<K3>
<perc>10.25</perc>
</K3>
<K4>
<perc>8.62</perc>
</K4>
<K5>
<perc>7.84</perc>
</K5>
<K6>
<perc>9.01</perc>
</K6>
<K7>
<perc>7.45</perc>
</K7>
<K8>
<perc>5.31</perc>
</K8>
<K9>
<perc>7.57</perc>
</K9>
<K10>
<perc>5.25</perc>
</K10>
<K11>
<perc>2.58</perc>
</K11>
<K12>
<perc>3.16</perc>
</K12>
<K13>
<perc>1.85</perc>
</K13>
<K14>
<perc>1.06</perc>
</K14>
<K15>
<perc>1.19</perc>
</K15>
<K16>
<perc>4.11</perc>
</K16>
<K17>
<perc>0</perc>
</K17>
<K18>

<perc>0</perc>
</K18>
<K19>
<perc>0</perc>
</K19>
</FractionalSedimentTransport>
</GrainSizeDist>

<GrainSizeDT>
<d_min>0.001</d_min>
<K1>
<dia>0.010</dia>
</K1>
<K2>
<dia>0.020</dia>
</K2>
<K3>
<dia>0.030</dia>
</K3>
<K4>
<dia>0.040</dia>
</K4>
<K5>
<dia>0.060</dia>
</K5>
<K6>
<dia>0.080</dia>
</K6>
<K7>
<dia>0.100</dia>
</K7>
<K8>
<dia>0.120</dia>
</K8>
<K9>
<dia>0.150</dia>
</K9>
<K10>
<dia>0.200</dia>
</K10>
<K11>
<dia>0.250</dia>
</K11>
<K12>
<dia>0.300</dia>
</K12>

<K13>
<dia>0.350</dia>
</K13>
<K14>
<dia>0.400</dia>
</K14>
<K15>
<dia>0.500</dia>
</K15>
<K16>
<dia>0.600</dia>
</K16>
<K17>
<dia>0.800</dia>
</K17>
<K18>
<dia>1.000</dia>
</K18>
<K19>
<dia>1.200</dia>
</K19>
</GrainSizeDT>

</GrainSizeDistFile>

A.2.5 Signal file format

Signals can be water (hydrograph) or sediment (sedigraph) discharge. These files are formatted text files with the extension *.sig. The structure is described in Table A.5. For sedigraphs the grain size distribution of the active layer of the relates cross-section (XSec) is considered.

Table A.5: Structure of the signal file

variable	description	unit
Name	name of the signal	-
Date	date when signal was generated	dd.mm.yyyy
unit	unit of the discharge	m^3/s
XSec	id of the cross-section where the signal is related	-
Signalname	name of the signal (shown during simulation)	-
Type	Type of signal	1 for water 2 for sediment
<td.dd.mm.yyyy-hh:mm,q>	format of the single entries	q in m^3/s
End	end of the signal	-
EOF	end of signal file	-

Example of signal file format for water discharge

Name Water

Date 09.11.2007

unit [m³/s]

XSec 0

Signalname Water

Type 1

<t21.08.2005-12:00,0.1>

<t21.08.2005-12:30,5>

<t21.08.2005-15:00,50>

<t21.08.2005-20:00,10>

<t21.08.2005-20:30,8>

<t21.08.2005-21:00,7>

<t21.08.2005-21:30,6>

<t21.08.2005-22:00,5>

<t21.08.2005-22:30,4>

<t21.08.2005-23:00,3>

<t21.08.2005-23:30,2>

<t22.08.2005-00:00,0.5>

End

EOF

Example of signal file format for sediment discharge

Name Bedload
Date 09.11.2007
unit [m3/s]

XSec 0
Signalname Bedload
Type 2

<t21.08.2005-12:00,0.001>
<t21.08.2005-12:30,0.1>
<t21.08.2005-15:00,0.5>
<t21.08.2005-20:00,0.2>
<t21.08.2005-20:30,0>
<t21.08.2005-21:00,0>
<t21.08.2005-21:30,0>
<t21.08.2005-22:00,0>
<t21.08.2005-22:30,0>
<t21.08.2005-23:00,0>
<t21.08.2005-23:30,0>
<t22.08.2005-00:00,0>

End

EOF

A.2.6 Output file format

Export as text files

For further analysis of the simulated channel two output files are generated. The first file lists all branches of the channel network. All nodes including the subsections are stored in topological order at the specified time steps. This simplifies the visualization of the longitudinal profiles in combination with specific output. In Table A.6 all possible stored variables are explained. The second export file lists the same output variables as time series for all nodes (uncluding the subsections).

Table A.6: Variables for txt the output file

variable	description	unit
Idx Sec	ID number of the section	-
Idx SubSec	ID number of the sub-section	-
Idx XSec	internal counter	-
RC_Counter	internal counter	-
XSec Name	name of the cross-section	-
Dist Root	distance to the channel outlet	m
Time absolute	absolute simulation time	dd.mm.yyyy — hh : mm
Time rel	relative simulation time	s
Original Axis Height	elevation of the axis at start of simulation	m
Act. Axis Height	elevation of the axis at actual simulation time	m
Height Water Level	elevation of the water level	m
Min. I0	minimum slope for selected formula set	m/m
Max. I0Min. I0	maximum, slope for selected formula set	m/m
I0Min. I0	actual slope	m/m
Fluid Velocity	flow velocity	m/s
Bedload Discharge	bedload discharge for the one grain model	m ³ /s
Bedload Avail.	accumulated availability of bedload over the whole channel length	m ³
Accumulated Bedload Transport	time integrated (accumulated) bedload transport	m ³
Height Bedload Layer	height of bedload layer	m
Water Depth	water and sediment mixture depth	m
Summ: Fractional Bedload Discharge	sum of all bedload fractions	m ³ /s
Fractional Bedload Discharge	bedload transport per fraction	m ³ /s
Perc	proportion of the grainsize distribution per fraction	-

Export as dxf files

For engineering applications the simulation results can be exported as DXF file. This already formatted file is prepared for plotting with CAD software. For all exported variables the maximum values are exported. The variables for the plot can be selected within the GUI of SETRAC.

Table A.7: Variables for the dxf output file

variable	description	unit	obligatory/optional
Original Axis Height	elevation of the axis at start of simulation	m	ob
Act. Axis Height	elevation of the axis at actual simulation time	m	ob
Left Bank	elevation of the left bank	m	ob
Right Bank	elevation of the right bank	m	ob
Height Water Level	maximum elevation of the water level	m	ob
Height Water Level	elevation of the water level	m	ob
Min. I0	minimum slope for selected formula set	m/m	op
Max. I0Min. I0	maximum, slope for selected formula set	m/m	op
I0Min. I0	actual slope	m/m	op
Fluid Velocity	maximum flow velocity	m/s	op
Bedload Discharge	maximum bedload discharge for the one grain model	m ³ /s	op
Bedload Avail.	accumulated availability of bedload over the whole channel length	m ³	op
Accumulated Bedload Transport	time integrated (accumulated) bedload transport	m ³	op
Height Bedload Layer	height of bedload layer	m	op
Mixture Depth	water and sediment mixture depth	m	op

Example of DXF export file

The original file shown in Figure A.4 is downscaled from A0 plot format. All optional variables are exported. In the header additional information about the file name and the simulation options as well as the formulas used for the simulation are shown.

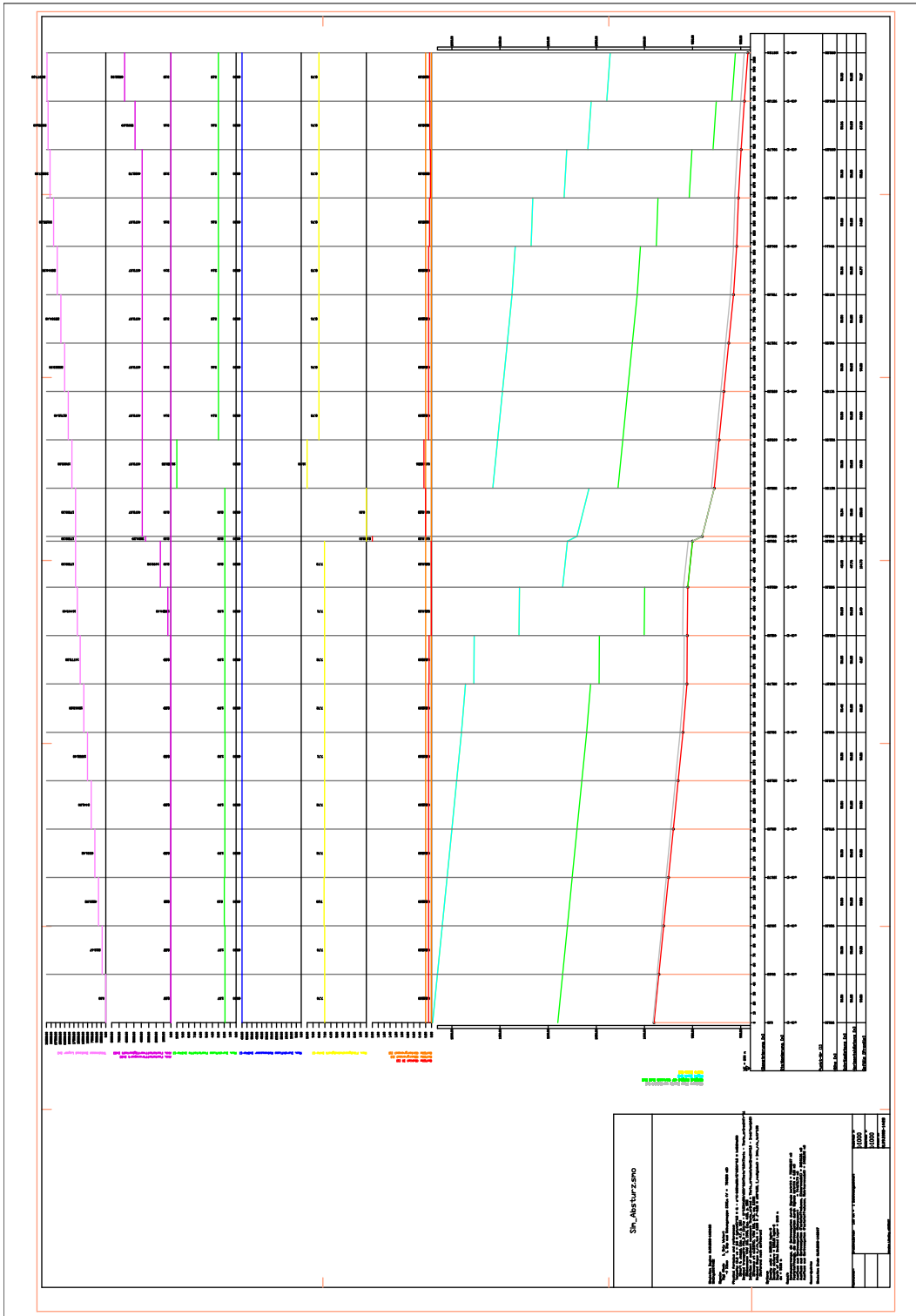


Figure A.4: Example of DXF file export in SETRAC.

B Precipitation-discharge simulation

Tables B.1 to B.7 show the selected models and parameters for the precipitation-discharge simulations in order to generate the input hydrographs needed for the SETRAC simulation. The simulations were calibrated with reconstructed flood hydrographs at the channel outlet. Wherever measurements were available, they were used for the re-calculation of the flood event.

Parameters for the calibration were:

- loss rate
- time of concentration
- base flow

Table B.1: Parameters for the precipitation-discharge simulations of the Sesslabach

Parameter	type
Model	HEC-HMS 2.2.2
Number of subbasins	4
Precipitation gauge	Kappl
Loss rate	SCS curve number
Transform	SCS unit hydrograph
Baseflow	recession
Channel routing	kinematic wave

Table B.2: Parameters for the precipitation-discharge simulations of the Schnannerbach

Parameter	type
Model	HEC-HMS 3.0.0
Number of subbasins	8
Precipitation gauge	Galzig
Loss rate	SCS curve number
Transform	SCS unit hydrograph
Baseflow	recession
Channel routing	kinematic wave

Table B.3: Parameters for the precipitation-discharge simulations of the Suggadinbach

Parameter	type
Model	HEC-HMS 3.0.1
Number of subbasins	13
Precipitation gauge	Vermunt and Tschagguns
Loss rate	SCS curve number
Transform	SCS unit hydrograph
Baseflow	recession
Channel routing	kinematic wave

Table B.4: Parameters for the precipitation-discharge simulations of the Chirelbach

Parameter	type
Model	HEC-HMS 3.0.0
Number of subbasins	26
Precipitation gauge	radar precipitation data
Loss rate	SCS curve number
Transform	SCS unit hydrograph
Baseflow	recession
Channel routing	kinematic wave

Table B.5: Parameters for the precipitation-discharge simulations of the Chiene mountain stream

Parameter	type
Model	HEC-HMS 3.0.0
Number of subbasins	21
Precipitation gauge	radar precipitation data
Loss rate	SCS curve number
Transform	SCS unit hydrograph
Baseflow	recession
Channel routing	kinematic wave

Table B.6: Parameters for the precipitation-discharge simulations of the Lüttschiene mountain stream

Parameter	type
Model	HEC-HMS 3.0.0
Number of subbasins	33
Precipitation gauge	radar precipitation data
Loss rate	SCS curve number
Transform	SCS unit hydrograph
Baseflow	recession
Channel routing	kinematic wave

Table B.7: Parameters for the precipitation-discharge simulations of the Laval case study

Parameter	type
Model	ETC 2.5
Number of subbasins	33
Precipitation gauge	Pompe
Loss rate	initial and constant
Transform	method of isochrone
Baseflow	none
Channel routing	kinematic wave